VERIFICATION OF A COMPUTER SIMULATOR FOR DIGITAL TRANSMISSION OVER TWISTED PAIRS

Fernando Costa

A dissertation submitted to the Faculty of Engineering, University of the Witwatersrand, Johannesburg, in fulfilment of the requirements for the degree of Master of Science in Engineering

Johannesburg, 1990

DECLARATION

I declare that this dissertation is my own, unaided work. It is being submitted for the degree of Master of Science in Engineering in the University of the Witwatersrand, Johannesburg. It has not been submitted before for any degree or examination in any other University.

Fernando Costa

(Signature of candidate)

9th day of November 1990

DEDICATION

To my Parents

Arlindo and Maria José

my Sister

Marlène

and

'Sabrina'

ABSTRACT

This dissertation verifies a Computer Simulation Package for modeling pulse transmission over digital subscriber loops. Multigauge sections on subscriber cables can be studied. The model used for each section incorporates skin, proximity and eddy current effects. The model allows important quantities such as near end echo and overall transmission distortion of pulses to be predicted. An experimental facility has been established in the laboratory for the purpose of validating the results produced by the simulator with results obtained over real cables. The experimental facility has as far as possible been automated by making use of computer controlled equipment for direct setup of the experiment, data transfer, and analysis. The results obtained from the pulse propagation program and that obtained from measurements are in close agreement, rendering the Computer Simulation Package useful for analysing the performance of multigauge digital subscriber loops.

ACKNOWLEDGEMENTS

I would like to thank Professor H.E. Hanrahan for his ideas and supervision of this dissertation.

The financial assistance of the Department of Posts and Telecommunications is gratefully acknowledge.

The cooperation and the laboratory facilities provided by S.T.C., South Africa is also appreciated.

CONTENTS

LIST OF FIGURES

LIST OF TABLES

Chapter 1

INTRODUCTION

The advent of digital transmission and digital switching in the telecommunications network comprises the foundation of the integrated digital network (IDN) [1]. Analog voice signals, coming through the local subscriber loops, are digitized using pulse-code modulation (PCM) and multiplexed using time-division multiplexing (TDM). The intermediate time-division digital switches can switch the individual signals without decoding them. Therefore, the voice signals can travel a long range using only a single digital encoding-decoding process at each exchange end of the connection.

The next step towards a digital network is to extend digital capability to the local subscriber loop and provide a digital service to the end user. This extension will not only enable end-to-end digital voice transmission but also offer the opportunity for a wide variety of digital data services, leading to an integrated services digital network (ISDN).

This chapter serves to introduce the ISDN interface of interest in this dissertation, a brief description of the transmission methods that have been proposed, and the main sources of impairments to be found in the digital subscriber loop. This is followed by a discussion of the overall aims of the current topic of research, and a résumé of the literature survey undertaken. The work achieved by previous research programs in the current field of study is also introduced. The chapter concludes with a brief overview of the work contained in the remainder of this dissertation.

1.1 Background of the Study Undertaken

Two major interfaces for the ISDN have been defined by the International Telegraph and Telephone Consultative Committee (CCITT). The two major interfaces are the basic-access interface (BAI) and the primary-rate interface (PRI). The former, supporting 2B channels and 1D channel (i.e., 2B + D), is intended for small capacity users (e.g., Residential subscribers) and will be provided on currently existing local subscriber loops. The latter, supporting 30B + D for Europe and 23B + D in North America, is intended for large capacity usage, such as private branch

exchanges (PBX). The B channels are 64 kilobits per second (kbits/s), and the D channel is 64 kbits/s for the primary rate interface and 16 kbits/s for the basic access interface.

The proposed ISDN interface block diagram is illustrated in *Figure 1.1*. The two most important interfaces are the S-interface, located within the customer premises, and the U-interface, which connects the telephone central-office end line termination (LT) to the customer premise network termination (NT).

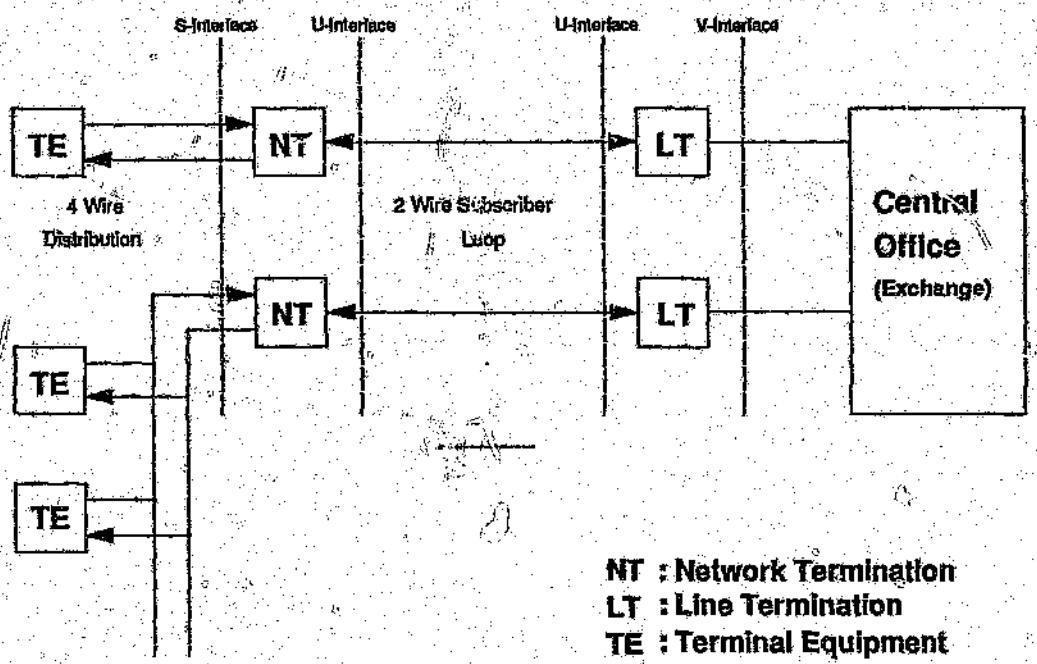

Figure 1.1 ISDN interface block diagram

The U-interface provides the minimal set of requirements to permit service between LT and NT over the subscriber loop. Data received by the customer premise NT is passed to the S-interface, which uses two pairs (one for each direction of transmission). It may operate in a point-to-point fashion or a multipoint connection bus with up to eight terminals attached to it [2].

Existing analog networks connect subscribers to the local exchange by a balanced wire pair (twisted-pair) designed to carry voice frequencies (i.e., base-band up to 3.4 kHz). The average cable plant investment in present installations is about 40 percent of the total network cost [3]. This enormous investment means that the digital services that can be offered to the majority of users will be restricted to those that can be provided using existing pairs to support basic access. The data rate required to carry 2B + D channels is 144 kbits/s. However, the transmission rate of the digital subscriber loop (DSL) must be higher in order to provide for framing, synchronization and maintenance functions. For example, the American National Standards Institute (ANSI) standard bit rate is 160 kbits/s in order to provided for these other functions [4].

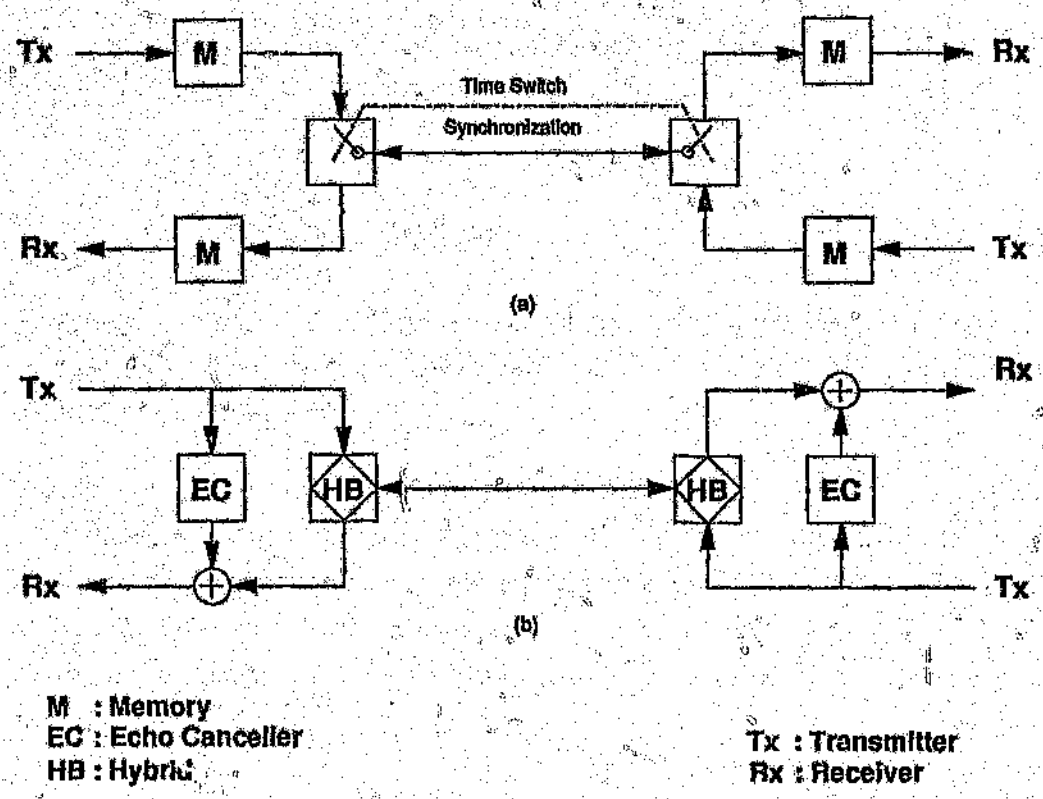

Figure 1.2 (a) Schematic of TCM Transmission Method
(b) Schematic of HEC Transmission Method

Various transmission schemes have been proposed to achieve full-duplex two-wire transmission [2]. The two transmission schemes that seem to offer better performance in terms of noise immunity and ease of implementation are burst mode, *Figure 1.2a*, also referred to as time compression multiplexing (TCM) mode, and the hybrid echo cancellation (HEC) mode, *Figure 1.2b*, also referred to simply as the hybrid mode [1,2,4,5].

Both of these modes isolate the data received from the far-end from that transmitted at the near-end. In the HEC mode the isolation is achieved by a hybrid and echo canceller while both the transmission and reception are occurring simultaneously. In the TCM mode, the intervals for transmission and reception are isolated in time and the separation of the two directions of transmission is thus simplified. The reader is referred to *Appendix A.1* for a brief discussion on these two transmission methods.

The main sources of impairments in digital subscriber loops are [5]:

(a) crosstalk,
(b) echo,
(c) impulse noise,
(d) intersymbol interference, and
(e) bridge taps.

The diagram of *Figure 1.3* illustrates most of the range-limiting factors in the subscriber loop. The reader is referred to *Appendix A.2* for a brief discussion on each of these range limiting factors.

The subscriber loop plant is far from the ideal situation where uniform gauge wires run from the subscriber to the local exchange. It was intended to provide adequate performance at voice frequencies and regard was not paid, in general, to high frequency characteristics. There is however no sharp cut-off frequency unless inductive loading is used, and this is rare in urban loops, where distances are moderate (i.e., up to approximately 6 km).

Any design of the bidirectional data transmission facility must therefore accommodate the wide disparity of cable compositions, bridge tap configurations, crosstalk, impulse noise, intersymbol interference and the variable impedances encountered from either end of the loop.

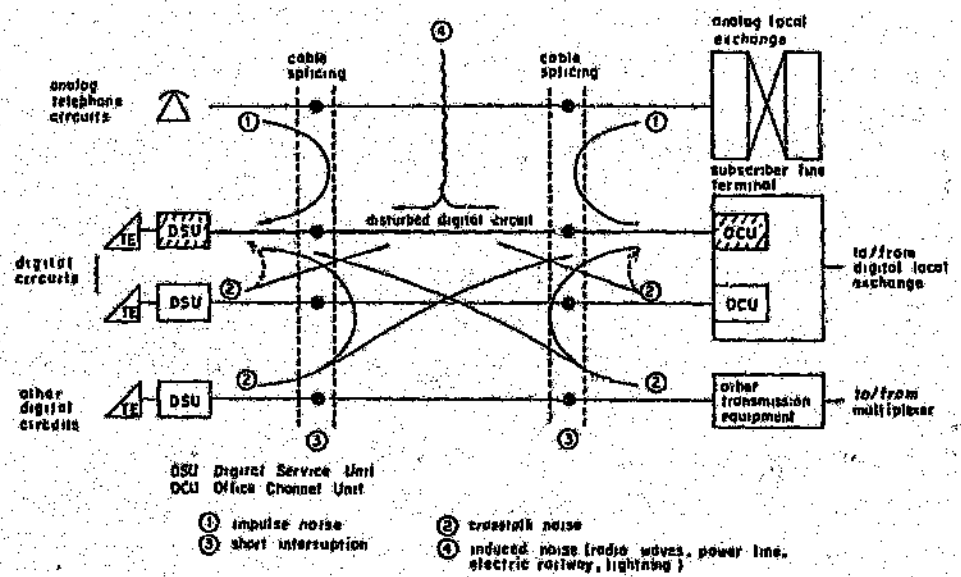

Source : Ref [6]

Figure 1.3 Range-limiting factors in subscriber loops

1.2 Statement of the Study Undertaken

In anticipation of the introduction of a switched end-to-end digital service on the telephone network, it is important to assess the digital transmission capability of the two-wire twisted-pair subscriber loop. In this dissertation, the transmission and implementation issues pertaining to the U-interface in order to provide the basic-access of 2B + D channels on the existing subscriber loop is the topic of research and discussion. The CCITT, recognizing the wide variation in cable plant conditions, plant modernization and servicing policies prevalent in different countries, has accepted that the U-interface specification should be a national responsibility. This allows the necessary flexibility to enable telecommunications authorities in different countries to select specifications appropriate to the particular loops prevalent in that country, while retaining those necessary features which ensures that the ISDN's in different countries are all compatible.

The challenge in South Africa is to identify the relevant characteristics of the cable plant, and to select the appropriate approach for the U-interface circuitry. Due to the diversity of the loop plant, exhaustive experimental analysis can be virtually excluded as a possible approach of establishing performance capabilities. The means of establishing this performance capability is by computer simulation.

A computer simulation package for modelling the subscriber loop, and to analyse digital pulse transmission over subscriber loops was created previously by Lowitt [7]. The pulse propagation program can be used to study TCM and HEC transmission modes together with different coding schemes. The work presented in this dissertation is a direct continuation of that work. This dissertation describes an experimental facility that has been setup for the purpose of characterizing subscriber cable loops, as well as to study pulse propagation along the loops. The results obtained from this experimental facility is used to partially validate the computer simulation package. The complete validation entails the review of the theoretical models used in order to assess the implications of any assumptions made, as well as the verification that the theoretical model has been correctly implemented in the program source code.

The simulation package is not without limitations. It considers transmission on a single pair only and does not also take into account the impairments described in *section 1.1*. The simulation package does however render itself to be easily upgraded to include new features such as a crosstalk model, due to its modular design. The simulation package is also required to be fully debugged, and to incorporate a friendly man-machine interface in order to render itself useful for general users.

1.3 Literature Review Pertaining to the Aims of this Study

Various methodologies for the characterization of the two-wire twisted-pair subscriber loop plant for high speed digital communications typical of evolving an ISDN has been considered in earlier works. Of particular interest is the work done by S.V. Ahamed *et al* [8], and J.W. Modestino *et al* [9].

The emphasis has been to assess the penetration of digital services on the loop plant population at a fixed grade of service measured either in terms of the bit error probability (Modestino *et al*), or by eye opening measurements (Ahamed *et al*).

Computer simulation was the means of establishing these performance capabilities. The simulation accesses data-bases containing information on a statistically significant population of the loops and also model other system components such as hybrids, equalizers, echo-cancellers, etc. The information contained in the data-bases was obtained from Loop Surveys; the Bell system Loop Survey (1973) and the G.T.E system Loop Survey (1982) was used respectively by Ahamed *et al* and Modestino *et al*. Typical of the information contained in the data-bases is, the length of each loop, composition, number of bridge-taps, etc., as well as electrical characteristics such as input impedance (from either end of the loop), attenuation, transfer functions, etc.

The computer simulation described by Ahamed *et al*, is based on a dedicated Eclipse minicomputer. The simulation represents the waveforms being transmitted by sixty four fourier harmonics. Each composite loop, with numerous loop sections and bridge-taps, is represented by its individual transfer function at each harmonic frequency. Two modes of transmission (the HEC and TCM) are investigated. Various coding methods are investigated even though the primary emphasis has been on the bipolar code. The results are displayed graphically by eye diagrams for individual loops and by scatter plots for all the loops in the data-base.

The computer simulation described by Modestino *et al*, places more emphasis on mathematical analysis, and does not rely on subjective criteria, like eye-opening results to determine the operating bit error probability. Each composite loop is represented by a mathematical equation that approximates its transfer function as was determined in the Loop Survey. The other system components are treated likewise. Attention is restricted to TCM schemes with bipolar line coding. The results are displayed as plots of bit error probability versus signal to noise ratio at various bit rates.

1.4 Overview of this Dissertation

The remainder of this dissertation has as its main objective the validation of the Cable Simulation Package.

Chapter 2 describes the cable simulation package that has been developed by Lowitt [7]. This not only entail a description of the software package but also describes the models used to represent the composite loop connection. *Chapter 3* describes a

test facility that has been designed to characterise a wide range of subscriber cable types, and to analyse the propagation of digital signals for any practical loop connection. The test facility is largely automated by making use of computer controlled equipment for direct setup of the experiments, data transfer, and analysis. *Chapter 4* is concerned with the verification of the cable characterization program of the Cable Simulation Package. The test facility that was designed in *Chapter 3* to characterise subscriber cables, is used to obtain results for comparison to that predicted by the cable characterization program. *Chapter 5* is concerned with the verification of the pulse propagation programs of the Cable Simulation Package, whereby the experimental results are provided by the test facility designed in *Chapter 3*, to analyse the pulse propagation of digital signals. *Chapter 6* summarises the findings of this investigation and proposes additional topics that would augment the present study.

Chapter 2

CABLE SIMULATOR

This chapter describes the computer simulation package for modelling pulse transmission over digital subscriber loops. The cable simulation package has been developed on an IBM compatible personal computer (PC), using Microsoft Pascal as the programming language. Microsoft Pascal[1] was used since it had the advantage of facilitating programming in modules and the ability to emulate a numeric co-processor in order to provide the required precision should one not be available in hardware. Changes to one module does not involve recompilation of the whole program since modules are compiled separately; although all the modules have to be re-linked. This feature leads to large complicated programs being easily managed. The overall program structure can be discerned by examining how the composite modules combine with one another, as each module performs a specific task.

The block diagram of *Figure 2.1* illustrates the digital subscriber loop configuration that can be analysed by the cable simulation package. For simplicity, this diagram represents the simulation in the unidirectional case only, although full-duplex transmission can be simulated as well.

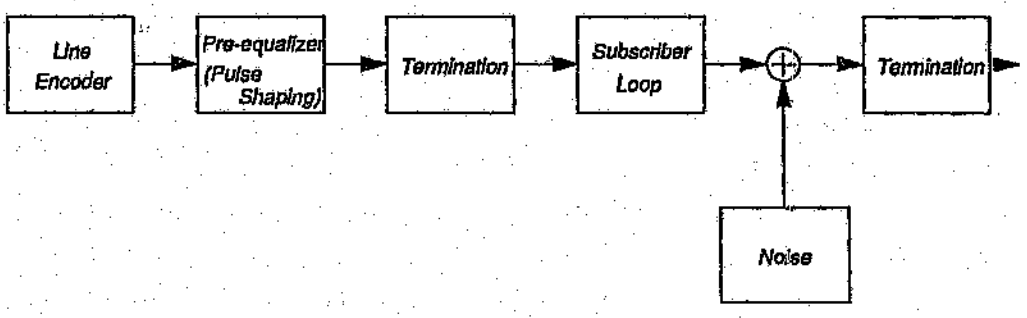

Figure 2.1 Digital subscriber loop simulator block diagram

[1] The decision to use Microsoft Pascal is an historical one of Lowitt[7]. With the advent of Turbo Pascal 4.0 and its unit structure, the choice in programming language could have been different if the decision were taken today.

The simulation package comprises several programs, which enables the user to analyse a specific aspect of the system without being required to re-execute other portions of the package. This is advantageous both to the user (i.e., saves time), and to the capability of the program being executed as it can make maximum use of the available workspace on the PC. The programs are all interactive, and a substantial effort has been made to create a friendly and efficient man-machine interface. Due to the nature of the simulation being very mathematically oriented, computation time is significant, and a status report is continually given as the various modeling aspects are performed and completed. This not only indicates that the program is "working", but also allows the user to monitor the logical progression of the theoretical analysis until completion.

2.1 Theoretical Basis

The foundation of the cable simulation package relies on the well established transmission line theory in order to characterize the cable connection specified by the user. Transmission line theory is reviewed as well as the model used to incorporate skin, proximity and eddy current effects. A frequency domain model which uses the Fast Fourier Transform as a tool is described, which enables pulse propagation to be studied on multigauge cable sections.

2.1.1 Transmission Line Theory

Transmission lines are modelled by series impedance elements having resistance R, and inductance L, per unit length, as well as shunt conductance G, and capacitance C, per unit length. These distributed circuit coefficient at a given frequency are determined only by the materials and dimensions of the line conductors and the surrounding medium, and do not vary with time, nor with line voltage or current. These four coefficients are used as an intermediate step between the physical dimensions and materials of the transmission line, and the ultimate signal propagation characteristics, known as the secondary characteristics.

There are two secondary parameters that are derived from the primary parameters [10]. Firstly, the characteristic impedance Z_o is given by

$$Z_o(\omega) = \sqrt{\frac{R + j\omega L}{G + j\omega C}} \qquad 2.1$$

and secondly, the propagation constant γ, is given by

$$\gamma(\omega) = \sqrt{(R + j\omega L)(G + j\omega C)} \qquad 2.2$$

The real and imaginary parts of γ are defined by the relation

$$\gamma = \alpha + j\beta \qquad 2.3$$

where α = attenuation constant (nepers per unit length)
β = phase constant (radians per unit length)

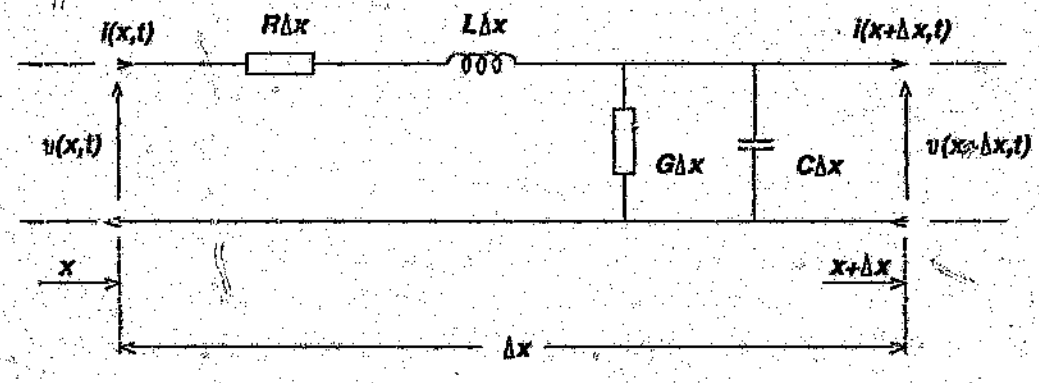

Source : Ref [10]

Figure 2.2 Representation of a short section of transmission line

The primary parameters are dependent on frequency over the range of interest[10]. The skin effect concerns the tendency of alternating current to crowd towards the surface of a conductor, thereby increasing the resistance of the conductor above its d.c resistance value. The skin effect correction factor for resistance is characterized by the parameter T_{sr} and is defined in equation (2.4) as the increase in resistance at each frequency relative to the d.c value.

$$T_{SR} = \frac{R(f)}{R_{dc}}$$

$$= \frac{q}{2} \cdot \frac{ber(q) \cdot bei'(q) - bei(q) \cdot ber'(q)}{[bei'(q)]^2 + [ber'(q)]^2} \qquad 2.4$$

where q is defined in equation (2.5) for any conductor of radius a,

$$q = \sqrt{2} \cdot \frac{a}{\delta} \qquad 2.5$$

and δ is the nominal depth of penetration (i.e., skin depth) for a round conductor, and is given by equation (2.6), where μ is the permitivity and σ is the conductivity of the conductor.

$$\delta = \frac{1}{\sqrt{\pi f \mu \sigma}} \qquad 2.6$$

In equation (2.4), use is made of the Bessel functions *ber* and *bei*, and there derivatives *ber'* and *bei'*. The primes indicate differentiation with respect to q. To solve for values of *ber*, *bei*, *ber'*, and *bei'*, the Bessel series expansions are used, (equations (2.7) to (2.10)), as they can be used without incurring an unacceptable computational penalty, providing better results as compared to look-up tables.

$$ber(q) = 1 - \frac{q^4}{2^2.4^2} + \frac{q^8}{2^2.4^2.6^2.8^2} - \ldots \qquad 2.7$$

$$bei(q) = \frac{q^2}{2^2} - \frac{q^6}{2^2.4^2.6^2} + \frac{q^{10}}{2^2.4^2.6^2.8^2.10^2} - \ldots \qquad 2.8$$

$$ber'(q) = -\frac{q^3}{2^2.4^4} + \frac{q^7}{2^2.4^2.6^2.8} - \frac{q^{11}}{2^2.4^2.6^2.8^2.10^2.12} + \ldots \qquad 2.9$$

$$bei'(q) = \frac{q}{2} - \frac{q^5}{2^2.4^2.6} + \frac{q^9}{2^2.4^2.6^2.8^2.10} - \ldots \qquad 2.10$$

The total inductance per unit length of line will be equal to the sum of the self inductance of each wire L_s and the mutual inductance L_m between each conductor. At low frequencies, the self inductance L_s is approximately equal to the inductance value at frequencies approaching d.c, i.e., L_{-dc}. When the skin effect is well developed, the self inductance L_s approaches zero and can thus be ignored. The skin effect correction factor for inductance is characterized by the parameter T_{SL} and is defined in equation (2.11) as,

$$T_{SL} = \frac{L_m(f)}{L_{-dc}}$$

$$= \frac{4}{q} \cdot \frac{bei(q) \cdot bei'(q) + ber(q) \cdot ber'(q)}{[bei'(q)]^2 + [ber'(q)]^2} \qquad 2.11$$

where q is defined as in equation (2.5).

The skin effect defined above is exact when the magnetic field intensity is uniform around the surface of each conductor. However, in telephone cables, the close proximity of the return conductor results in field distortions. This has the effect of increasing the a.c resistance by a further factor T_{PR}. The proximity effect correction factor for resistance can be approximated by equation (2.12) [11], with an error of less than 1% for any value of q provided that $\alpha < 0.5$, which is true for all the telephone cables under consideration, (see *Table 4.1* 'Cable Library').

$$T_{PR} = \frac{1}{\sqrt{1 - \alpha^2 \cdot a(q)}} \qquad 2.12$$

where α is defined for a conductor of diameter d, and a centre to centre spacing s between the two conductors in each pair,

$$\alpha = \frac{d}{s} \qquad 2.13$$

and $a(q)$ is defined by equation (2.14), where q is defined as in equation (2.5).

$$a(q) = 0.526\left[1 + \mathrm{Tanh}\left(1.14 - \frac{3.078}{q}\right)\right] \qquad 2.14$$

As frequency increases, there are additional loses due to eddy currents being induced in neighbouring conductors. This effect can be represented by an additional component in the conductance resistance defined as ΔR_e. An approximation for ΔR_e is given in equation (2.15) [10].

$$\Delta R_e = \frac{\Delta R}{10} \quad for \quad q > 5$$

$$\Delta R_e = \frac{\Delta R}{16} \quad for \quad 2.5 < q < 5$$

$$\Delta R_e = \frac{\Delta R}{24} \quad for \quad q < 2.5 \qquad 2.15$$

where ΔR is given by equation (2.16) and q is defined as in equation (2.5).

$$\Delta R = q \cdot \frac{d}{s} \cdot R_{dc} \qquad 2.16$$

The resulting equation for the resistance of the cable as a function of frequency and the inductance of the cable as a function of frequency is given respectively by equation (2.17) and equation (2.18) [10].

$$R(f) = R_{dc} \cdot T_{SR} \cdot T_{PR} + \Delta R_e \qquad \Omega/km \qquad 2.17$$

$$L(f) = L_{dc} + \mu_r \cdot 10^{-4} \cdot T_{SL} \qquad H/km \qquad 2.18$$

The conductance parameter G is frequency sensitive and its effect is more pronounced in paper insulated cables. In good quality plastic insulated, G can be taken as a constant, and is in general very small. The model for the frequency dependence of G is embodied in equation (2.19).

$$G(f) = g \cdot f^k \qquad 2.19$$

where g is the base value, and the index k depends on the type of cable and would be zero in an ideal cable. For paper insulated cables, k varies in the range 1.0 to 1.5.

Of all the primary parameters, capacitance is the least variable with frequency and is assumed to be constant.

2.1.2 Multigauge Cable Model

A transmission line of characteristic impedance Z_o is usually depicted as illustrated in *Figure 2.3*, where the line is driven by a generator E_G, internal impedance Z_G, and is terminated at the distance l (measured from the generator end), by an impedance Z_T.

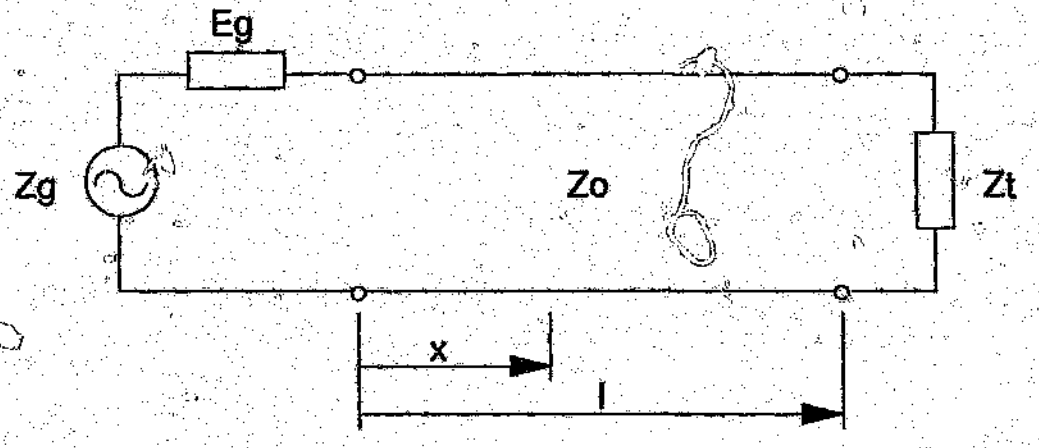

Figure 2.3 Single cable section depicting generator and terminator components

A wave travelling down the line will be attenuated. The propagation of a wave travelling from the generator end towards the termination end is given by equation (2.20).

$$V_{For}(\omega,x) = e^{-\gamma x} V_{For}(\omega,0) \qquad (2.20)$$

where x = Length of cable section.

$V_{For}(\omega,0)$ = Fourier transform of the forward travelling voltage at the generator end.

$V_{For}(\omega,x)$ = Fourier transform of the forward travelling voltage at point x along the cable section.

If the terminating impedance Z_T is different to the characteristic impedance Z_o, a reflection takes place at the termination end of the line. The reflection coefficient is given by equation (2.21).

$$\rho_{For} = \frac{Z_o(\omega) - Z_T(\omega)}{Z_o(\omega) + Z_T(\omega)} \qquad 2.21$$

The propagation of the backward travelling wave is described by equation (2.22).

$$V_{Ref}(\omega, x) = e^{-\gamma\omega(l-x)} V_{Ref}(\omega, l-x) \qquad 2.22$$

The backward travelling wave suffers a reflection at the generator end, according to equation (2.23).

$$\rho_{Ref} = \frac{Z_G(\omega) - Z_o(\omega)}{Z_G(\omega) + Z_o(\omega)} \qquad 2.23$$

When the line is driven by a source with internal impedance Z_G, the voltage impressed upon the line as a forward travelling wave is given by equation (2.24).

$$V_{For}(\omega, 0) = V_G(\omega) \frac{Z_G(\omega)}{Z_G(\omega) + Z_o(\omega)} \qquad 2.24$$

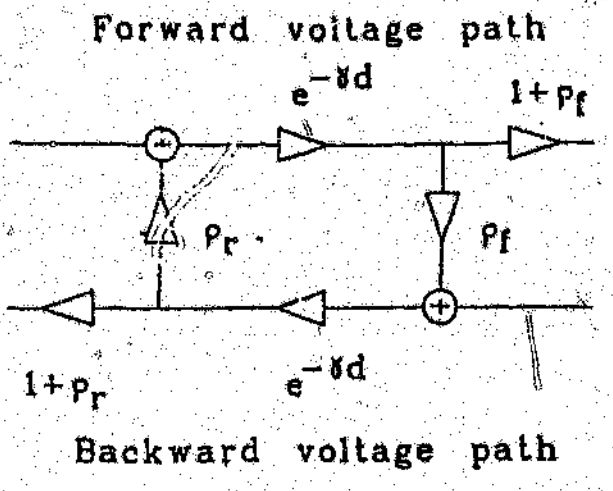

Source : Ref [12]

Figure 2.4 Model for a single cable connection

The diagram of *Figure 2.4* illustrates the model used for a single section of cable. The upper path depicts the forward travelling wave, while the lower path depicts the backward travelling wave. At the generator end, the factor A_G is introduced to describe the potential divider effect shown in equation (2.24).

Modelling of a multigauge subscriber loop is performed by interconnecting the single section model of *Figure 2.4*. *Figure 2.5* is an example for a three section cable connection, where the individual models for the three sections are distinguished by an extra subscript.

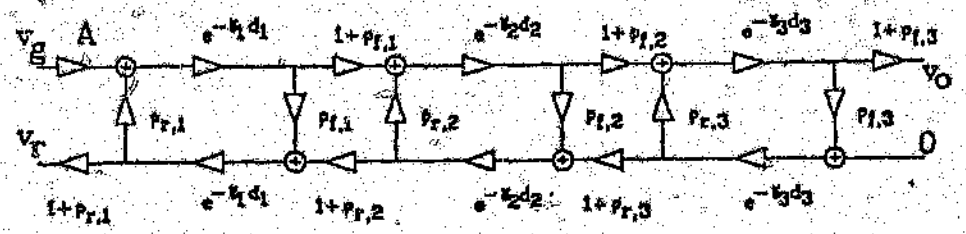

Source : Ref [12]

Figure 2.5 Model for a three section cable connection

It is clear from *Figure 2.5* that the reflections at either end of each section give rise to the multiplicity of forward and backward travelling components. The type of series solution used for single cable sections proves difficult in this situation. Discipline is required to manage the data flow and calculations in the simulation. One approach is described by Lowitt[7], while *Figure 2.6* indicates a second methodology[12] for keeping track of the various components.

Figure 2.6 differs from the model depicting the three section connection of *Figure 2.5* by replicating the forward and backward paths as many times as is necessary. Whenever a reflection occurs the element depicting the reflection coefficient connects with the next lower line in the diagram rather than feeding back to the upper line. The sum of all the backward travelling waves due to the first reflection at the ends of cable section 1, 2, and 3 arrive at the receiving end at point

x, while later reflections arrive at points *y*, *z*, etc. The sum of these reflections together with the output of element *A* gives the near end echo. At the termination end, the total received waveform is the output of the summer shown.

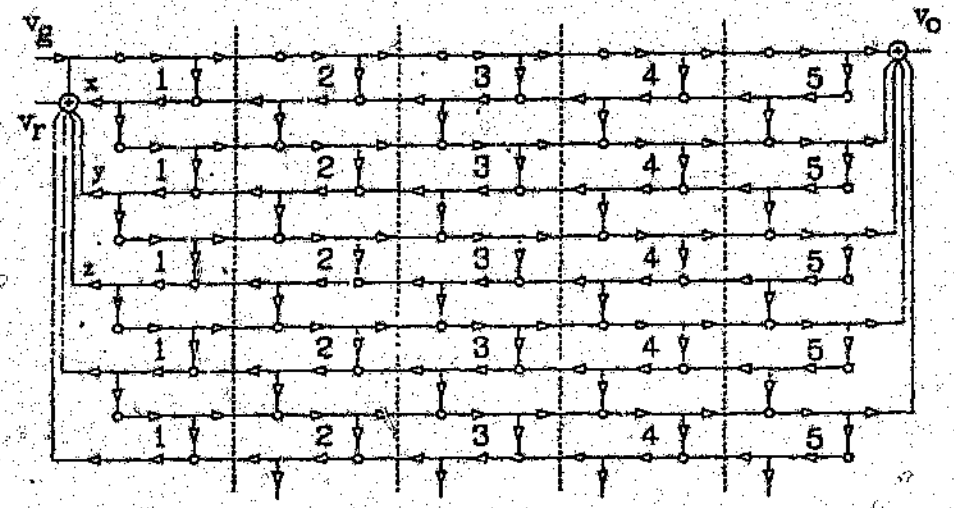

Source : Ref [12]

Figure 2.6 Expansion of cable model showing reflected components

There exists a minimum number of paths required to give an accurate representation of the near end and received waveforms. Not all reflections are modelled and those of very low amplitude are not calculated.

The model illustrated in *Figure 2.6* is known as the transient state model, since each cable section is characterized as a transfer function and each join with a reflection coefficient. The various transmitted and reflected signals can be explicitly described, and full-duplex transmission can be simulated as bidirectional transmission is readily modelled as the superposition of transmission in both directions.

A second model known as the steady state model has also been developed. This model reduces the entire cable connection to a single equivalent transfer function. Implicit in this model is the reflections which results from mismatches along the

connection and is absorbed into the transfer function expressions. This model can therefore not give explicit expressions for the signal that will be reflected at the discontinuities created by the differing cable joins. It can therefore only be used to simulate half-duplex transmission schemes.

The simulation represents the waveforms being transmitted by 256 fourier harmonics. Each composite loop, with numerous loop sections is represented by its individual transfer function at each harmonic frequency. The number of points in the Fast Fourier Transform has been limited to 256 due to the program stack been limited to 64kbytes. It has subsequently been determined that with careful usage, the number of points used in the Fast Fourier Transform can be increased to 1024 providing that large arrays are declared globally or placed on the heap memory space.

2.2 Original Simulator - *Version 0.0*

The cable simulation package structure as developed by Lowitt [7] is illustrated in the block diagram of *Figure 2.7*. The simulation can be divided into two main sections. The first characterises the subscriber loop connection (i.e., program ***CabSim***), and the second simulates the propagation of digital signals along the connection (i.e., program ***Waves***, ***EyeDgm***, and ***EyePat***). Several other auxiliary programs are provided to manipulate and plot the results produced from these programs.

The program ***CabSim*** is used to characterise the subscriber loop which is specified by the user. Multigauge connections comprising sections selected from a 'Cable Library', or specified by the user in terms of the d.c primary parameters and cable geometry are characterised in the frequency domain. Two models are available to characterise the subscriber loop; namely, the steady state and the transient state model.

Both these models rely on computing the secondary parameters (i.e., characteristic impedance and propagation factor) of the composite sections. The secondary parameters are calculated from the primary parameters. Various effects such as skin effect, proximity effect and eddy current effect are taken into account when computing the frequency dependant versions of the primary parameters.

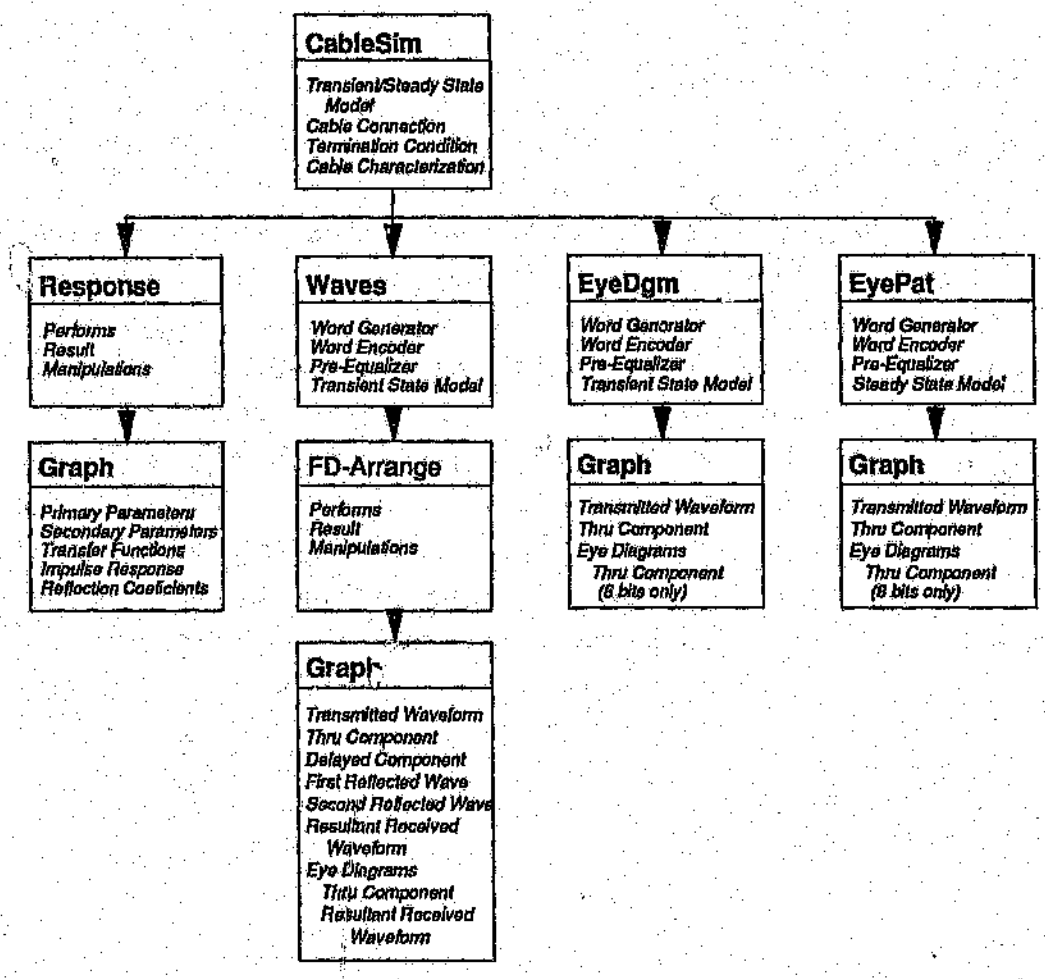

Figure 2.7 Original simulator program block diagram - *Version 0.0*

The characteristic impedance values are used to determine the reflection coefficient which characterise the joins between cable sections. The propagation factor is necessary to characterise the voltage transfer function for each section.

The program ***Response*** is used to manipulate the results produced by ***CabSim*** for plotting purposes. The results available include the following :

(a) primary parameters,

(b) secondary parameters,

(c) reflection coefficient,
(d) transfer functions, and
(e) impulse response.

The program ***Graph***, which is a dedicated graph plotting program, is used to display these results.

The program ***Waves*** utilises the transient state cable connection model to simulate pulse transmission in full-duplex mode along the connection. This program allows the user to select the bit pattern (i.e., data sequence) to be transmitted, the coding strategy (i.e., either ternary, bipolar or orthonormal coding), and in the case of bipolar or ternary c. ling, a window for pulse shaping (i.e, pre-equalizer). A hanning, raised cosine, hamming, tophat and rectangular window is available. The window is applied to each bit period in the data sequence. The program ***Waves*** assumes perfect impedance matching conditions at the end terminations even though the cable characterization program ***CabSim*** provides the option of establishing mismatches at the end terminations, and generates the reflection coefficient to characterise these mismatches. The simulation in its present form implies perfect matching at the termination ends.

The program ***Arrange*** is used to manipulate the results produced by program ***Waves*** for plotting purposes. The results available include the following :

(a) the transmit signal waveforms from both ends,
(b) the received signal waveforms at both ends, and
(c) the various reflected signal waveforms.

The program ***Graph*** can then be used to display these results graphically.

The manipulations performed by the program ***Arrange*** is required due to the modulation property, i.e.,

$$x(t-a) \quad \Leftarrow FT \Rightarrow \quad e^{-j\omega a}$$

which has the effect of shifting the origin of the time domain representation of the waveforms relative to the common origin in time. Since this axis is effectively a "wrap-arround", it means that what might appear to be a zero point in time, would be a point $t = a$, which has been delayed and now wraps into the beginning. The program ***Arrange*** therefore provides the user with the flexibility to shift the origin of the received signals (i.e., results produced by program ***Waves***) by "un-wrapping"

the axis and re-arranging it. This program also positions the various reflected signals relative to the main received signal. For example, those signals that are delayed are set to zero for the time corresponding to the time delay they experience relative to the main received signal. This enables superposition of the signals to proceed correctly.

There are also two other programs that can be used to analyse unidirectional transmission. The first is ***EyeDgm***, which utilises the transient state model. The second is ***EyePat*** which utilises the steady state model. These two programs generate eye diagrams of the received signals. The eye diagrams can be graphically displayed with the use of the program ***Graph***. The program Graph is however only capable of displaying up to the first eight bits of the signal.

2.3 Modified Simulator - *Version 1.0*

The programs contained in the cable simulation package *version 0.0* (described in *Section 2.2*), was revised, and in several cases, rewritten. The program ***CabSim***, ***Response*** and ***Graph*** were revised in order to improve the man-machine interface, and also debugged further. The programs ***Waves***, ***EyeDgm***, ***EyePat*** and ***Arrange*** had to be rewritten due to the fact that they did not produce sensible results, or any results at all. They were also difficult to use due to a poor effort on the man-machine interface as well as inadequately debugging. The decision to rewrite these programs instead of merely correcting them came about because these programs were developed using global variables only in an attempt to conserve stack space on the computer. This approach to programming makes it extremely difficult to analyse only certain sections of the complete program. The modified version of the cable simulation package contains extensive parameter passing declarations in its procedures, but has included variable declarations to the parameters passed in order to still conserve the stack space.

The revised version of the cable simulation package is illustrated in *Figure 2.8*. The program ***CabSim*** has been renamed to ***CableSim***. The 'Cable Library' contained in this program has been updated from three different type of cables in *version 0.0* to six different type of cables in *version 1.0*. The results produced by ***CableSim*** are structured and contain adequate titles for the various tables of data, enabling the result file to be dumped directly to a printer.

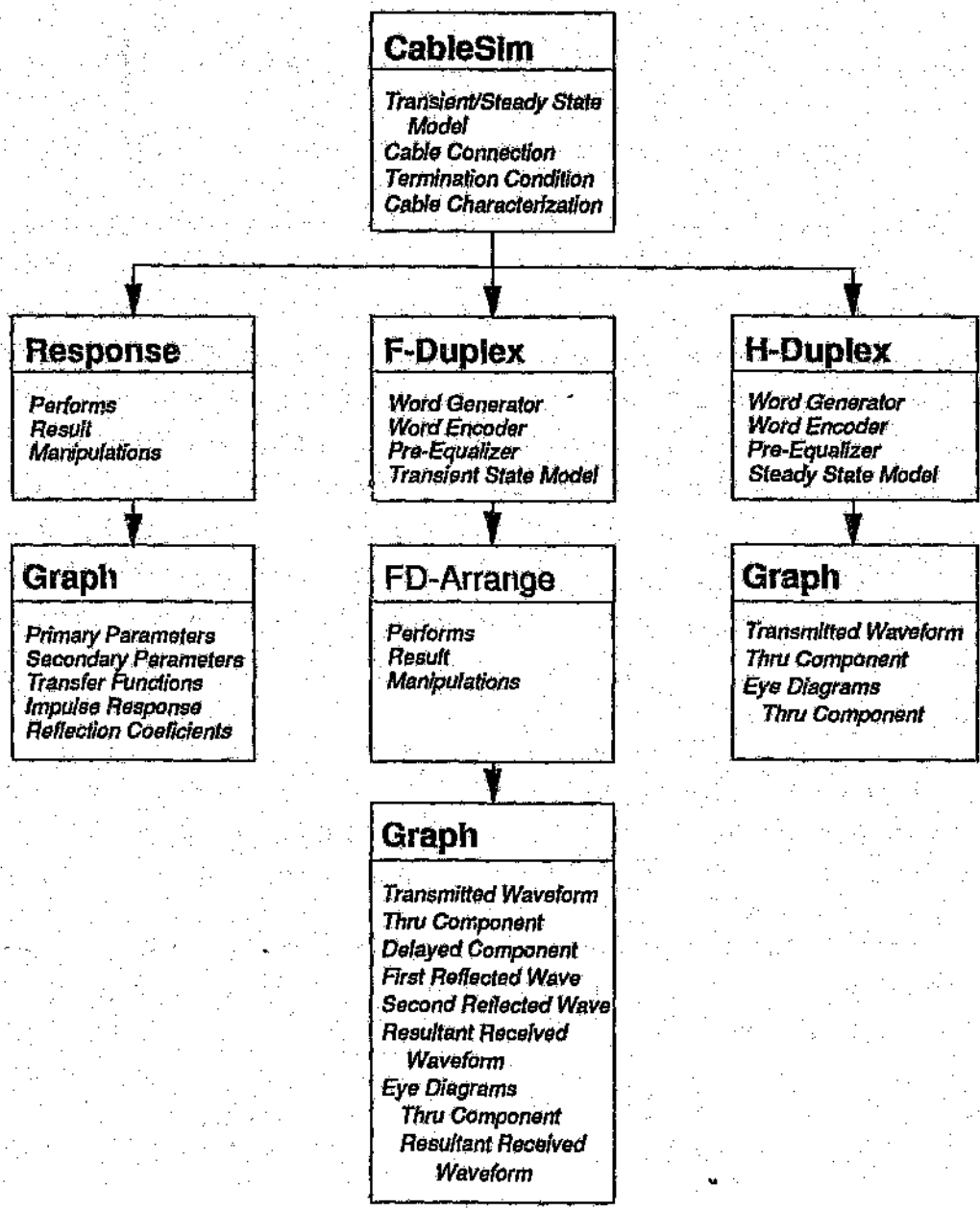

Figure 2.8 . Modified simulator program block diagram - *Version 1.0*

The programs ***Response*** and ***Graph*** have remained with the same name. They do however include refinements to the man-machine interface. The program ***Graph*** is now no longer restricted to displaying only the first eight bits of a received or transmitted waveform in the eye diagram, but of displaying all the bit periods in the eye diagram irrespective of the number of bits used to create the transmitted signal.

The program ***F-Duplex*** (i.e., Full-duplex simulation), now replaces the program ***Waves***. The program ***F-Duplex*** also includes eye diagram facilities (thus causing the program ***EyeDgm*** to be redundant), as well as several new features and functions. The line code selection has been upgraded to include AMI (Alternate Mark Inversion) code. Other popular line codes such as 4B3T and 2B1Q can be easily included in the program. Information about the cable connection (as was specified by the user in the program ***CableSim***), the line code, the pulse shaping window, as well as the bit rate of the data sequence being simulated, is also displayed. The bit rate is not specified directly by the user, but is a function of the fold frequency and the number of points to be used in the fast fourier transform (specified in the program ***CableSim***), as well as the number of bits in the data sequence (specified within the program ***F-Duplex***).

The program ***H-Duplex*** (i.e., Half-Duplex Simulation), replaces the program ***Eye-Pat***. It has also been upgraded in order to provide the new features and functions incorporated in the program ***F-Duplex***.

The program ***FD-Arran*** (i.e., Full-Duplex Arrange), now replaces the program ***Arrange***. This program has been modified in order to produce the various eye diagram results produced by the program ***F-Duplex***.

The revised cable simulation package, as is illustrated in *Figure 2.8*, has been used to obtain all the simulation results that has been quoted in this dissertation.

2.4 Conclusions

This chapter has described a computer simulation package that can be used for modelling pulse transmission over multigauge subscriber loops. The model used for each section incorporates skin, proximity, and eddy current effects. The model

is configured to allow forward and backward travelling waves to be clearly identified. The simulator thus allows important quantities such as near end echo and overall transmission distortion to be predicted.

Chapter 3

EXPERIMENTAL SETUP

A comprehensive test facility has been designed that can be used to characterize a wide range of cable types, and analyse the performance of pulse propagation for any specified cable connection. Although this facility can be used to provide data needed for the development of digital transmission equipment that will operate effectively within the constraints of the installed cables; its main objective is to provide data needed for the validation of the Cable Simulation Package.

It is necessary to prove the performance of the Cable Simulation Package against field data, with the experimental system operating over real cables in the existing subscriber cable environment. While this is an essential part of the overall evaluation, it would be costly to carry out all the required evaluations in the field, so a realistic test facility is required in the laboratory where there is the additional advantage of a full range of test instruments; and cable types.

The large number of measurements required are processed as efficiently and effectively as possible by the use of computer controlled test equipment and direct collection of the data for processing. This has been achieved with the use of the IEEE GPIB-488 bus interface standard. The IEEE GPIB-488 bus controller being hosted on the PC. Several software programs have therefore been developed in order to :

(a) facilitate the remote operation of the test instruments,
(b) automatically transfer the measured data, and
(c) to analyse and display the measured data on the PC.

The experimental facility has been divided into two separate parts. The first is used to characterize the various types of cables, and the second used to obtain time domain waveforms.

3.1 Cable Test Bed

For a mixed gauge situation, it is not feasible to build a lumped component cable simulator with sufficient accuracy [3], so it is necessary to use real cables in laboratory

tests. Ideally the laboratory should have direct access to a wide range of cable types and lengths of ducted cables. Some practical compromise such as having the lengths of cable on a drum, have to be made. Deviations in transmission performances compared to ducted cables are not expected to be significant, although differences in crosstalk behaviour may impose some restrictions on the test bed use.

The diagram given in *Figure 3.1*, illustrates the physical construction of a typical subscriber cable found underground.

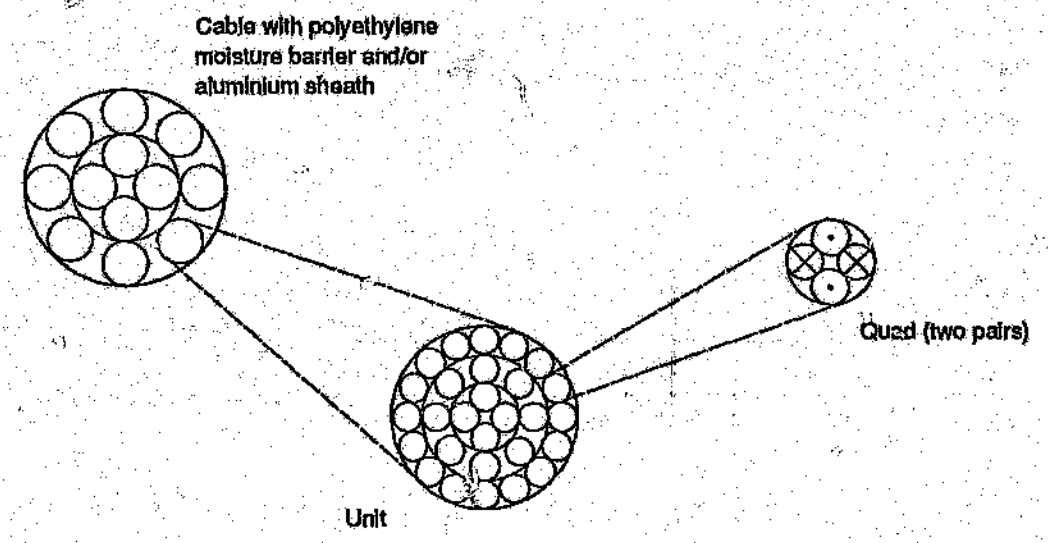

Figure 3.1 Typical construction layout of a subscriber cable

The subscriber cable consists of several units (layered concentrically around the centre), which are encapsulated by a aluminium sheath and a polyethylene moisture barrier. Each unit in turn consists of several quads which are also layered concentrically. Each quad, in general, contains four conductors (i.e., two pairs), which are twisted together. All the quads and units remain within their designated layer throughout the entire cable length. They do however rotate and move around their designated layers in order to increase the cable flexibility enabling the cable to be wound on large drums. The two pairs within a quad are twisted together not only for flexibility considerations, but mainly to minimize crosstalk.

The cable types that have been installed in the laboratory, in a relatively stable temperature environment (i.e., 24 degrees centigrade), is summarised in *Table 3.1*. These cables are terminated on a distribution frame and incorporate some form of screening to minimize interaction. For each type, two lengths are available, enabling a fair selection of length, gauge and insulation types to be patched at the distribution frame. Manual patching thus provides for a much wider selection of conditions in the laboratory than it would be economic to explore in the field.

The characterization measurements to be performed on each type of cable in the cable test bed has been repeated on two pairs. The first pair selected is situated in the outer layer next to the cable sheath and is referred to as *Sample 1*. The second pair is selected in the innermost layer and is referred to as *Sample 2*.

Table 3.1 Cable Test Bed

Gauge	Insulation	Filling	Pairs	Screen	Sheath	Type	Lengths
19 (0.91mm)	PE	Air	80	Z-Screen	PE	PCM	223m 1001m
22 (0.63mm)	PE	Air	80	Z-Screen	PE	PCM	219m 1006m
24 (0.51mm)	PE	Air	75	Layer Seperated	PE	Distribution Cable	217m 1004m
26 (0.41mm)	PE	Air	75	Layer Seperated	PE	Distribution Cable	193m 929m

Key : PE - Polyethylene

This test bed will be extensively used for the evaluation of the Cable Simulation Package. Tables of data regarding its electrical properties were not available and had to be determined. This involves determining the attenuation, phase and impedance as functions of frequency.

The Cable Simulation Package uses transmission line theory in order to develop a model of the subscriber loop.

3.2 Cable Characterization

The primary parameters cannot be determined by direct measurement on the cable, and must be determined either from the physical cable geometry and material constants, or from the secondary parameters. The former method involves theoretical approximations [13], and is therefore unsuitable. The latter requires the availability of the secondary parameter data, which can be determined indirectly from input impedance measurements on the cables. This method entails measuring the input impedance of a sample length of cable under two termination conditions, namely; under open-circuit (Z_{oc}) and short-circuit (Z_{sc}) conditions. A short-circuit and open-circuit being two readily available terminal load impedances.

Provided that Z_{sc} and Z_{oc} are measured at the same frequency, for the same line section of length l, then Z_o, α and β are determined by equations (3.1), (3.2) and (3.3). These equations are derived from the basic transmission line equations, the derivation of which is presented in *Appendix B.1.*

$$Z_o = \sqrt{Z_{sc} Z_{oc}} \tag{3.1}$$

$$\alpha = \frac{1}{2l} \ln \left| \frac{1+\sqrt{\frac{Z_{sc}}{Z_{oc}}}}{1-\sqrt{\frac{Z_{sc}}{Z_{oc}}}} \right| \tag{3.2}$$

and

$$\beta = \frac{1}{2l} \left\{ \angle \frac{1+\sqrt{\frac{Z_{sc}}{Z_{oc}}}}{1-\sqrt{\frac{Z_{sc}}{Z_{oc}}}} + 2n\pi \right\} \tag{3.3}$$

where $n = 0, 1, 2, ...$

l = length of the cable in meters

This method does not however determine a unique value of β, but a series of values differing consecutively by (π/l) radians per meter.

As an approximation, the relation $\beta = 2\pi/\lambda_e$ (where λ_e is the electrical wavelength on the line), can be used. Since the lines under consideration contain a plastic dielectric, it is expected that λ_e may be as much as thirty percent shorter than the free space value. There does however exist a better way of determining the value of β, by making use of the two different lengths available in the cable test bed for each type of cable. By performing the same impedance measurement on a shorter length of line, lower values of n will occur in the equation for β, and there will be less doubt as to which is the correct value. This is clearly illustrated in *Figure 3.2*, where β was determined from impedance measurements performed on two different lengths of the same type of cable, spanning the same frequency range. In each of these graphs, the factor $(n\pi/l)$, (see equation (3.3)), has been excluded in calculating β.

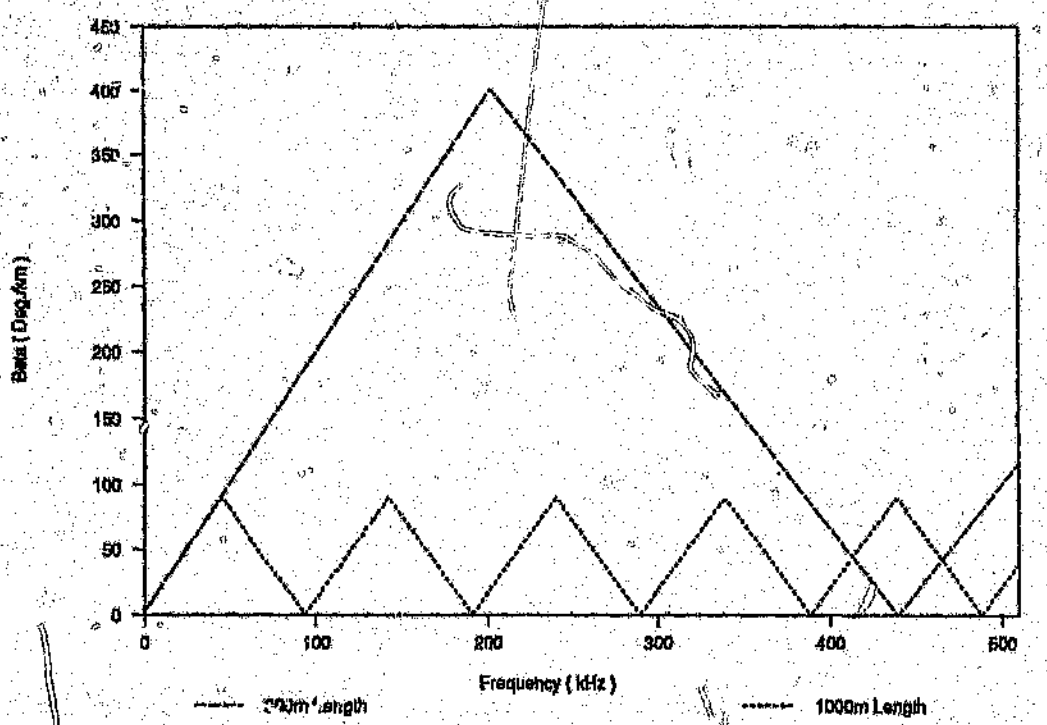

Figure 3.2 Measured phase constant for two different lengths of the same cable type excluding the factor $(n\pi/l)$

Two precautions must be observed in performing the input impedance measurements. Firstly, the impedance-measuring instrument used must be capable of measuring "balanced" impedances since the parallel-wire line conductors are symmetrical. Secondly, the length of line l, cannot be completely arbitrary but must be chosen so that both Z_{sc} and Z_{oc} have values appropriate to the impedance-measuring instrument. It is obvious, that for an extremely short section of any line, Z_{sc} might be too small and Z_{oc} too large to be accurately measurable.

Equations (3.4), (3.5), (3.6) and (3.7) are general design equations for determining the distributed circuit coefficient that a transmission line would have to possess to give a set of desired operating characteristics specified by the values of α, β and Z_o at frequency ω. The derivation of these equations is presented in *Appendix B.2*.

$$R = \alpha R_o - \beta X_o \qquad 3.4$$

$$L = \frac{\beta R_o + \alpha X_o}{\omega} \qquad 3.5$$

$$G = \frac{\alpha R_o + \beta X_o}{R_o^2 + X_o^2} \qquad 3.6$$

and

$$C = \frac{-\alpha X_o + \beta R_o}{\omega (R_o^2 + X_o^2)} \qquad 3.7$$

where

$$Z_o = R_o + jX_o \qquad 3.8$$

Care must be taken when these formulas are implemented in order not to introduce computation errors caused by the difference in order of magnitude of some of the variables.

3.2.1 Experimental Facility : Cable Characterization Analysis

It is clear that the foregoing procedure rely on a variety of measurements and computations which would be both tedious and time consuming without the aid of

computers and computer controlled test equipment. Extensive use has therefore been made of the IEEE GPIB-488 digital interface in order to provide an efficient and effective method of analysis. The activity of all the devices connected to the IEEE GPIB-488 bus interface is controlled by the GPIB controller which is hosted on an IBM compatible personal computer (PC). The PC is also used to collect measurement data from the various test equipment for analysis and storage purposes. Results obtained may be displayed on the screen, stored to a file, or written to an output device such as a plotter or printer.

The HP4195A Network/Spectrum analyser, together with the HP35676A Reflection/Transmission Test Kit has been used to perform the impedance measurements required on the test bed cables. The results of the two measurements required, Z_{oc} and Z_{sc}, to be performed on each cable are stored to disk on the Network/Spectrum analyser before being transferred to the PC for additional analysis.

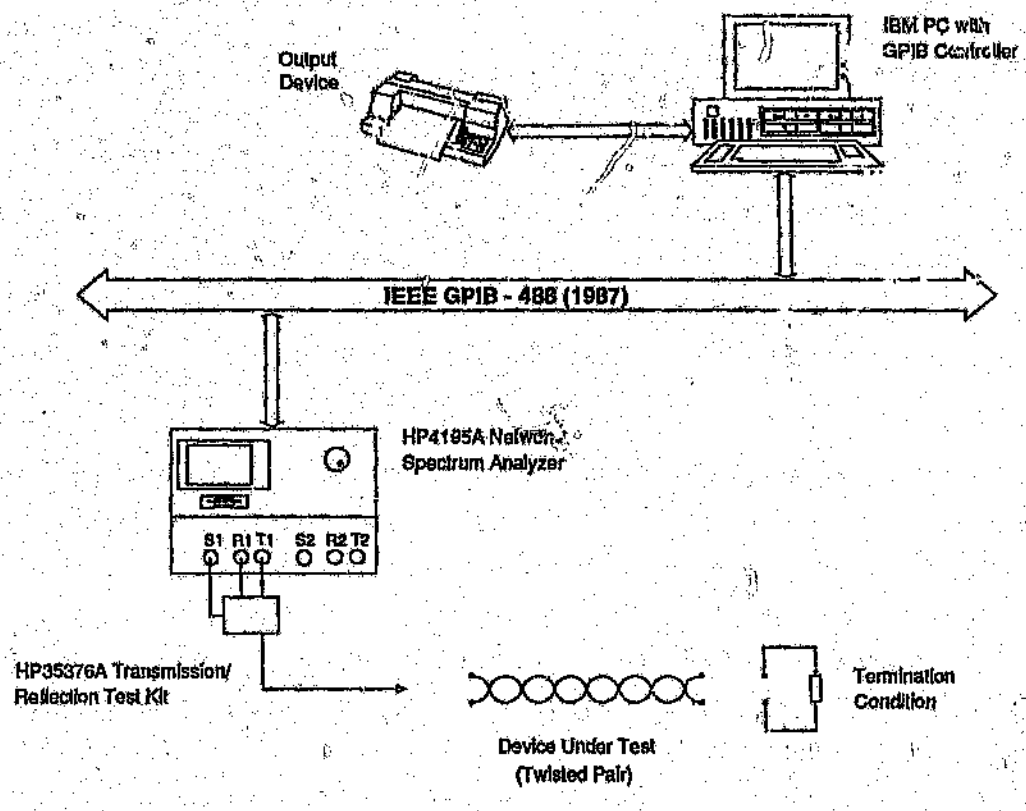

Figure 3.3 Diagram of the cable characterization experimental setup

An outline configuration for the measurement facility required to determine the input impedance of the various cables under different termination conditions is shown in *Figure 3.3*.

The following sections provide a description of each instrument used, stating its capability and limitations applicable to the experiments.

Network/Spectrum Analyser - HP4195A [14, 15]

The HP4195A is an intelligent Network/Spectrum analyzer which consists of a Control Unit and a Measurement Unit. The control unit contains a colour graphics CRT for displaying the measured results, and a 3.5 inch micro flexible drive for storing/recalling data and internally stored user programs. The measurement unit has two channels, each of which has its own source output, reference, and test receiver input on the front panel. The instrument bandwidth is 10Hz to 500MHz.

The HP4195A has measurement calibration capabilities, which is an accuracy enhancement procedure that transfers the measured accuracy and uncertainty of standard devices to the measurement accuracy and uncertainty of a test device. Since the characteristics of standards are known to a high degree of accuracy, the system (HP4195A plus external devices needed to measure a test device), can measure one or more standards, then use the results of these measurements to greatly enhance the measurement accuracy. Four sets of calibration standard values are stored in the HP4195A. Each set consists of open termination's conductance and parallel capacitance, short termination's resistance and series inductance, and load termination's resistance and series inductance.

The HP4195A can be used to perform impedance measurements. A reflection coefficient measurement method is used when making impedance measurements. To measure reflection parameters, a directional coupler (i.e., bridge), shown in *Figure 3.4*, is required to pick up the reflected signal. A power splitter is also required to feed the signal to both the reference channel and the directional coupler. The setup for this measurement is accomplished by connecting the HP35676A Reflection/Transmission Test Kit as illustrated in *Figure 3.3*. The receiver detects two signals (i.e., Reference and Test) and the amplitude ratio and the phase difference of the two signals are converted into the required impedance measurement format.

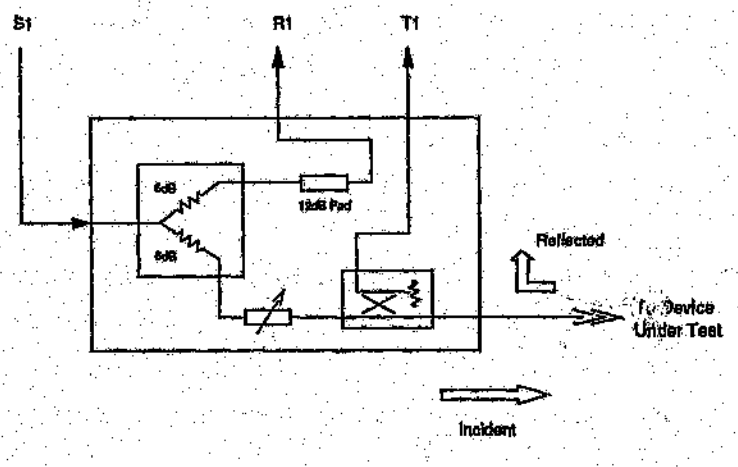

Source : Ref [16]

Figure 3.4 HP35676A reflection/transmission test kit block diagram

Reflection/Transmission Test Kit - HP35676A [16]

The HP35676A Reflection/Transmission Test Kit contains components to assist the HP4195A Network/Spectrum analyzer in performing calibrated complex reflection and transmission measurements over a frequency range 5Hz to 200MHz.

It is calibrated for reflection measurements by using the internal one port full calibration function of the HP4195A. The calibration function requires that a short, open and reference load (50Ω) be attached in place of a test device during calibration. A complete description of the HP4195A calibration procedure is given in the HP4195A Network Analyzer Operating Manual [14].

The HP4195A is also able to calibrate and compensate for external cables and test adapters connected between the signal divider and the device under test. When calibrating with external cables and test adapters, simply apply the short, open and reference load at the physical point where the test device will be connected.

The HP4195A together with the Reflection/Transmission Test Kit is not capable of measuring "balance" impedances. There are three solutions to this problem, namely :

(a) to purchase a "balanced" Reflection/Transmission Test Kit,
(b) to design a unbalance-to-balance transformer (BALUN), and
(c) to un-earth the HP4195A Network/Spectrum Analyser.

The commercially available "balanced" Reflection/Transmission Test Kit for the HP4195A that operates within the region of interest was not available. To design a BALUN that could be used to match a unbalanced load to a balanced load was feasible [17], as the characteristics of the BALUN would be compensated for by the external adapter calibration and compensation facility provided by the HP4195A. The last option of disconnecting the earth strap from the mains is by far the easiest method to implement. The results obtained are accurate provided that certain conditions are adhered to.

The illustration of *Figure 3.5* depicts a simple diagram of how a balanced network can be measured using a unbalanced measuring device.

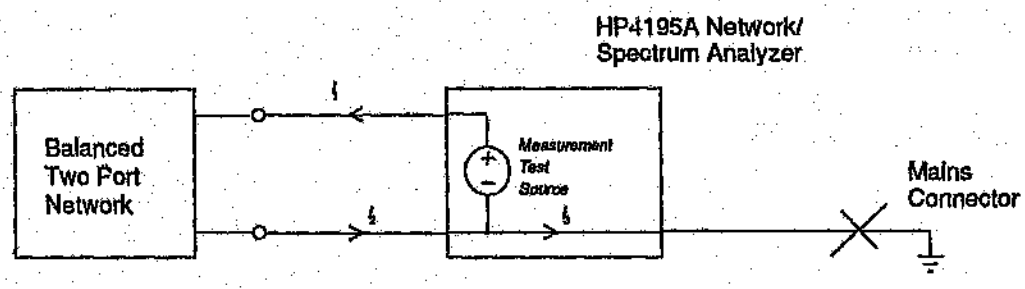

Figure 3.5 Measuring a balanced network with a unbalance measuring device

In an unbalanced impedance measuring device, one of the two measurement probes is connected to the instrument chassis which in turn is connected to earth via the mains cable as is illustrated in *Figure 3.5*. In order for such an instrument to be capable of measuring balanced networks, it is not sufficient to merely disconnect the earth wire from the mains. This technique of disconnecting the earth cable from the mains will only provide accurate results if the physical dimensions of the instrument (including the length of the power cord), is a negligible fraction of the shortest wavelength used in the measurement being performed. Under these

conditions, the currents i_1 and i_2 are identical since i_3 will be negligible, and a balanced measurement criterion is achieved. The highest frequency of interest is 1MHz which corresponds to a wavelength of 300m and thus the results obtained are of sufficient accuracy.

Analysis Capabilities On The PC

Several programs have been written on the PC in Turbo Pascal in order to accomplish all the computations (specified in *section 3.2*), required to determine the primary and secondary parameters. Each program performs only one task. This allows the user to actively monitor the results obtained after each task is completed. The sequence in which each program must be executed is illustrated in *Figure 3.6*.

Each program upon completion writes the results to a ASCII file in a structured format. The file can therefore be copied to a printer or screen for analysis, or it can be accessed by a graphing package in order to generate graphical results of each parameter(s). Also illustrated in each program block of *Figure 3.6*, is the result output filename format. As an example, a particular cable is considered. The cable section is of the gauge type 22 with a length of 200m.

Each program can be executed either interactively, or in a batch mode environment by setting up a batch file. This feature is advantageous due to the intensity of the computations performed (which increases execution time), and also due to the low requirement of user interaction. Whichever mode of execution is used, the result files generated after each task are not destroyed and can be viewed after all the tasks are completed. Each program in *Figure 3.6* is briefly discussed in the following paragraphs.

For the example considered, the open and short circuit measurements were performed on a pair situated next to the cable sheath (i.e., *Sample 1*), and each measurement result is stored on the HP4195A Network/Spectrum analyzer. The program *HP4195A* seizes control of the IEEE GPIB 488 interface. It addresses the HP4195A Network/Spectrum analyzer and transfers the open-circuit and short-circuit measurements stored on the disk to the hard-disk storage medium on the PC. This program requires as input, the cable gauge, cable length and measurement sample number. The cable of interest is thus specified and the required files containing the

short and open circuit impedance measurement results are transferred. If the required files are not available, an error is reported, and the user is informed to perform the required impedance measurements first.

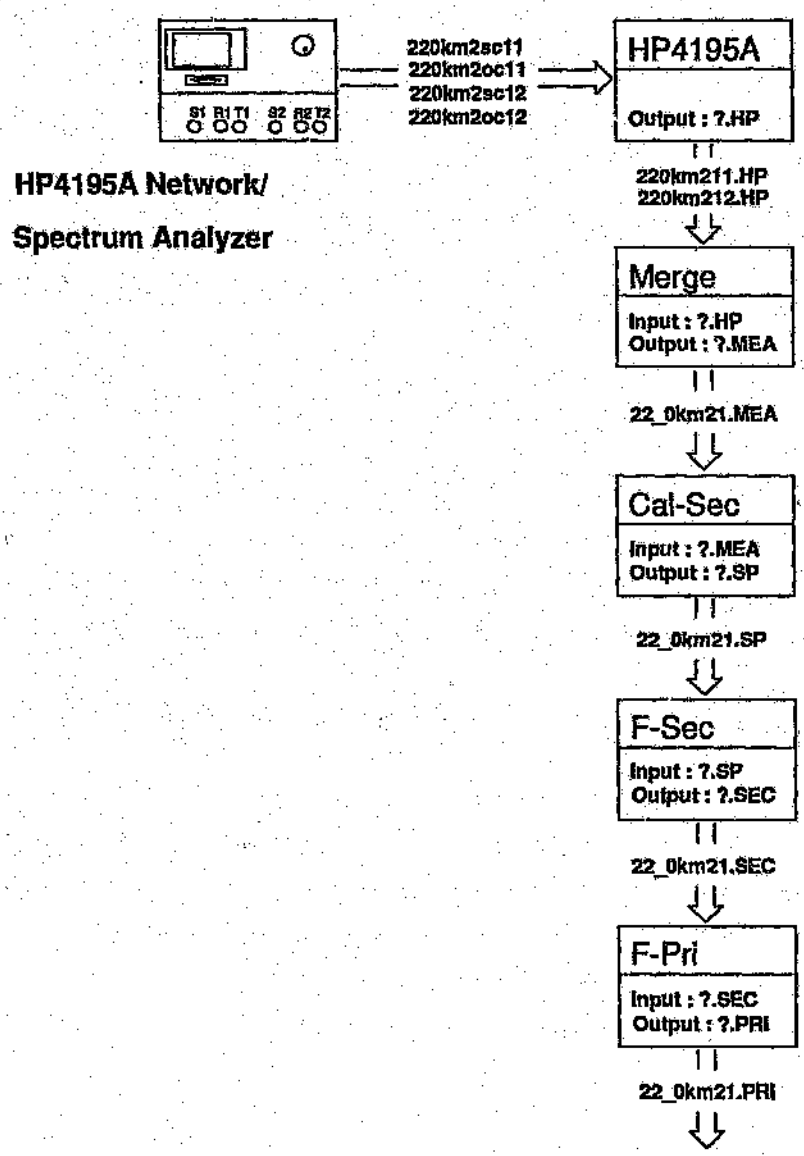

Figure 3.6 Cable characterization analysis sequence on the PC

Due to the limitation by the Disk Operating System (DOS) on the length of the filename, the filename extension (i.e., last three characters) are extensively used in order to indicate the type of results contained in the file. In this case, as the files contain data as was measured by the HP4195A Network/Spectrum analyzer, all the files transferred will have the extension '***HP***'.

The program ***Merge*** is used to join the respective measurement results (only if the measurements were performed in separate ranges), into one file. The cable measured data is now completely specified by the cable gauge, cable length and sample number.

The extension in this case is '***MEA***' as the data contained in the file is the complete measured data of that particular cable. Every file with the extension '***MEA***' therefore contains all the input impedance measurements data pertaining to a cable which is specified by the filename.

The program ***Cal-Sec*** calculates the secondary parameters in accordance with equations (3.1), (3.2) and (3.3) given in *section 3.2*. This program requires as input a filename with an extension '***MEA***'. The filename completely specifies the cable of interest. The results for the characteristic impedance and the propagation factor as a function of frequency is stored to a file of the same name but with the extension '***SP***'. This file does not contain unique values for β, but the basic value and n times the multiple which should be added, (see equation (3.3)).

The program ***F-Sec*** is now used to determine the unique values for β in accordance with the theory presented in *section 3.2*. This program requires as input a file with the extension '***SP***', and operates only on the column for β. The results are written to a file of the same name, but with the extension '***SEC***'. The file with an extension '***SEC***' therefore contains a table of the secondary parameters (i.e., $\Re eal(Z_o)$, $\Im mag(Z_o)$, α and β), as a function of frequency. The filename again completely specifies the cable measured.

The program ***F-Pri*** is now used to calculate the primary parameters in accordance with the equations (3.4), (3.5), (3.6) and (3.7) given in *section 3.2*. The program requires as input, a file with the extension '***SEC***', and stores the results to a file with the same name but with the extension '***PRI***'. The file with the extension '***PRI***' therefore contains a table of the secondary parameters (i.e., R, L, G and C), as a function of frequency.

In all the above computations, care has been taken in order not to introduce errors due to computation errors being caused by inadequate real number precision.

Selected results obtained with this measurement facility is discussed in *Chapter 4*, with the complete set of results for all the cables contained in the cable test bed, given in *Appendices D to F*.

3.3 Propagation Analysis of Digital Signals

An experimental facility that is capable of transmitting line-coded signals, and recording the received and transmitted signals on subscriber loops, is required in order to obtain results that will enable the verification of the propagation model of digital signals contained in the Cable Simulation Package.

The line-coded signals in subscriber loops are characterized by a spectra which has a zero d.c level content, a spectral peak in the range of 30 to 50kHz and which can usually be considered to be band limited to approximately 150kHz by equalization filters used at the termination ends. Line drivers and receivers are required for measurement purposes to have a flat frequency response up to at least 500kHz, preferably wider for the line drivers. The waveforms are required to be captured for analysis purposes. Analog to digital converters with sampling rates in excess of 10MHz are required since the waveforms must be oversampled in order to retain the signal shape.

3.3.1 Experimental Facility : Pulse Propagation Analysis

The block diagram of the experimental system used to analyse the propagation characteristics of digital signals on various cable connections is illustrated in *Figure 3.7*.

The line-coded signal are obtained from the pulse generator and word generator combination, and fed through to the line driver. Each end of the cable is terminated at a specified impedance. Receivers are used at each end of the connection to detect the waveforms present. These detected waveforms are captured by the two-channel programmable digitizer, and transferred to the PC via the IEEE GPIB 488 digital interface, for display, analysis, and storage purposes.

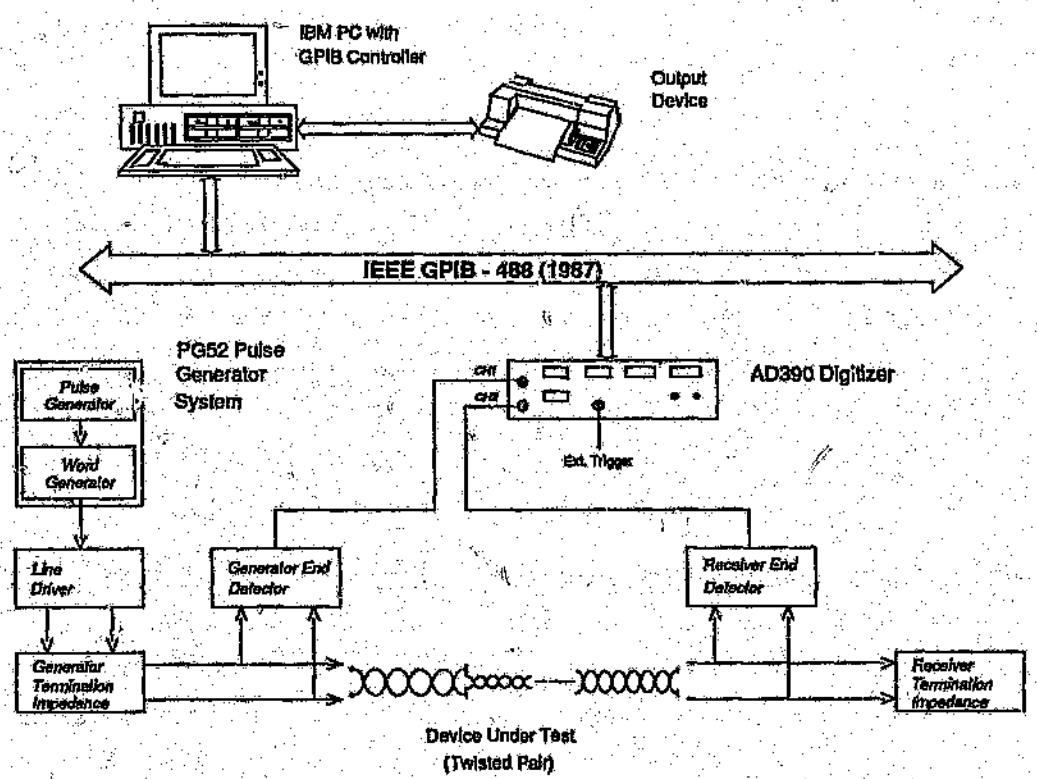

Figure 3.7 Diagram of the pulse propagation experimental setup

The IEEE GPIB 488 digital interface was again exploited to provide an efficient and effective method of analysis and measurement automation. An extensive program was written in order to :

(a) remotely control the operation of the digitizer,
(b) transfer the data captured to the PC,
(c) provide analysis capabilities on the data captured,
(d) store and retrieve measured data, and
(e) provide graph plotting routines.

The graphical capabilities include the setting up of time diagrams and eye diagrams, as well as graph storage, graph retrieval and graph hardcopy facilities.
This program was designed to be user friendly and makes extensive use of menus, command status reports, and help information.

The following sections provide a description of each instrument used, stating it's capability and limitations applicable to the experiment.

PG52 Modular Pulse Generator System [18]

The PG52 Pulse Generator is completely modular in construction, a system being assembled from a wide range of signal generating and processing units available, to produce the desired output waveform. Repetition frequencies up to 30MHz and pulse widths down to 10nsec can be obtained from the system. Different output modules are designed to operate into a 50Ω load. The flexibility of the system is obtained by driving this range of output modules from the clock, width or delay, gate or word generator waveform processing modules, to construct an unlimited range of pulse or ramp waveforms.

The plug in units are all self-contained and require only d.c power supplies, which are obtained from the main frame. Signal paths are made externally, through BNC/BNC connectors, to ensure maximum flexibility in interconnection. The interconnection required between modules, which are briefly discussed in the following paragraphs, are detailed in the operators manual.

(a) PG52 1A Clock Generator Module

This module provides the basic clock rates for the system. It covers the frequency range 0.1Hz to 30MHz in free-running, externally triggered or gated mode. The trigger mode may also be triggered manually for single shot applications, or used as an aperiodic +10 or +100 count-down. A sweep facility alternatively allows the internal frequency to be controlled over any selected 10:1 range by an external input.

(b) PG52 A Standard Output Module

This module provides outputs into 50Ω with rise and fall times of typically 5nsec. The positive and negative levels of the output pulse may be varied independently over the range 0 to +10 volts and 0 to -10 volts respectively. Attenuated ranges allow those levels to be reduced successively from 10 volt to 100 mvolt.

A pulse invert facility allows both the generation of negative pulses and output duty cycles approaching 100%. The two input sockets allow the generation of output pulses from two independent sources.

(c) PG52 P8 Word Generator Module

This module generates pulse patterns of up to 16 bits in length and can operate in a continuous or externally triggered cycle mode. The output can be switched to be in a non-return-to-zero form or, a return to zero form. A synchronizing output signal is provided at the end of the word to allow modules to be cascaded in order to extend the word length beyond 16 bits.

The word generator can be driven directly from a clock and into a output module to provide a non-return to zero waveform cycling through any required pulse pattern up to 16 bits in length. The last bit output of the word generator is used as a trigger pulse for all other devices.

Differential Line Driver

In order to obtain a good noise rejection performance, a differential line driver circuit was designed to transmit the digital signal over the twisted-pair connection. The design of the line driver circuit is presented in *Appendix C*. The graphs of *Figure X.8* and *Figure X.9* respectively illustrates the magnitude and phase response characteristic of the non-inverting and inverting line driver.

The line drivers are of unity gain, and are therefore current boosters. The non-inverting line driver has a bandwidth of 1.6MHz, measured at its -3dB point. The frequency response is flat up to 300kHz thereafter rising gradually and peaking at 1.0 MHz with a gain of 0.6dB's. The inverting line driver has slightly different characteristics due to the additional inverting amplifier required. The inverting line driver has a bandwidth of 1.7MHz, with a flat frequency response up to 325kHz rising gradually and peaking at 1.04MHz with a gain of 0.9dB's. The phase response is linear in the range of interest, and as expected the phase response between the non-inverting and inverting line driver is 180 degrees.

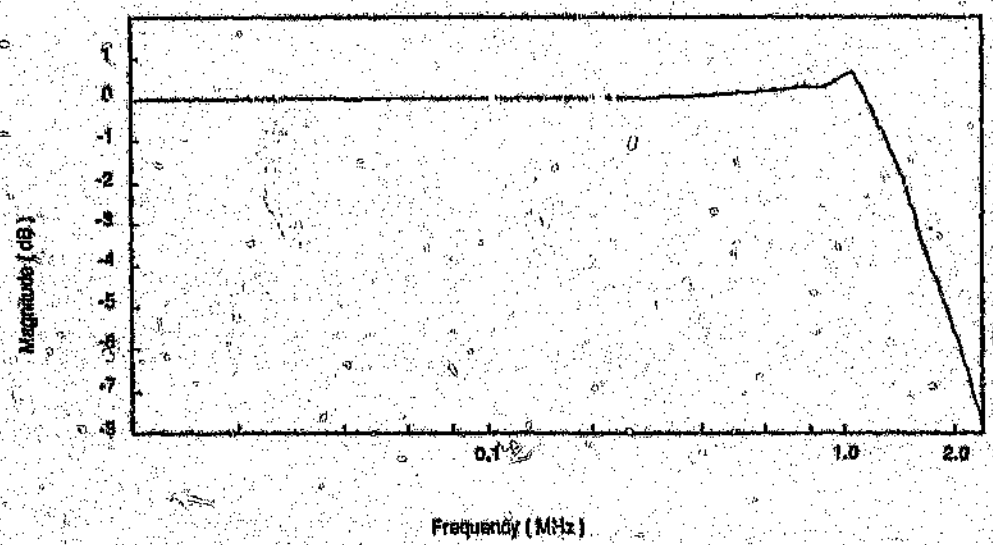

(a)

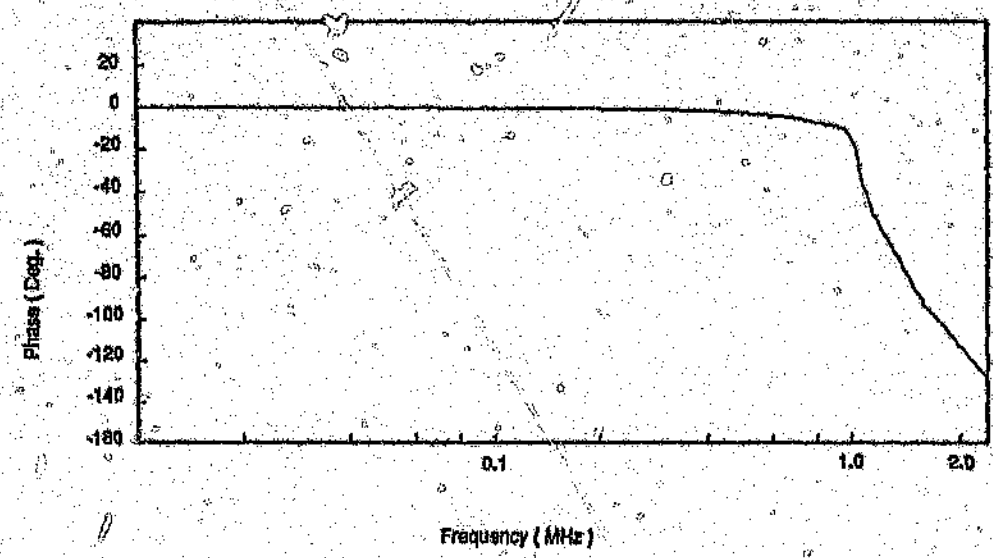

(b)

Figure 3.8 Non-inverting line driver frequency response
(a) Magnitude response
(b) Phase response

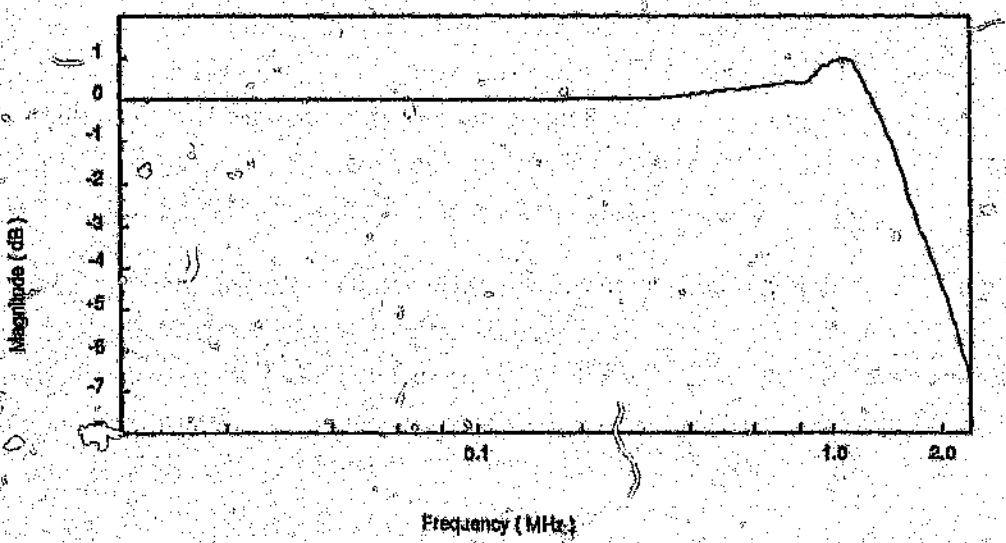

(a)

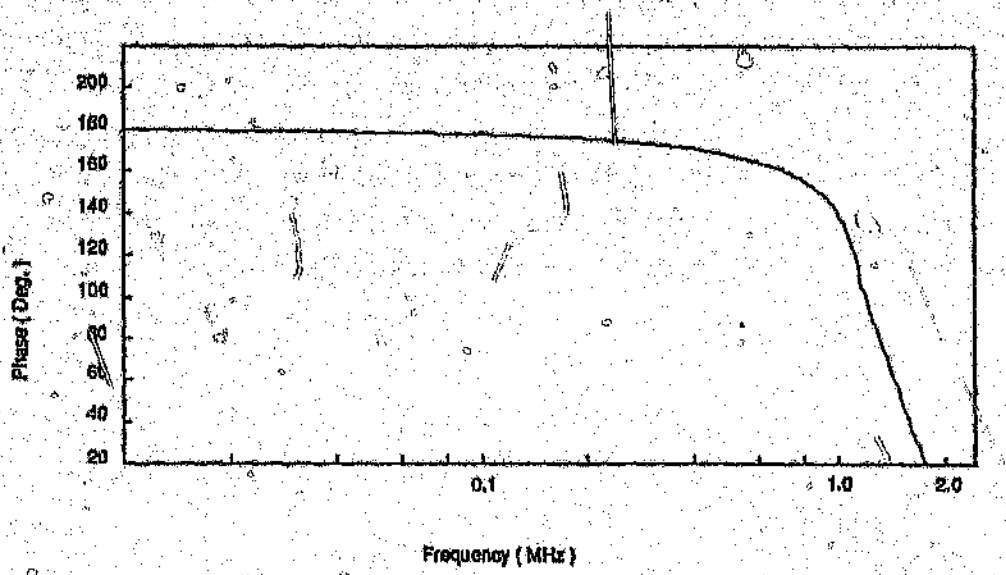

Note : *Y-axis zero suppressed*

(b)

Figure 3.9 Inverting line driver frequency response
(a) Magnitude response
(b) Phase response

Differential Line Receivers

A high gain d.c coupled differential amplifier with single ended output, high input impedance and high common mode rejection ratio is required to detect the signals present on the twisted-pair. It is also important not only to monitor the receiver end of the twisted-pair, but also to monitor the transmitter end as it will detect any signal that is reflected back towards the line drivers.

The design of the differential receiver circuits is presented in *Appendix C*. The graphs of *Figure 3.10* and *Figure 3.11* respectively illustrates the magnitude and phase response characteristic of the transmitter and receiver end detectors. The transmitter end detector has a flat frequency response at a gain of 12.2dB's, and a bandwidth of 245kHz. The receiver end detector has gain of 57dB's and a bandwidth of 135kHz.

Termination

The output impedance of the differential line driver used to transmit the digital signals along the twisted-pair is negligible in comparison to the input impedance of the connection. This arrangement ensures maximum flexibility in defining the termination impedance. The differential line detectors on the other hand have a very high input impedance thus providing the same flexibility. This enables the termination networks used to be independent of the equipment found on either end of a cable connection. The termination network can simply be a resistor, lumped impedance network, or a hybrid.

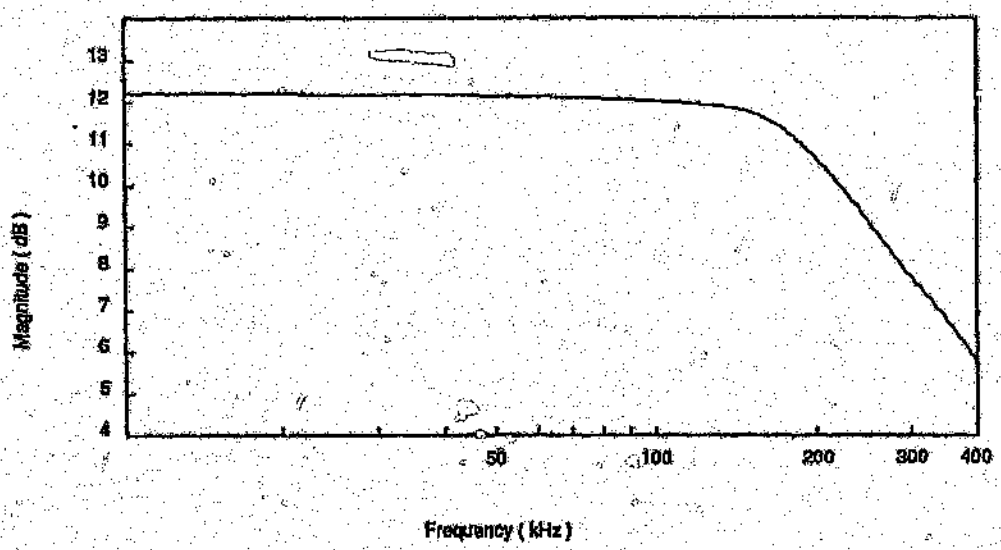

Note : *Y-axis zero suppressed*

(a)

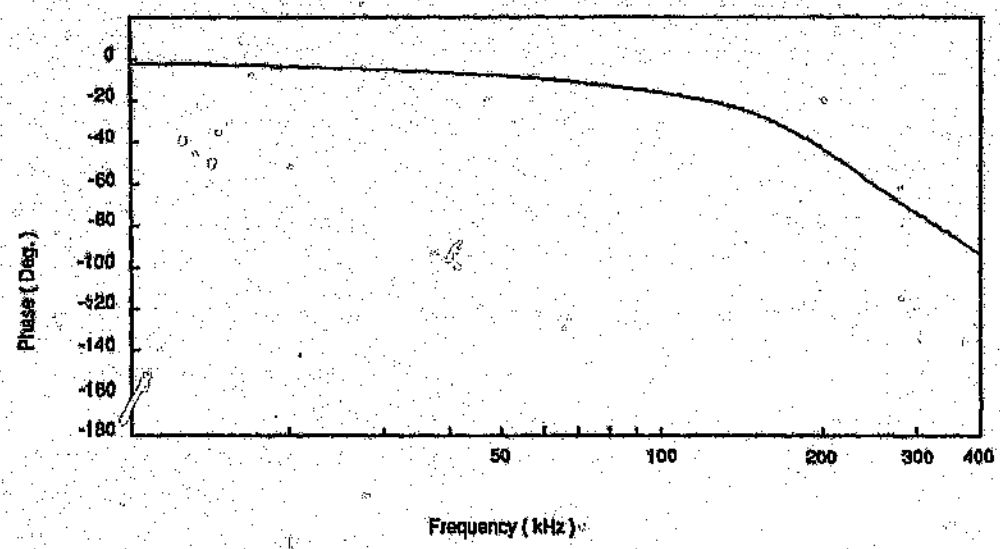

(b)

Figure 3.10 Transmitter end detector frequency response
(a) Magnitude response
(b) Phase response

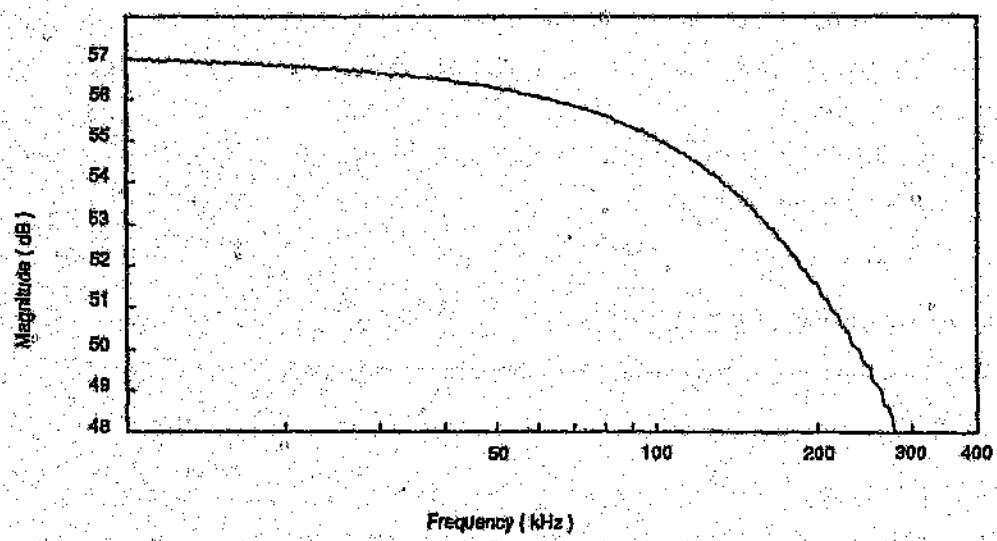

Note : *Y-axis zero suppressed*

(a)

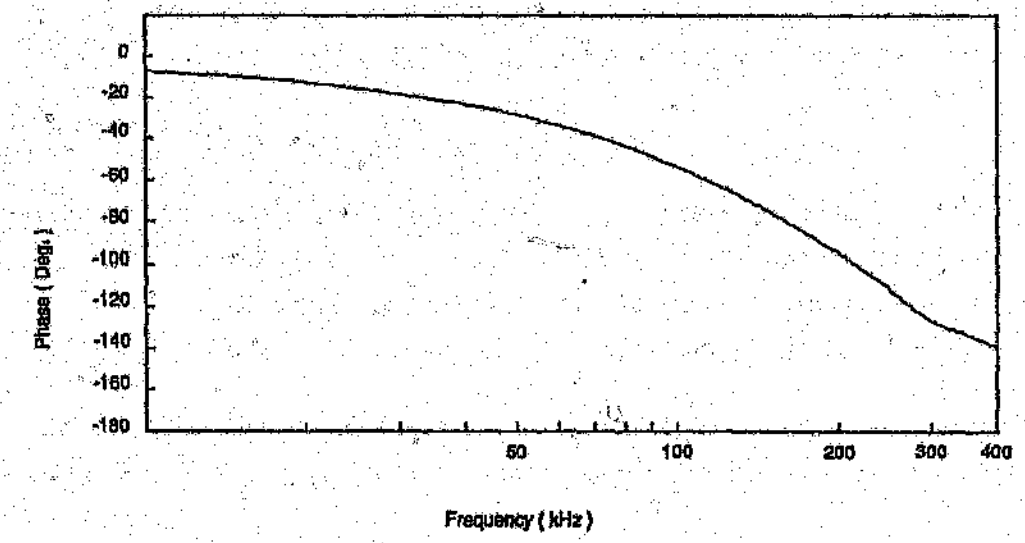

(b)

Figure 3.11. Receiver end detector frequency response
(a) Magnitude response
(b) Phase response

390AD Programmable Digitizer [19]

The 390AD is a high-performance, fully programmable waveform digitizer with two-channel input, 10 bit voltage resolution, maximum sampling rate of 60MHz, and bandwidth of d.c to 15MHz. It can record a high speed, single shot event simultaneously into two channels. The 390AD is equipped with a GPIB connector (IEEE GPIB 488) for waveform processing and automatic measurement using an external controller.

The 390AD includes circuits to automatically calibrate the gain and d.c drift, which ensures high stability, excellent dynamic accuracy, effective bits, transient response, differential gain and differential phase.

The purpose of the IEEE GPIB 488 bus is to provide an effective communications link over which messages can be carried between instruments in a clear and orderly manner. Instruments designed to operate according to the standard can be connected directly to the bus and operated by a controller with appropriate programming. All settings except for the control of power supply, and external monitor controls such as vertical and horizontal position, expansions, and display times, are programmable.

Waveform Analysis Capabilities on the PC

Automation of the digital signal propagation experimental setup has been achieved by remotely controlling the digitizer from a PC via the GPIB-488 interface. A menu driven program has been created in order to facilitate the setting up procedure of the digitizer, the transfer of information captured, and the quick display of the data.

The diagram of *Figure 3.12* illustrates the menu structure of this program. It can be seen that the program provides many other features that have been grouped into the four menus.

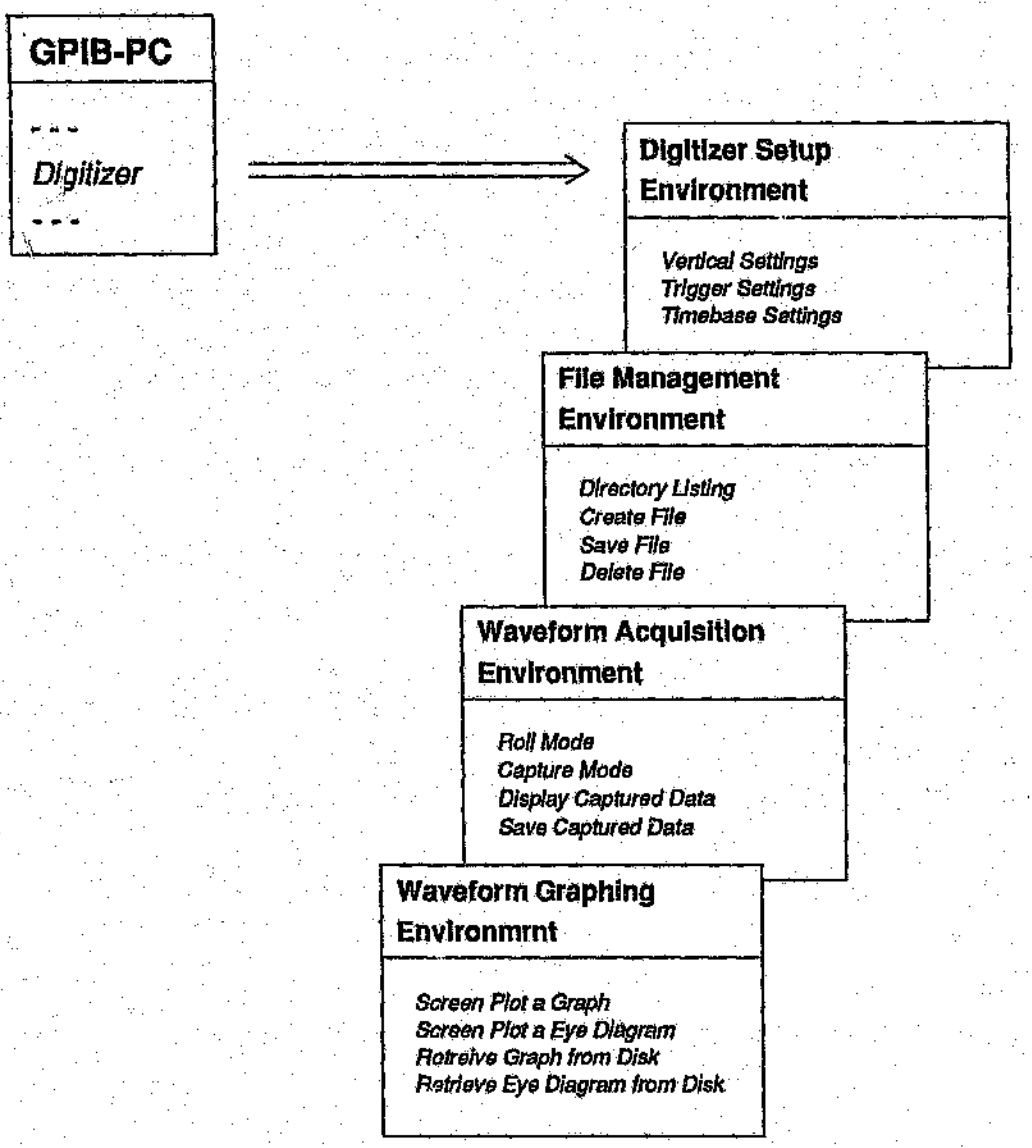

Figure 3.12 Host computer menu structure for the 390AD programmable digitizer

The digitizer setup environment provides complete remote programmability o. the instrument. For easy operation the setup menu has been grouped into three sections in the same manor as the operators guide, namely, the vertical se- ng, trigger setting, and the timebase settings. The file management environment allows the user easy

access to directory listings of data, graph or eye diagrams that have previously been stored. It also allows file creation, file selection, file deletion, and data storage. The waveform acquisition environment provides two modes of data acquisition. The first is the roll mode which continuously displays the data being captured. The second is a single shot mode that enables data to be captured on the occurrence of an event. Only the single shot mode can be used to store the digitized information. This information can however be displayed before a decision is taken to store the data. The waveform graphing environment provides display capabilities that allows both channels waveforms to be displayed simultaneously. It also provides facilities to zoom, pan, label axis, graph titles, graph storage, as well as hardcopy facilities. The screen plotting facilities for eye diagram are the same as that for the waveforms except for the zoom facility.

3.4 Conclusion

This chapter has defined the cable test bed available in the laboratory that is to be used as part of the two experimental facilities described. The first experimental facility is used to characterize the different cables according to the well known transmission line equations. The results obtained from this is used to set up the 'cable library' contained in the Cable Simulation Package as well as to verify the Primary parameters, secondary parameters, transfer functions, and reflection coefficients of the various cables and cable connections. The results of this experimental facility is discussed in *Chapter 4*. The second facility is used to analyse the pulse propagation patterns and characteristics. The measured results obtained are compared against the results predicted by the simulation package by means of pulse pattern and eye diagram plotting functions. These results are presented in *Chapter 5*.

The measurement facility is as far as possible automated by making use of computer controlled equipment for direct setup of the experiments, data transfer, and analysis. Extensive programming was required in order to achieve the level of automation. These programs are menu driven in order to facilitate user operation.

Chapter 4

FREQUENCY DOMAIN VERIFICATION

This chapter is concerned with the verification of the program ***CableSim***. This program characterizes the cable connection, that is specified by the user, by utilizing the data provided in the 'Cable Library' for each type of cable. The characterization consists of calculating the following parameters in the given order :

(a) primary parameters,
(b) secondary parameters,
(c) transfer function,
(d) reflection coefficient, and
(e) impulse response.

The various routines, or program code, used to calculate the above parameters in the program ***CableSim*** is firstly verified. This involves analysing the theoretical models derived by Lowitt [7], and then ensuring that the resulting mathematical equations are correctly implemented in the program code.

The results produced by ***CableSim*** for each cable type is then graphically compared to the measured results obtained. The parameters have been specified as per km quantities (where applicable). Two sets of measured results are displayed for each parameter, (see *section 3.1*). *Sample 1* and *Sample 2* respectively indicate measurements performed on pairs in the outer and centre region of the cable. *Sample 1* will therefore contain measured results from a pair that is not only surrounded by other pairs, but which is also in close proximity to the aluminium sheath that surrounds the complete cable. *Sample 2* will contain measured results from a pair that is completely surrounded by other pairs only.

The input impedance measurement results are discussed first as it is from these measurements that the primary and secondary parameters are obtained according to the theory presented in *section 3.2*.

4.1 Cable Simulation Package - 'Cable Library'

The 'Cable Library' contained in the program ***CableSim*** has been updated from three cable types to six cable types. The different types of cables contained in the new library are tabulated in *Table 4.1*.

Table 4.1 Cable library contained in the cable simulator package

Gauge Type	24 Pulp/Cu	19 Pulp/Cu	26 PE/Cu	24 PE/Cu	22 PE/Cu	19 PE/Cu
R_{dc} (Ω/km)	168	53	275	174	111	54
L (μH/km)	460	600	658	615	695	720
C (nF/km)	49	38	52	52	41	41
G (pS/km)	5.9	6.2	35	35	35	86
k	1.3	1.33	1.0	1.0	1.0	1.0
s (mm)	1.0	1.8	0.61	0.82	1.21	2.24
d (mm)	0.51	0.91	0.4	0.51	0.63	0.91

Key : PE - Polyethylene
Pulp - Paper
Cu - Copper

The 'cable library' thus consists of two paper insulated cables and four polyethylene insulated cables; the conductors in all cases being copper. The cable test bed did not however contain any paper insulated cables, and thus only the polyethylene insulated cables have been used in the experiments. The data contained for the polyethylene insulated cables in *Table 4.1* was determined from the characterization measurements performed on the cable test bed, the results of which is described in this chapter. The data contained for the paper insulated cables is as was specified by Lowitt [7].

The results for the polyethylene insulated cables tabulated in *Table 4.1* are within the range as is specified [20] by the South African Dept. of Posts and Telecommunications. *Table 4.2* has been extracted from this specification and provides information on the nominal, minimum, and maximum conductor diameter as well as the average resistance and insulation thickness.

Table 4.2 Diameter and resistance of various gauges as specified by the South African Dept. of Post and Telecommunications

Conductor Diameter (mm)			Max. Average Resistance for Conductor @ 20 C	Insulated Conductor	
Nom.	Min.	Max.	(Ω/km)	Min. Radial Thickness (mm)	Max. Overall Diameter (mm)
0.4	0.39	0.41	141.4	0.14	0.84
0.5	0.49	0.51	90.31	0.18	1.02
0.63	0.62	0.64	56.94	0.22	1.22
0.9	0.89	0.91	27.91	0.25	1.61

Source : Ref [20]

The maximum average resistance given in *Table 4.2* is the value that is measured at d.c. The specification further states that the average mutual capacitance of the pairs in a manufacturing length of cable, measured at 800 or 1000Hz must not exceed 56nF/km.

4.2 Input Impedance Measurement Results

The input impedance measurements were performed using the experimental facility illustrated in *Figure 3.4* of *section 3.2.1*. The measurements were performed separately on both lengths provided for each cable type, and for all the types contained in the cable test bed.

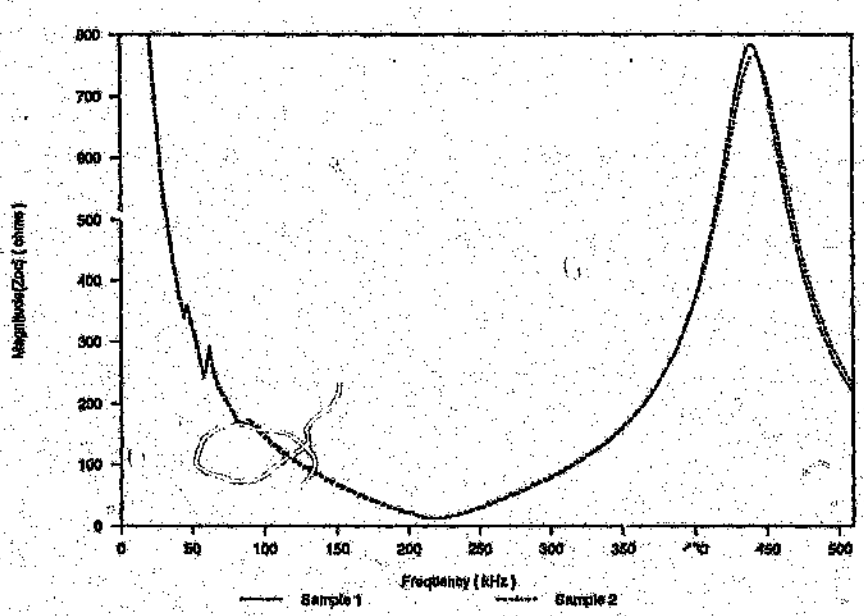

(a)

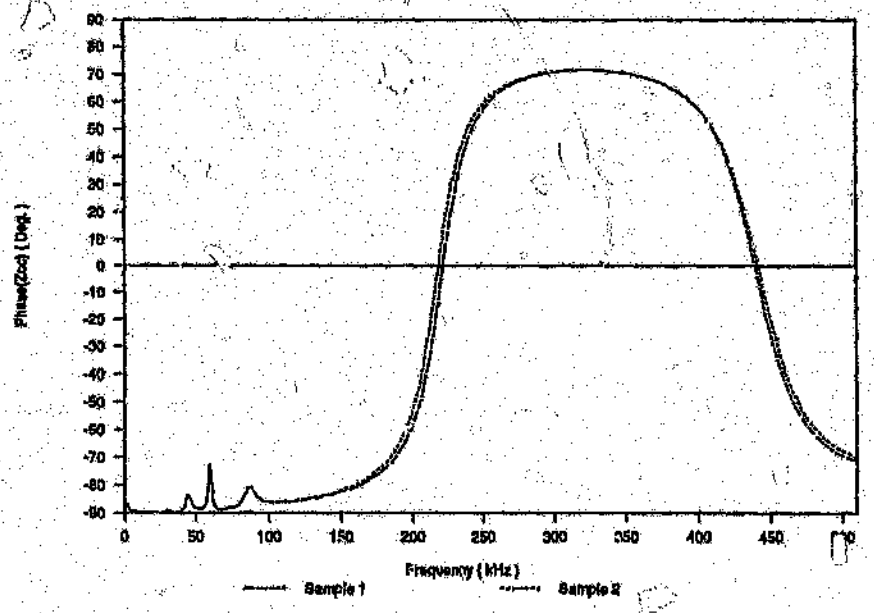

(b)

Figure 4.1 Input impedance, Z_{oc}
Magnitude (a) and phase (b) response of a 10m section of cable gauge type 19 terminated under *open-circuit* conditions.

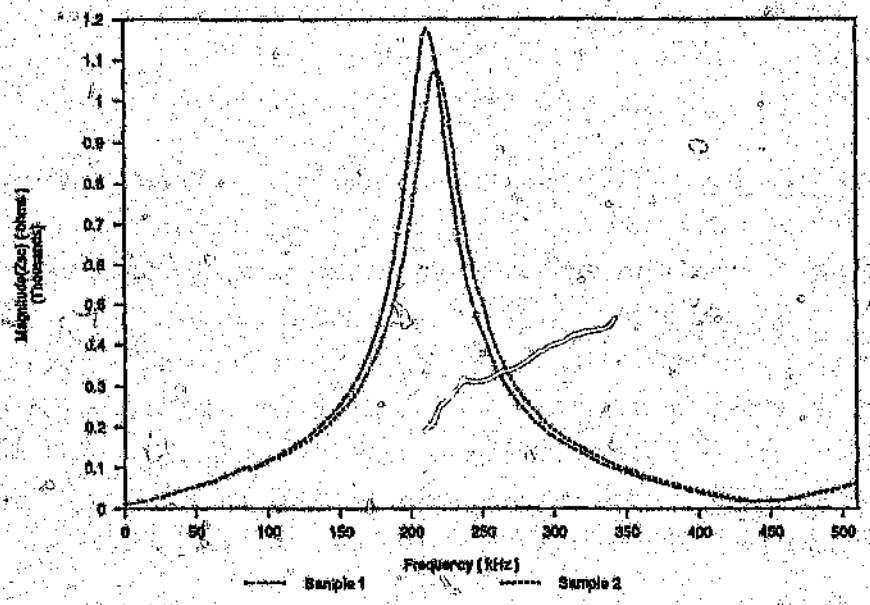

(a)

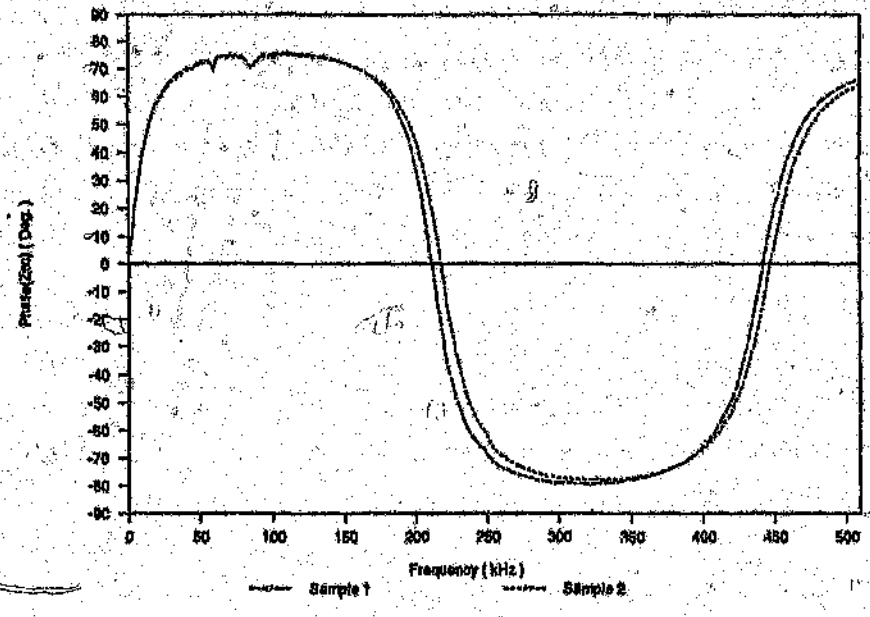

(b)

Figure 4.2 Input impedance, Z_{ss}
Magnitude (a) and phase (b) response of a 200m section of cable gauge type 19 terminated under *short-circuit* conditions.

The graphs of *Figure 4.1* and *Figure 4.2* illustrates the results obtained for the 200m length of gauge 19 type cable, when the termination end was an open-circuit and a short-circuit respectively. The complete set of results obtained for all the cables in the test bed is presented in *Appendix D*.

The peak resistance value measured for Z_{oc} occurs when the electrical half wavelength on the line is equal to the length of the cable being measured. In the case for Z_{scc} the resistance value tends to zero when the same conditions are reached. It can be seen that the instruments measurement range was not exceeded in performing these measurements. This is also evident from the fact that although the Z_{oc} and Z_{sc} measurements were performed separately, the electrical half wavelength occur at precisely the same frequency. In *Figure 4* [illegible] he reason why the magnitude of Z_{sc} is not zero at d.c is due to the inherent [illegible]ance of the cable. This resistance value is the same value as that which has been specified in the 'Cable Library' of *Table 4.1*.

The input impedance measurement results do however contain an unexpected abnormality in the low frequency region between 10kHz and 30kHz. These abnormalities are in the form of several "spikes", and are present in every type of cable measured irrespective of the cable length and pair positioning. The fact that these effects appear in all the cable measurement, requires that they be investigated even though they are not predominant. These effects also propagate through to all the other quantities that are determined from the input impedance measurements, as will be seen later on in this chapter.

These spikes could be caused by crosstalk effects from communicating equipment attached to other pairs. This was however impossible as full control was obtained over the cable test bed and no other equipment was attached to it for the duration of the experiment. The effects must therefore be caused by abrupt changes encountered along the length of the twisted pair, with the result being that the test signal is reflected at these particular frequencies. Deformities in the cable is not unlikely and is in fact unavoidable due to the cable manufacturing process.

These cables are manufactured to a standard length of 1000m or to a maximum length of 4000m, which makes it impossible for any cable to be made in one continuous, uninterrupted process. The process is in fact stopped at regular intervals of several meters depending upon the number of pairs contained in the cable. These inter-

ruptions are due mainly to the cable manufacturing machinery being incapable of producing the entire length in one manufacturing run, and also due to the conductors being broken during the assembling of the cable. These broken conductors are then repaired either by brazing, silver soldering, or by pressure jointing. During each interruption and restarting procedure, it remains impossible for the machinery to retain the required constant twist rate of each pair in the cable, thus causing discontinuities to occur in each twisted pair in the cable.

The result of these discontinuities are clearly shown in the following sections which analyses several cable characteristic. Although in some cases these effects seem large, this is merely due to the scale chosen for the graphs. It is also important to note that these discontinuities occur in the frequency band in which most line codes, used in digital transmission systems, contain their peak energy spectra. It therefore remains to be seen if these discontinuities will adversely effect the time domain results presented in *Chapter 5*.

4.3 Primary Parameters

The primary parameters of each cable type constituting a connection is dependent on frequency. The frequency dependant nature of the primary parameters is due mainly to the skin effect, the proximity effect and the eddy current effect. The d.c values of the primary parameters for the various types of cables are stored in the 'cable library', together with other quantities such as the conductor diameter and the centre to centre spacing of each pair.

The graph of *Figure 4.3* plots resistance per kilometre as a function of frequency for a cable of gauge 19. Similar graphs for the other cables in the cable test bed can be found in *Appendix E*. The results obtained indicates that the resistance model does correlate with the measured results to a certain degree, although it is not expected to be exact since the proximity correction factor caters for the proximity of only one conductor whereas each conductor pair is actually surrounded by many more pairs in close proximity. The abrupt 'stepping' that is seen to occur along the predicted resistance curve is due to the eddy current effect correction factor of equation (4.12).

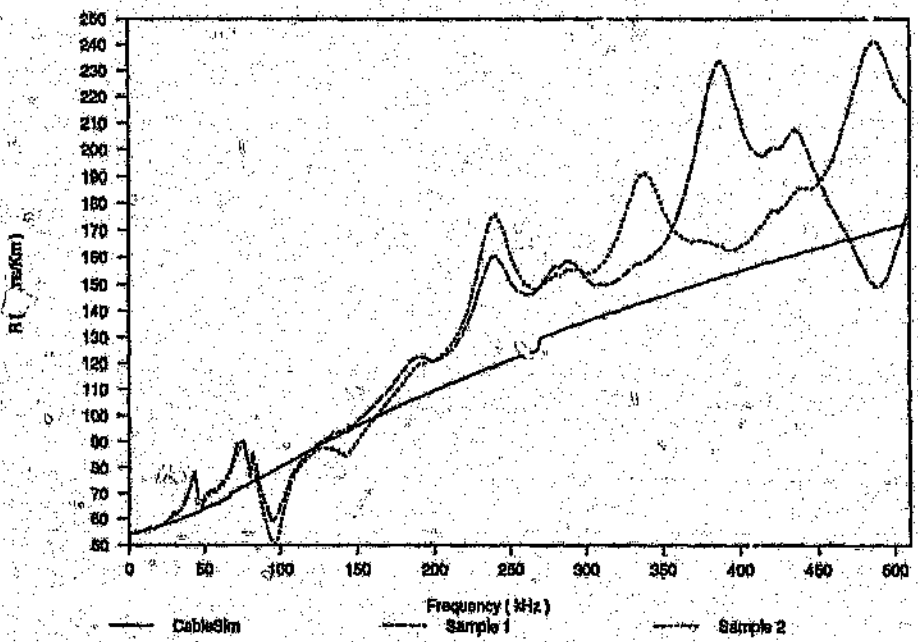

Note : *Y-axis zero suppressed*

Figure 4.3 Gauge 19 - Resistance

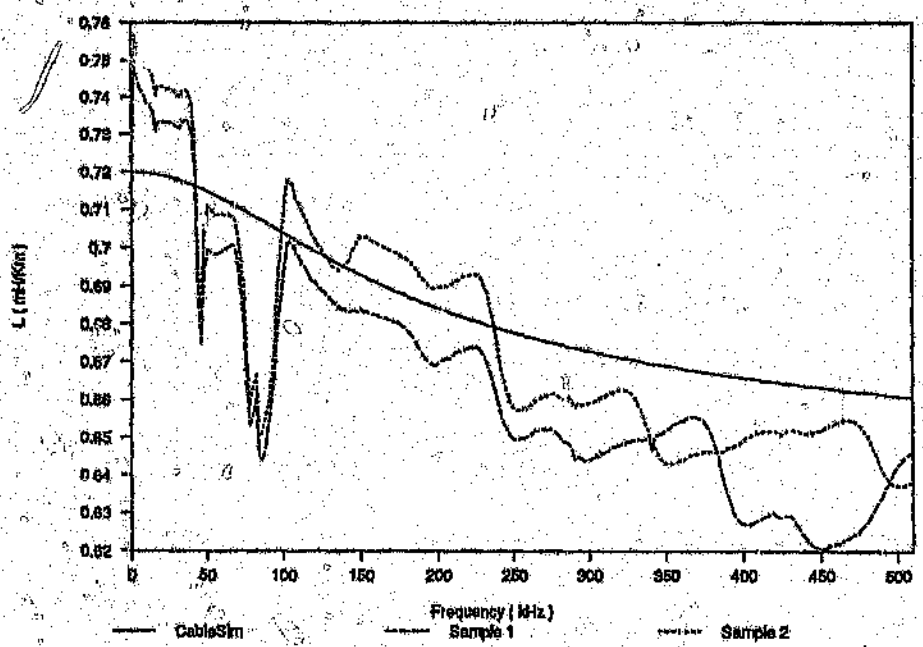

Note : *Y-axis zero suppressed*

Figure 4.4 Gauge 19 - Inductance

For convenience, *Table 4.3* tabulates the resistance per kilometre at several frequencies for the different types of cables contained in the cable test bed. For each type of cable, the simulated value as well as the two measured values are given. The frequency points in *Table 4.3* have not been selected at random and were chosen to be the half bit rate frequency of the line codes used in the time domain experiments presented in *Chapter 5*.

Table 4.3 Resistance at various frequencies for different cable types

Frequency (kHz)		32	64	72	108	144	162	216	324
GUAGE 19	*CableSim*	59.4	67.7	71.3	82.9	94.2	99.4	113.5	140.8
	Sample 1	62.2	75.7	89.4	77.4	95.5	104.9	128.6	153.4
	Sample 2	61.9	74.6	86.2	75.4	85.5	99.9	131.6	173.3
GUAGE 22	*CableSim*	116.0	123.5	125.6	136.3	151.1	157.5	176.8	213.2
	Sample 1	120.1	132.4	142.2	134.9	153.4	150.1	168.6	248.1
	Sample 2	118.1	128.2	136.0	120.0	128.5	138.7	164.3	223.8
GUAGE 24	*CableSim*	179.5	186.3	188.4	198.8	210.4	216.5	235.7	282.9
	Sample 1	178.2	163.8	167.5	197.4	214.6	224.0	244.7	302.3
	Sample 2	177.9	163.0	168.2	190.9	204.7	210.8	234.6	296.5
GUAGE 26	*CableSim*	281.4	287.1	288.9	298.3	309.3	315.2	334.0	374.7
	Sample 1	281.3	277.8	281.2	287.9	302.3	305.1	323.7	380.7
	Sample 2	279.2	276.8	277.4	286.9	304.8	311.6	343.6	397.6

Note : *All values are in Ω/km*

The graph of *Figure 4.4* illustrates the correlation between the predicted and measured results obtained for a cable of gauge 19. The complete set of results for all the other cables in the test bed is illustrated in *Appendix E*. For convenience, *Table 4.4* again lists selected values obtained for the inductance of all the cable types in the cable test bed.

It is important to note that the zero has been suppressed in several graphs shown in this chapter as well as in the appendices. Hence the variations are not as bad as is first seen and must be considered in view of the scale chosen.

The conductance parameter G is frequency sensitive and its effect is more pronounced in paper insulated cables. In good quality plastic insulated, G can be taken as a constant, and is in general very small.

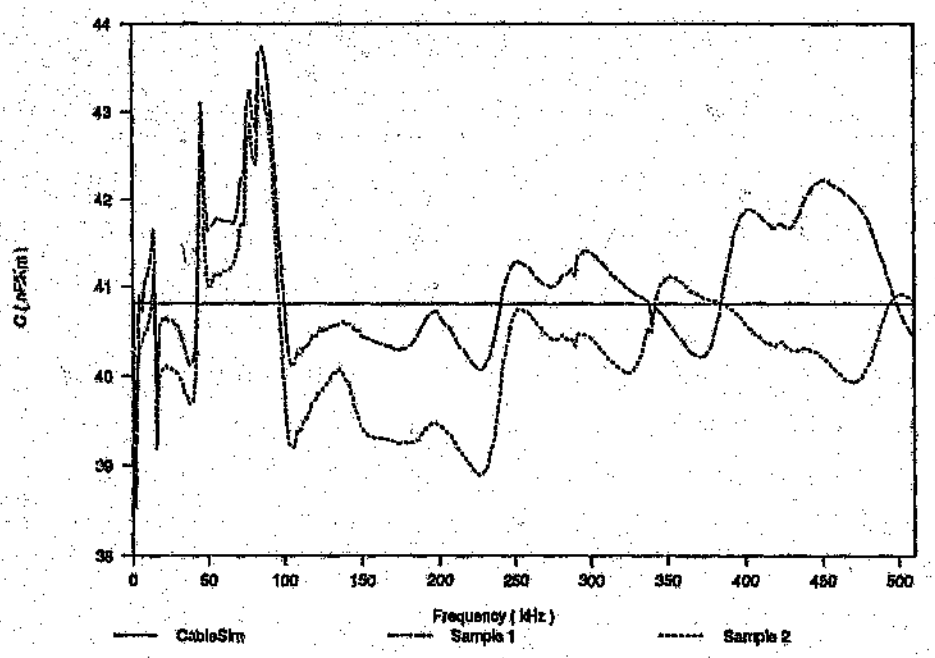

Note : *Y-axis zero suppressed*

Figure 4.5 Gauge 19 - Capacitance

There are no results for conductance as it proved extremely difficult to extract this small quantity from the measured results, verifying the fact that the plastic insulated cables are almost ideal.

Of all the primary parameters, capacitance is the least variable with frequency and is assumed to be a constant. This is easily verified by the graph of *Figure 4.5*, which illustrates the predicted 'constant' capacitance and the two measured results. The complete set of results are again presented in *Appendix E*, and a table of selected values being given in *Table 4.5*. The capacitance measurements also clearly indicate the increased capacitance caused by the deformities caused during manufacture.

Table 4.4 Inductance at various frequencies for different cable types

Frequency (kHz)		32	64	72	108	144	162	216	324
GUAGE 19	*CableSim*	0.72	0.71	0.71	0.70	0.69	0.69	0.68	0.67
	Sample 1	0.73	0.70	0.69	0.70	0.68	0.68	0.67	0.65
	Sample 2	0.74	0.71	0.69	0.71	0.69	0.70	0.69	0.66
GUAGE 22	*CableSim*	0.69	0.69	0.69	0.69	0.69	0.68	0.68	0.67
	Sample 1	0.72	0.69	0.68	0.68	0.66	0.66	0.67	0.65
	Sample 2	0.71	0.69	0.67	0.71	0.70	0.69	0.7	0.7
GUAGE 24	*CableSim*	0.61	0.61	0.61	0.61	0.61	0.61	0.61	0.60
	Sample 1	0.59	0.57	0.61	0.61	0.60	0.59	0.58	0.56
	Sample 2	0.59	0.58	0.61	0.62	0.61	0.6	0.6	0.58
GUAGE 26	*CableSim*	0.66	0.66	0.66	0.66	0.66	0.66	0.65	0.65
	Sample 1	0.65	0.61	0.66	0.66	0.65	0.65	0.65	0.64
	Sample 2	0.66	0.61	0.68	0.68	0.67	0.67	0.66	0.63

Note : *All values are in mH/km*

4.4 Secondary Parameters

The secondary parameters of each cable type constituting a connection is calculated using the frequency dependant values of the primary parameters. The simplified expressions presented by Lowitt [7], has not been implemented. Instead use has been made of the well known transmission line equation presented in *Appendix B*.

Table 4.5 Capacitance at various frequencies for different cable types

Frequency (kHz)		32	64	72	108	144	162	216	324
GUAGE 19	*CableSim*	40.8	40.8	40.8	40.8	40.8	40.8	40.8	40.8
	Sample 1	40.4	41.8	42.4	40.3	40.5	40.4	40.3	40.97
	Sample 2	40.0	41.2	41.7	39.4	39.7	39.3	39.1	40.0
GUAGE 22	*CableSim*	41.3	41.3	41.3	41.3	41.3	41.3	41.3	41.3
	Sample 1	40.6	42.2	42.4	42.0	42.6	43.0	41.3	41.6
	Sample 2	41.7	43.0	43.7	41.2	41.3	41.2	40.1	39.2
GUAGE 24	*CableSim*	52.0	52.0	52.0	52.0	52.0	52.0	52.0	52.0
	Sample 1	52.6	55.9	51.9	51.0	51.4	51.5	52.0	52.0
	Sample 2	52.5	55.0	52.3	51.1	51.3	51.4	51.1	51.1
GUAGE 26	*CableSim*	52.0	52.0	52.0	52.0	52.0	52.0	52.0	52.0
	Sample 1	52.8	56.2	52.3	52.0	52.3	52.5	52.1	51.7
	Sample 2	52.3	56.3	52.0	51.7	51.9	51.9	51.7	52.6

Note : *All values are in nF/km*

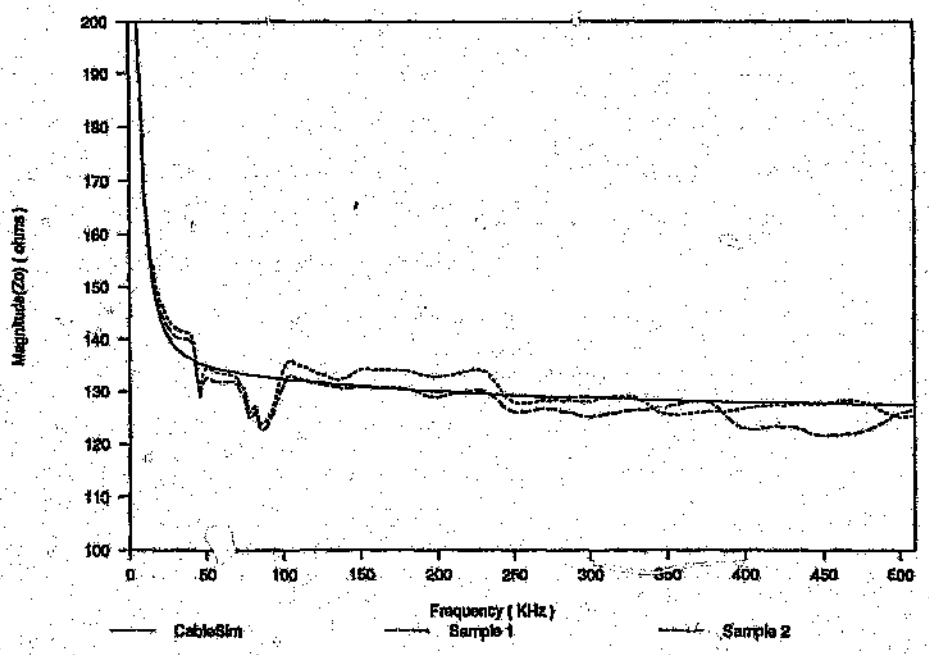

Note : *Y-axis zero suppressed*

Figure 4.6 Gauge 19 - Magnitude(Characteristic Impedance)

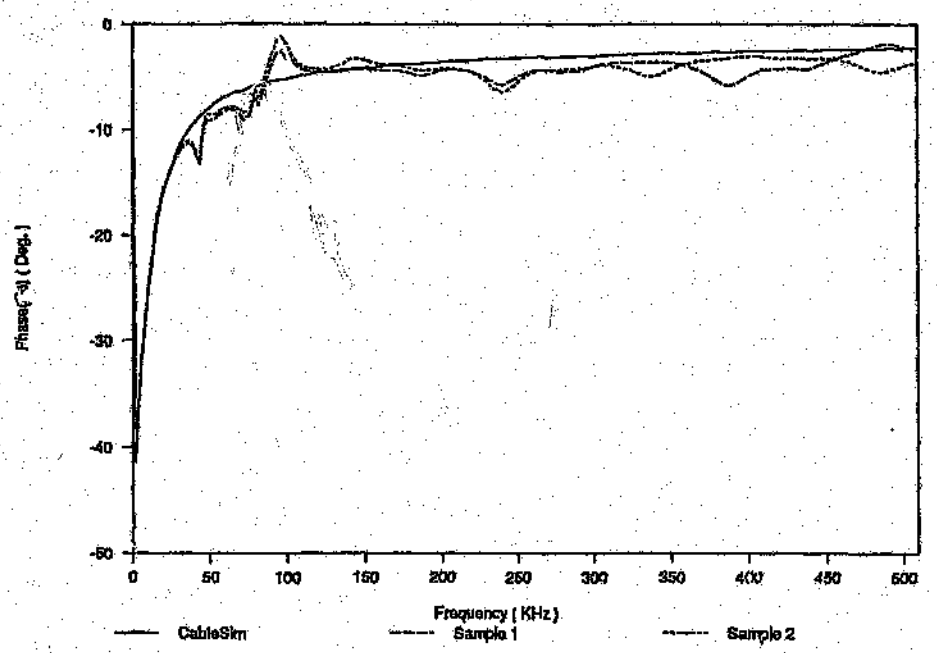

Figure 4.7 Gauge 19 - Phase(Characteristic Impedance)

The graphs of *Figure 4.6* and *Figure 4.7* illustrates the excellent correlation obtained between the measured and the predicted results obtained for the cable of gauge 19. The complete set of results for the other cable types in the cable test bed is presented in *Appendix F*. The 'dips' which is evident in all the measured results are due to deformities in the cable manufacturing process and are not caused by bridge taps as might be suspected. The characteristic impedance is usually given in the units of ohms, although it is independent of cable length.

Table 4.6 Magnitude*(Characteristic Impedance)* at various frequencies for different cable types

Frequency (kHz)		32	64	72	108	144	162	216	324
GUAGE 19	*CableSim*	137.9	133.9	133.5	132.1	131.2	130.7	129.8	128.6
	Sample 1	140.9	131.7	130.1	132.6	130.6	130.7	129.8	126.3
	Sample 2	141.7	133.4	131.4	135.3	133.3	134.2	133.7	129.2
GUAGE 22	*CableSim*	147.9	135.5	134.4	131.9	130.7	130.3	129.2	127.8
	Sample 1	152.1	134.5	132.9	129.8	126.7	125.1	128.8	126.2
	Sample 2	148.9	132.7	129.8	132.8	131.0	131.0	133.1	134.2
GUAGE 24	*CableSim*	144.4	121.6	119.4	114.3	112.1	111.5	110.1	108.7
	Sample 1	142.4	111.9	117.4	115.3	112.0	110.9	108.0	105.7
	Sample 2	142.4	113.6	117.0	115.2	112.4	111.4	110.2	108.0
GUAGE 26	*CableSim*	172.5	136.6	132.8	123.3	119.3	118.1	115.9	114.0
	Sample 1	170.9	127.6	131.8	123.0	118.2	116.6	114.9	113.2
	Sample 2	171.3	127.7	132.7	124.4	120.3	119.0	117.1	112.3

Note : *All values are in* Ω's

It is seen that the characteristic impedance does attain an approximately constant value above a few hundred kilohertz. The phase also tends to approximately a constant value. The line codes used for transmission however have most of their energy spectra concentrated in the lower frequencies, precisely where the characteristic impedance changes the most with frequency. This results in considerable difficulty in trying to match the line with any terminating equipment such as a hybrid, resulting in a substantial effort being placed into the investigations of implementing adaptive hybrids.

Table 4.7 Phase*(Characteristic Impedance)* at various frequencies for different cable types

Frequency (kHz)		32	64	72	108	144	162	216	324
GUAGE 19	*CableSim*	-11.2	-6.6	-6.2	-4.9	-4.3	-4.0	-3.5	-2.9
	Sample 1	-11.8	-8.1	-9.0	-4.1	-4.4	-4.4	-4.4	-3.7
	Sample 2	-11.6	-7.8	-8.4	-3.8	-3.3	-3.8	-4.4	-4.4
GUAGE 22	*CableSim*	-19.9	-11.9	-10.9	-8.1	-6.8	-6.4	-5.4	-4.5
	Sample 1	-20.3	-13.9	-13.9	-8.2	-7.7	-6.4	-5.1	-6.3
	Sample 2	-20.1	-13.1	-13.0	-5.9	-4.7	-4.7	-4.4	-4.5
GUAGE 24	*CableSim*	-27.7	-18.5	-17.1	-12.8	-10.4	-9.6	-8.0	-6.5
	Sample 1	-28.7	-16.1	-13.9	-12.7	-11.1	-10.5	-9.0	-8.1
	Sample 2	-28.8	-15.8	-14.2	-11.9	-10.0	-9.3	-8.0	-7.5
GUAGE 26	*CableSim*	-32.4	-23.7	-22.1	-16.9	-13.8	-12.6	-10.3	-7.9
	Sample 1	-33.0	-25.0	-21.2	-15.8	-13.4	-12.2	-9.9	-8.3
	Sample 2	-32.9	-25.0	-20.6	-15.5	-13.3	-12.3	-10.7	-9.1

Note : *All values are in* Ω's

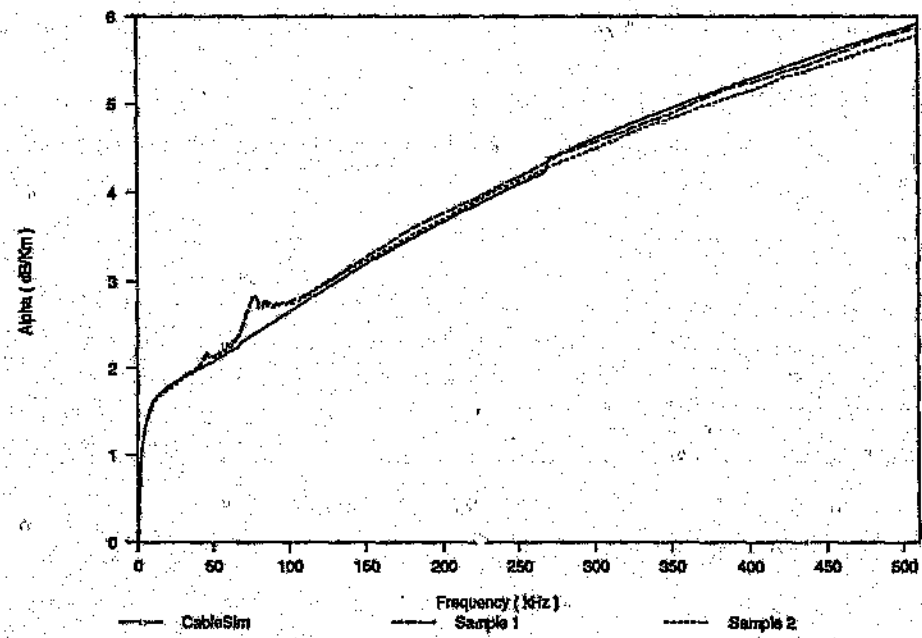

Figure 4.8 Gauge 19 - Attenuation constant

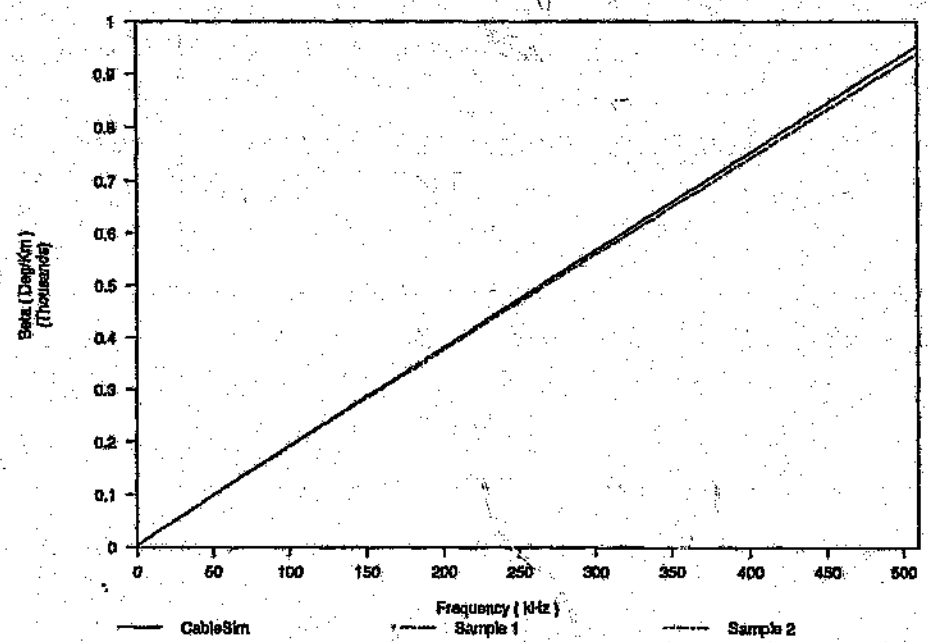

Figure 4.9 Gauge 19 - Phase constant

The spectra of the line coded signals is kept as low as possible because as will soon be seen, the attenuation on the cable increases drastically with increases in frequency.

Table 4.6 and *Table 4.7* tabulates the magnitude and phase of the characteristic impedance for the different types of cables at various frequencies.

Table 4.8 Attenuation constant at various frequencies for different cable types

Frequency (kHz)		32	64	72	108	144	162	216	324
GUAGE 19	*CableSim*	1.907	2.215	2.336	2.739	3.133	3.318	3.816	4.776
	Sample 1	1.918	2.318	2.654	2.824	3.207	3.409	3.893	4.719
	Sample 2	1.895	2.294	2.614	2.793	3.179	3.353	3.852	4.669
GUAGE 22	*CableSim*	3.624	4.047	4.135	4.536	5.059	5.285	5.971	7.273
	Sample 1	3.547	4.012	4.196	4.516	4.942	5.156	5.809	7.020
	Sample 2	3.586	4.081	4.291	4.602	5.061	5.287	5.947	7.177
GUAGE 24	*CableSim*	6.101	7.017	7.167	7.749	8.289	8.559	9.389	11.38
	Sample 1	6.044	7.261	7.090	7.644	8.265	8.584	9.554	11.37
	Sample 2	6.003	7.117	7.038	7.568	8.194	8.512	9.473	11.30
GUAGE 26	*CableSim*	8.396	9.967	10.20	10.98	11.60	11.88	12.72	14.42
	Sample 1	8.407	10.20	10.14	10.92	11.56	11.89	12.75	14.58
	Sample 2	8.258	10.00	9.89	10.70	11.32	11.65	12.65	14.58

Note : *All values are in dB's/km*

The graphs of *Figure 4.8* and *Figure 4.9* illustrates the correlation between the measured and predicted results obtained for the attenuation constant and the phase constant per kilometre of a cable of gauge 19. It can be seen that the attenuation constant increases approximately as the square of the frequency, (i.e., similar to $R(f)$). The phase constant remains linear. The complete set of results for the other cable types is presented in *Appendix F*, and *Table 4.8* and *Table 4.9* provides an overview of the results for all the cable types at various frequencies.

Table 4.9 Phase constant at various frequencies for different cable types

Frequency (kHz)		32	64	72	108	144	162	216	324
GUAGE 19	*CableSim*	64	125	140	209	277	310	411	611
	Sample 1	64	126	141	207	274	307	406	603
	Sample 2	64	126	141	206	274	307	406	602
GUAGE 22	*CableSim*	66	126	141	210	278	312	413	614
	Sample 1	67	128	144	210	278	312	412	611
	Sample 2	67	129	144	211	279	313	413	612
GUAGE 24	*CableSim*	77	138	154	225	297	333	441	655
	Sample 1	77	136	151	223	293	328	432	638
	Sample 2	77	136	152	223	294	329	434	639
GUAGE 26	*CableSim*	87	150	166	239	312	349	461	685
	Sample 1	88	151	166	238	311	348	458	676
	Sample 2	88	152	167	240	315	352	463	682

Note : *All values are in* Deg./*km*

4.5 Reflection Coefficients

Signal reflections occur along a cable connection due to mismatches encountered. A mismatch exists at the joins between cable sections of different characteristic impedance, as well as between each end section and the corresponding end terminating impedance. The reflection coefficient therefore represents the extent of the mismatch between the characteristic impedance of adjacent sections.

The graph of *Figure 4.10* illustrates the reflection coefficient as a function of frequency between a cable section of gauge 19 and gauge 22 (i.e., $\rho_{19->22}$). The reflection coefficient for any two cable sections always converges to a constant value which is expected since the characteristic impedance of all the cable types also converge to a constant value. In the case of a cable section of gauge 22 and gauge 19 (i.e, $\rho_{22->19}$), the reflection coefficient is equal in magnitude to $\rho_{19->22}$ but opposite in sign, (i.e., there is a phase difference of 180 degrees). The graphs for the reflection coefficients of all the other possible combinations are presented in *Appendix G*. The list given in *Table 4.10* compares the reflection coefficients for the various combinations at various frequencies.

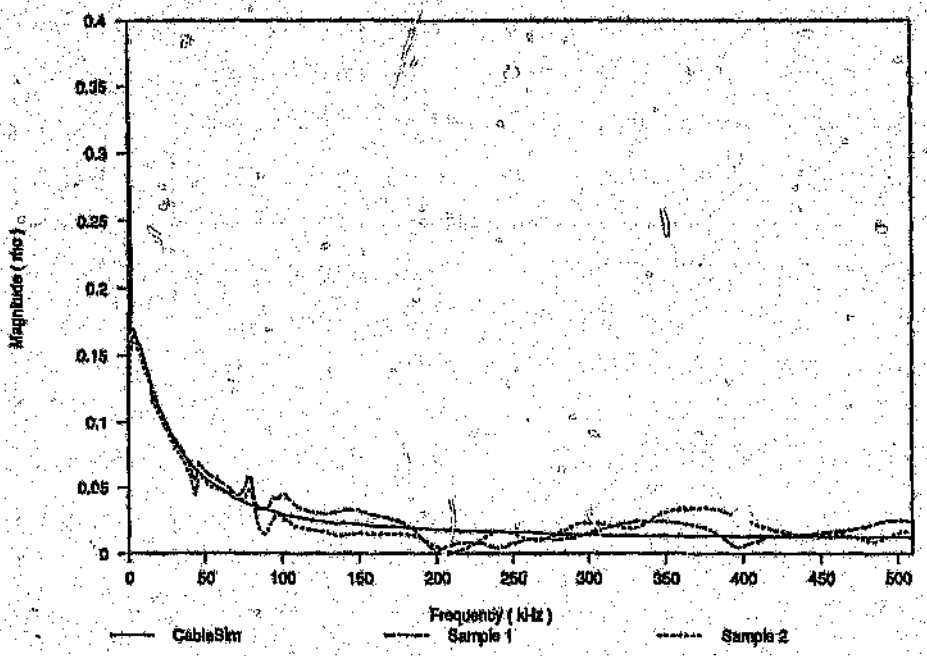

Figure 4.10 Gauge 19=>22 - Reflection coefficient ($\rho_{19->22}$)

Table 4.10 Reflection coefficients at various frequencies for different cable connections

Frequency (kHz)		32	64	72	108	144	162	216	324
GUAGE 19 22	*CableSim*	0.0836	0.0466	0.0410	0.0279	0.0226	0.0206	0.0171	0.0137
	Sample 1	0.0851	0.0513	0.0400	0.0373	0.0325	0.0282	0.0075	0.0226
	Sample 2	0.0791	0.0462	0.0407	0.0206	0.0148	0.0142	0.0021	0.0193
GUAGE 19 24	*CableSim*	0.1473	0.1145	0.1100	0.0998	0.0950	0.0934	0.0907	0.0893
	Sample 1	0.1488	0.1075	0.0665	0.1023	0.0966	0.0982	0.1004	0.0965
	Sample 2	0.1518	0.1062	0.0771	0.1072	0.1030	0.1040	0.1014	0.0932
GUAGE 19 26	*CableSim*	0.2180	0.1501	0.1391	0.1104	0.0957	0.0909	0.0819	0.0741
	Sample 1	0.2115	0.1489	0.1073	0.1086	0.0938	0.0891	0.0776	0.0678
	Sample 2	0.2106	0.1528	0.1075	0.1109	0.1014	0.0951	0.0862	0.0808
GUAGE 22 24	*CableSim*	0.0698	0.0787	0.0797	0.0822	0.0827	0.0828	0.0828	0.0825
	Sample 1	0.0800	0.0939	0.0618	0.0710	0.0686	0.0703	0.0944	0.0896
	Sample 2	0.0790	0.0810	0.0530	0.0883	0.0893	0.0900	0.0924	0.1113
GUAGE 22 26	*CableSim*	0.1341	0.1028	0.0979	0.0837	0.0758	0.0735	0.0689	0.0645
	Sample 1	0.1251	0.1005	0.0643	0.0712	0.0614	0.0616	0.0707	0.0570
	Sample 2	0.1316	0.1061	0.0677	0.0902	0.0866	0.0817	0.0846	0.0973
GUAGE 24 26	*CableSim*	0.0976	0.0735	0.0686	0.0523	0.0425	0.0392	0.0326	0.0265
	Sample 1	0.0981	0.1012	0.0860	0.0423	0.0341	0.0292	0.0319	0.0342
	Sample 2	0.0986	0.0999	0.0842	0.0496	0.0445	0.0423	0.0388	0.0241

4.6 Transfer Function

There are two transfer function models that can be used to characterize a cable connection in the frequency domain, namely; the steady state and the transient state model.

The steady state model reduces the cable connection into one equivalent transfer function and can therefore not be used to provide explicit information about the reflections from discontinuities caused by the cable joins along the connection. The results presented in *Figure 4.11* was obtained for a cable section of gauge 19 and length 1km. The cable section was terminated by a resistive load of 120Ω.

The transient state model does not reduce the connection to one equivalent model, but characterizes each cable section in the connection with a transfer function, and each discontinuity in the connection with a reflection coefficient. This model therefore lends itself to analysis of the reflections from discontinuities, although in its present form, it implies perfect matching conditions at the cable connection ends. The results illustrated in *Figure 4.12* were obtained for the same cable configuration as for the steady state case, except for the termination ends being open-circuited.

The complete result for all the other types of cables gauges are presented in *Appendix H* and *Appendix I* for the Steady State and Transient State transfer function. It can be seen that the Steady State Transfer function and the Transient State Transfer function are almost identical for frequencies above 60kHz.

The impulse response of these transfer functions are also shown. The impulse response corresponding to the transfer functions given above in *Figure 4.11* and *Figure 4.12* are respectively shown in *Figure 4.13* and *Figure 4.14*. It can be seen that the impulse response are almost identical. The initial flat delay corresponds to the propagation time along the cable, and the ringing delay which follows the flat delay is an important parameter used to determine the number of taps that would be required for a transversal filter.

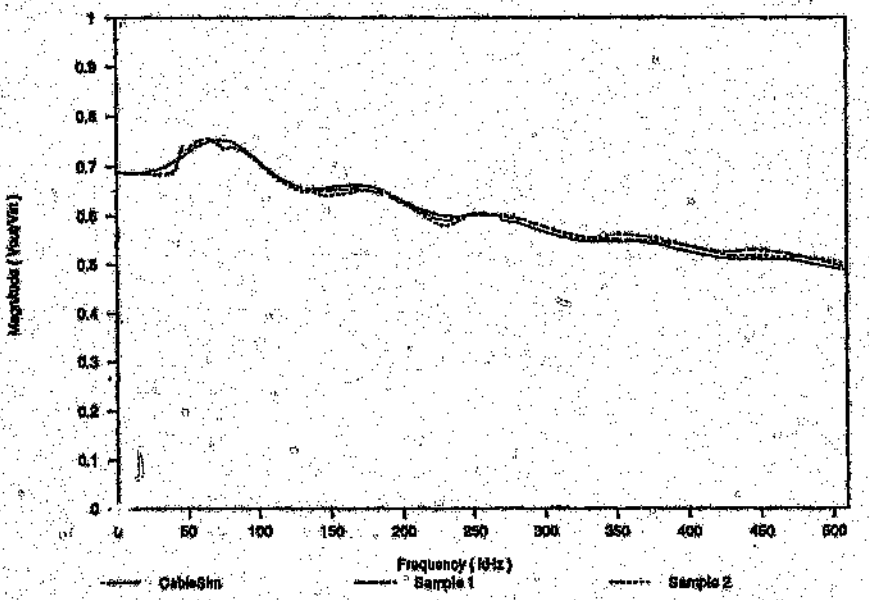

(a)

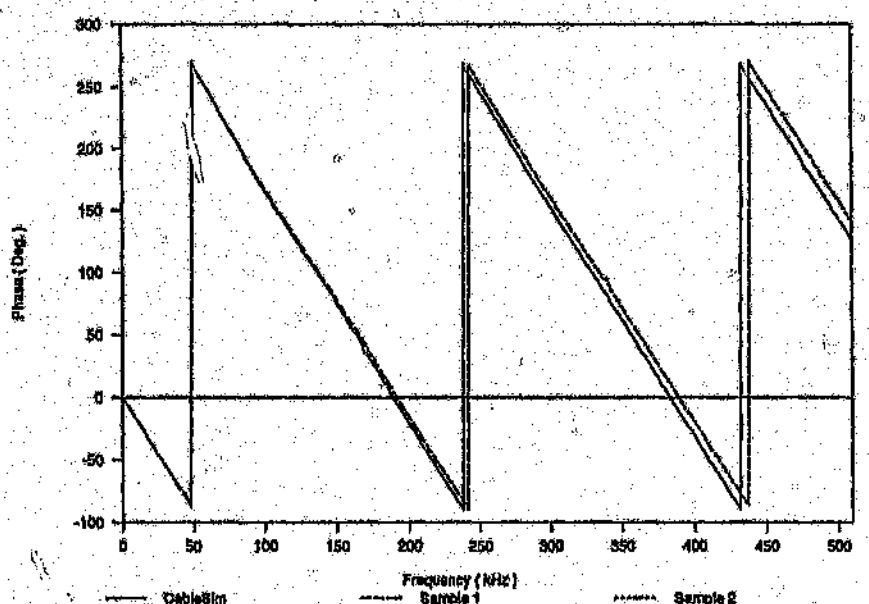

(b)

Figure 4.11 Gauge 19 - Steady state transfer function
($Length = 1km$, $Z_{load} = 120+j0\Omega$)
(a) Magnitude response
(b) Phase response

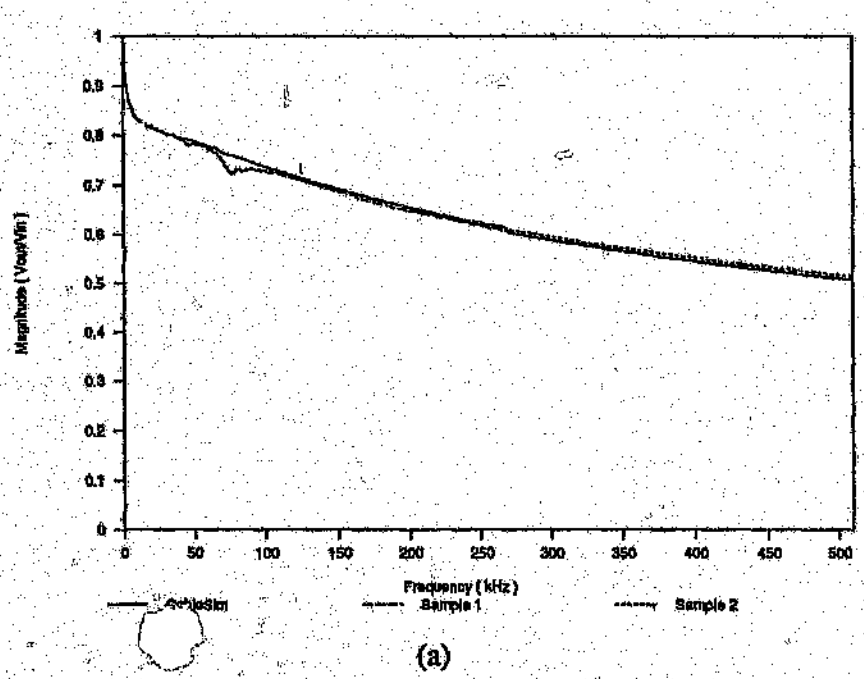

(a)

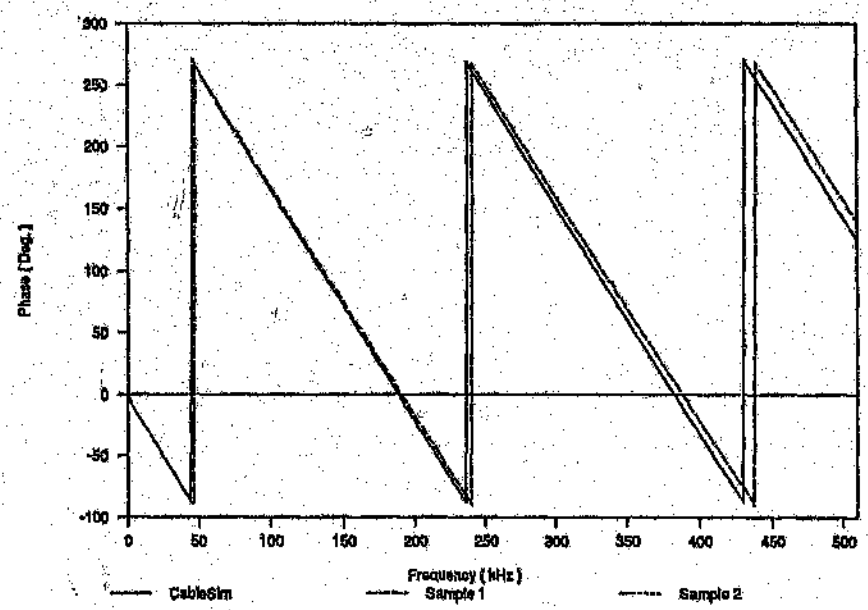

(b)

Figure 4.12 Gauge 19 - Transient state transfer function
(*Length = 1km*)
(a) Magnitude response
(b) Phase response

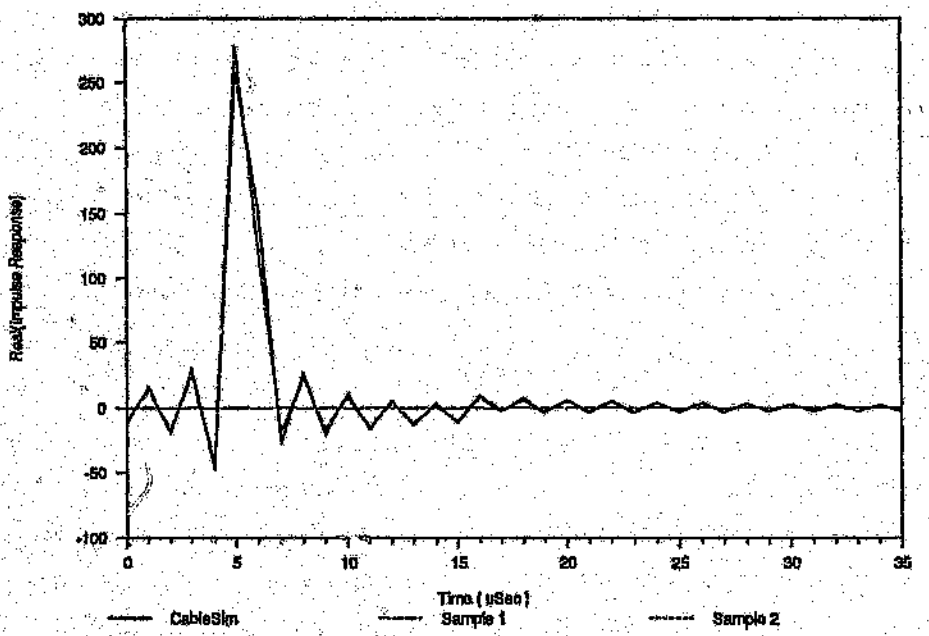

Figure 4.13 Gauge 19 - Steady state impulse response
(*Length = 1km*, $Z_{load} = 120+j0\Omega$)

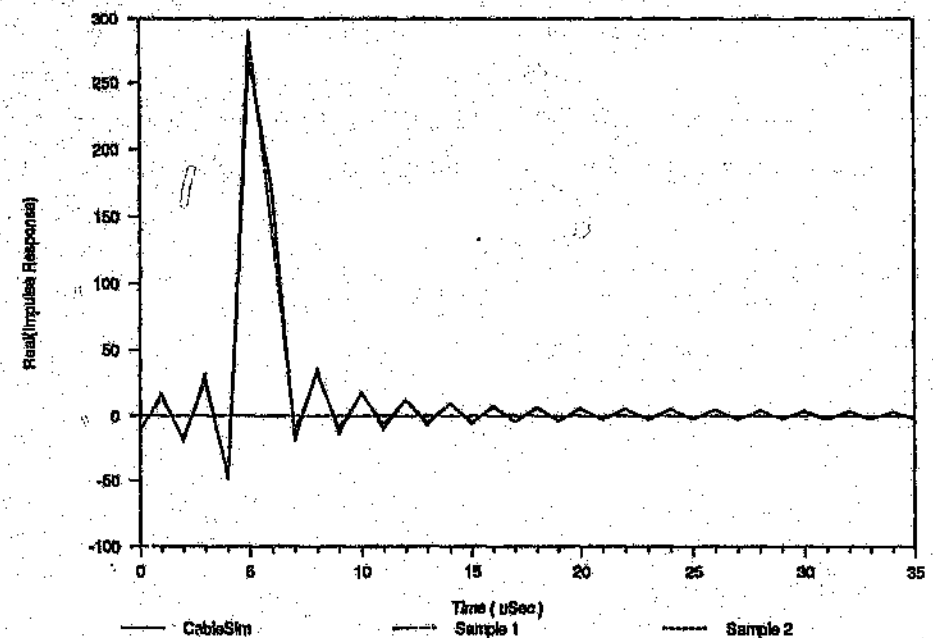

Figure 4.14 Gauge 19 - Transient state impulse response
(*Length = 1km*)

Subsequently, the steady state model is used for the unidirectional case only, and the transient state model is used for the full-duplex case. Having said this, it is also important to note that although the TCM mode of transmission is essentially a unidirectional system, the full-duplex case can be used with an even greater success by considering the signal propagation in the one direction only, and determining the consequences of the reflections from this waveform that is propagated back to the transmitter. The magnitude of this delayed signal as well as its time delay will provide useful information on the required guard time in a TCM system.

4.7 Conclusions

The data required by the 'cable library' has been determined from the input impedance measurements performed on the various cables in the test bed. The primary parameters, secondary parameters, transfer functions and reflection coefficients predicted by the Cable Simulation Package are in close agreement with that as was obtained from the characterization measurements performed. These results thus indicates the validity of the well established transmission line model, together with the correction factors for skin effect, proximity effect, and eddy current effects. It must again be mentioned that the model for the proximity effect correction factor used only takes into account the proximity of one conductor on another, whereas in real cables, each conductor is closely surrounded by many other conductors. This approximation has had minimal effects in the frequency range used, but should be investigated further if the Cable Simulation Package is extended to much hi frequencies.

Chapter 5

TIME DOMAIN VERIFICATION

This chapter is concerned with the verification of the program ***F-Duplex***, which simulates the propagation of pulses along the connection specified by the program ***CableSim***. The program allows any binary bit sequence to be specified by the user. A word encoder module provides facilities for different line codes to be generated including the Jessops-Waters coding alphabet[21] used to obtain a ternary bit pattern. Pre-equalization facilities are also provided for the specified transmit signal.

The pulse propagation experimental facility described in *section 3.3* of *Chapter 3*, has been used to obtain the results measured on real cable connections for comparison with the simulated results. The single pulse responses, waveform shapes and eye diagrams presented in the following sections were selected as examples for discussion, whilst other loop configurations analysed have been summarized in tables. In order to ease the comparison between the simulated and measured results, the gain of the detection amplifiers has been taken into consideration in all the results presented.

5.1 Single Pulse Response

The transmission capabilities of a particular cable connection can be determined from the single pulse response analysis. Three crucial results emerge from the single pulse response study:

(a) the deterioration of the received pulse,
(b) the extent of the long decaying tails left behind by the pulse, and
(c) the magnitude and shape of the reflections of the sent pulse at the sending end.

The graphs illustrated in *Figure 5.1* is a typical example of the pulse response shape obtained at the receiver end. *Figure 5.1(a)* is the result predicted by the pulse propagation program, and *Figure 5.1(b)* the corresponding measured result. The cable connection in this case consists of 2.01km of gauge type 22 followed by 3.01km of gauge type 24.

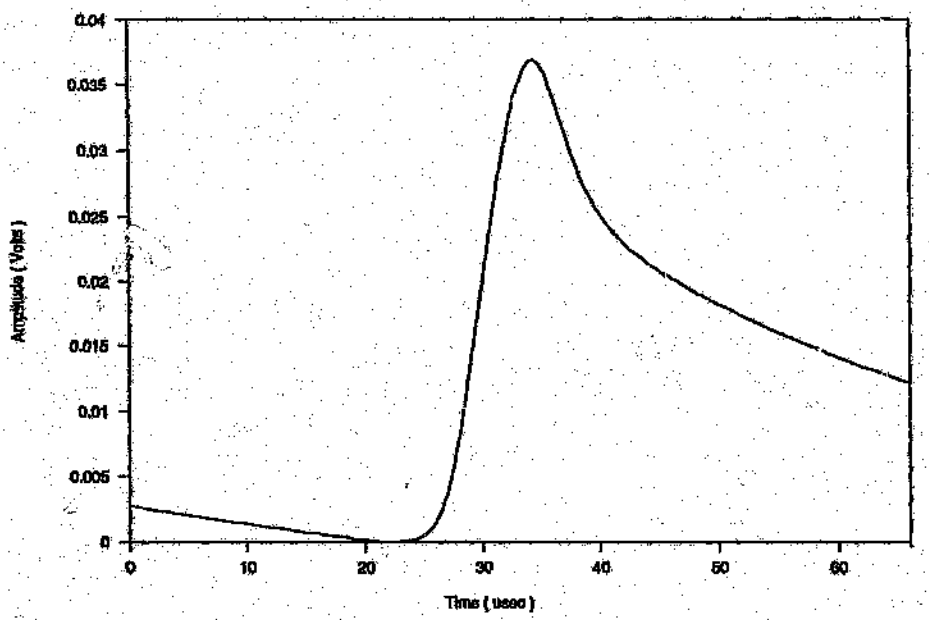

(a)

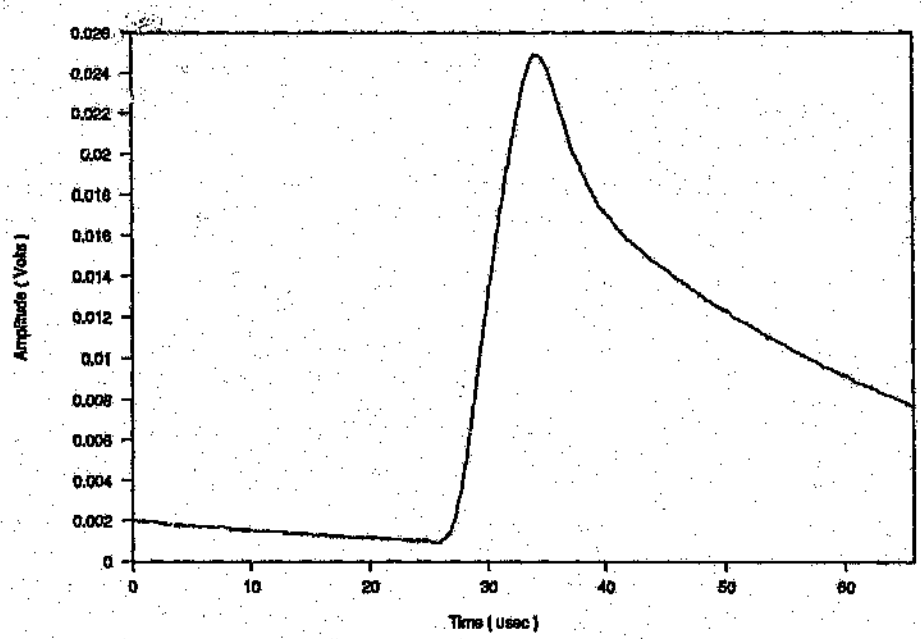

(b)

Figure 5.1 Computationally (a) and experimentally (b) generated pulse response over a two-section (2.01km of 22 AWG; 3.01km of 24 AWG) multi-gauge connection at 144kbits/sec.

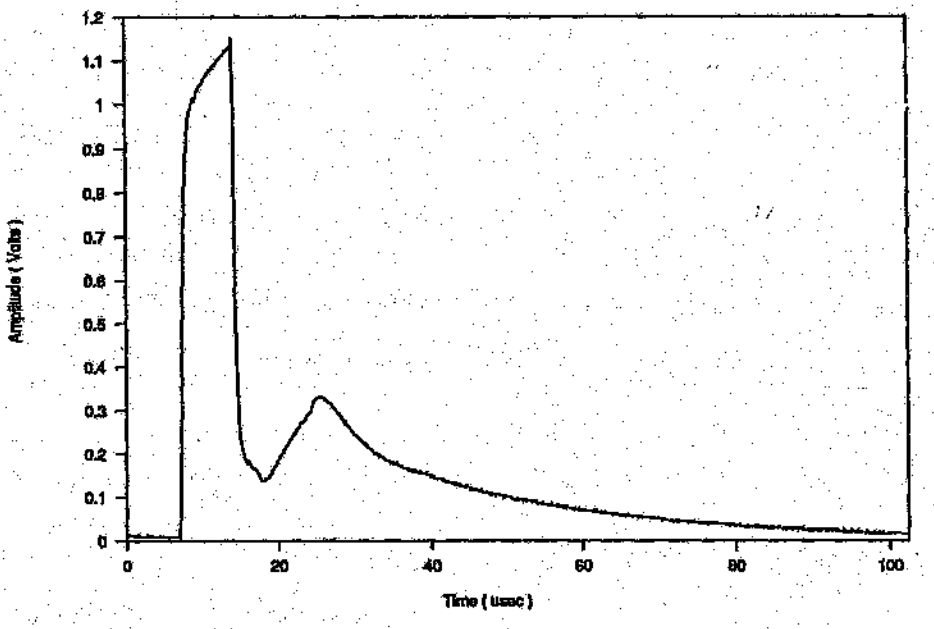

Figure 5.2 Transmission and reflection of a single pulse on a two-section (1km of 19 AWG; 1.86km of 26 AWG) multigauge connection measured at the generator end. The pulse rate is 144kbits/sec, and the connection is resistively matched at each end.

The simulation assumed perfect matching conditions at both ends of the connection, whilst experimentally the termination ends were only resistively matched. The transmitted pulse used was unbalanced and rectangular in shape with a pulse width of 6.95μseconds, which is the bit period required to achieve a line bit rate of 144kbits/sec.

The peak value of the pulse arriving at the receiver end has been attenuated by approximately 28dB's and 32dB's respectively for the simulated and measured result. The difference in the attenuation is caused by the mismatched conditions encountered at both ends of the connection. The rise time was found to be consistently fast, and approximately equal to one bit interval. The tails on the other hand decay very slowly, spreading into the bit periods of other pulses. Any following pulse would therefore be offset from their zero position because of the prior pulses.

In order to illustrate the effect caused by the discontinuity encountered at the join of two cables of different gauge; a 1km section of gauge 19 was connected to a 1.86km section of gauge 26. The connection was excited by a rectangular pulse with a period of 15,6μ seconds (i.e, 64kbits/sec), applied to the section of gauge 19 as it provides the lowest propagation attenuation of the two cables (see *Table 4.8* in *section 4.4*). The reflection coefficient between gauge 19 and gauge 26 has been determined in *Table 4.10* to be the worst at this bit rate with a value of 0.22. The resulting shape of the reflected pulse on the transmitter side as was experimentally determined is illustrated in *Figure 5.2*. There are two peaks embedded in the transmitted pulse tail. The positive peak being approximately the amplitude of an expected pulse arriving from the opposite end of the connection. The reflected signal would therefore be a source of interference, and unless the reflection is cancelled out by an echo canceller, the eye diagram would be considerably distorted.

5.2 Pulse Patterns and Eye Diagrams

This section discusses the results obtained from the transmission of pulse pat over a specified cable connection. Extensive use has been made of diagrams in order to illustrate the correlation between the simulated and measured results. These diagrams are in the form of pulse patterns and their corresponding eye diagrams. For each cable connection investigated, four different line bit rates are studied and their results recorded. The line bit rate of interest is 64kbits/sec, and 144kbits/sec as the latter is the bit rate used in the existing Diginet system and the former is the data rate required to support basic access in an ISDN. Two more line rate have however been included to the list. They are 216kbits/sec and 324kbits/sec line data rates. The former being the line rate required for a TCM system operating at an effective line rate of 144kbits/sec and the latter is approximately the line rate required if overheads such as timing, framing and maintenance functions are not to be provided as part of the 144kbits/sec for the basic access to an ISDN.

There are two case studies presented. The first case is concerned with a multigauge cable connection consisting of two different cable section. This connection extends over a distance of 5km and the resulting eye diagrams at the receiver ends are adequately opened for all four line bit rates investigated. The second case analyses

a multigauge cable connection consisting of three different cable sections. This connection extends over a distance of 6km and the resulting eye diagrams illustrates a almost completely closed eye.

5.2.1 Case Study 1

The first case study is concerned with a cable connection consisting of two different cable sections as illustrated in *Figure 5.3*. The total length of the connection is 5.02km, where section one comprises a length of 2.01km of gauge type 22, followed by section two of length 3.01km of gauge type 24.

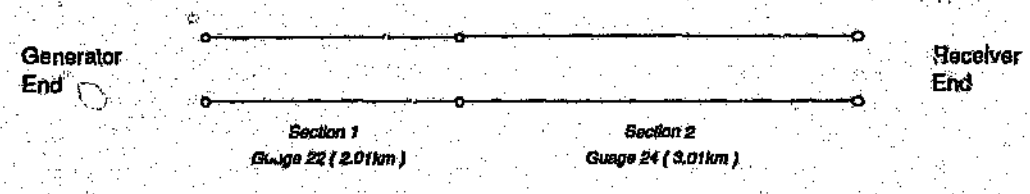

Figure 5.3 Case Study 1 : Two-section multigauge cable connection (*Total length = 5km*)

The pulse propagation program ***F-Duplex*** of the Cable Simulation Package assumes "perfectly" matched conditions at both ends of the cable connection. Experimentally the cable connection was only resistively matched at the ends by using a lumped resistor network. For each of the four bit rates investigated on the connection, the receiver end was terminated with the characteristic impedance value of the last section (i.e., section two), at half the bit rate frequency as predicted by the program ***CableSim***. The generator end was terminated with the input impedance for the connection as was predicted by the program ***CableSim***, at half the bit rate frequency. The input impedance and termination impedance used for the four different bit rates investigated are summarised in *Table 5.1*.

The connection shown in *Figure 5.3* was excited by a binary bit pattern consisting of 16 bits for all the four different line bit rates under investigation. The binary pattern used was chosen to be

1100101011001010

which contains a selection of different bit patterns, such as 010, 101, 0110, 1001, etc. If the binary pattern was to consist of states that further increased the average d.c. voltage over a number of consecutive bits (e.g., the bit pattern 01110); this would only serve to decrease the eye opening at the receiver end due to the start of the decaying tails being offset by a higher average d.c. voltage value. In general, line codes are chosen such that the number of transitions is maximized in order to maintain a zero d.c. average voltage as well as to enable timing and synchronization information to be easily extracted.

Table 5.1 Termination impedances for case study 1, given at half the bit rate frequency

Bit Rate (kbits/sec)	Half Bit Rate Frequency (kHz)	Generator End Impedance (Ω)	Receiver End Impedance (Ω)
64	32	143 - *j* 0	128 - *j* 0
144	72	135 - *j* 0	114 - *j* 0
216	108	131 - *j* 0	112 - *j* 0
324	162	131 - *j* 0	110 - *j* 0

The coding strategy used was the Bipolar code which translates a binary "one" into a positive voltage level (i.e., +1volt), and a binary "zero" into a corresponding negative voltage level (i.e., -1volt). The rectangular window was used on each bit for pulse shaping. The results obtained from the Cable Simulation Package and that measured over real cables for the connection are presented in *Figure 5.4* through *Figure 5.11*. Each figure illustrates the received pulse pattern at the receiver end and its corresponding eye diagram.

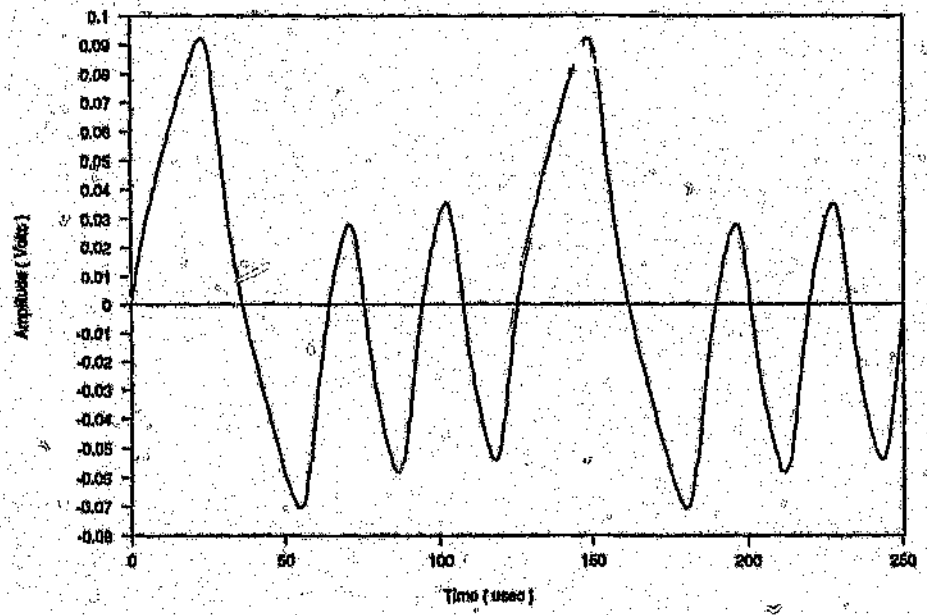

(a)

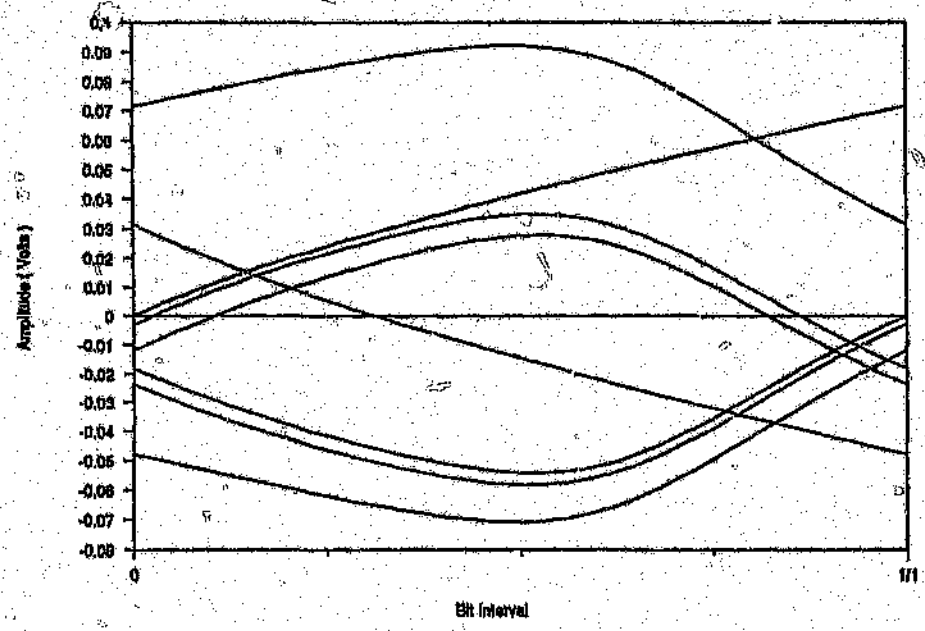

(b)

Figure 5.4 Computationally generated pulse pattern (a) and eye diagram (b) of a two-section (2.01km of 22 AWG; 3.01km of 24 AWG) multigauge connection at 64 kbits/sec. The number of points in the FFT is 256, and the fold frequency is 1024kHz.

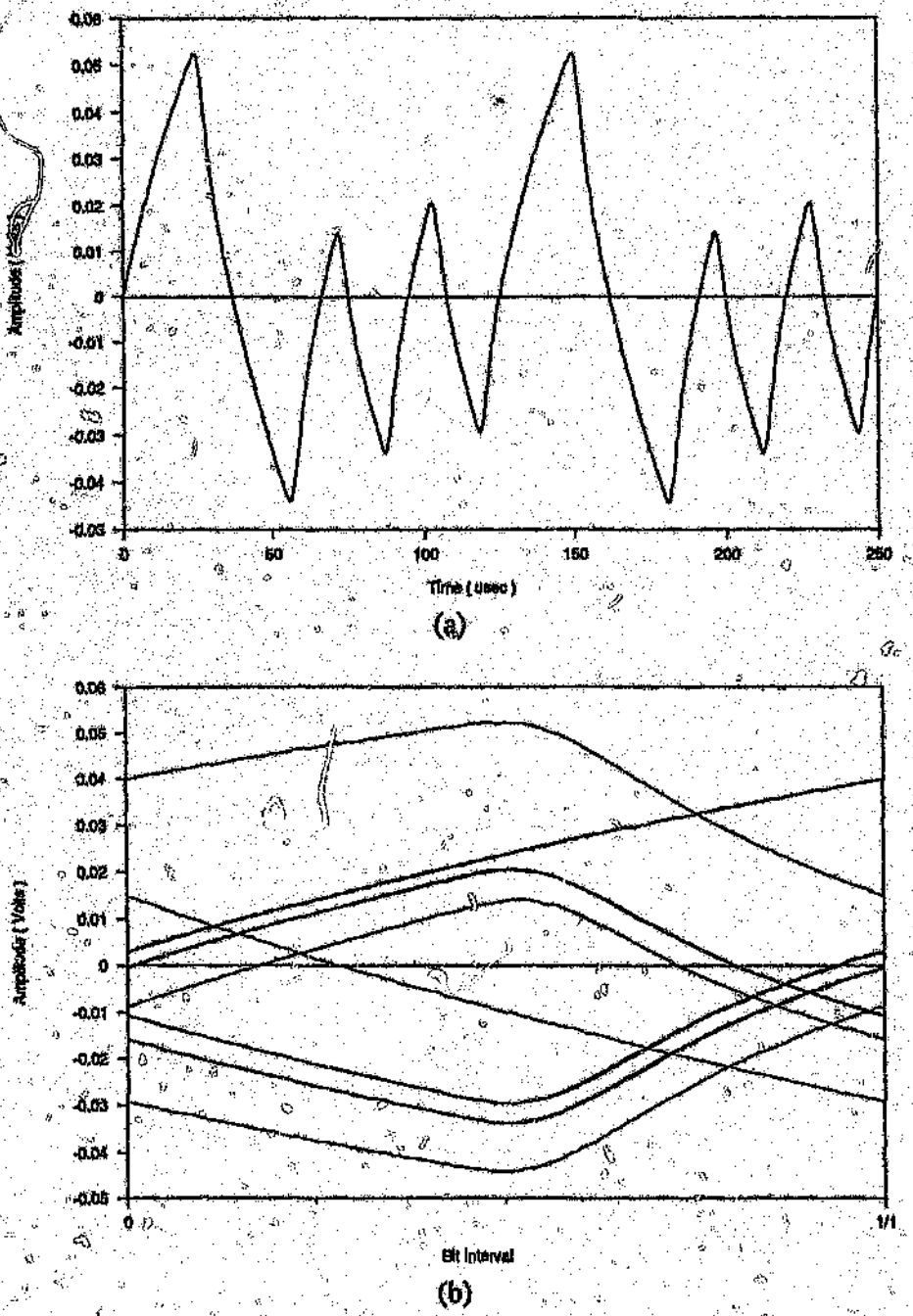

Figure 5.5 Experimentally generated pulse pattern (a) and eye diagram (b) of a two-section (2.01km of 22 AWG; 3.01km of 24 AWG) multigauge connection at 64 kbits/sec. The digitizer sampling frequency is 10MHz.

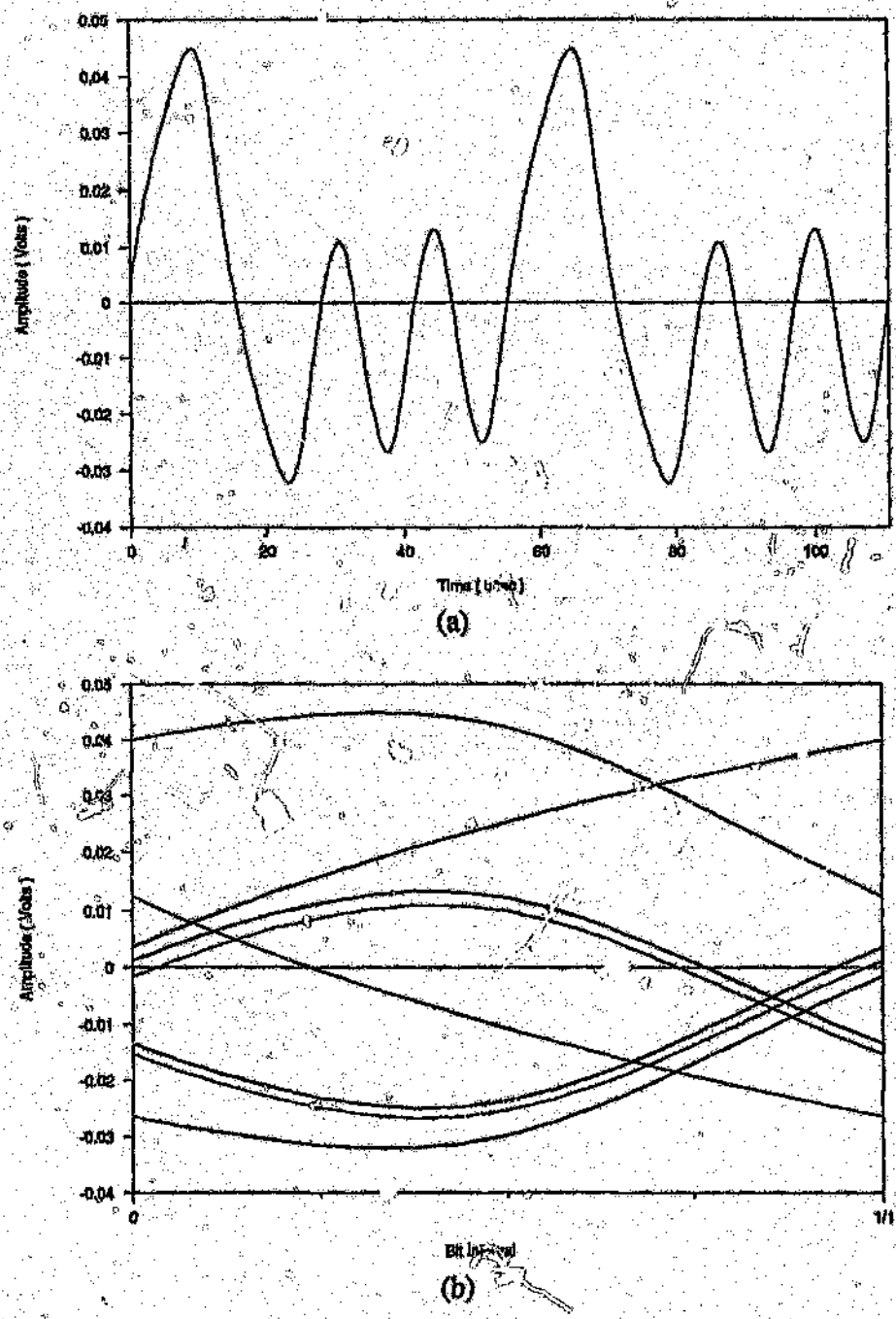

Figure 5.6 Computationally generated pulse pattern (a) and eye diagram (b) of a two-section (2.01km of 22 AWG; 3.01km of 24 AWG) multigauge connection at 144 kbits/sec. The number of points in the FFT is 128, and the fold frequency is 1152kHz.

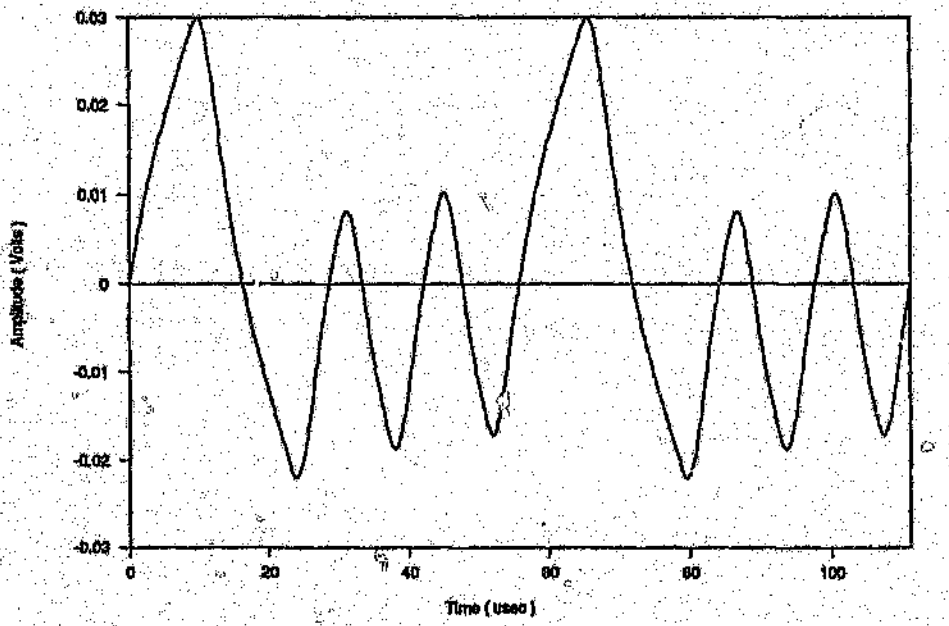

(a)

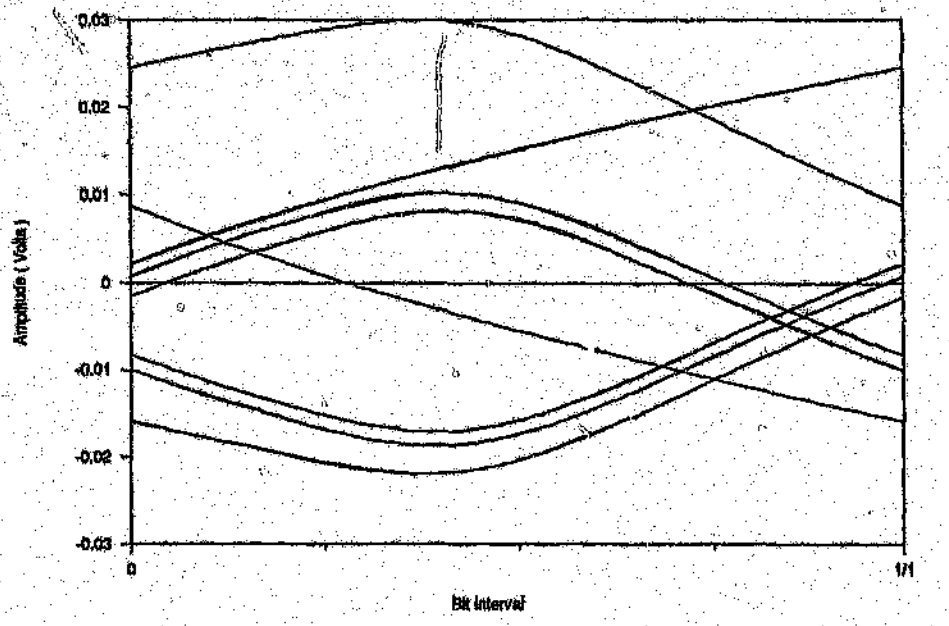

(b)

Figure 5.7 Experimentally generated pulse pattern (a) and eye diagram (b) of a two-section (2.01km of 22 AWG; 3.01km of 24 AWG) multigauge connection at 144 kbits/sec. The digitizer sampling frequency is 20MHz

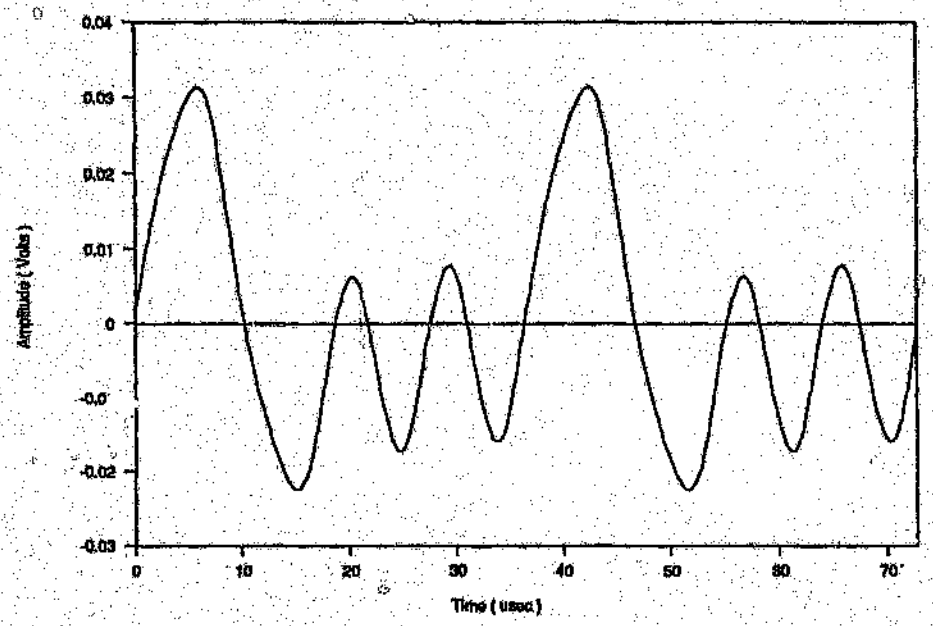

(a)

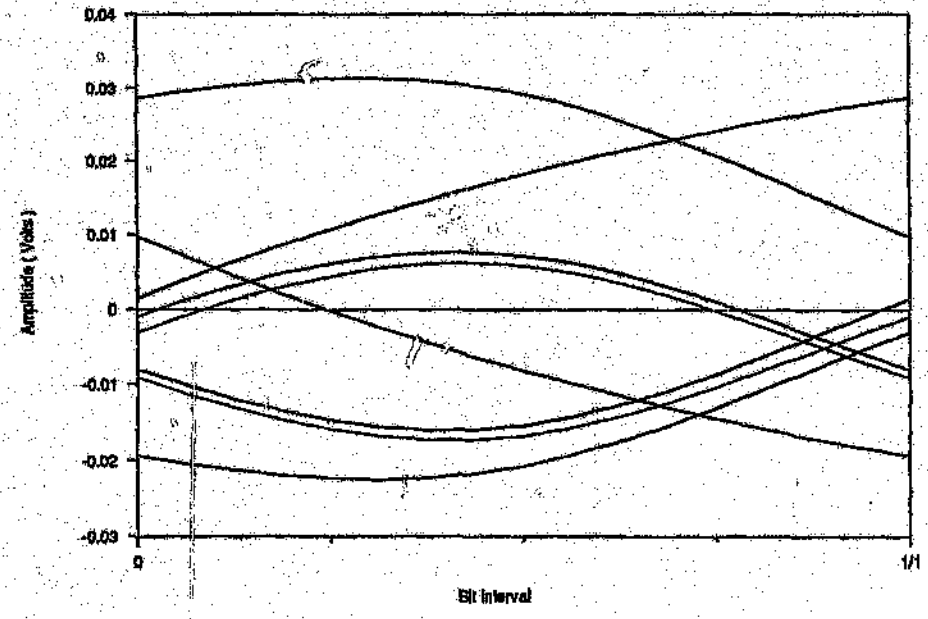

(b)

Figure 5.8 Computationally generated pulse pattern (a) and eye diagram (b) of a two-section (2.01km of 22 AWG; 3.01km of 24 AWG) multigauge connection at 216 kbits/sec. The number of points in the FFT is 128, and the fold frequency is 1728kHz.

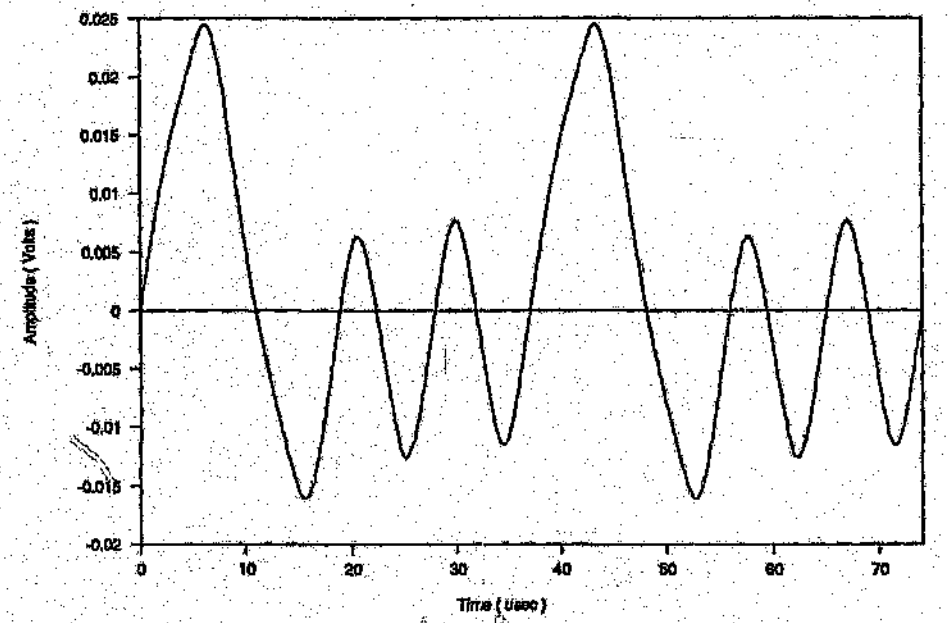

(a)

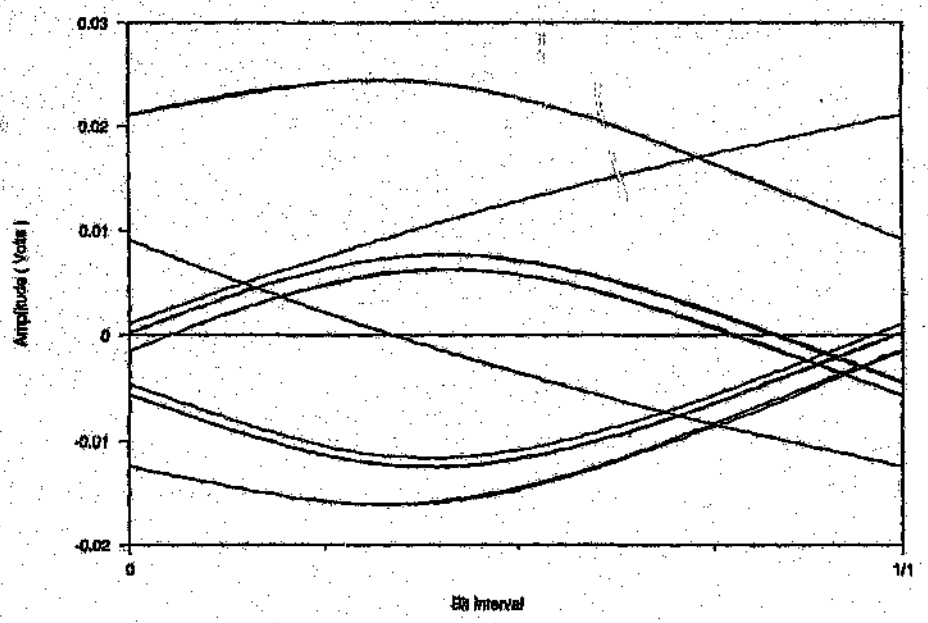

(b)

Figure 5.9 Experimentally generated pulse pattern (a) and eye diagram (b) of a two-section (2.01km of 22 AWG; 3.01km of 24 AWG) multigauge connection at 216 kbits/sec. The digitizer sampling frequency is 30MHz.

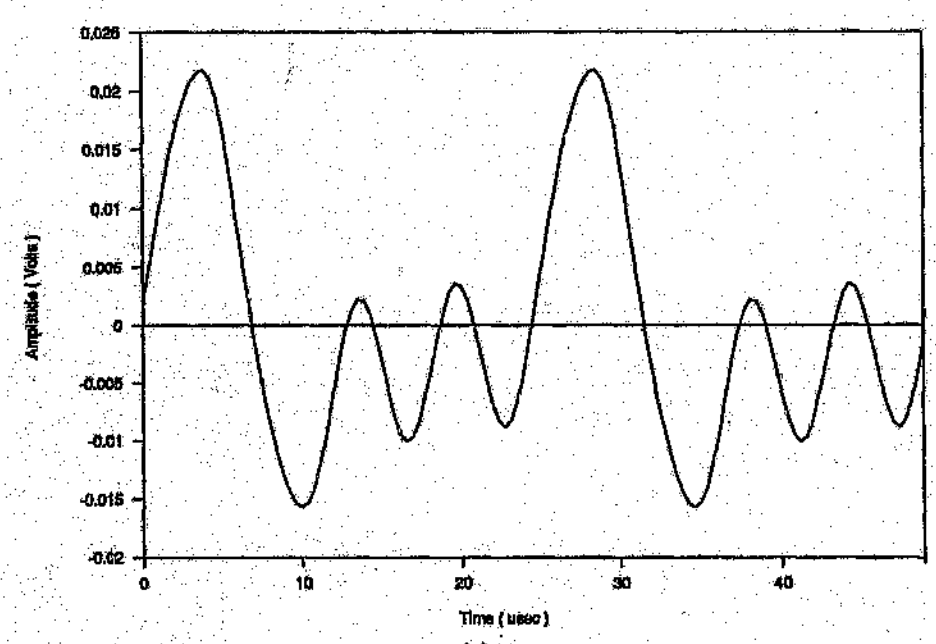

(a)

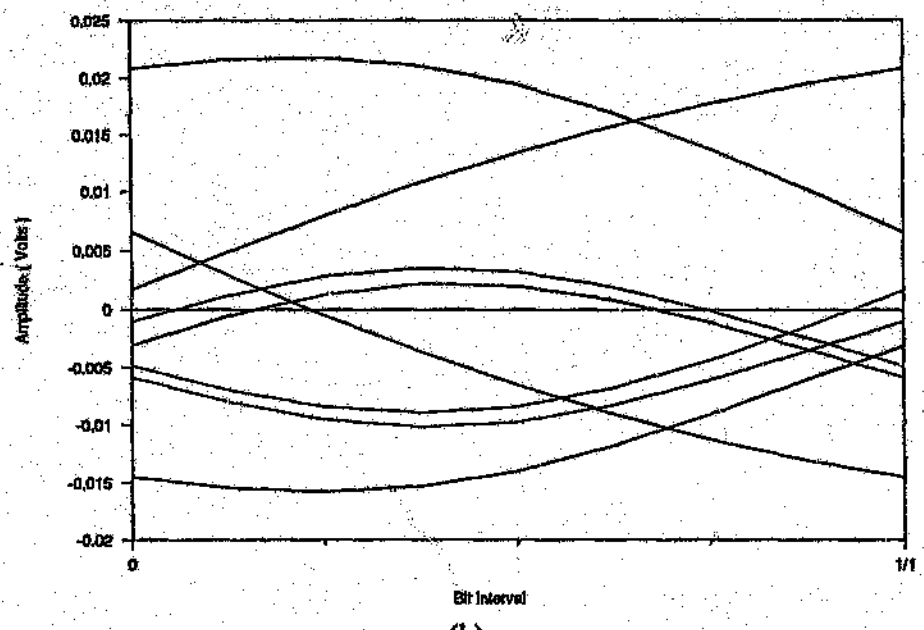

(b)

Figure 5.10 Computationally generated pulse pattern (a) and eye diagram (b) of a two-section (2.01km of 22 AWG; 3.01km of 24 AWG) multigauge connection at 324 kbits/sec. The number of points in the FFT is 64, and the fold frequency is 1296kHz.

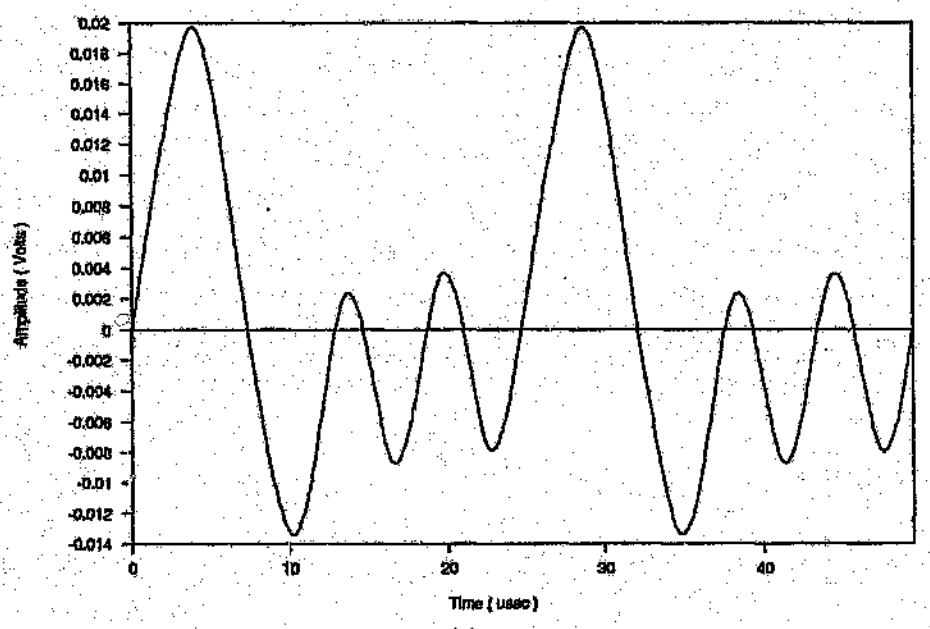

(a)

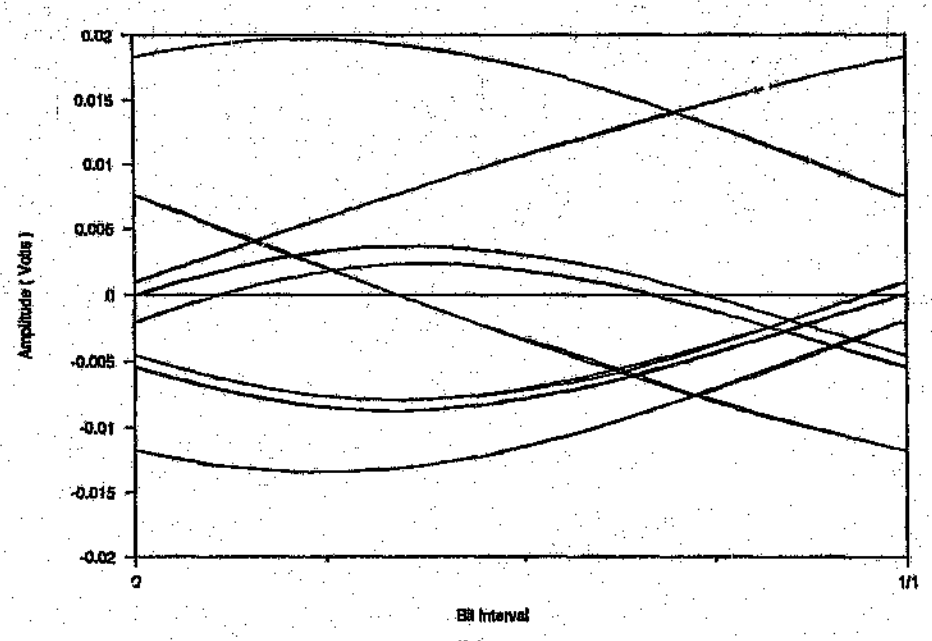

(b)

Figure 5.11 Experimentally generated pulse pattern (a) and eye diagram (b) of a two-section (2.01km of 22 AWG; 3.01km of 24 AWG) multigauge connection at 324 kbits/sec. The digitizer sampling frequency is 30MHz.

It can be seen from *Figure 5.4* through *Figure 5.11* that the results produced by the simulation package are indeed similar to the results obtained from measurements performed on real cables. In order to facilitate analysis, the received pulse pattern attenuation and eye opening values has been summarised and presented in *Table 5.2* for the four bit rates investigated. The table indicates a noticeable difference in the attenuation values especially on the lower bit rates. This difference is to be expected even though in *Chapter 4* it was shown that the attenuation and reflection coefficients results determined by measurement for each type for cable in the cable test bed are in close agreement with that predicted by the Cable Simulation Package. There are two reasons for expecting a difference.

Table 5.2 Pulse pattern attenuation and percentage eye opening results for case study 1

Bit Rate (kbits/sec)	Pulse Pattern Attenuation (dB)		Eye Opening (%)	
	Simulated	Measured	Simulated	Measured
64	-21.8	-26.3	29.5	27.0
144	-28.3	-31.7	27.5	24.4
216	-31.4	-33.9	27.8	24.4
324	-34.5	-35.6	24.5	18.4

The first and most important fact is that the experiments performed on the cable test bed did not achieve perfect matching conditions at each end of the cable connection. Although the ends were resistively matched, the reactive component required to obtain a "perfect" matched condition is comparable in magnitude to the "real" resistance especially at the lower bit rates investigated. The difference in the required matching impedance can be seen by comparing the data contained in *Table 5.1* to that of *Table 5.3*. The second reason is due to the fact that the cable test bed did not contain continuous lengths of more than 1km for each type of cable, and therefore the longer lengths for a particular type of cable section was obtained by joining pairs at the end of the cable with other pairs contained within the same cable. This type

of discontinuity may not at first seem important, but considering that each cable end has all its pairs split approximately 2m before reaching the distribution frame, it certainly must be taken into consideration especially if further studies are to be performed at much higher bit rates.

Table 5.3 Termination impedances required for perfect matching conditions for case study 1, given at half the bit rate frequency

Bit Rate (kbits/sec)	Half Bit Rate Frequency (kHz)	Generator End Impedance (Ω)	Receiver End Impedance (Ω)
64	32	$143 - j52$	$128 - j67$
144	72	$135 - j25$	$114 - j35$
216	108	$131 - j16$	$112 - j26$
324	162	$131 - j14$	$110 - j19$

The eye opening as predicted by the Cable Simulation Package and as measured from the cable test bed for the various line bit rates are similar in value as well as in the general pattern for each bit. In all the eye diagrams of *Figure 5.4* through *Figure 5.11*, the outer lines are formed by the *-1, +1, +1, -1* and *+1, -1, -1, +1* transitions. Although the *-1, +1, -1* and *+1, -1, +1* transitions further reduces the eye opening, the main cause of the eye closure is due to the long decaying tail of the *+1, +1, -1* transition. The eye opening would degrade even further if the situation occurred when more than two consecutive *+1*'s were to be transmitted. The Bipolar Line code thus has the disadvantage that it is not d.c b l, resulting in the popularity of other line codes such as Alternate Mark I... ...on (AMI) which maintains a balanced d.c voltage on the line. A popular method of reducing this intersymbol interference is to shape the transmitted pulses in such a way that the interference is minimized. This correction is provided by filters otherwise known as equalizers.

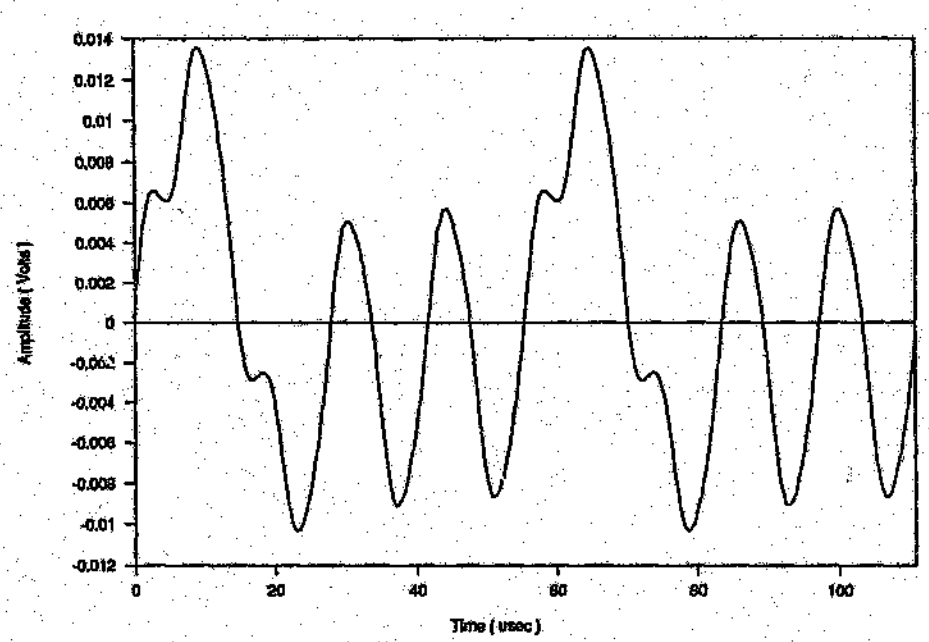

(a)

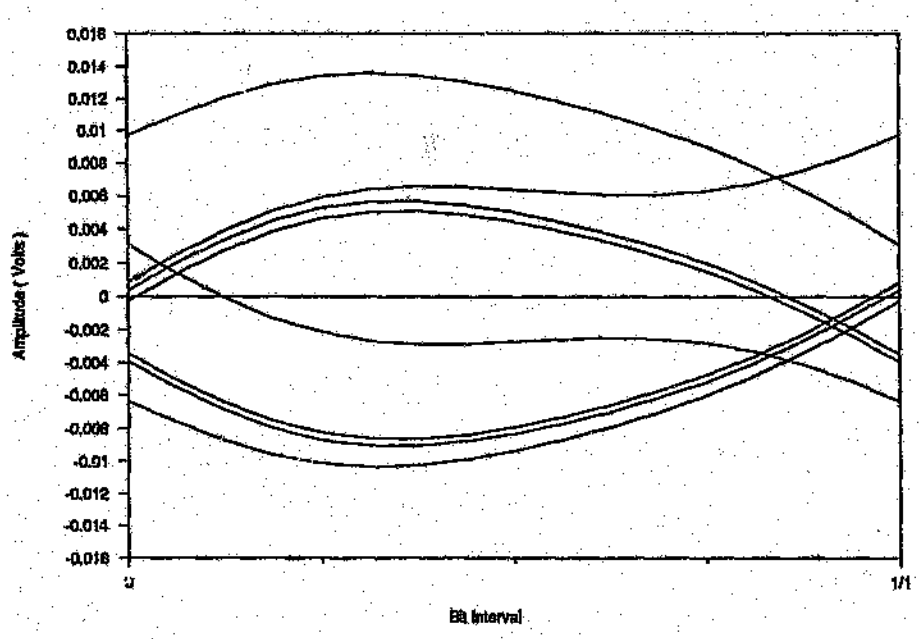

(b)

Figure 5.12 Computationally generated pulse pattern (a) and eye diagram (b) of a two-section (2.01km of 22 AWG; 3.01km of 24 AWG) multigauge connection at 144kbits/sec, using the *Tophat* window function for pulse shaping.

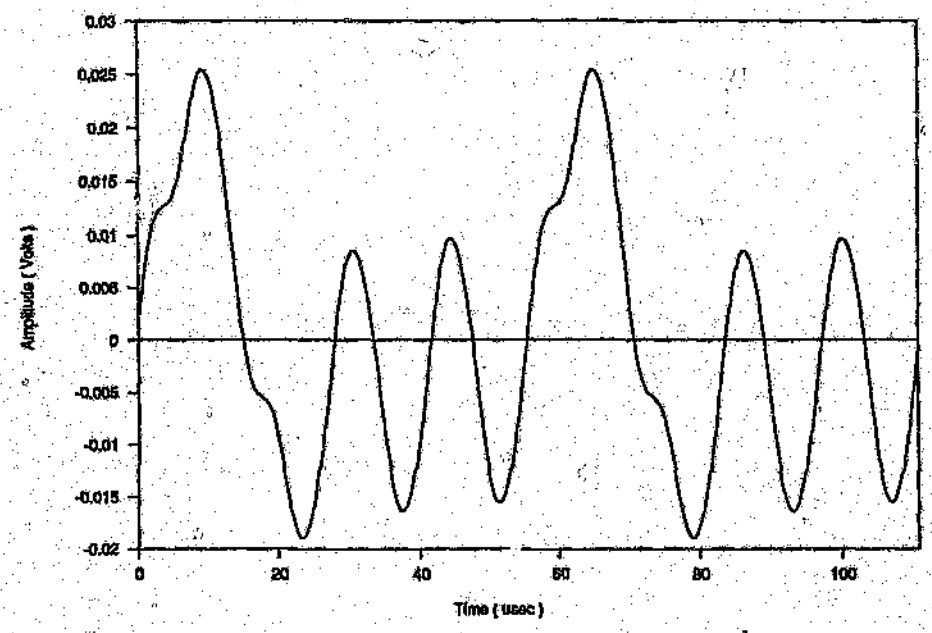

(a)

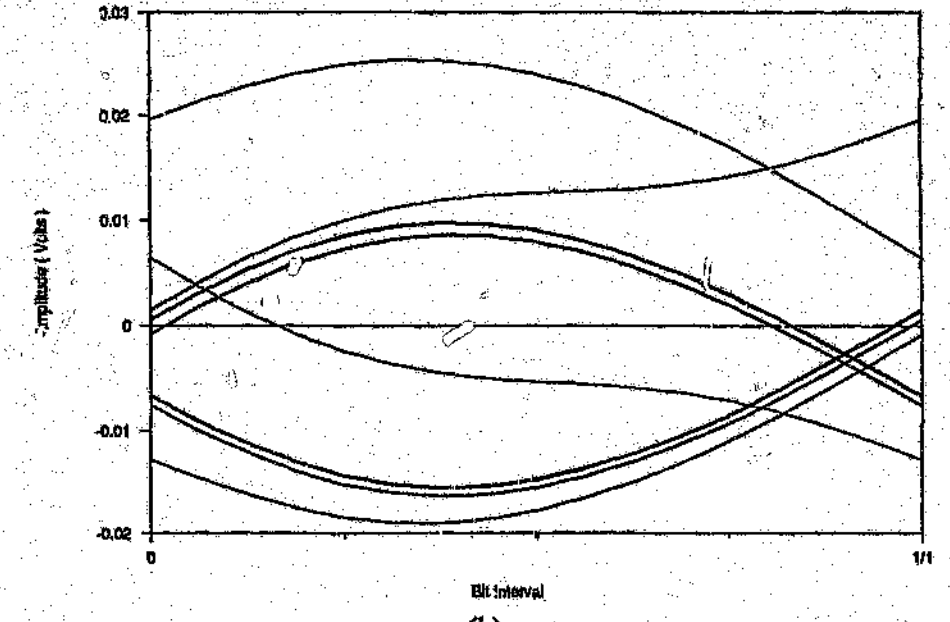

(b)

Figure 5.13 Computationally generated pulse pattern (a) and eye diagram (b) of a two-section (2.01km of 22 AWG; 3.01km of 24 AWG) multigauge connection at 144 kbits/sec, using the *Hanning* window function for pulse shaping.

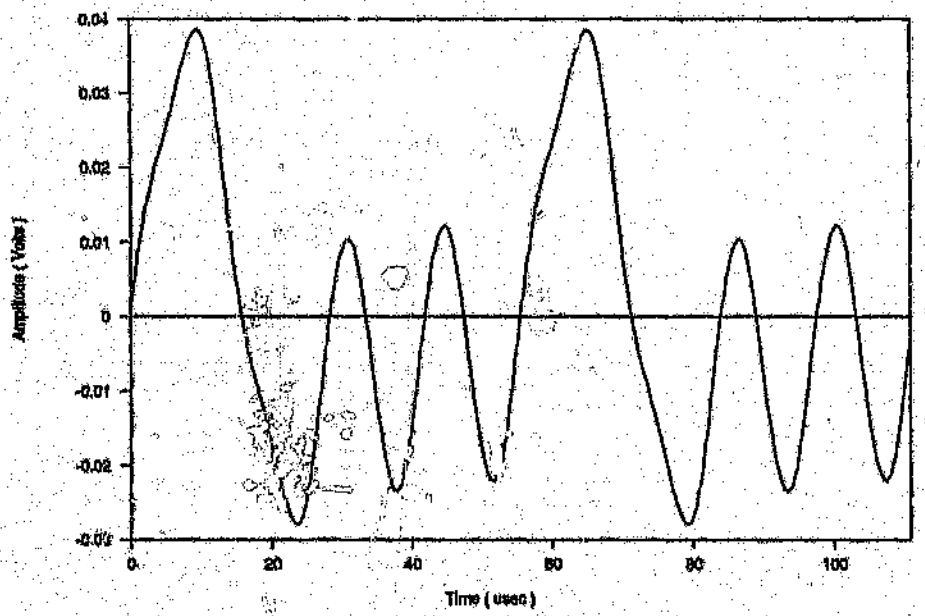

(a)

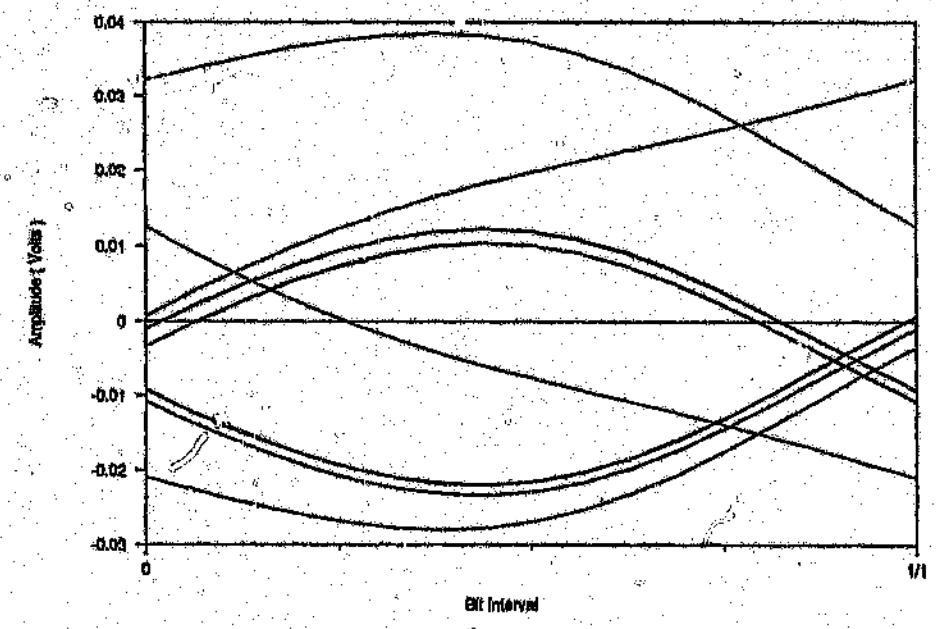

(b)

Figure 5.14 Computationally generated pulse pattern (a) and eye diagram (b) of a two-section (2.01km of 22 AWG; 3.01km of 24 AWG) multigauge connection at 144 kbits/sec, using the *Hamming* window function for pulse shaping.

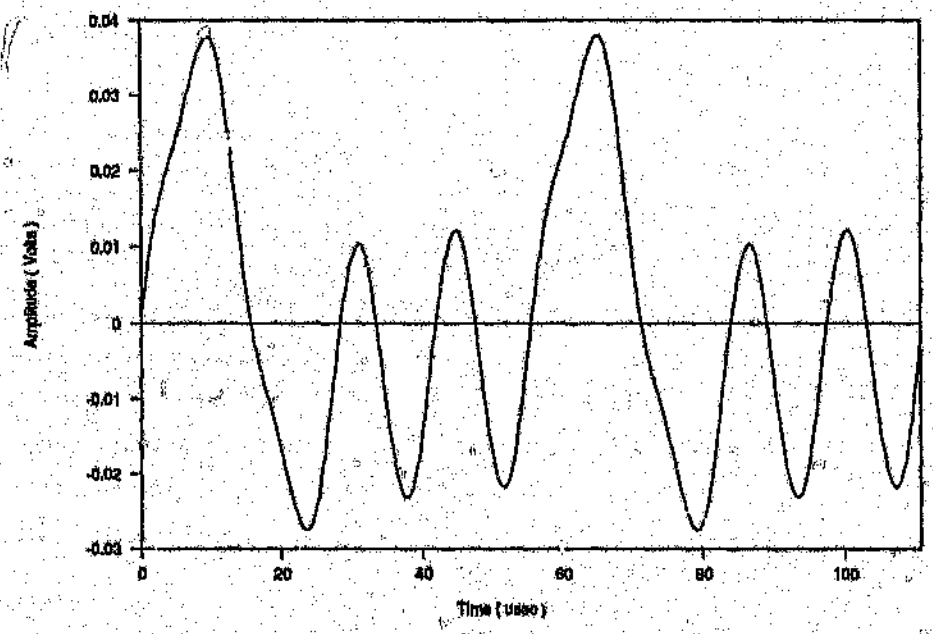

(a)

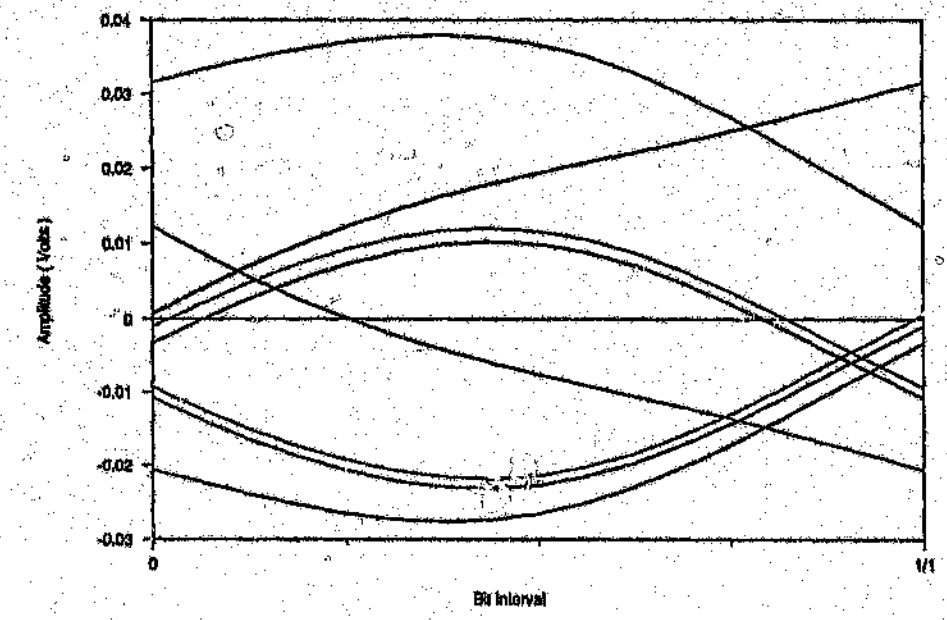

(b)

Figure 5.15 Computationally generated pulse pattern (a) and eye diagram (b) of a two-section (2.01km of 22 AWG; 3.01km of 24 AWG) multigauge connection at 144 kbits/sec, using the *Raised Cosine* window function for pulse shaping.

The pulse propagation program ***F-Duplex***, has the capability of providing several windows for pulse shaping, namely:

(a) hanning,
(b) raised cosine,
(c) hamming,
(d) tophat, and
(e) rectangular window.

The diagrams of *Figure 5.12* to *Figure 5.15* illustrates the received pulse pattern at the receiver end and its corresponding eye diagram for the connection of *Figure 5.3* for the case when the line bit rate is 144kbits/sec and different pulse shaping techniques are applied to the transmitted Bipolar code. Due to the non-availability of the pulse shaping filter equipment required, there are no experimentally measured results available.

Table 5.4 summarises the eye opening for the various pulse shaping functions as predicted by the Cable Simulation Package for a line bit rate of 144kbits/sec.

Table 5.4 Eye opening results obtained from several pulse shaping functions for a line bit rate of 144kbits/sec

Window Function	Eye Opening (%)
Rectangular	27.5
Hanning	31.0
Raised Cosine	27.9
Hamming	27.6
Tophat	33.3

From the eye diagrams of *Figure 5.12* through *Figure 5.15*, it can be seen that the effect of the pulse shaping function used is not only aimed at increasing the eye

opening, but also has the effect to cause the time interval at the maximum eye opening to be enlarged. This can easily be seen in *Figure 5.12* and *Figure 5.13* for the case of the Tophat and the Hanning window functions.

5.2.2 Case Study 2

This case study is concerned with a cable connection consisting of three different cable sections as illustrated in *Figure 5.16*. The total length of the connection is 5.9km, where section one comprises a length of 2.01km of gauge type 22; section two comprises a length of 1.86km of gauge type 26, and finally section three comprises a length of 2.01km of gauge type 24.

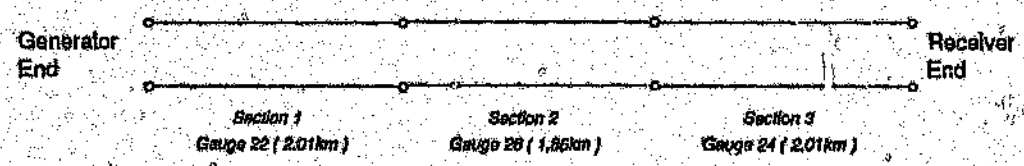

Figure 5.16 Case Study 2 ; Three-section multigauge cable connection (*Total length = 6km*)

As for the case study of *section 5.2.2*, the experimental results were obtained under the condition that the cable connection was only resistively matched at both ends. The input impedance values used and the impedance values required to obtain a perfect match are tabulate in *Table 5.5* and *Table 5.6* for the four line rates investigated.

Table 5.5 Termination impedances for case study 2, given at half the bit rate frequency

Bit Rate (kbits/sec)	Half Bit Rate Frequency (kHz)	Generator End Impedance (Ω)	Receiver End Impedance (Ω)
64	32	146 - *j* 0	128 - *j* 0
144	72	135 - *j* 0	114 - *j* 0
216	108	129 - *j* 0	112 - *j* 0
324	162	130 - *j* 0	110 - *j* 0

Table 5.6 Termination impedances required for perfect matching conditions for case study 2, given at half the bit rate frequency

Bit Rate (kbits/sec)	Half Bit Rate Frequency (kHz)	Generator End Impedance (Ω)	Receiver End Impedance (Ω)
64	32	143 - *j* 48	128 - *j* 67
144	72	135 - *j* 23	114 - *j* 35
216	108	131 - *j* 16	112 - *j* 26
324	162	131 - *j* 13	110 - *j* 19

The cable connection of *Figure 5.16* was excited by a binary bit pattern consisting of 16 bits for all four line bits rates investigated. The binary pattern used was the same as that used for case study 1 of *section 5.2.2*, namely,

1100101011001010

which was encoded to a Bipolar code with a rectangular window function for pulse shaping. The results obtained from the cable simulation package and that measured over real cables for the connection are presented in *Figure 5.17* through *Figure 5.24*. Each figure illustrates the received pulse pattern and its corresponding eye diagram at the receiver end.

It can be seen from *Figure 5.17* through *Figure 5.24* that the results produced by the Cable Simulation package are indeed similar to the results obtained from the measurements performed on real cables even though in this case the eye opening is minimal. The received pulse pattern attenuation and eye opening values are tabulated in *Table 5.7* for the four line rates investigated. The higher attenuation recorded for the experimental data is again due to the imperfect matching conditions achieved. The eye opening as predicted by the cable simulation package and as measured from the cable test bed for the various line bit rates are similar not only in shape but also in the value of the percentage eye opening. The reason for the eye closure is clearly seen to be the decaying tail of the *+1, +1, -1* transition.

Table 5.7 Pulse pattern attenuation and percentage eye opening results for case study 2

Bit Rate (Kbits/sec)	Pulse Pattern Attenuation (dB)		Eye Opening (%)	
	Simulated	Measured	Simulated	Measured
64	-29.7	-33.8	2.3	1.5
144	-38.4	-41.3	1.3	1.9
216	-42.7	-44.5	4.4	4.1
324	-46.8	-47.2	7.4	5.7

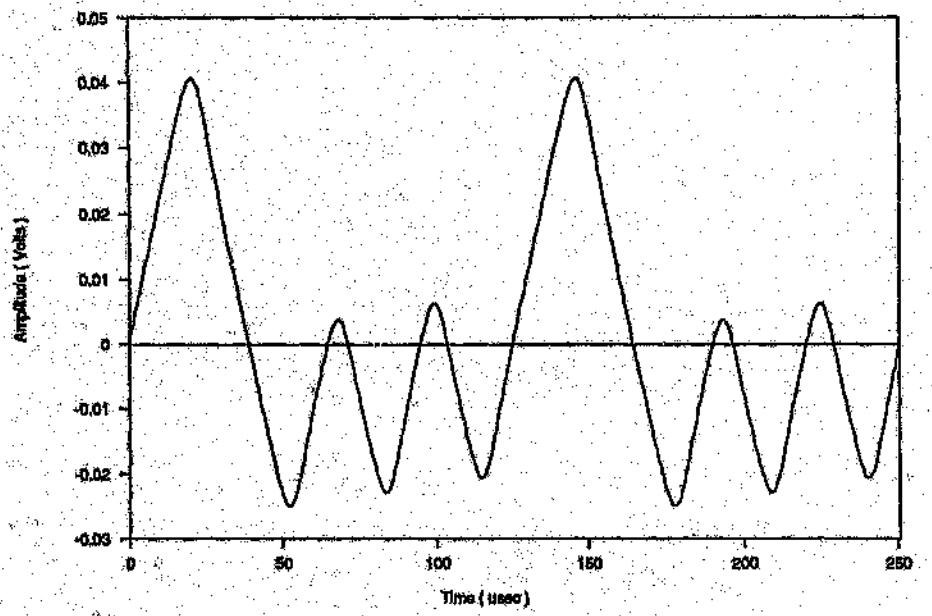

(a)

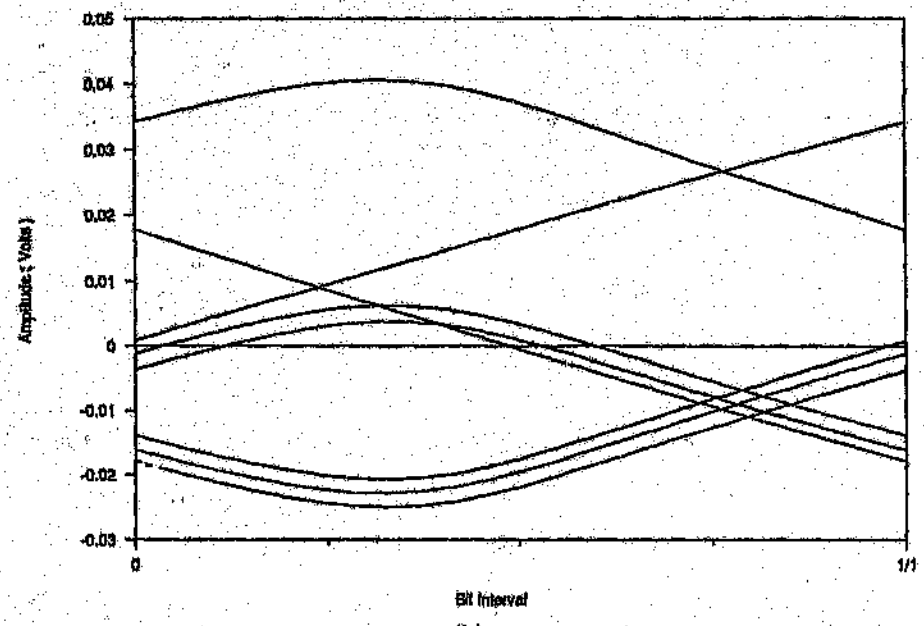

(b)

Figure 5.17 Computationally generated pulse pattern (a) and eye diagram (b) of a three-section (2.01km of 22 AWG; 1.86km of 26 AWG; 2.01km of 24 AWG) multigauge connection at 64 kbits/sec. The number of points in the FFT is 256, and the fold frequency is 1024kHz.

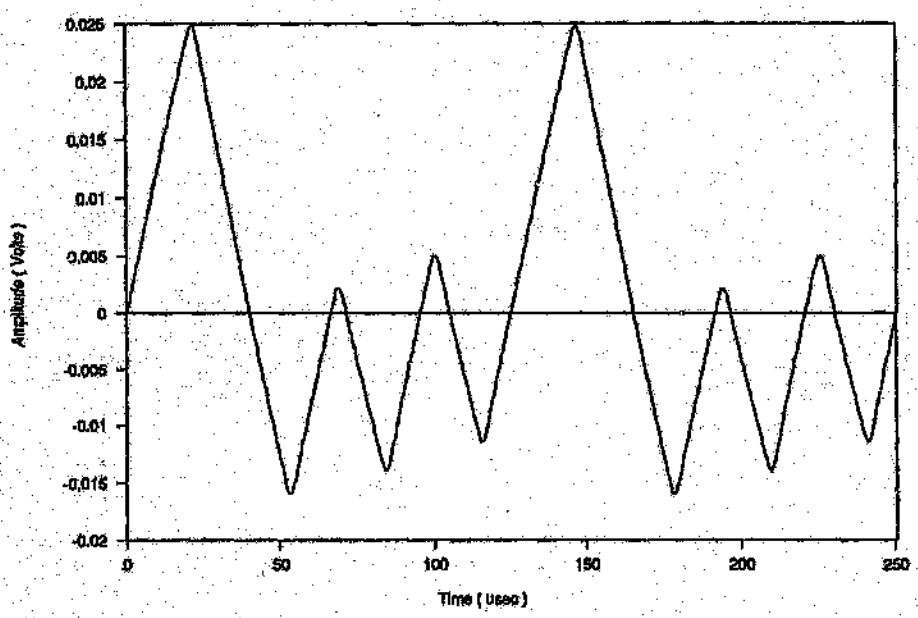

(a)

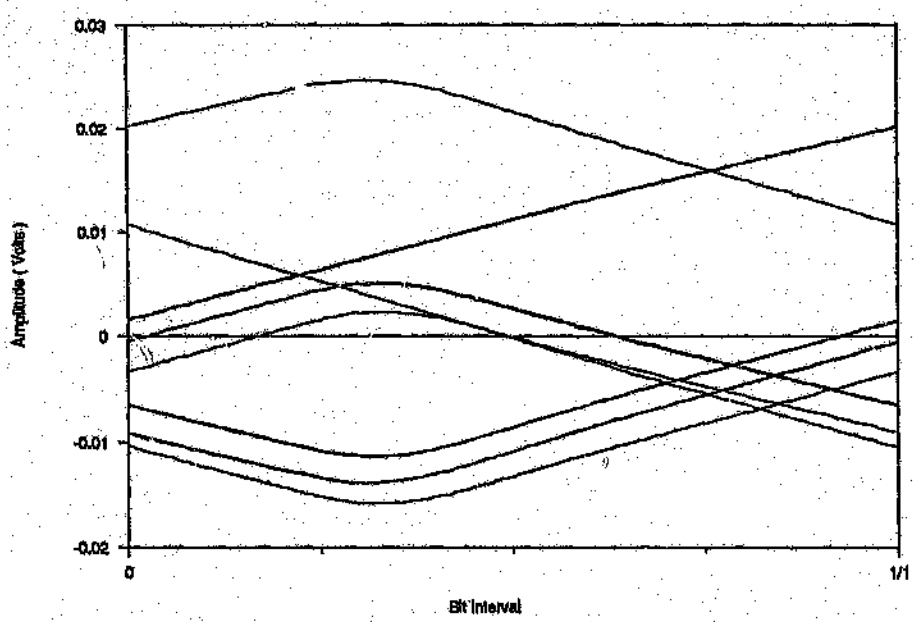

(b)

Figure 5.18 Experimentally generated pulse pattern (a) and eye diagram (b) of a three-section (2.01km of 22 AWG; 1.86km of 26 AWG; 2.01km of 24 AWG) multi[illegible]ge connection at 64 kbits/sec. The digitizer sampling frequency is 10MHz.

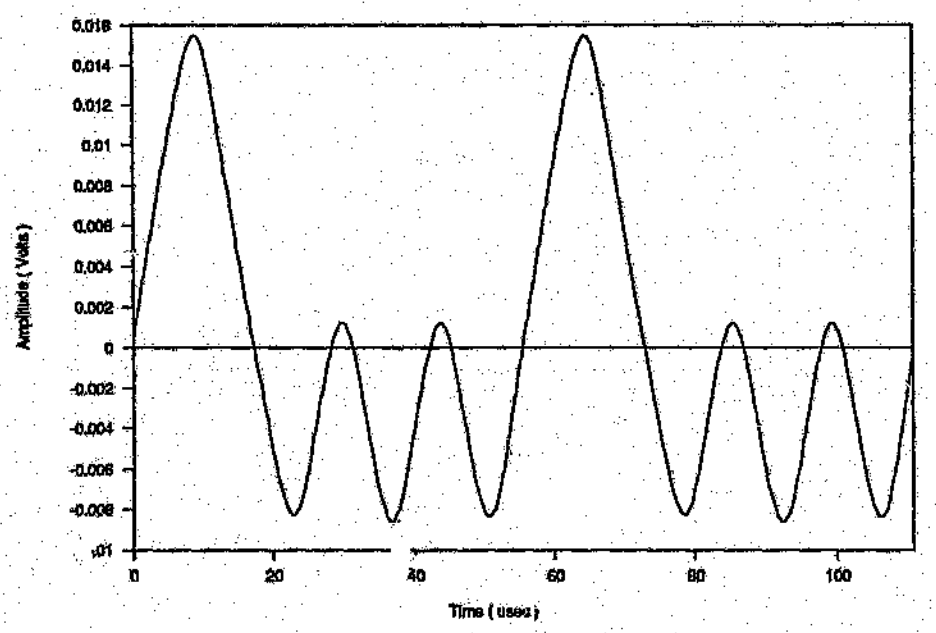

(a)

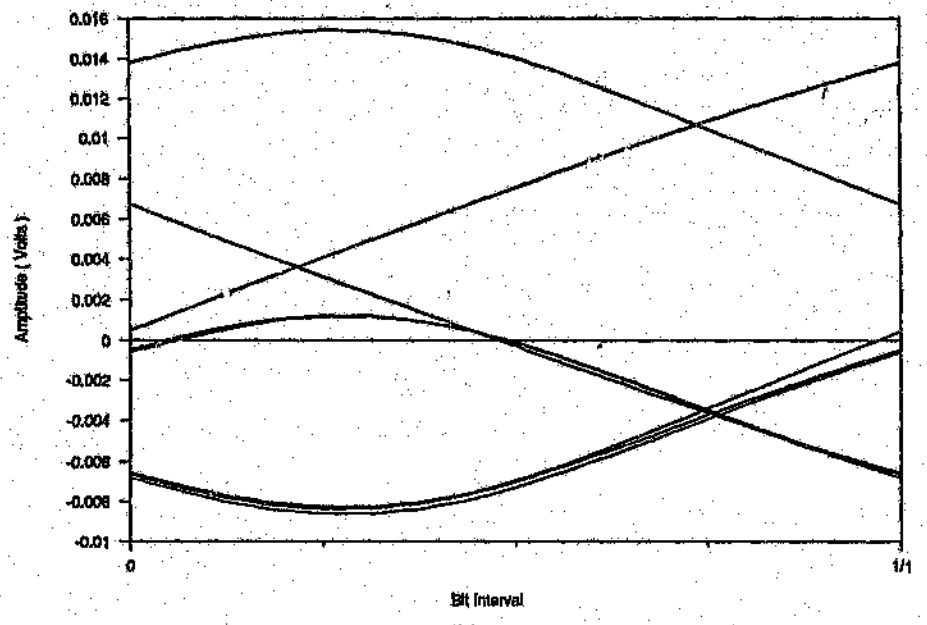

(b)

Figure 5.19 Computationally generated pulse pattern (a) and eye diagram (b) of a three-section (2.01km of 22 AWG; 1.86km of 26 AWG; 2.01km of 24 AWG) multigauge connection at 144 kbits/sec. The number of points in the FFT is 128, and the fold frequency is 1152kHz.

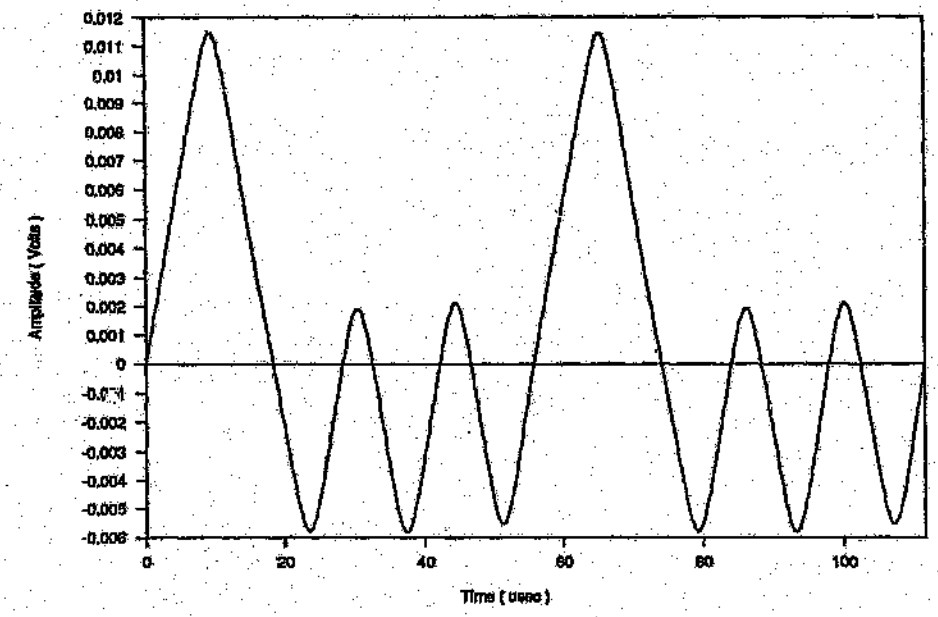

(a)

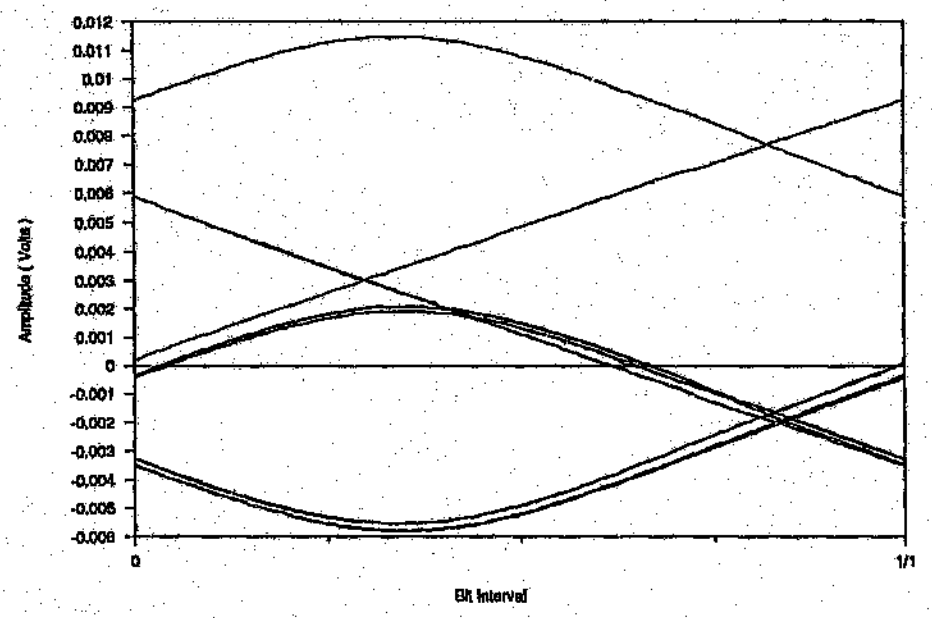

(b)

Figure 5.20 Experimentally generated pulse pattern (a) and eye diagram (b) of a three-section (2.01km of 22 AWG; 1.86km of 26 AWG; 2.01km of 24 AWG) multigauge connection at 144 kbits/sec. The digitizer sampling frequency is 20MHz.

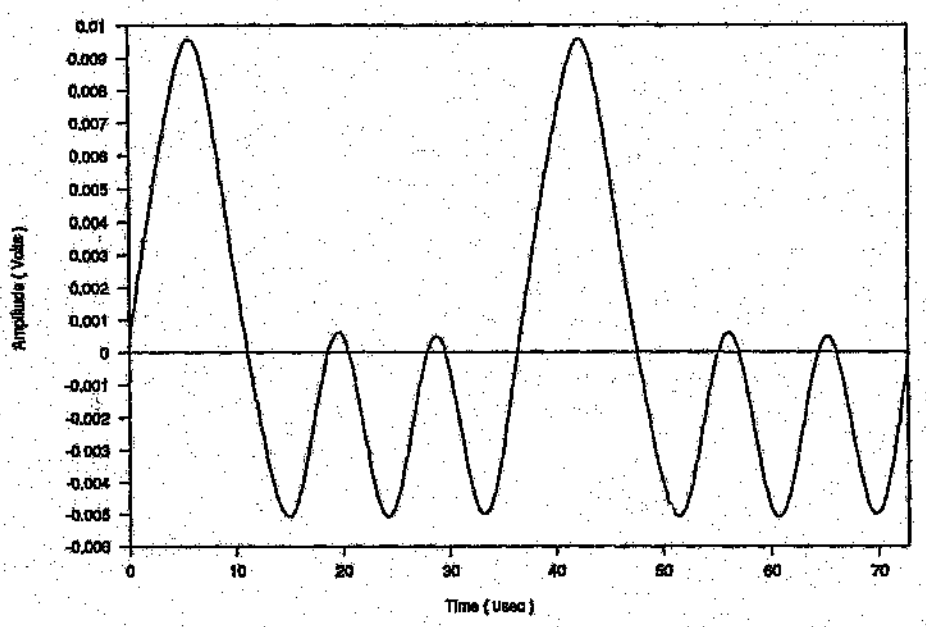

(a)

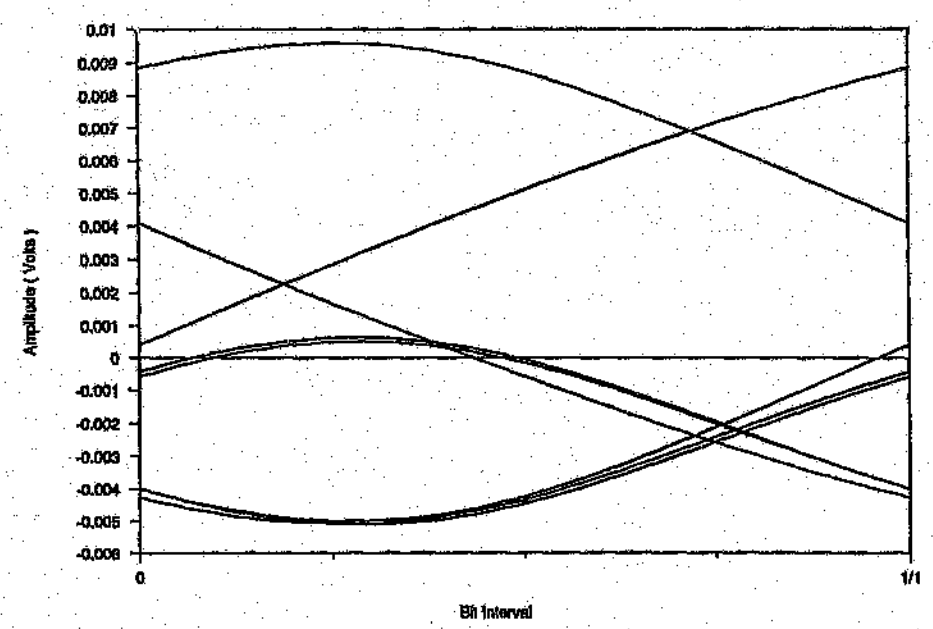

(b)

Figure 5.21 Computationally generated pulse pattern (a) and eye diagram (b) of a three-section (2.01km of 22 AWG; 1.86km of 26 AWG; 2.01km of 24 AWG) multigauge connection at 216 kbits/sec. The number of points in the FFT is 128, and the fold frequency is 1728kHz.

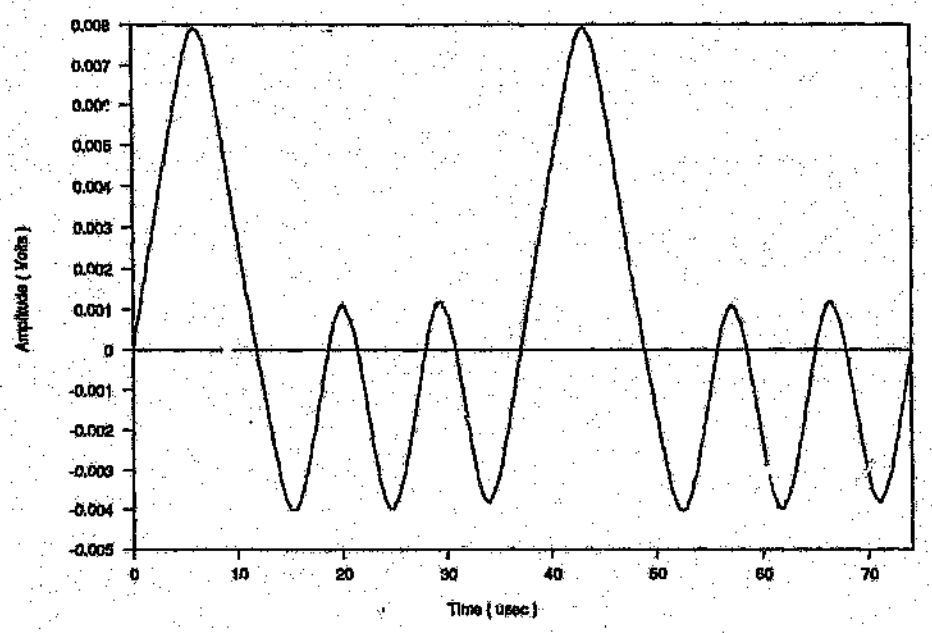

(a)

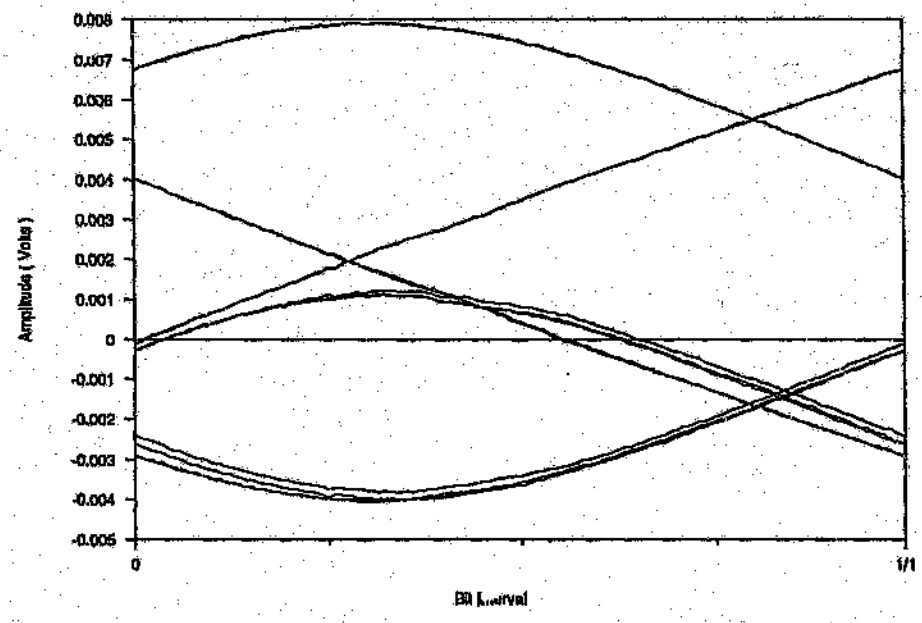

(b)

Figure 5.22 Experimentally generated pulse pattern (a) and eye diagram (b) of a three-section (2.01km of 22 AWG; 1.86km of 26 AWG; 2.01km of 24 AWG) multigauge connection at 216 kbits/sec. The digitizer sampling frequency is 30MHz.

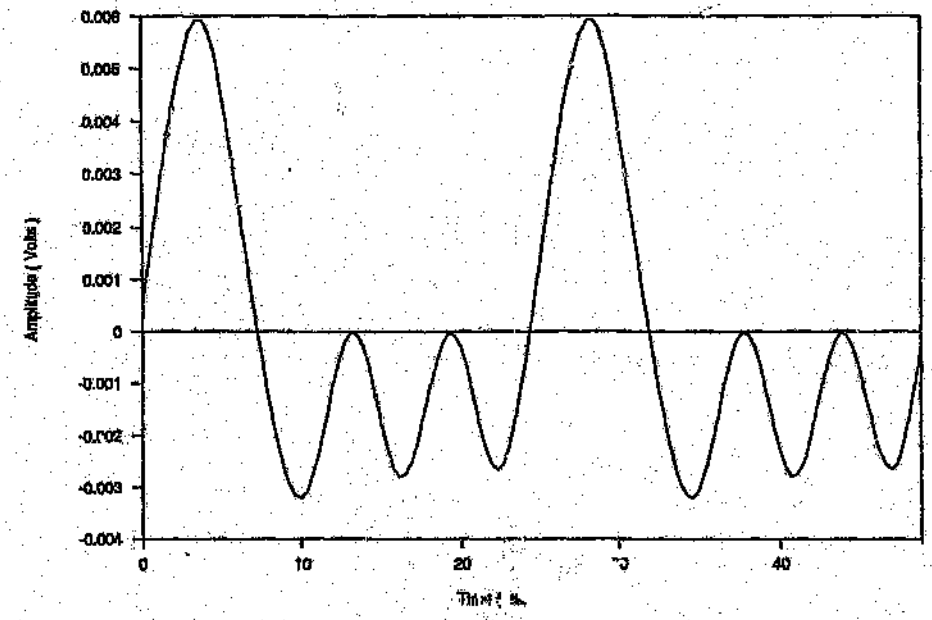

(a)

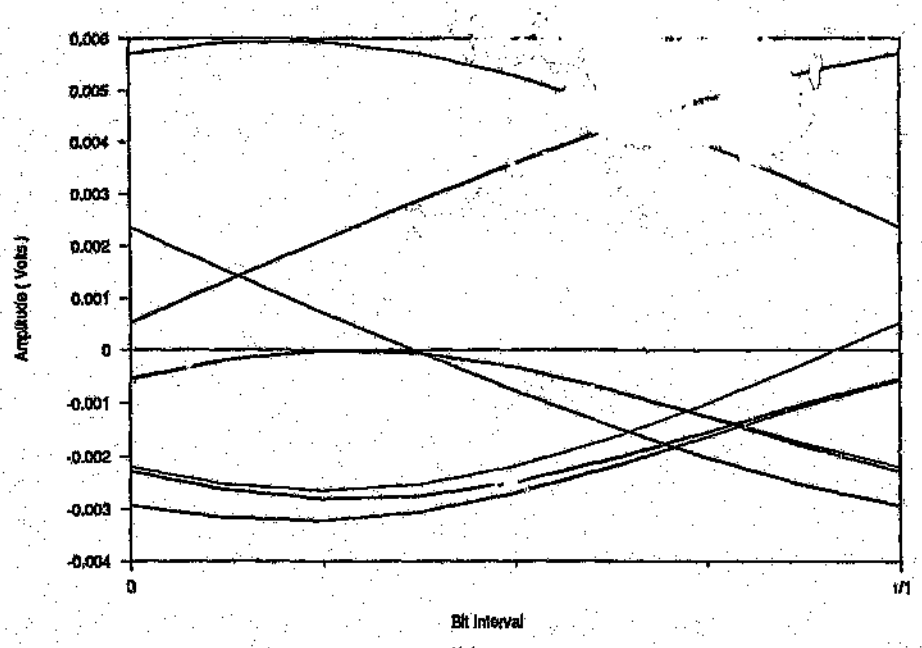

(b)

Figure 5.23 Computationally generated pulse pattern (a) and eye diagram (b) of a three-section (2.01km of 22 AWG; 1.86km of 26 AWG; 2.01km of 24 AWG) multigauge connection at 324 kbits/sec. The number of points in the FFT is 64, and the fold frequency is 1296kHz.

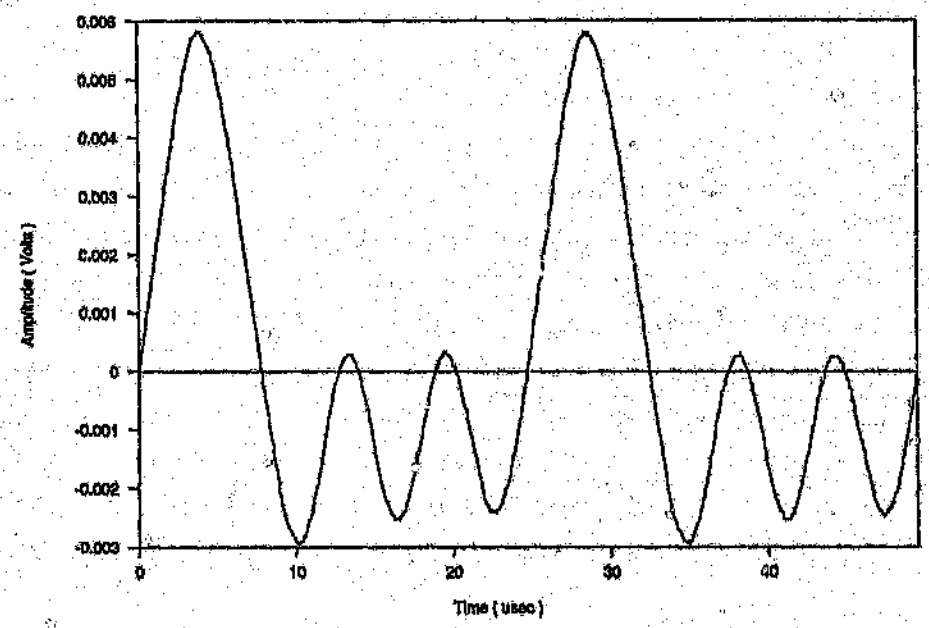

(a)

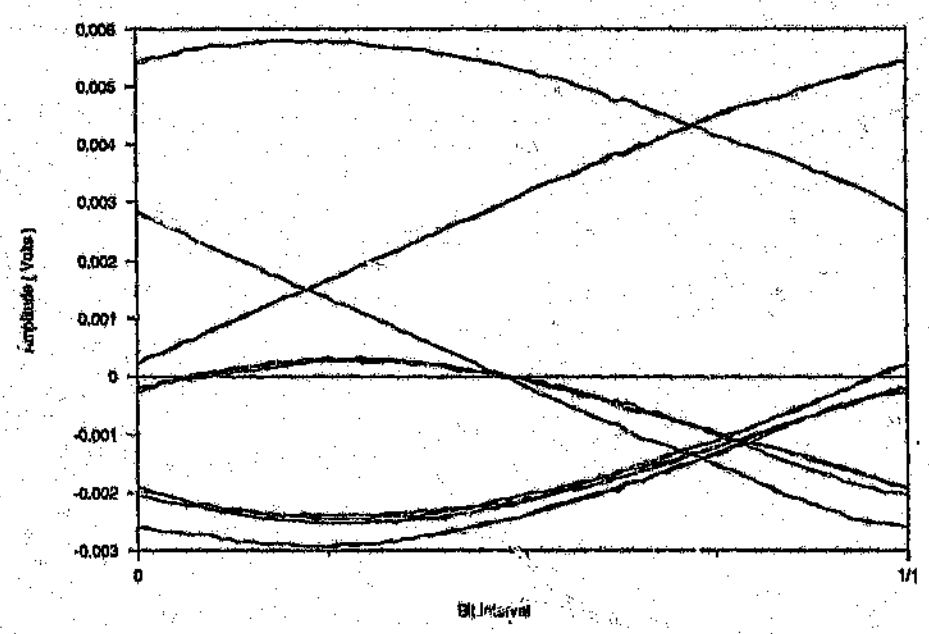

(b)

Figure 5.24 Experimentally generated pulse pattern (a) and eye diagram (b) of a three-section (2.01km of 22 AWG; 1.86km of 26 AWG; 2.01km of 24 AWG) multigauge connection at 324 kbits/sec. The digitizer sampling frequency is 30MHz.

5.3 Conclusions

This chapter has presented the results obtained from the pulse propagation program of the Cable Simulation Package and those measured on real cable connections. The emphasis has not been to identify cable connections that provide adequate transmission capabilities, but to illustrate the pulse propagation characteristics for diverse transmission conditions irrespective of the cable connection used. The pulse patterns and eye diagrams results presented for the two case studies is indicative of the correlation obtained in the shape of the pulse patterns between the simulation results and the measured results even though the attenuation values differ somewhat. The single pulse response has illustrated the effect that the long decaying tails of the pulses have on the eye closure as well as the effect of the signals that are reflected back to the pulse sending end. The results of different pulse shaping functions has also been presented in order to illustrate the benefits that can be derived.

Chapter 6

CONCLUSION

In this dissertation, the transmission and implementation issues pertaining to the U-interface in order to provide the basic-access of 2B + D channels on the existing subscriber loop has been the topic of research and discussion. The challenge in South Africa is to identify the relevant characteristics of the cable plant, and to select the appropriate approach for the U-interface circuitry. Due to the diversity of the loop plant, exhaustive experimental analysis can be virtually excluded as a possible approach of establishing performance capabilities. The means of establishing this performance capability is by computer simulation.

A computer simulation package that can be used for modelling pulse transmission over multigauge subscriber loops has been described. The model used for each section incorporates skin, proximity, and eddy current effects, and is configured to allow forward and backward travelling waves to be clearly identified. The simulator thus allows important quantities such as near end echo and overall transmission distortion to be predicted. The simulation package is not without limitations. The models do not take into account any impairment found on real cables, such as crosstalk, echo, impulse noise, intersymbol interference, etc. It is also limited in the frequency domain due to the simulation representing the waveforms, transfer functions and other pertinent parameters by only 256 fourier harmonics.

An experimental facility was designed around a cable test bed available in the laboratory. The first experimental facility is used to characterize the different cables according to the well known transmission line equations. The results obtained from this was used to set up the 'cable library' contained in the Cable Simulation Package as well as to verify the primary parameters, secondary parameters, transfer functions, and reflection coefficients of the various cables and cable connections. The second facility is used to analyse the pulse propagation patterns and characteristics. The measured results obtained were compared against the results predicted by the simulation package by means of pulse pattern and eye diagram plotting functions.

The measurement facility was as far as possible automated by making use of computer controlled equipment for direct setup of the experiments, data transfer, and analysis. Extensive programming was required in order to achieve the level of automation. These programs are menu driven in order to facilitate user operation.

The data required by the 'cable library' has been determined from the input impedance measurements performed on the various cables in the test bed. The primary parameters, secondary parameters, transfer functions and reflection coefficients predicted by the Cable Simulation Package are in close agreement with that as was obtained from the characterization measurements performed. These results thus indicates the validity of the well established transmission line model, together with the correction factors for skin effect, proximity effect, and eddy current effects. It must again be mentioned that the model for the proximity effect correction factor used only takes into account the proximity of one conductor on another, whereas in real cables, each conductor is closely surrounded by many other conductors. This approximation has had minimal effects in the frequency range used, but should be investigated further if the Cable Simulation Package is extended to much higher frequencies.

The results obtained from the pulse propagation program of the Cable Simulation Package and those measured on real cable connections are in close agreement not only in value but also in the actual shapes of the wave patterns. The emphasis has not been to identify cable connections that provide adequate transmission capabilities, but to illustrate the pulse propagation characteristics for diverse transmission conditions irrespective of the cable connection used. The pulse patterns and eye diagrams results presented for the two case studies is indicative of the correlation obtained in the shape of the pulse patterns between the simulation results and the measured results even though the attenuation values differ somewhat. The single pulse response has illustrated the effect that the long decaying tails of the pulses have on the eye closure as well as the effect of the signals that are reflected back to the pulse sending end. The results of different pulse shaping functions has also been presented in order to illustrate the benefits that can be derived.

In conclusion, it is clear that additional work can improve the capabilities of the cable simulator package. A noise model which would account for most of the impairments found to exist on real cables would be of value in assessing the pen-

etration capabilities of several coding schemes. A module which would perform post-equalization would also be useful. Additional line transmission codes can also be easily implemented in order to provide a greater selection. The cable simulation package in its present form can be successfully used by users in general with the confidence that the results predicted are representative of the performance that can be achieved in real multigauge connections.

REFERENCES

[1] Lin, N.S., and Tzeng, C.P.J., **"Full-Duplex Data Over Local Loops,"** *IEEE Communications Magazine*, Vol. 26, No. 2 (Feb. 1988), pp. 31-42.

[2] Guinea, J.A., Stacey, C., and Batruni, R., **"Digital Transmission in the Subscriber Loop,"** *IEEE Magazine on Circuits and Devices*, (Sep. 1986), pp. 14-28.

[3] Rous, R.F., and Weston, J.D., **"Subscriber Cable Performance Evaluation,"** *Electrical Communications*, Vol. 56, No. 1 (1981), pp. 80-86.

[4] Ahamed, S.V., **"Simulation and Design Studies of Digital Subscriber Lines,"** *Bell System Technical Journal* Vol. 61, No. 6 (July - Aug. 1982), pp. 1003-1076.

[5] Komiya, R., Yoshida, K., and Tamaki, N., **"The Loop Coverage Comparison Between TCM and Echo Canceller Under Various Noise Considerations,"** *IEEE Transactions on Communications*, Vol. COM-34, No. 11 (Nov. 1986), pp. 1058-1067.

[6] Messerschmitt, D.G., **"Design Issues in the ISDN U-Interface Transceiver,"** *IEEE Journal on Selected Areas in Communications*, Vol. SAC-4 (Nov. 1986), pp. 1281-1293.

[7] Lowin, I.T., **"Design Considerations for U-Interface Circuitry for an ISDN in South Africa,"** *MSc (Eng.) Dissertation*, Electrical Engineering Department, University of the Witwatersrand, (1988).

[8] Ahamed, S.V., Bohn, P.P., and Gottfried, N.L., **"A Tutorial on Two-Wire Digital Transmission in the Loop Plant,"** *IEEE Transactions on Communications*, Vol. COM-29, No. 11 (Nov. 1981), pp. 1554-1564.

[9] Modestino, J.W., Massey, C.S., Bollen, R.E., and Prabhu, R.P., **"Modeling and Analysis of Error Probability Performance for Digital Transmission Over the Two-Wire Loop Plant,"** *IEEE Journal on Selected Areas in Communications*, Vol. SAC-4, No. 8 (Nov. 1986), pp. 1317-1330.

[10] Johnson, W.C., "Transmission Lines and Networks," McGraw-Hill New York, N.Y., (1950).

[11] Arnold, A.H.M., "Proximity Effects in Solid and Hollow Round Conductors", *Proceedings of the IEE*, Vol. 88, (1941), pp 349-359.

[12] Hanrahan, H.E., Lowitt, I.T., and Costa, F., "A Simulation and Test Facility for Digital Subscriber Loops", First SAIEE/CSSA Conference on ISDN, Johannesburg, 16-19 May 1988.

[13] Jordan, E.C., and Balmain, K.G., "Electromagnetic Waves and Radiating Systems," Prentice-Hall, Inc. N.Y., Second Edition (1968).

[14] Hewlett Packard Corporation, HP4195A Network/Spectrum Analyzer - Operations Manual, Second Edition (Feb. 1988), Manual Part Nº 04195-90000.

[15] Hewlett Packard Corporation, HP4195A Network/Spectrum Analyzer - User's Guide, (March 1988), Manual Part Nº 5950-2942.

[16] Hewlett Packard Corporation, HP356" .eflection/Transmission Test Kit - Operating and Service Manual, First Edition (Feb. 1985), Manual Part Nº 35676-90000.

[17] Sevick, J., "Transmission Line Transformers", *American Radio Relay League*, Newington, (1987).

[18] Advance Instruments, Inc., PG 52 Modular Pulse Generator System - Instructions Manual, (July 1972), Manual Part Nº 30163.

[19] Tektronix Corporation, 390AD Programmable Digitizer - Operators Manual", Second Revision (Jan. 1983), Manual Part Nº 070-4450-00.

[20] South African Dept. of Posts and Telecommunications, "Specification for Cables, underground, solid polyethylene insulated, aluminium polyethylene laminate sheathed, PCM and data type", Specification Nº 373A, (Nov. 1983), pp 1-11.

[21] Buchner, J.B., "**Ternary Line Codes**", *Philips Telecom Review*, (June 1976), pp 77-86.

[22] Geiger, G., and Lerach, L., "**ISDN-Oriented Modular VLSI Chip-set for Central-office and PABX Applications,**" *IEEE Journal on Selected Areas in Communications*, Vol. SAC-4 (Nov. 1986), pp. 1268-1274.

[23] Szechenyi, K., Zapf, F., and Sallaerts, D., "**Integrated Full-Digital U-Interface Circuit for ISDN Subscriber Loop,**" *IEEE Journal on Selected Areas in Communications*, Vol. SAC-4 (Nov. 1986), pp. 1337-1349.

[24] Anderson, J.O., Bauer, A., and Carlquist, B., "**An LSI Implementation of an ISDN Echo Canceller: Design and Network Aspects,**" *IEEE Journal on Selected Areas in Communications*, Vol. SAC-4 (Nov. 1986), pp. 1350-1358.

[25] Kanemasa, A., "**An ISDN Subscriber Loop Transmission System Based on Echo Cancellation, Design and Network Aspects,**" *IEEE Journal on Selected Areas in Communications*, Vol. SAC-4 (Nov. 1986), pp. 1359-1366.

[26] Chipman, R.A., "**Schaum's Outline of Theory and Problems of Transmission Lines**", McGraw-Hill New York, N.Y., (1968).

[27] Horowitz,P., and Hill, W., "**The Art of Electronics**", Cambridge University Press, Cambridge, (1980).

Appendix A

TRANSMISSION METHODS AND IMPAIRMENTS IN DIGITAL SUBSCRIBER LOOPS

A.1 Transmission Methods

Various transmission schemes have been proposed to achieve full-duplex two-wire transmission [2]. The two transmission schemes that seem to offer better performance in terms of noise immunity and ease of implementation are burst mode, *Figure A.1a*, also referred to as time compression multiplexing (TCM) mode, and the hybrid echo cancellation (HEC) mode, *Figure A.1b*, also referred to simply as the hybrid mode [1, 2, 4, 5].

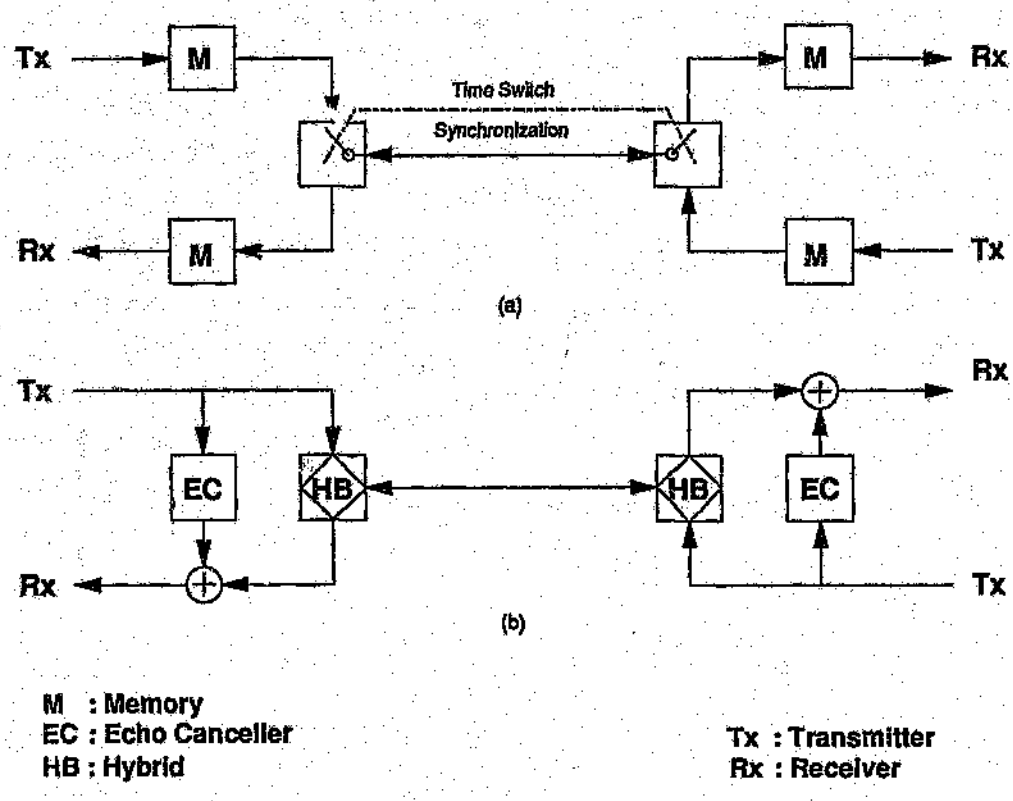

Figure A.1 (a) Schematic of TCM Transmission Method
(b) Schematic of HEC Transmission Method

Both of these modes isolate the data received from the far-end from that transmitted at the near-end. In the HEC mode the isolation is achieved by a hybrid and echo

canceller while both the transmission and reception are occurring simultaneously. In the TCM mode, the intervals for transmission and reception are isolated in time and the separation of the two directions of transmission is thus simplified.

A.1.1 TCM Transmission Method

In the TCM mode, the intervals for the transmission and reception are isolated in time and the separation of the two directions of transmission is thus simplified. In practical systems [2], the exchange has a time slot defined to transmit it's data burst (i.e., blocks of bits) simultaneously to all the network termination. Each network termination receives the data after a corresponding delay and replies back to the exchange end. This type of isolation demands a line rate in the loop plant in excess of twice the data rate, (approx. 2.3 to 2.5 times the data rate). The extent to which the line rate exceeds twice the data rate depends on the burst length, the transit time for a pulse to travel down the line, and the duration for which both the transmitter and receiver are idle while line transients subside.

The determination of the number of bits per burst is a compromise between two factors. Firstly, the number of bits per burst should be kept large enough to reduce the line rate, and secondly, small enough to avoid long signal delay on the line, which is undesirable for voice traffic.

This mode is attractive because of the reduced complexity of the transceiver design. Depending on the loop plant characteristics, this mode can be used in long range subscriber loops, although in general they do show shortcomings due to the higher attenuation and crosstalk at these frequencies. It is therefore successfully used in short range transmissions.

A.1.2 HEC Transmission Method

In a transmission system using a HEC mode, a hybrid is used to separate the transmitted signal from the received signal and to perform the two to four wire conversion. It therefore uses the same principal as in conventional telephony but with no restrictions on hybrid loss [4], (i.e., a bridge with a balancing network is used to match the subscriber loop). Methods of implementing an adaptive balancing network are more attractive due to the variable subscriber loop impedances. Due to the imperfect impedance matching of the adaptive hybrid to the subscriber loop, there will be a leakage of the near-end (local) transmitted signal through the adaptive

hybrid to the near-end (local) receiver. This unwanted signal is called echo, and is superimposed on the received signal that was transmitted from the far-end. An echo canceller is used to cancel this unwanted echo, and the residual signal is composed by the far-end transmitted data and the system noise.

This mode maintains a line rate equal to the data rate. Consequently, this mode will offer better performance than the TCM mode in the sense that either higher data rate or longer transmission range can be achieved.

The hardware complexity of the HEC mode system is higher than that of the burst mode system due mostly to the complexity of the echo canceller. However, the fast development of integrated-circuit technology has rapidly reduced the cost of extra hardware, and LSI realization of the echo-cancellation mode system has been demonstrated to be feasible [22, 23, 24, 25].

A.2 Impairments in the Transmission Medium

The main sources of impairments in digital subscriber loops are crosstalk, echo, impulse noise, intersymbol interference, and bridge taps. The diagram of *Figure A.2*, illustrates most of the range-limiting factors in the subscriber loop.

A.2.1 Crosstalk

Crosstalk is one of the most significant limitations in digital subscriber loops. Pairs bundled together are capacitively coupled, producing undesirable signal-leak between them. Two distinct coupling paths is illustrated in *Figure A.2*, namely, near-end crosstalk (NEXT) and far-end crosstalk (FEXT).

Compatibility considerations must therefore account for crosstalk between the digital line and other systems. The two important factors are :

(a) when the digital line is the disturbed system, and

(b) when it is the disturbing system.

To deal with the former case, the minimum receive power of the digital transmission system must be maximized. In the latter case, the maximum transmitted power of the digital line must be limited. The combined effect is to limit the range of transmission of the data.

In *Figure A.2*, it is evident that FEXT suffers the same channel loss as the signal while NEXT does not. A HEC system therefore suffers more from the NEXT noise induced by other systems. On the contrary, a TCM system does not suffer from NEXT when bursts sent are synchronized with the exchange clock.

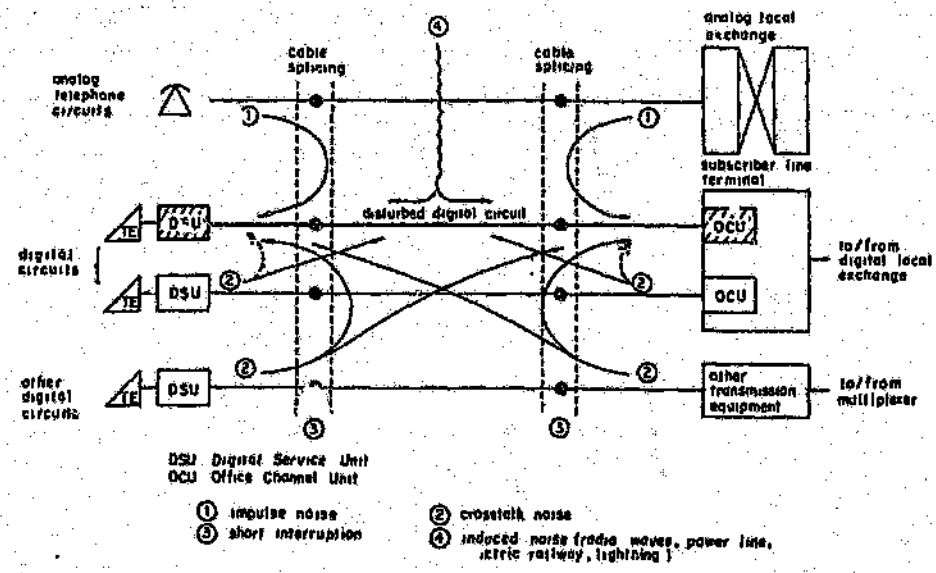

Source : Ref [6]

Figure A.2 Range-Limiting Factors in Subscriber Loops

A.2.2 Impulse Noise

Impulse noise is characterized by infrequent high amplitude bursts of noise. Impulse noise coming through existing analog telephone circuits comes mainly from two sources; one is the call connection procedure in an exchange, and the other is the metering pulses for determining charges, which depends on the call hold time and the destination. This charge metering pulse is used in a crossbar switch. Electronic exchange systems which use the electronic charge record do not generate metering pulse noise.

Impulse noise on subscriber loop plants thus varies according to the number and calling rate of analog telephone circuits, and cable crosstalk characteristics.

A.2.3 Echo

In a HEC system, the receiver will be isolated from the transmitter provided that the hybrid is matched to the channel input impedance at all frequencies. In practical situation, this perfect matching conditions is impossible to achieve; variations in cable impedances with frequency are strongest at lower frequencies, and minimal at higher frequencies. The impedance matching is therefore better at higher frequencies than at lower frequencies. A hybrid transformer will thus normally provide better echo attenuation at higher frequencies than at lower frequencies, resulting in relatively large echo power at low frequencies being coupled to the receiver.

A.2.4 Intersymbol Interference

In band-limited channels with frequency dependent attenuation and delay, pulses are dispersed and span several bit periods, which interferes with other pulses. This effect is known as intersymbol interference (ISI). A useful graphical representation of the data signal that allows immediate evaluation of the amount of ISI is an eye diagram, (i.e., eye diagrams are the superposition of individual received pulses in the same time slot, each time slot being the width of one bit period). A large vertical open eye implies a small ISI, which corresponds to a large noise margin for the receiver decision device.

There are two ways of reducing intersymbol interference. The first method is to separate the pulses by reducing the pulse width within the bit time period. This is wasteful of bandwidth and causes, due to the Hartley-Shannon law, an impairment of the signal to noise ratio. The second method is to shape the transmitted signal in such a way that the interference is minimized. The signal waveshape is chosen to provide a maximum at the true sampling point, while it has a zero level at all other sampling points.

This correction is provided by filters (otherwise known as equalizers). Ideally the equalization filter will exhibit a frequency dependence which is the exact inverse of that recorded for the transmission cable. The equalization process is normally performed in two stages. A pre-equalizer generates a suitable pulse shape, and provides initial compensation for the transmission medium. Further pulse shaping and final compensation for the medium occurs at the post-equalizer, situated at the distant end of the transmission path.

A.2.5 Bridge Taps

A standard recourse in the loop plant wiring was to reach nodes in a loop that were treated as feeders and spread them in a star fashion to multiple termination points by the use of extra pairs bridged or tapped across the main pair. This results in a very handy technique when geographical flexibility is desired. Unfortunately, this wiring practice limits the data transmission plant performance, requiring larger equalization complexity.

The presence of the bridge taps on the main subscriber loops affects the trailing part of the loop impulse response. In the frequency domain the bridge tap effect results in transmission zero's on the lines frequency response. The frequencies affected are determined by [illegible]ngth of the bridge taps.

Appendix B

DETERMINATION OF THE TRANSMISSION LINE SECONDARY AND PRIMARY PARAMETERS

B.1 Determination of the Secondary Parameters from Impedance Measurements [26]

When a arbitrary length of any general transmission line is terminated in an open-circuit or short-circuit, its input impedance is determined completely by the propagation factor α and β, the characteristic impedance Z_o and the line length l. The input impedance Z_i of a uniform transmission line of length l and characteristic impedance Z_o terminated in a load Z_T is given by

$$Z_i = Z_o \left\{ \frac{Z_T + Z_o \tanh[(\alpha + j\beta)l]}{Z_o + Z_T \tanh[(\alpha + j\beta)l]} \right\} \qquad B1.1$$

If the line is short-circuited at its termination, i.e., $Z_T = 0$ (but $\alpha \neq 0$, then equation (B1.1) reduces to

$$Z_{sc} = Z_o \tanh[(\alpha + j\beta)l] \qquad B1.2$$

The input impedance of the same line with open-circuit termination, i.e., $Z_T = infinity$, then equation (B1.1) reduces to

$$Z_{oc} = Z_o \coth[(\alpha + j\beta)l] \qquad B1.3$$

Provided that Z_{sc} and Z_{oc} are measured at the same frequency, for the same line section of length l, then Z_o, α, β, and l will have the same values in both of the equations (B1.2) and (B1.3). Multiplying together the corresponding sides of these equations gives

$$Z_o = \sqrt{Z_{sc} Z_{oc}} \qquad B1.4$$

This is a valuable and valid equation by which the characteristic impedance of any type of uniform transmission line can be obtained from two impedance measurements made on a sample length of the line, using two readily available terminal load impedances.

The attenuation factor α and the phase propagation factor β can also be calculated from the measured impedances Z_{sc} and Z_{oc}.

Dividing corresponding sides of equations (B1.2) and (B1.3),

$$\frac{Z_{sc}}{Z_{oc}} = \tanh^2[(\alpha + j\beta)l] \qquad B1.5$$

Expanding this hyperbolic tangent in exponential form using $\gamma = \alpha + j\beta$, we get,

$$\sqrt{\frac{Z_{sc}}{Z_{oc}}}=\frac{(1-e^{-2\gamma l})}{(1+e^{-2\gamma l})} \qquad B1.6$$

which gives

$$e^{2\gamma l}=\frac{1+\sqrt{\frac{Z_{sc}}{Z_{oc}}}}{1-\sqrt{\frac{Z_{sc}}{Z_{oc}}}} \qquad B1.7$$

Taking natural logarithms on both sides,

$$(\alpha+j\beta)l=\frac{1}{2}\ln\left\{\frac{1+\sqrt{\frac{Z_{sc}}{Z_{oc}}}}{1-\sqrt{\frac{Z_{sc}}{Z_{oc}}}}\right\} \qquad B1.8$$

The logarithm of a complex number expressed in polar form $Ae^{j\phi}$ is defined by

$$\ln\{Ae^{j\phi}\}=\ln\{A\}+j\{\phi+2n\pi\}$$

The attenuation factor α (nepers/m) is therefore given by

$$\alpha=\frac{1}{2l}\ln\left|\frac{1+\sqrt{\frac{Z_{sc}}{Z_{oc}}}}{1-\sqrt{\frac{Z_{sc}}{Z_{oc}}}}\right| \qquad B1.9$$

when l is in meters. The phase propagation factor β (radians/m) is given by

$$\beta=\frac{1}{2l}\left\{\angle\frac{1+\sqrt{\frac{Z_{sc}}{Z_{oc}}}}{1-\sqrt{\frac{Z_{sc}}{Z_{oc}}}}+2n\pi\right\} \qquad B1.10$$

where $n = 0, 1, 2, \ldots$

This method does not however determine a unique value of β, but a series of values differing consecutively by (π/l) rad/m.

B.2 Solutions of the Inverse Form R, G, L, C = $f(\alpha, \beta, R_o, X_o, \omega)$

The secondary parameters Z_o and γ, are determined from the primary parameters by, [26]

$$Z_o = R_o + jX_o = \sqrt{\frac{R + j\omega L}{G + j\omega C}} \qquad B2.1$$

and

$$\gamma = \alpha + j\beta = \sqrt{(R + j\omega L)(G + j\omega C)} \qquad B2.2$$

These are well known transmission line equations that are used to determine the secondary parameters given the primary parameters. Least known, is the solution of the inverse form, i.e., determining the primary parameters from the secondary parameters.

Multiplying the corresponding sides of equations (B2.1) and (B2.2), gives

$$(R_o + jX_o)(\alpha + j\beta) = R + j\omega L \qquad B2.3$$

rearranging, gives

$$R + j\omega L = (R_o\alpha - \beta X_o) + j(\beta R_o + \alpha X_o) \qquad B2.4$$

Equating the real terms of equation (B2.4),

$$R = \alpha R_o - \beta X_o \qquad B2.5$$

and from the imaginary terms of equation (B2.4),

$$L = \frac{\beta R_o + \alpha X_o}{\omega} \qquad B2.6$$

Dividing corresponding sides of equation (B2.2) by those of equation (B2.1) gives

$$\frac{\alpha + j\beta}{R_o + jX_o} = G + j\omega C \qquad B2.7$$

rearranging, gives

$$G + j\omega C = \frac{\alpha R_o + \beta X_o}{R_o super2 + X_o^2} - j\frac{(\alpha X_o - \beta R_o)}{R_o super2 + X_o^2} \qquad B2.8$$

Equating the real terms of equation (B2.8),

$$G = \frac{\alpha R_o + \beta X_o}{R_o^2 + X_o^2} \qquad B2.9$$

and from the imaginary terms of equation (B2.8),

$$C = \frac{-\alpha X_o + \beta R_o}{\omega (R_o^2 + X_o^2)} \qquad B2.10$$

Equations (B2.5), (B2.6), (B2.9) and (B2.10) appear to be general design equations for determining the distributed circuit coeficients that a transmission line would have to possess to give a set of desired operating characteristics specified by the values of α, β, R_o and X_o at frequency ω. The situation is, however, not as simple and straightforward as this statement suggests. The characteristic impedance of a transmission line can be very nearly a pure resistance (especially true at higher frequencies), and the conductance G for polyethylene insulated cables is negligible. The condition therefore arrises with equation (B2.9) which then suggests that $\alpha = 0$, which is incorrect because the distributed line resistance R has not been required to be zero (and never is in practice). It is possible for X_o to be small enough to be unimportant (relative to R_o), with $G = 0$, but even such a small value of X_o can be significant in equations (B2.5) and (B2.9), since for the high frequency line under discussion β is always numerically much larger than α.

Appendix C

CABLE DRIVER AND RECEIVER CIRCUIT DESIGN

In order to transmit digital signals, differential line drivers and receivers are used in order to obtain good noise rejection [27]. The block diagram of *Figure C.1*, illustrates the typical scenario used to gather experimental data. The cable shield can be connected to the instrument case at both ends since no signals travels on the shield; but by tying the shield to the case through a small inductor, the d.c voltage is kept small while preventing large radiofrequencies currents.

For very long cables, it is useful to prevent large ground currents flowing in the shield at radiofrequencies.

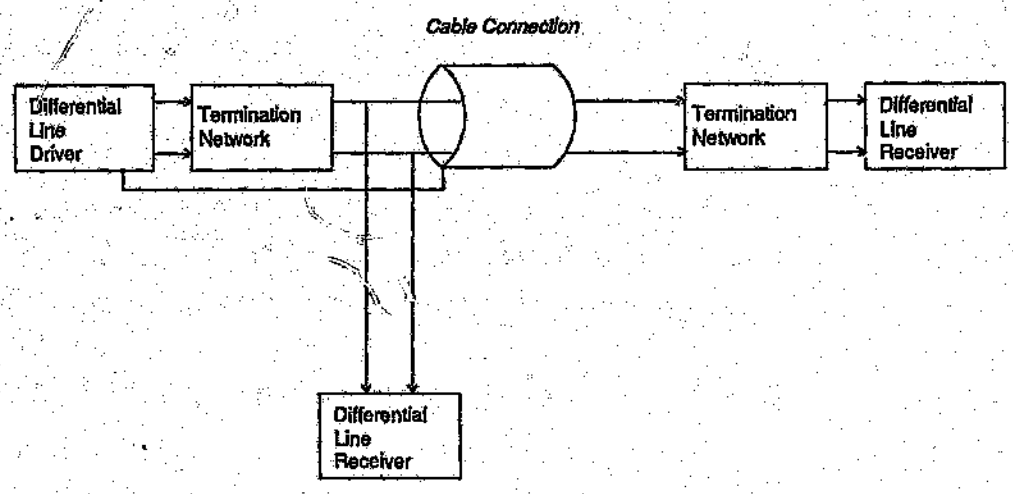

Figure C.1 Block Diagram of a High Speed Differential Cable Driver and Receiver

The termination network can consist of a hybrid or simply of a resistor. Although only one transmitter receiver circuit is required, the receiver circuit on the transmitor side is required in order to determine what effect the reflection have on the transmitt signal.

C.1 Cable Driver

The differential line driver consists of a class AB push-pull current amplifier for each line conductor in the cable pair with the signal of one line being symetrically inverted to the other as is illustrated in *Figure C.2*.

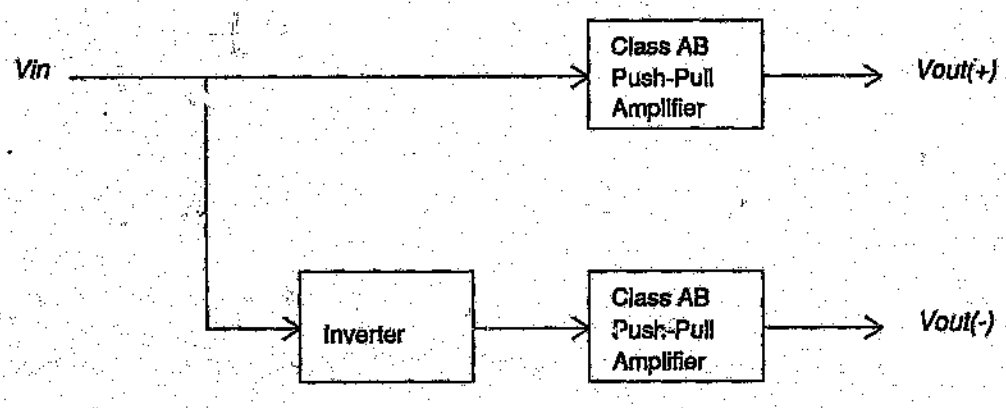

Figure C.2 Differential Line Driver Block Diagram

The two signals Vout(+) and Vout(-) will be completely symetrical provided that the inverting amplifier has a gain of unity and a flat frequency response which exceeds the frequency response of the push-pull current amplifier.

C.1.1 Inverting Amplifier

The high-slew-rate inverting amplifier illustrated in *Figure C.3* has been used to obtain the inverted form of the transmit signal for the differential line driver circuit.

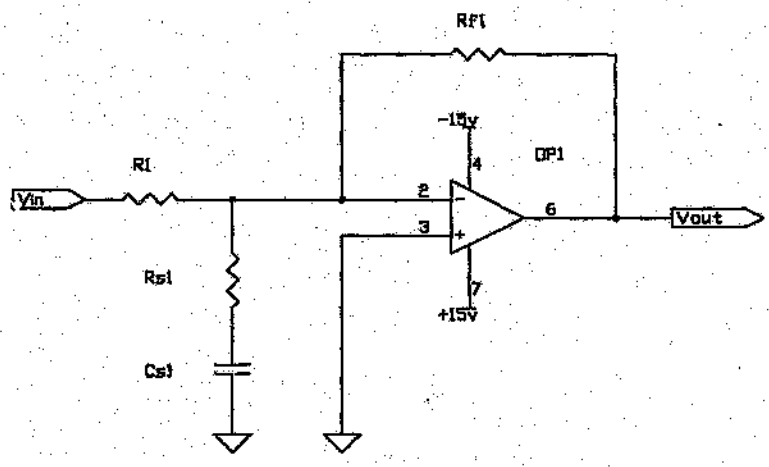

Figure C.3 Inverting Amplifier Circuit Diagram

The voltage is controlled by the ratio of the feedback resistance to the input resistance, given by equation (C.1).

$$\frac{V_o}{V_{in}} = -\frac{R_{fl}}{R_1} \qquad C.1$$

The component values for this circuit being tabulated in *Table C.1.*

Table C.1 Inverting Amplifier Circuit Component Values

Component Type	Component Value		
Resistors			
R_1	1k0Ω	1/4 W	2%
R_{a1}	270Ω	1/4 W	2%
R_{fl}	1k0Ω	1/4 W	2%
Capacitors			
C_{a1}	500pF		
Operational Amplifiers			
OP1	OPA27		

C.1.2 Signal Amplifier

The signal amplifier consists of a push-pull booster attached to the output of an op-amp, as illustrated in *Figure C.4.* The push-pull transistor pair is biased into quiescent conduction by the resistors R_{b1} and R_{b2}, in order to illiminate crossover distortion. Crossover distortion occurs because the output of the transistors trail the input at the base by a voltage drop arrising due to the base-emitter diode drop inherent in transistor devices. Thus neither Q_1 or Q_2 are conducting when the input signal is within ±0.6v, causing the output to remain at zero volts.

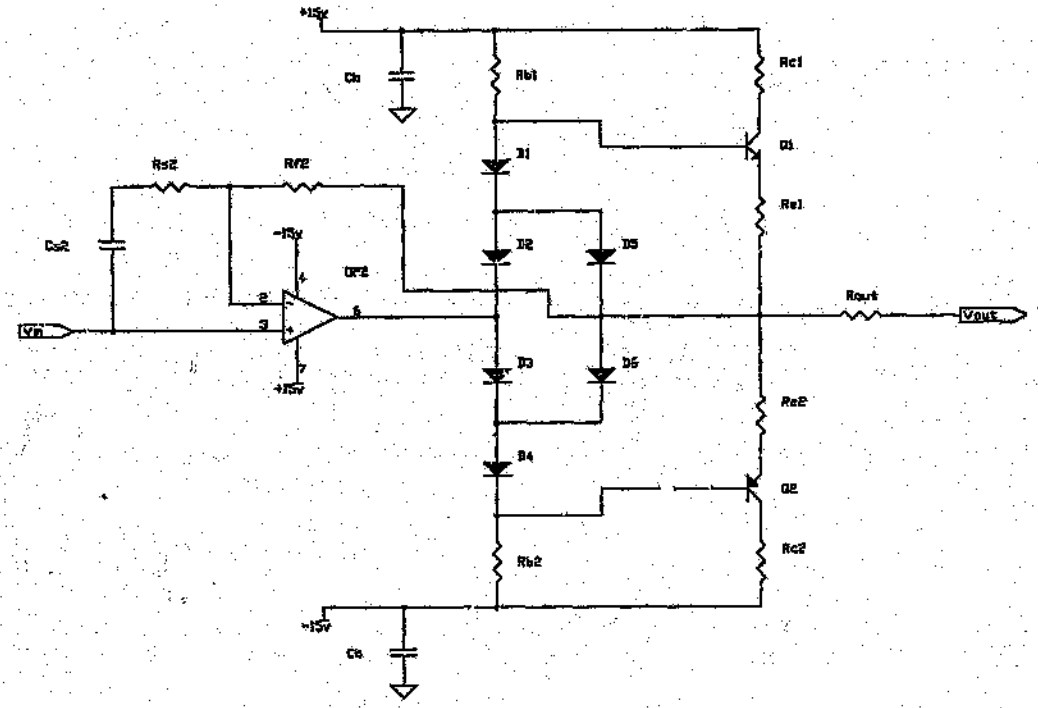

Figure C.4 Class AB Push-Pull Current Amplifier Circuit Diagram

The bias resistors R_{b1} and R_{b2} brings the diodes D_1 to D_6 into forward conduction, holding Q_1's base a diode voltage drop above the input signal and Q_2's base a diode voltage drop below the input signal. Now as the input signal crosses through zero, conduction passes from one transistor to the other; one of the transistors is always conducting. The feedback to the op-amp further reduces this distortion by forcing the output to track the input signal. The diodes D_1, D_2, D_3 and D_4 are to be mounted in close proximity with the output transistors Q_1 and Q_2 so that the voltage drops across the diodes and the base-emitter junctions of the output transistors will track with temperature. The diodes D_5 and D_6 provides short circuit protection on the load. The drive current being bypassed arround the output transistors through D_1 and D_5 for the positive half cycle and through D_4 and D_6 durring the negative cycle. Drive current limiting occurs whenever R_{e1} or R_{e2} sees more than one diode drop (i.e., 0.6 volts). An expression for the maximum output current is :

$$I_{MAX} = \frac{0.6}{R_{a1}} \qquad C.2$$

Table C.2 tabulates data for two complementary symetrical transistor pairs that were available.

Table C.2 Transistor Specification

Transsistor Type	Freq. (MHz)	Ic_{max} *m*Amps	h_{FE} Min	Ic_{bias} *m*Amps	Power Diss. (W)
2N2219A	300	800	50	1	800
2N2222A	300	800	50	1	400
2N2907A	200	600	100	1	400
2N2905A	200	600	100	1	600

The major advantage of using the *2N2219A - 2N2905A* pair instead of the *2N2222A - 2N2907A* pair was the increase in power dissipation capabilities.

In order to correctly bias the transistor pairs, we consider the state when point *A* and *B* are at a zero volt potencial, corresponding to an input signal voltage of zero volts.

(a) Biasing the NPN transistor - 2N2222A

From *Table C.2*, the collector bias current I_{cbias} is 1mAmp, and the transistor gain HFE is equal to 50. In order to correctly bias the transistor, the required bias current is :

$$I_{b1(bias)} = \frac{I_{c1(bias)}}{H_{FE}}$$

$$= 20\mu A \qquad C.3$$

The current required to drive the diodes D_1, D_2 and D_5 is of the order of 132 µAmps. The total current required to pass through resistor R_{b1} is thus 152 µAmps. The voltage across R_{b1} will be :

$$V_{Rb1} = V_{cc} - 2(0.7)$$

$$= 13.6V \qquad C.4$$

Thus the required value for the resistor R_{b1} is :

$$R_{b1} = \frac{V_{Rb1}}{I_{Rb1}}$$

$$= 89.6k\Omega \qquad C.5$$

Selecting a standard resistor value of 82kΩ for R_{b1}, the power dissipation is :

$$P_{diss(Rb1)} = \frac{V_{Rb1}^2}{R_{b1}}$$

$$= 2mW \qquad C.6$$

(b) Biasing the PNP transistor - 2N2907A

Similarly to the case of the NPN transistor above, the resistor R_{b2} required to bias the PNP transistor is 82kΩ.

For a short-circuited load, the drive current is bypassed arround the output transistors through D_1 and D_5 durring the positive half cycle, and through D_4 and D_6 durring the negative half cycle of the input signal. This will happen whenever R_{e1} or R_{e2} sees more than one diode voltage drop across it. If we limit the maximum output current to 500mAmps, then

$$R_{e1} = R_{e2} = 1.4\Omega \qquad C.7$$

and the power disipated is equal to 0.35W.

The collector resistors R_{c1} and R_{c2} were found to be redundant and were replaced by a 0Ω link. The capacitors C_1 and C_2 are used to bypass the power supply.

The output impedance of the driver circuit is approximately equal to the output resistor R_{out}. This resistance is connected on the front panel of the instrument and thus enables various output impedance conditions to be obtained. Other more complex circuits such as a hybrid may also be connected.

The bandwidth response obtained for the driver circuit is illustrated in *Figure C.5* for the non-inverting line driver, and in *Figure C.6* for the inverting line driver.

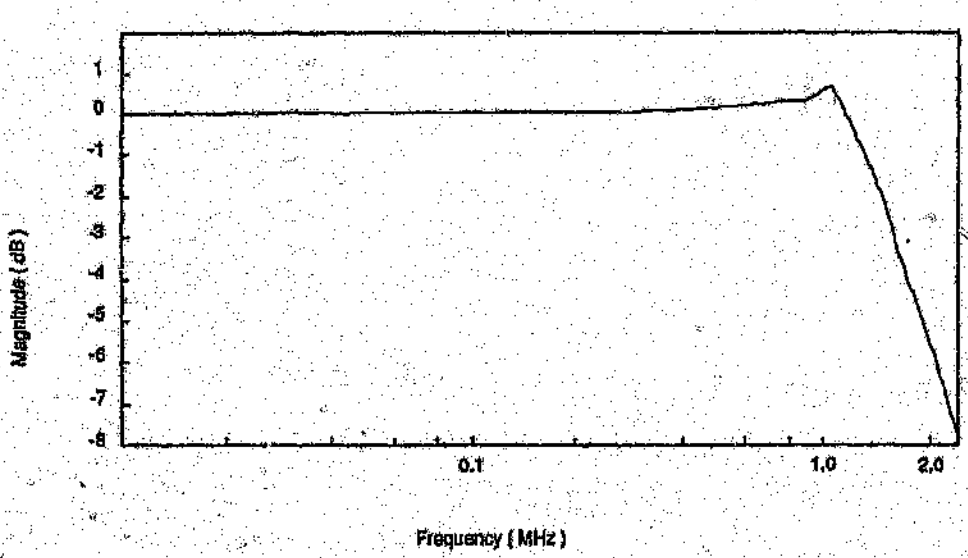

(a)

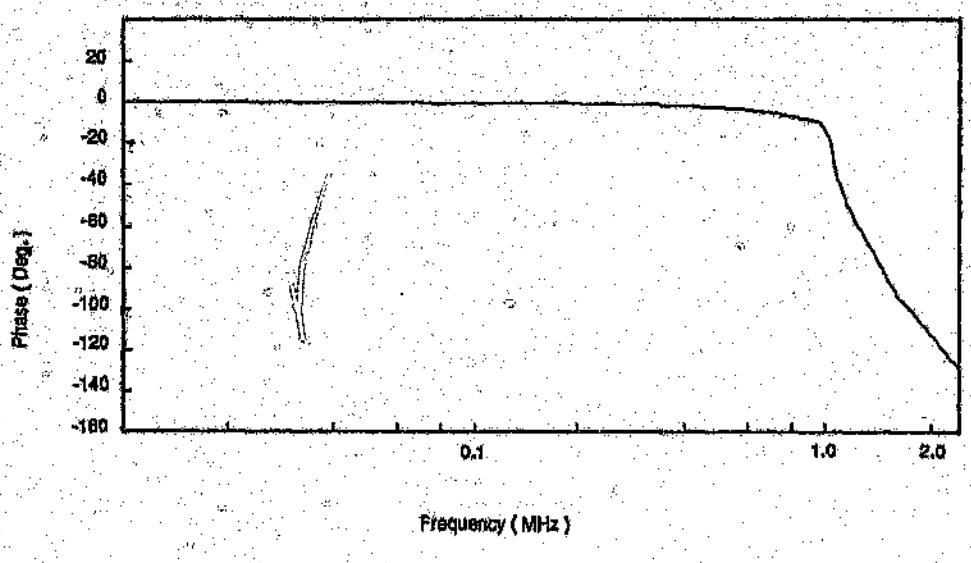

(b)

Figure C.5 Non-Inverting Line Driver
(a) Magnitude Response
(b) Phase Response

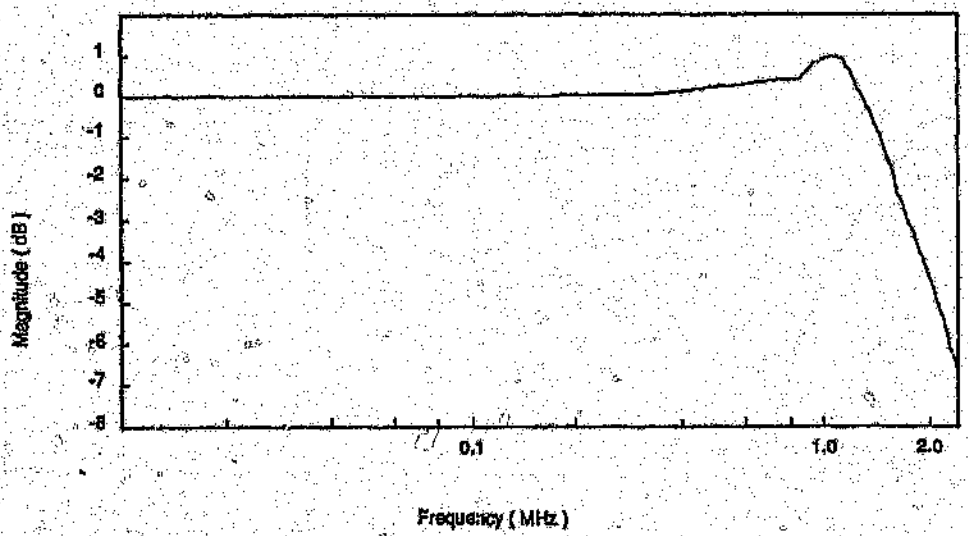

(a)

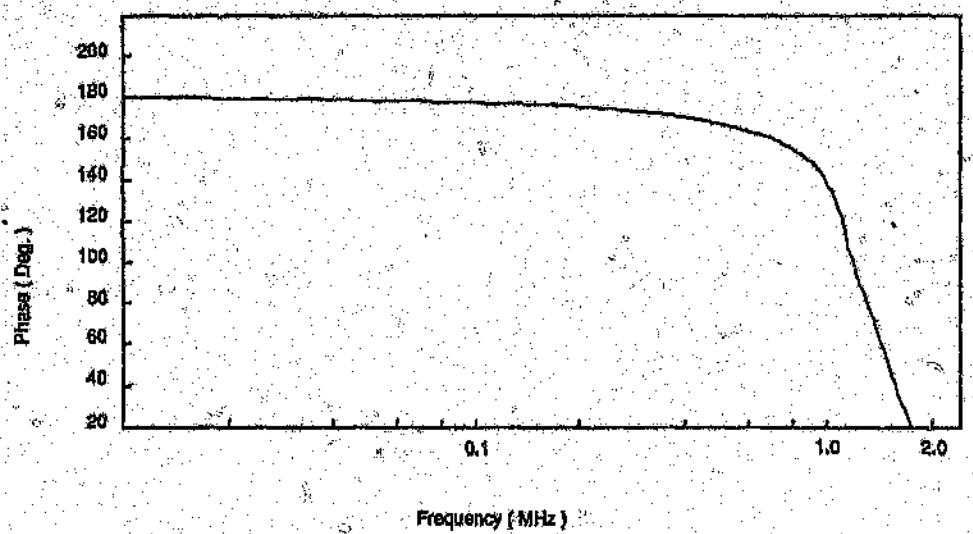

Note : *Y-axis zero suppressed*

(b)

Figure C.6 Inverting Line Driver
(a) Magnitude Response
(b) Phase Response

The *Table C.3* tabulates the component values used.

Table C.3 Line Driver Circuit Component Values

Component Type	Component Value		
Resistors			
R_{a2}	270Ω	1/4 W	2%
R_{a2}	1k0Ω	1/4 W	2%
R_{b1}	82k0Ω	1/4 W	2%
R_{b2}	82k0Ω	1/4 W	2%
R_{c1}	0Ω	1/4 W	2%
R_{c2}	0Ω	1/4 W	2%
R_{e1}	1.2Ω	1/2 W	2%
R_{e2}	1.2Ω	1/2 W	2%
R_{var}	TBD		
Capacitors			
C_{a2}	39pF		
C_b	0.01μF		
Diodes			
D_1	IN4007		
D_2	IN4007		
D_3	IN4007		
D_4	IN4007		
D_5	IN4007		
D_6	IN4007		
Transistors			
Q_1	2N2222A	NPN type	
Q_2	2N2907A	PNP type	
Operational Amplifiers			
OP2	OPA27		

C.2 Cable Receiver

A high gain d.c coupled differential amplifier with single ended output, high input impedance and high common mode rejection ratio is required to detect the severly distorted and attenuated signals. A instrumentation amplifier posseses all these charateristics and has been used for the receiver and the transmitter end.

C.2.1 Instrumentation Amplifier

The amplifier used is illustrated in the circuit diagram of *Figure C.7*. In order to attain a high input impedance, non-inverting amplifiers are used before the differential amplifier.

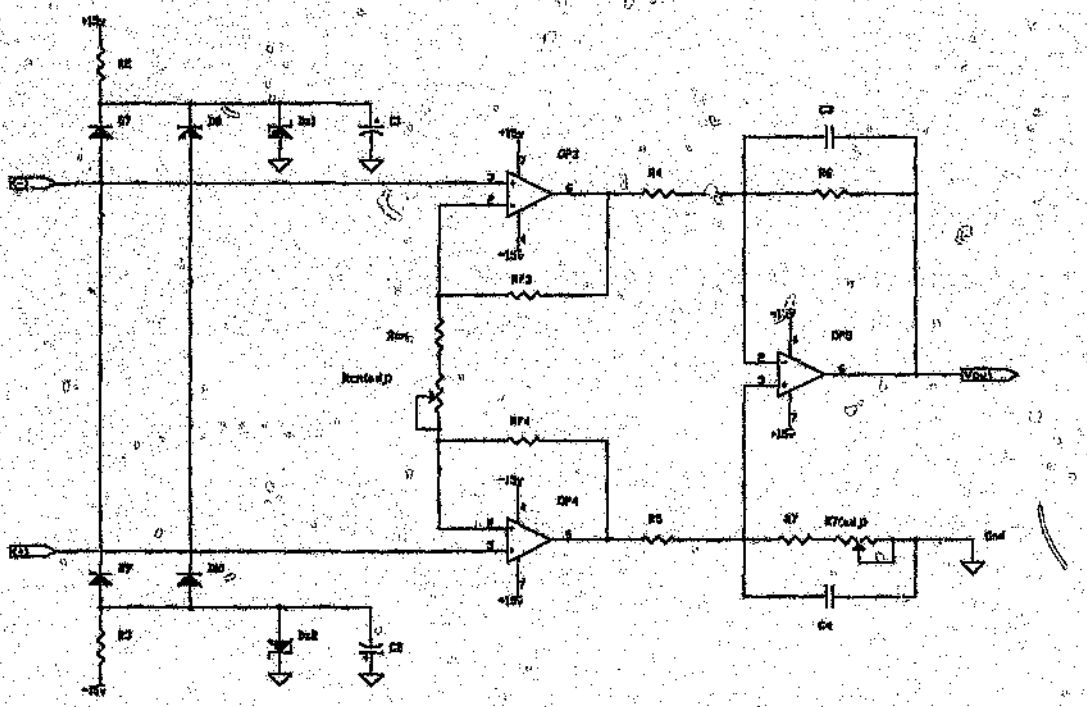

Figure C.7 Differential Amplifier Circuit Diagram

For a differential input signal, *OP3* and *OP4* act as non-inverting amplifiers of gain

$$A_{VI} = 1 + \left[\frac{2R_{f3}}{R_{cm}}\right] \qquad C.8$$

where $R_{f3} \approx R_{f4}$.

However the gain is unity for common-mode signals since the voltages V_1 and V_2 are in phase, and no current flow is developed through R_{f3}, R_{cm}, $R_{cm(adj)}$ and R_{f4}. The second stage is simply an op-amp connected as a differential amplifier of gain

$$A_{V2} = \frac{R_6}{R_4} \qquad C.9$$

where $R_6 = R_7$ and $R_4 = R_5$.

The total gain of the instrumentation amplifier is

$$A_V = \left[1 + \frac{2R_\beta}{R_{cm}}\right] \cdot \left[\frac{R_6}{R_4}\right] \qquad C.10$$

The variable resistor $R_{7(adj)}$ can be used to take up the resistance tolerances of R_4, R_5 and R_6 for the best common mode rejection. The variable $R_{cm(adj)}$ is used to vary the gain of the instrumentation amplifier without degrading the common-mode rejection.

The diodes D_7 to D_8, the 10 volt zeners D_{z1} and D_{z2}, the resistors R_2 and R_3, together create a protection circuit by preventing common mode excursions beyound ±10 volts.

(a) Receiver End Detect

The reciever end differential amplifier has a freqeuncy response as illustrated in *Figure C.8*. The bandwidth of the amplifier is 135kHz and the gain is 57dB's. *Table C.4* tabulates the component values used.

Table C.4 Receiver End Differential Amplifier Circuit Component Value

Component Type	Component Value		
Resistors			
R_2	1k0Ω	1/4 W	2%
R_3	1k0Ω	1/4 W	2%
R_4	20k0Ω	1/4 W	2%
R_5	20k0Ω	1/4 W	2%
R_6	20k0Ω	1/4 W	2%
R_7	19k6Ω	1/4 W	2%
R_{cm}	560Ω	1/4 W	2%
R_{13}	300Ω	1/4 W	2%
R_{14}	300Ω	1/4 W	2%
$R_{cm(adj)}$	100Ω	20 turn trim-pot	
$R_{7(adj)}$	500Ω	20 turn trim-pot	
Capacitors			
C_1	1.0μF	Tantalum	
C_2	1.0μF	Tantalum	
C_3	500pF	Ceramic	
C_4	500pF	Ceramic	
Diodes			
D_7	IN4007		
D_8	IN4007		
D_9	IN4007		
D_{10}	IN4007		
D_{z1}	15 volt zener		
D_{z2}	15 volt zener		
Operational Amplifiers			
OP3	OPA27		
OP4	OPA27		
OP5	OPA27		

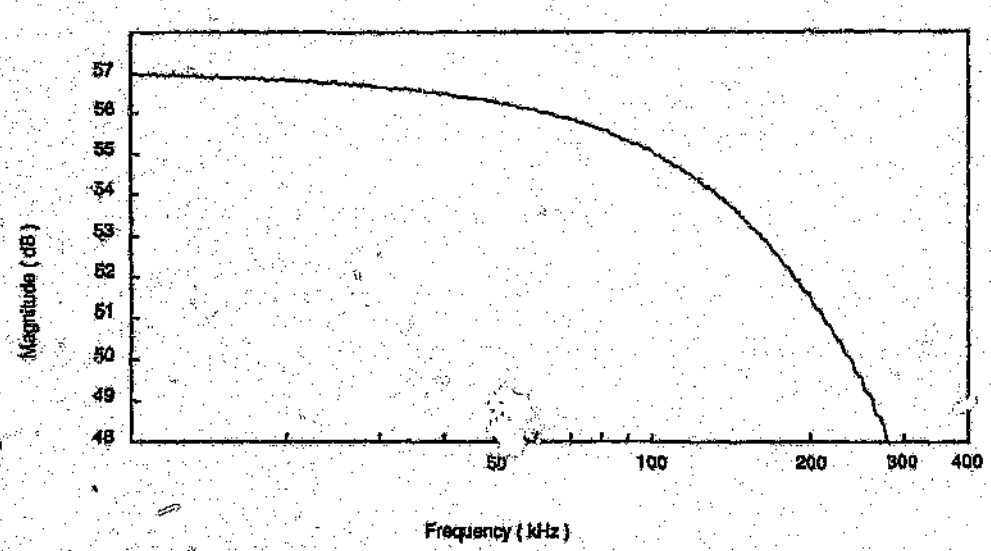

Note : *Y-axis zero suppressed*

(a)

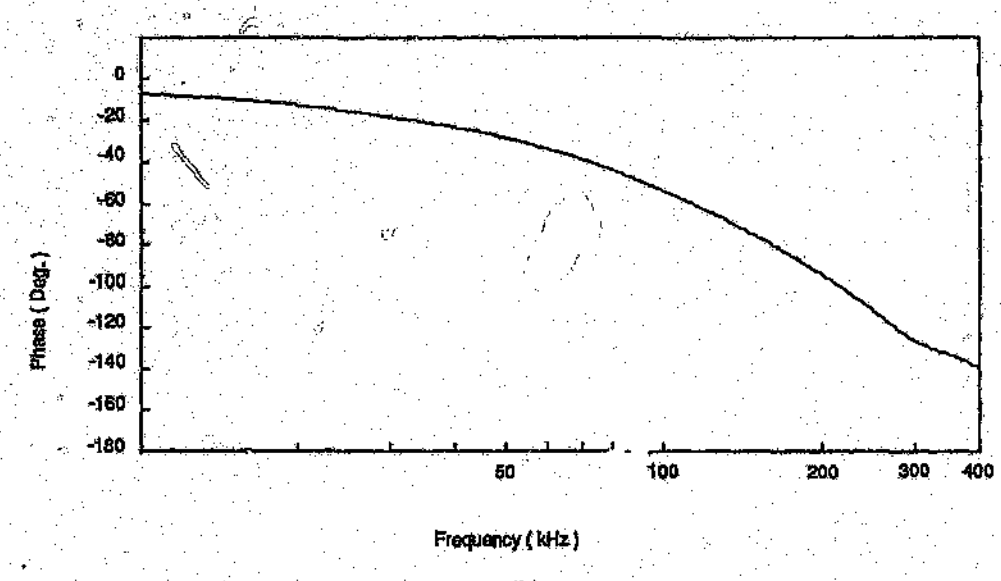

(b)

Figure C.8 Receiver End Detector
(a) Magnitude Response
(b) Phase Response

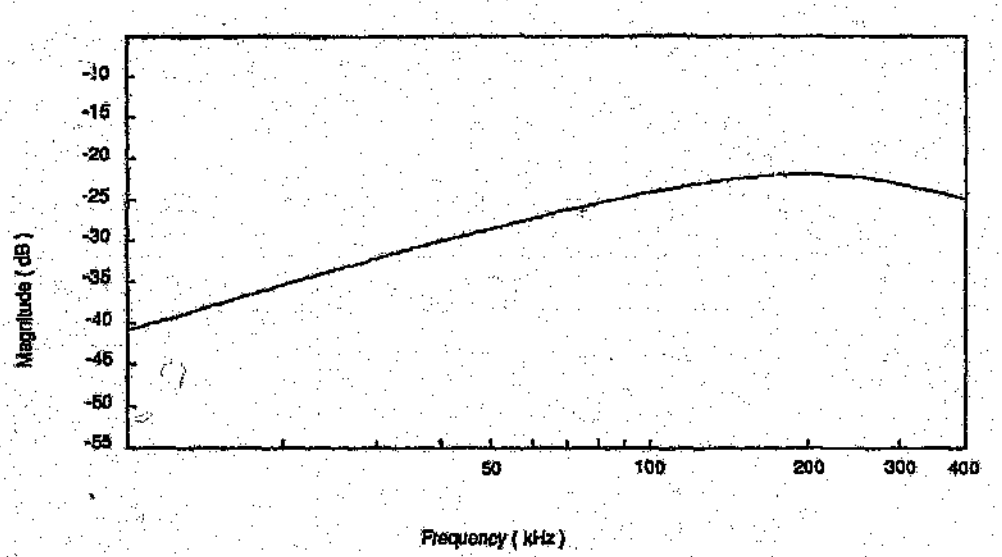

Note : *Y-axis zero suppressed*

(a)

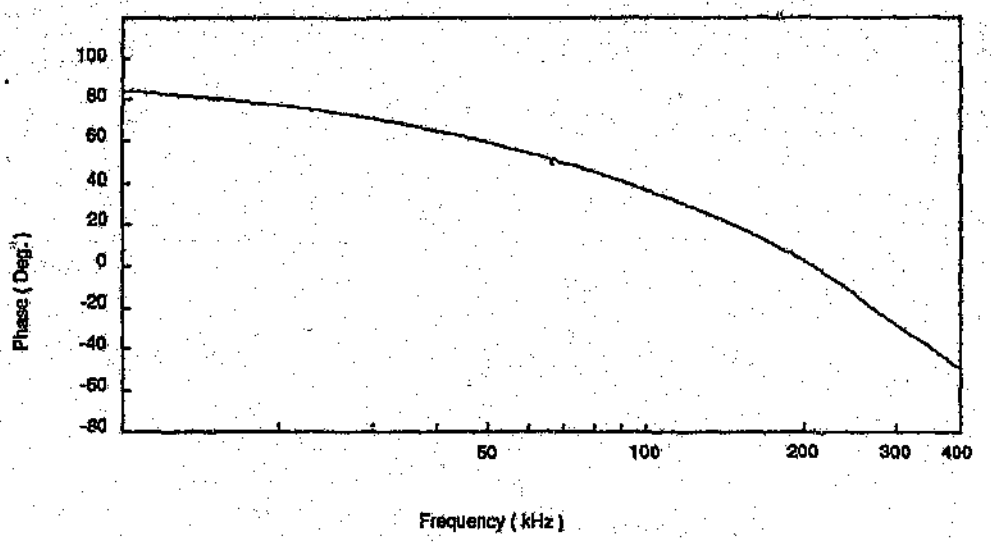

Note : *Y-axis zero suppressed*

(b)

Figure C.9 Receiver Common-Mode Rejection Ratio
(a) Magnitude Response
(b) Phase Response

(b) Transmitter End Detect

The Table C.5 tabulates the component values used.

Table C.5 Transmitter End Differential Amplifier Circuit Component Values

Component Type	Component Value		
Resistors			
R_2	1k0Ω	1/4 W	2%
R_3	1k0Ω	1/4 W	2%
R_4	1k0Ω	1/4 W	2%
R_5	1k0Ω	1/4 W	2%
R_6	20k0Ω	1/4 W	2%
R_7	19k6Ω	1/4 W	2%
R_{cm}	560Ω	1/4 W	2%
R_{f3}	5k1Ω	1/4 W	2%
R_{f4}	5k1Ω	1/4 W	2%
$R_{cm(adj)}$	100Ω	20 turn trim-pot	
$R_{\gamma(adj)}$	500Ω	20 turn trim-pot	
Capacitors			
C_1	1.0μF	Tantalum	
C_2	1.0μF	Tantalum	
C_3	500pF		
C_4	500pF		
Diodes			
D_7	IN4007		
D_8	IN4007		
D_9	IN4007		
D_{10}	IN4007		
D_{z1}	10 volt zener		
D_{z2}	10 volt zener		
Operational Amplifiers			
OP3	OPA27		
OP4	OPA27		
OP5	OPA27		

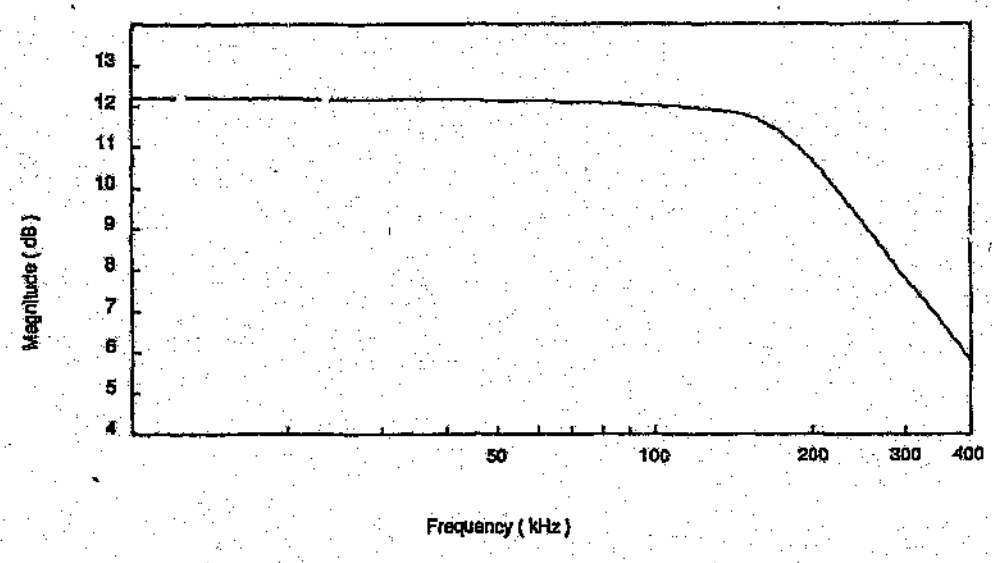

Note : *Y-axis zero suppressed*

(a)

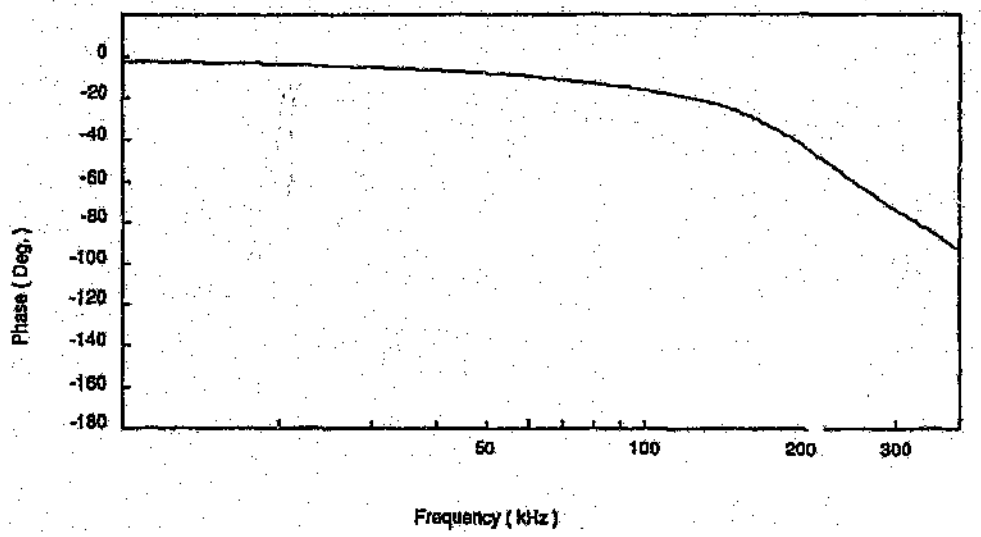

(b)

Figure C.10 Transmitter End Detector
(a) Magnitude Response
(b) Phase Response

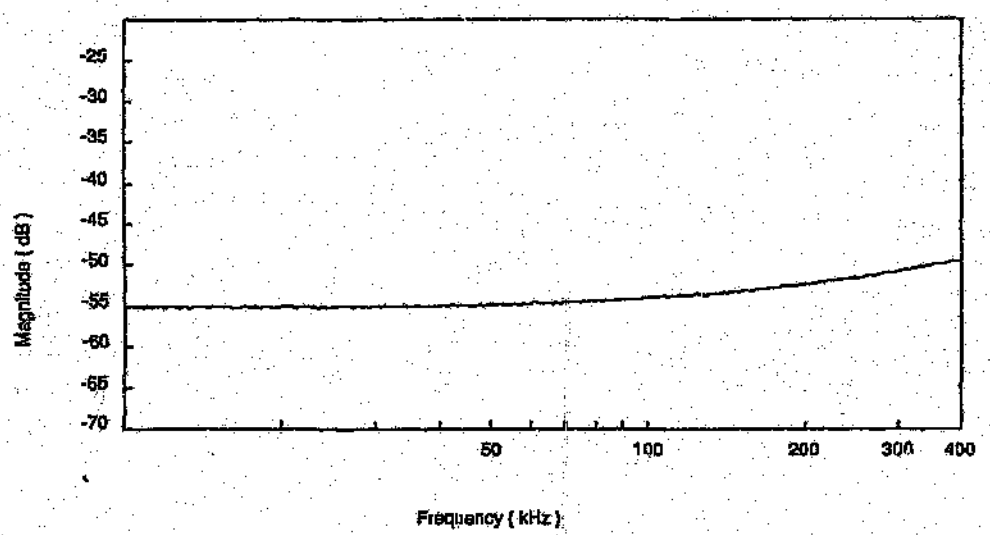

Note : *Y-axis zero suppressed*

(a)

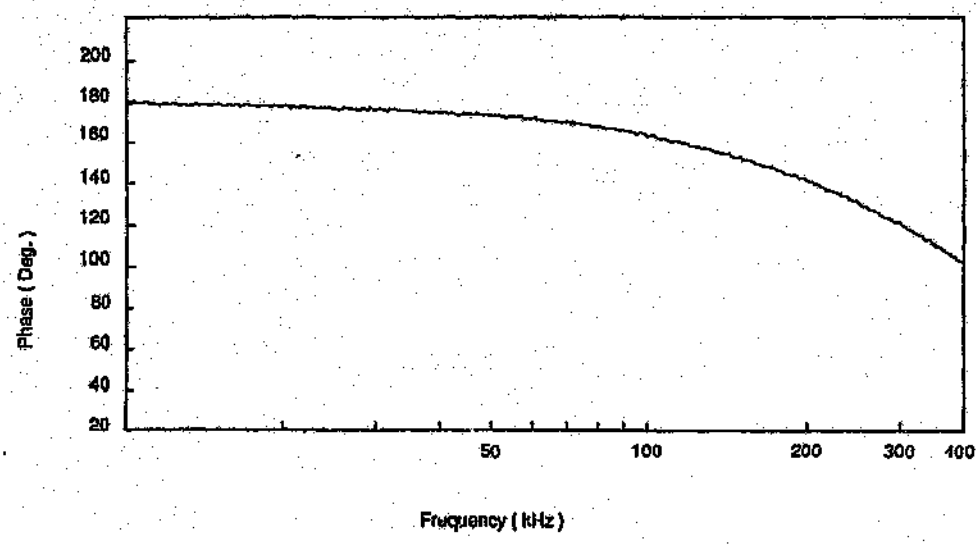

Note : *Y-axis zero suppressed*

(b)

Figure C.11 Transmitter End Detector Common-Mode Rejection Ratio
(a) Magnitude Response
(b) Phase Response

C.3 PCB Design

The differential line driver and the two receiver amplifiers circuits have been implemented on a commom printed circuit board. The silk screen layer is illustrated in *Figure C.12* and the solder side layout is illustrated in *Figure C.13*. The component side of the PCB was made into a ground plain.

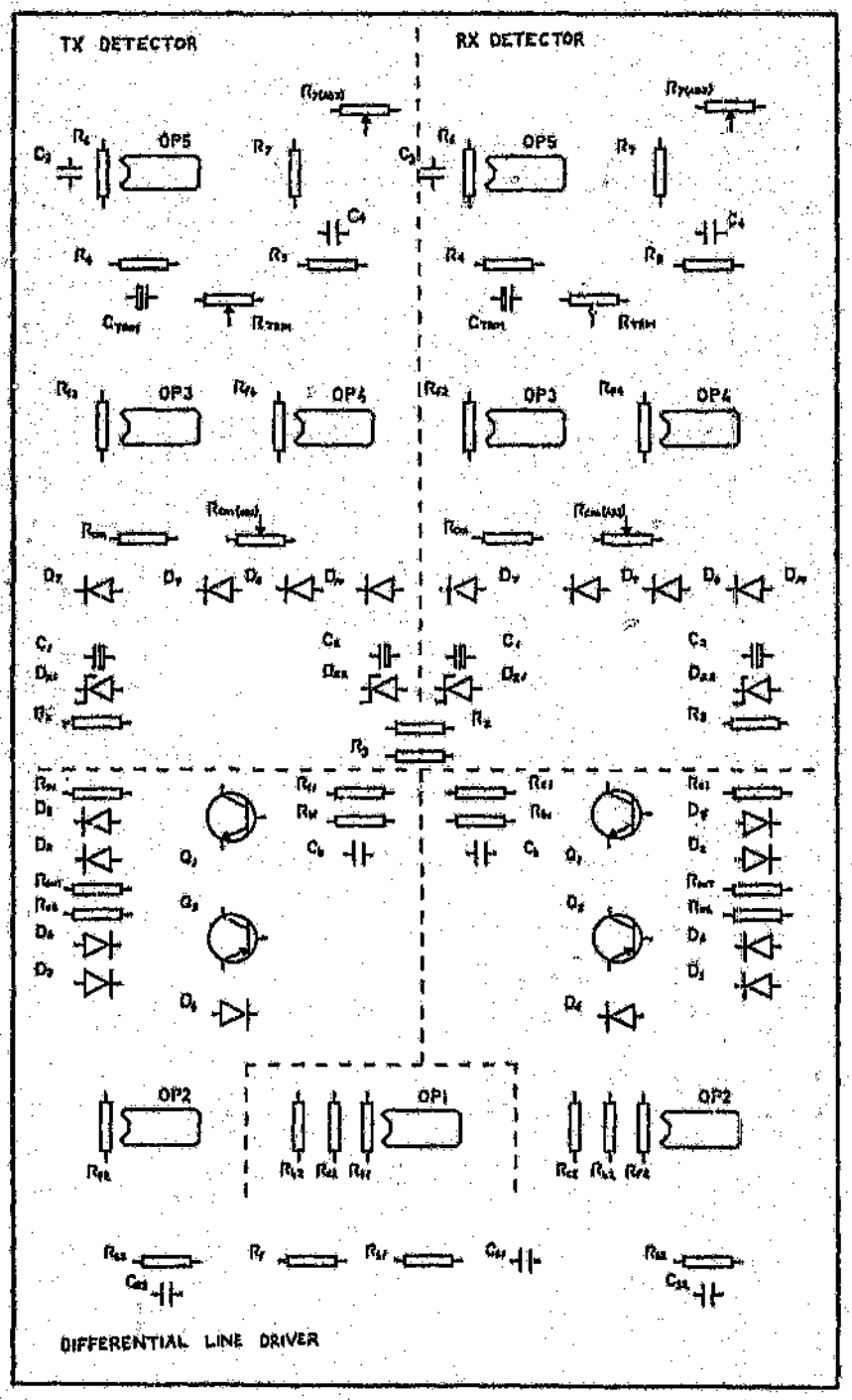

Figure C.12 Silk Screen Layer

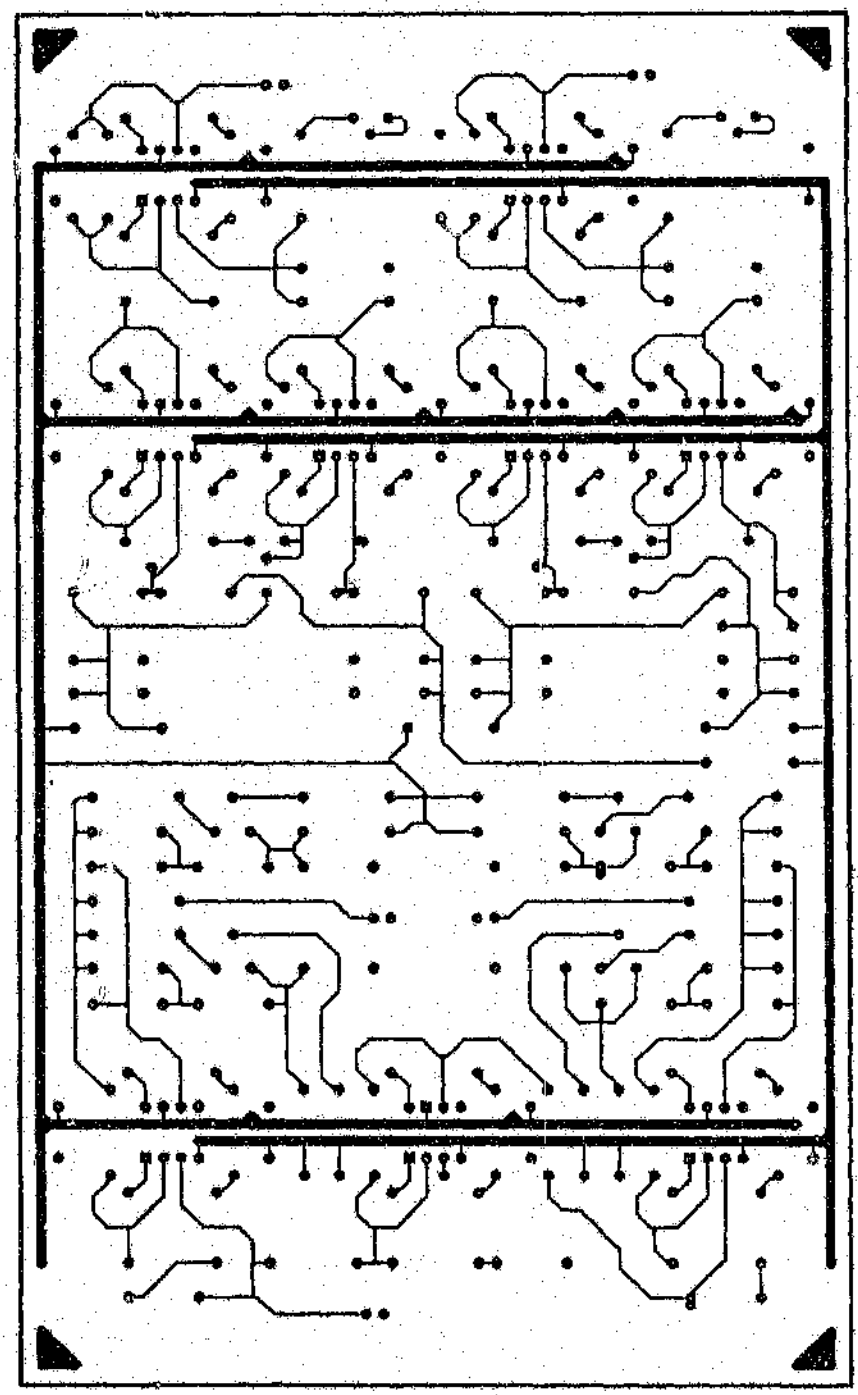

Figure C.13 Solder Side Layout

Appendix D

INPUT IMPEDANCE MEASUREMENTS

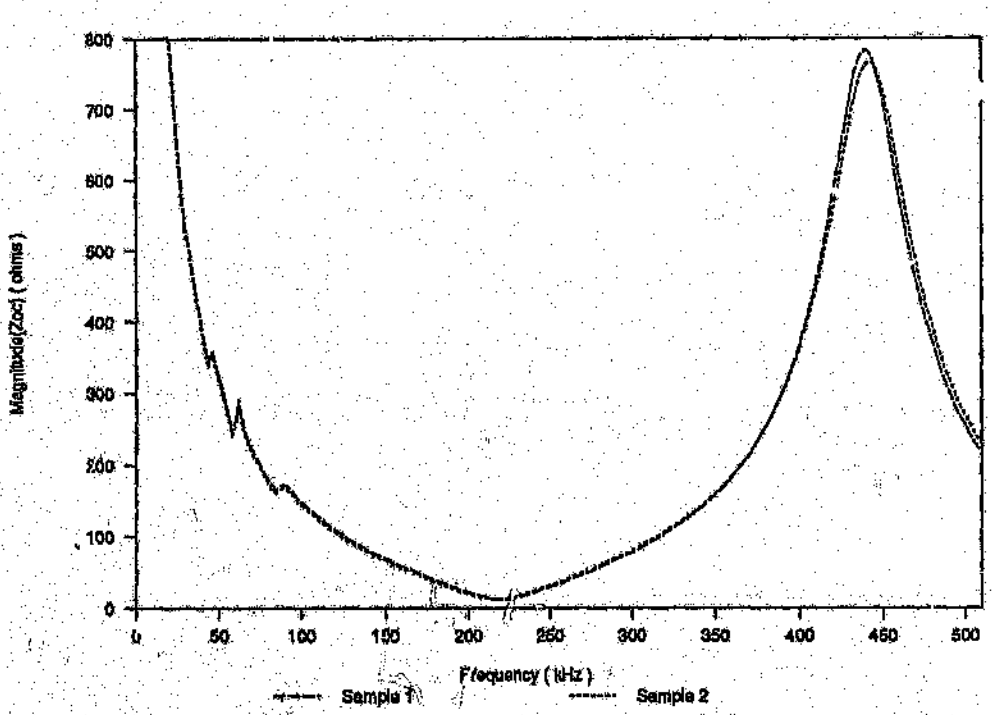

(a)

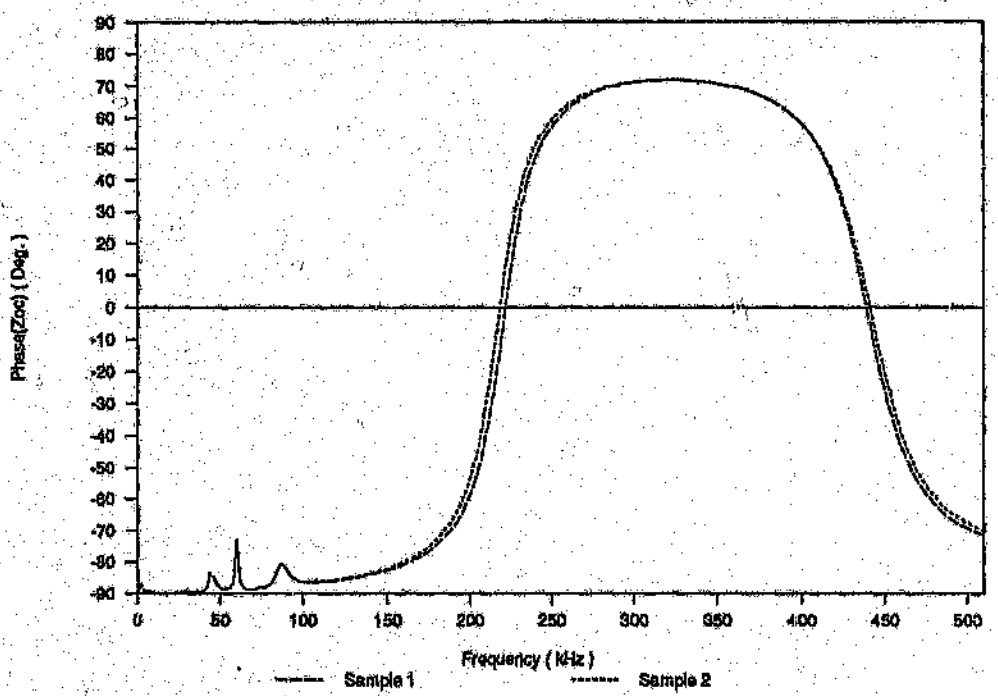

(b)

Figure D.1 Input Impedance, Z_{oc}
Magnitude (a) and phase (b) response of a 200m section of cable gauge type 19 terminated under *open-circuit* conditions.

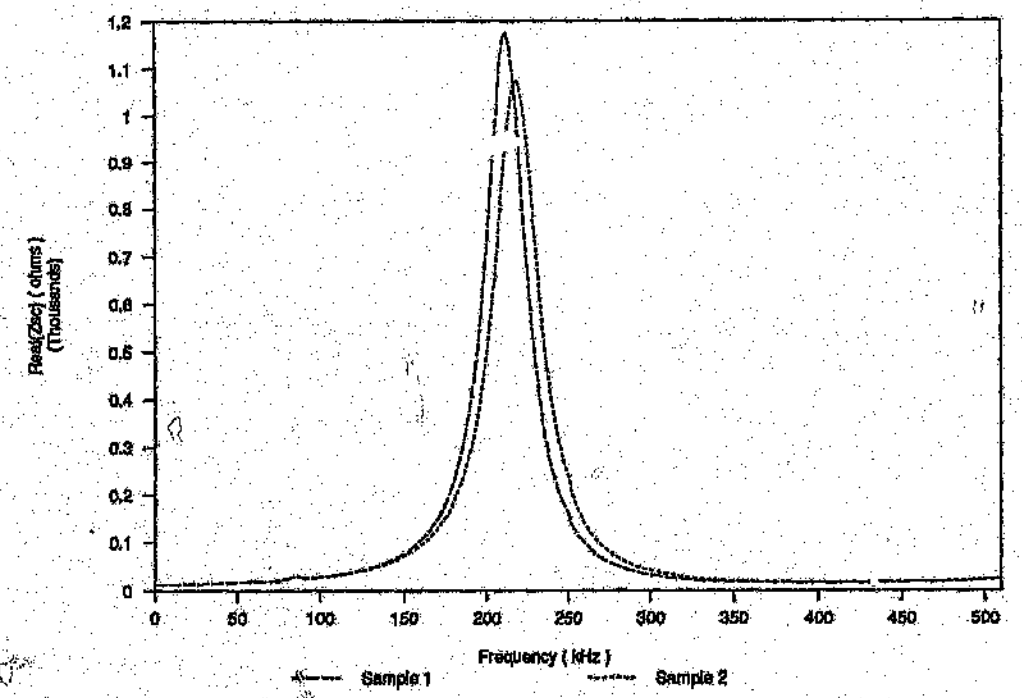

(a)

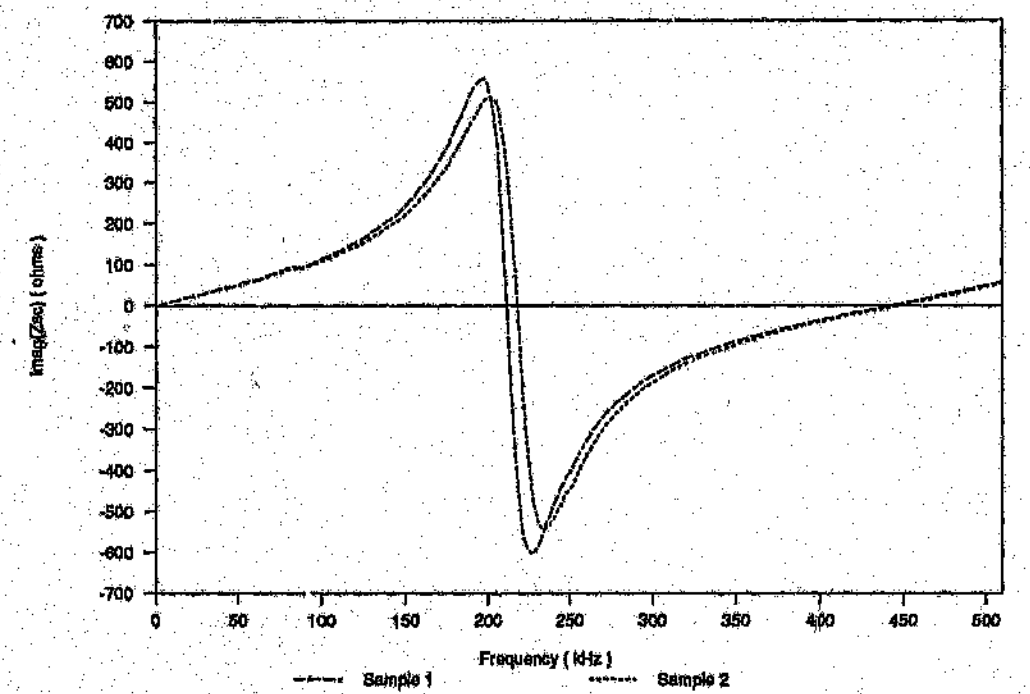

(b)

Figure D.2 Input Impedance, Z_{sc}
Magnitude (a) and phase (b) response of a 200m section of cable gauge type 19 terminated under *short-circuit* conditions.

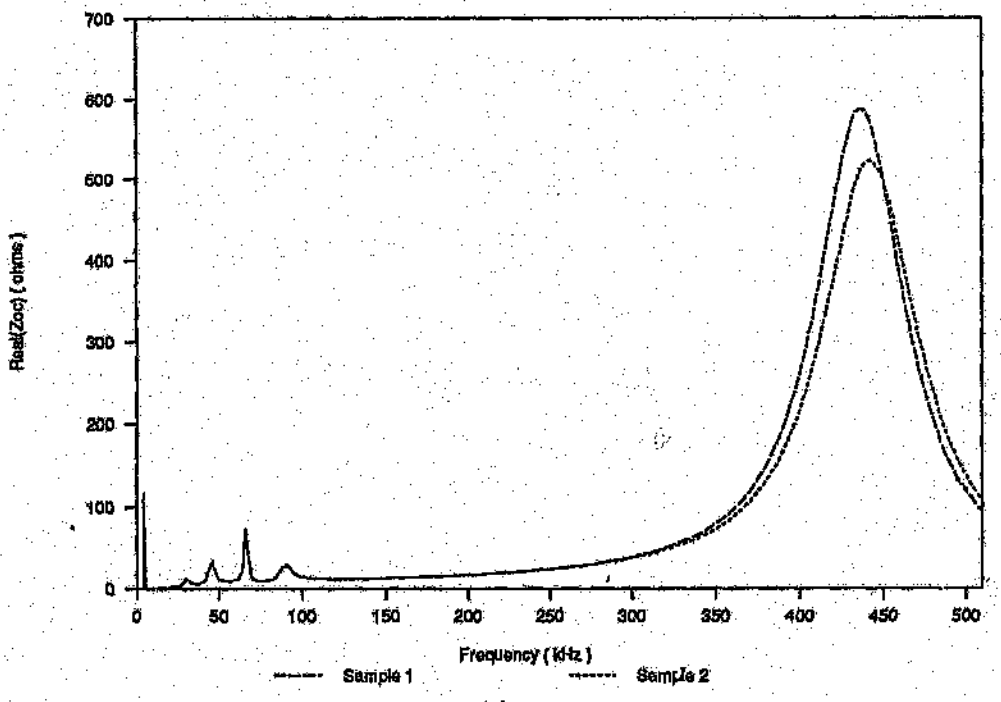

(a)

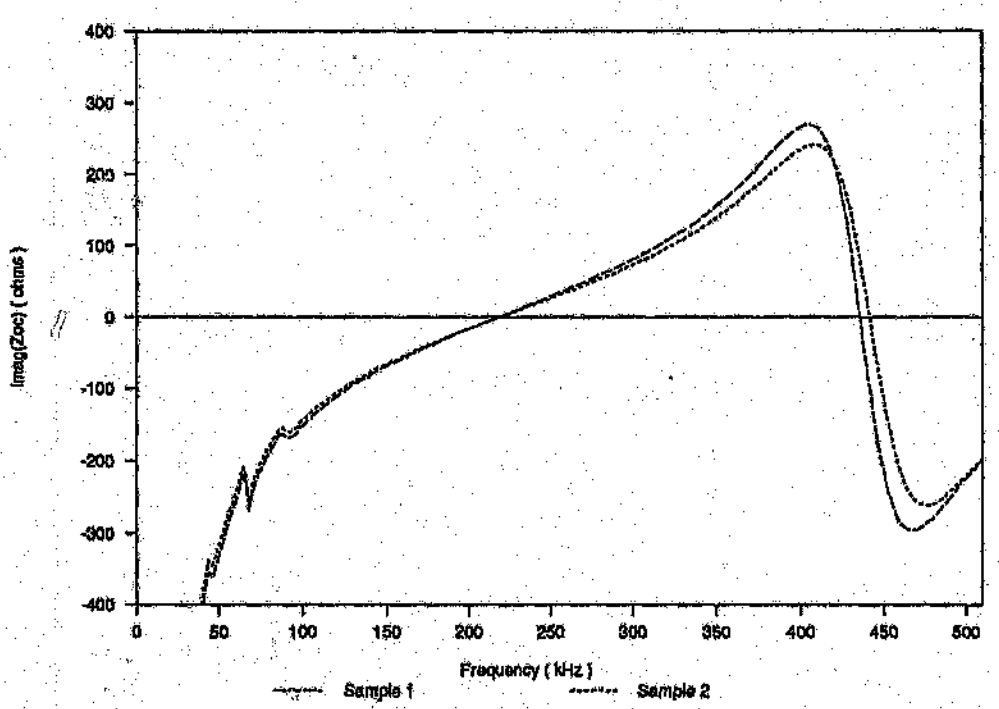

(b)

Figure D.3 Input Impedance, Z_{oc}
Magnitude (a) and phase (b) response of a 200m section of cable gauge type 22 terminated under *open-circuit* conditions.

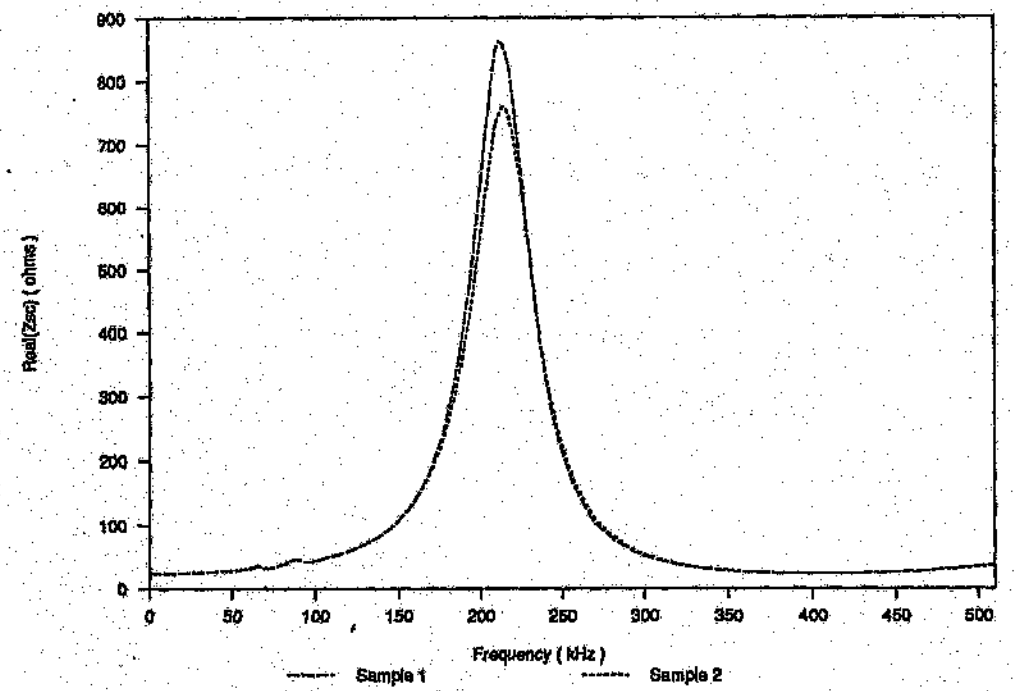

(a)

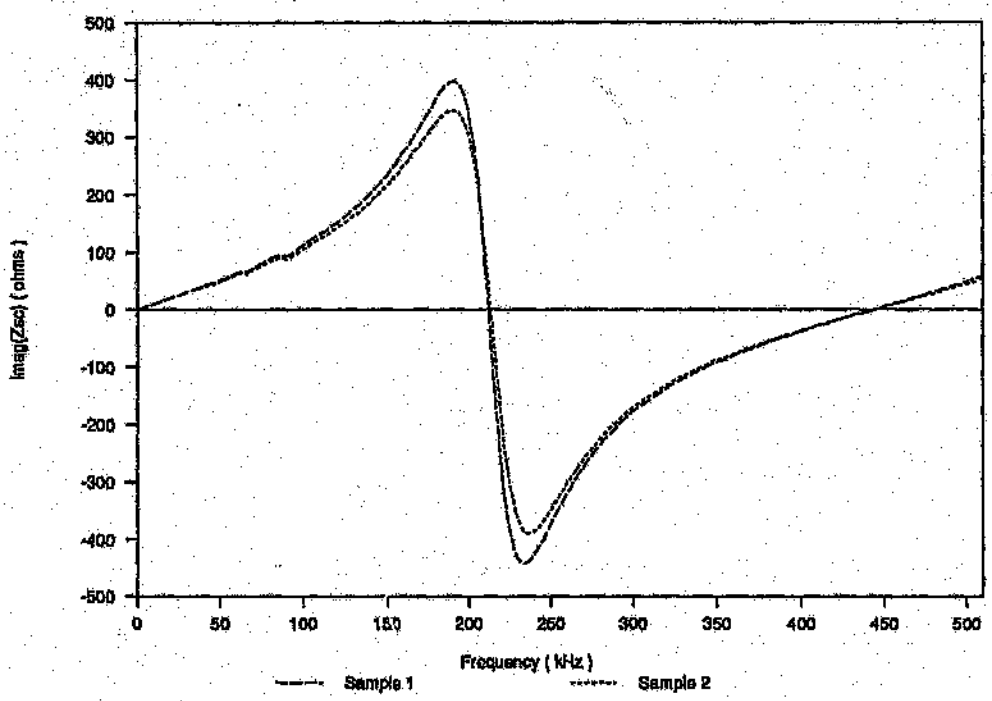

(b)

Figure D.4 Input Impedance, Z_{oc}
Magnitude (a) and phase (b) response of a 200m section of cable gauge type 22 terminated under *open-circuit* conditions.

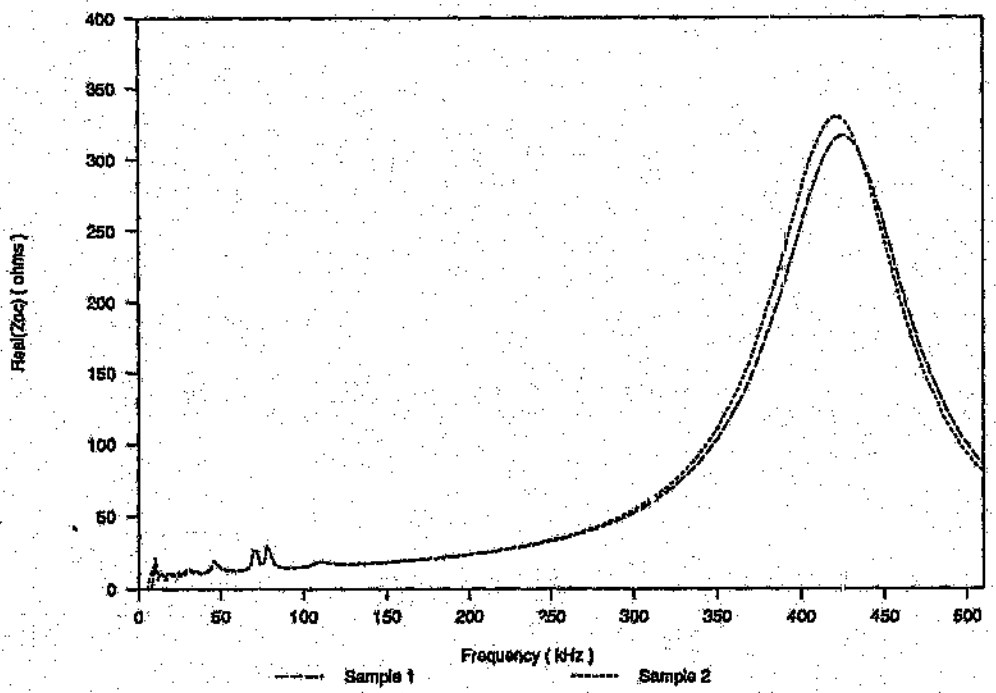

(a)

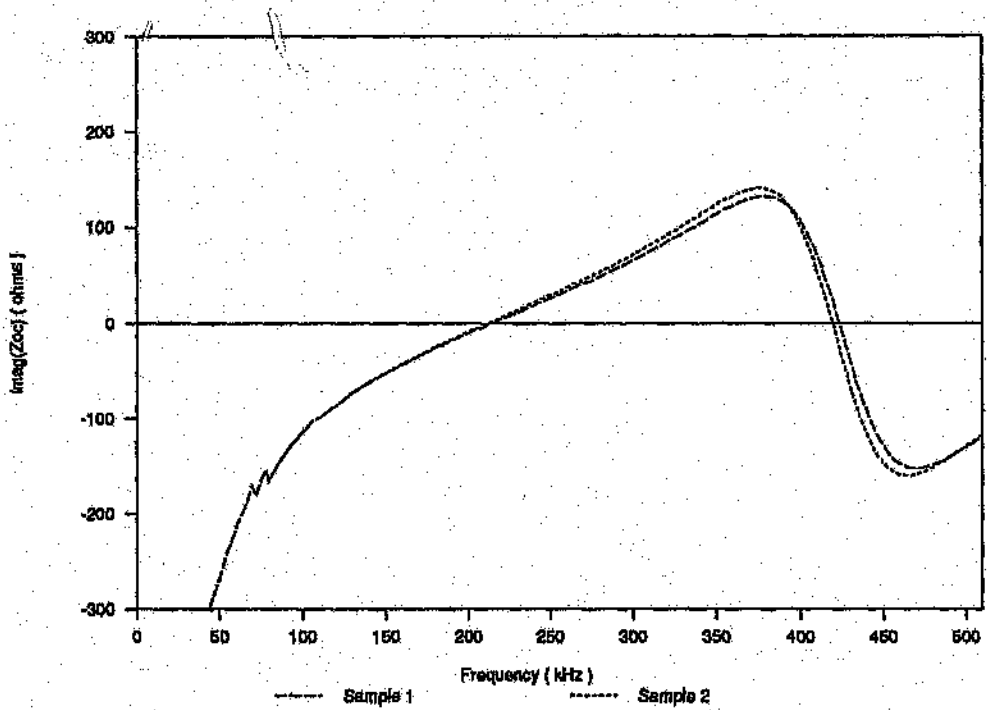

(b)

Figure D.5 Input Impedance, Z_{oc}
Magnitude (a) and phase (b) response of a 200m section of cable gauge type 24 terminated under *open-circuit* conditions.

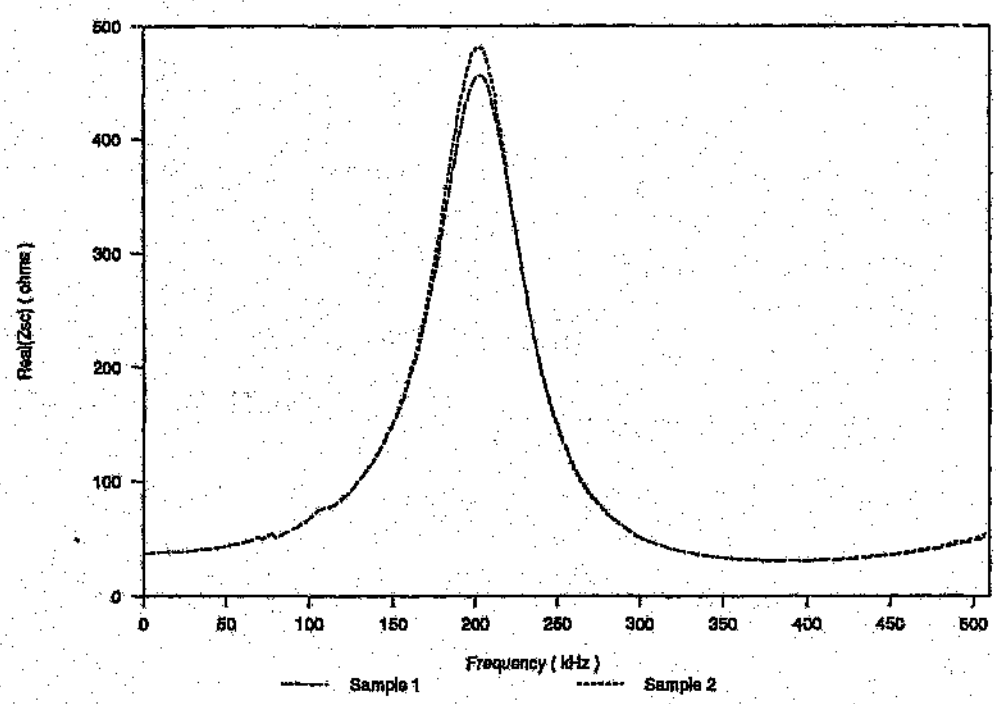

(a)

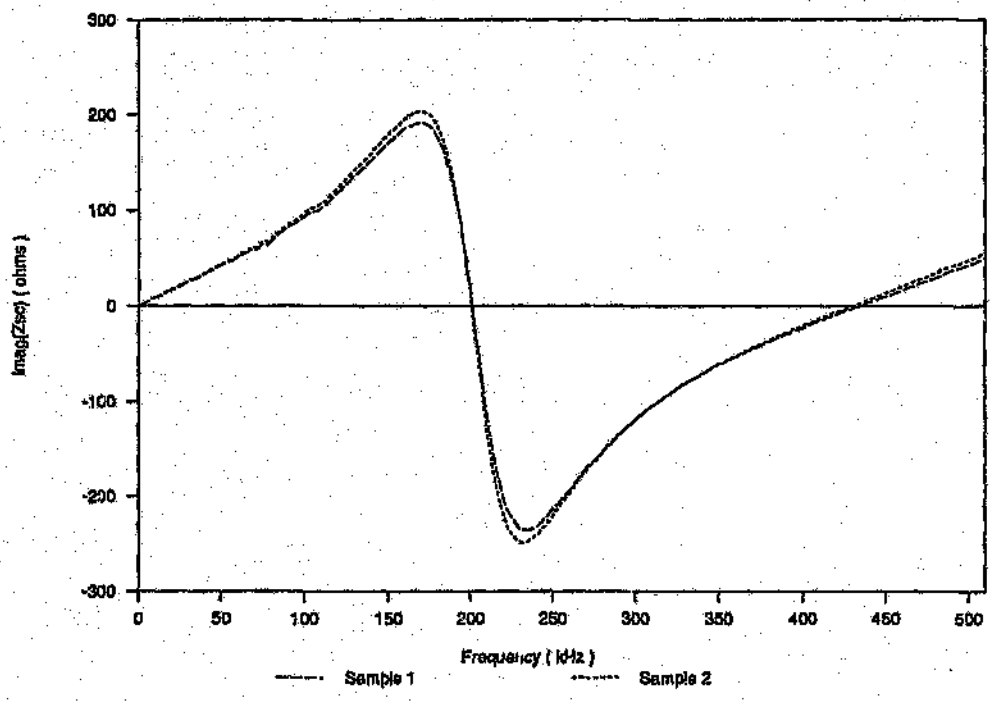

(b)

Figure D.6 Input Impedance, Z_{oc}
Magnitude (a) and phase (b) response of a 200m section of cable gauge type 24 terminated under *open-circuit* conditions.

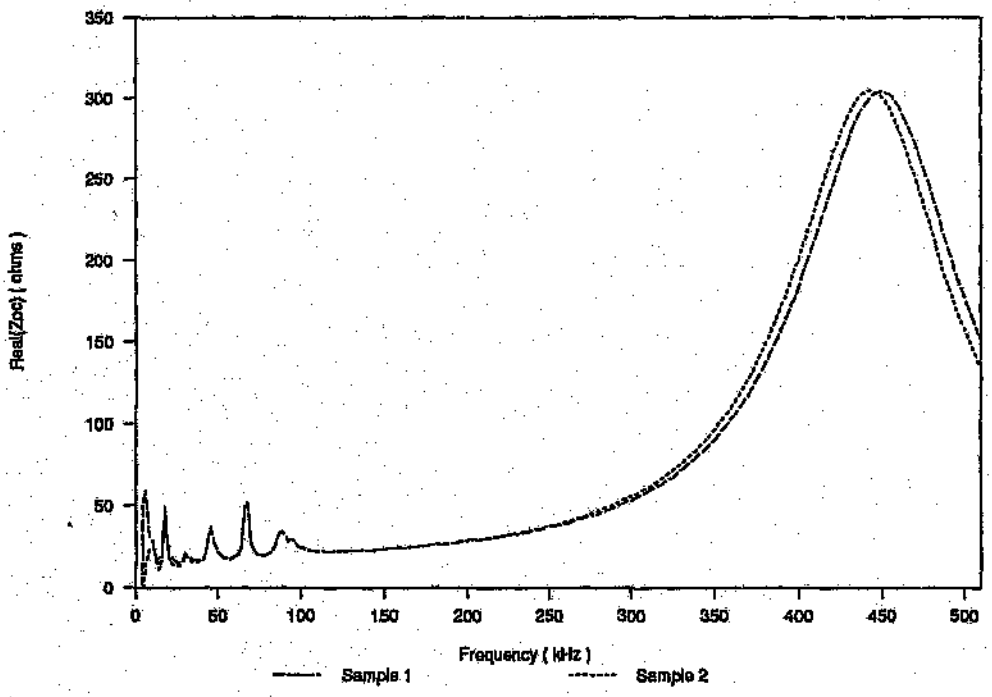

(a)

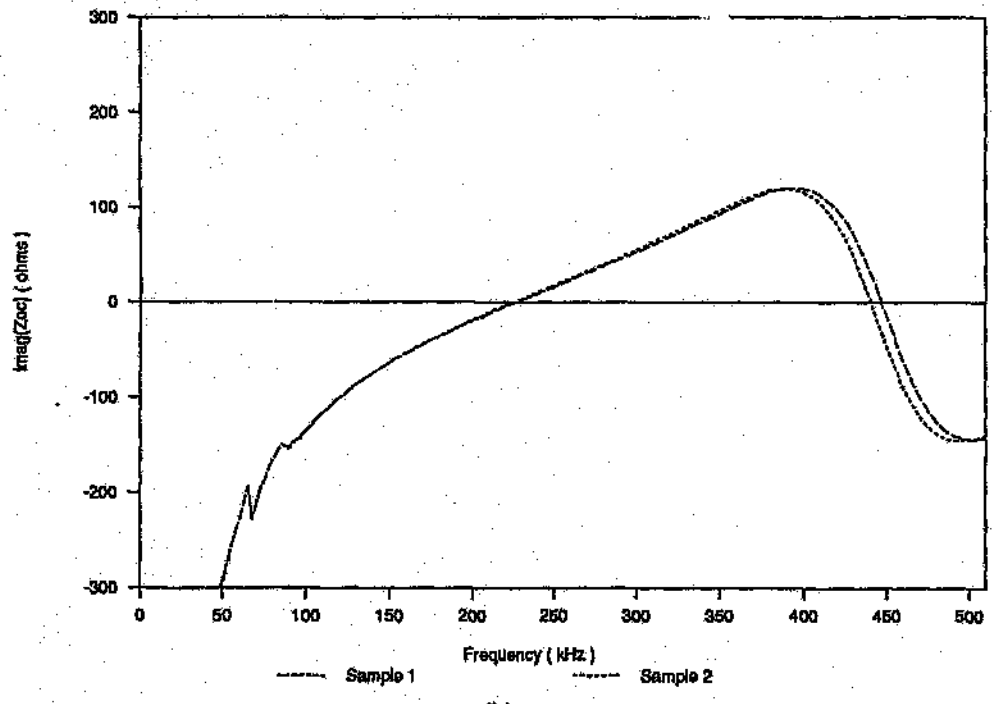

(b)

Figure D.7 Input Impedance, Z_{oc}
Magnitude (a) and phase (b) response of a 200m section of cable gauge type 26 terminated under *open-circuit* conditions.

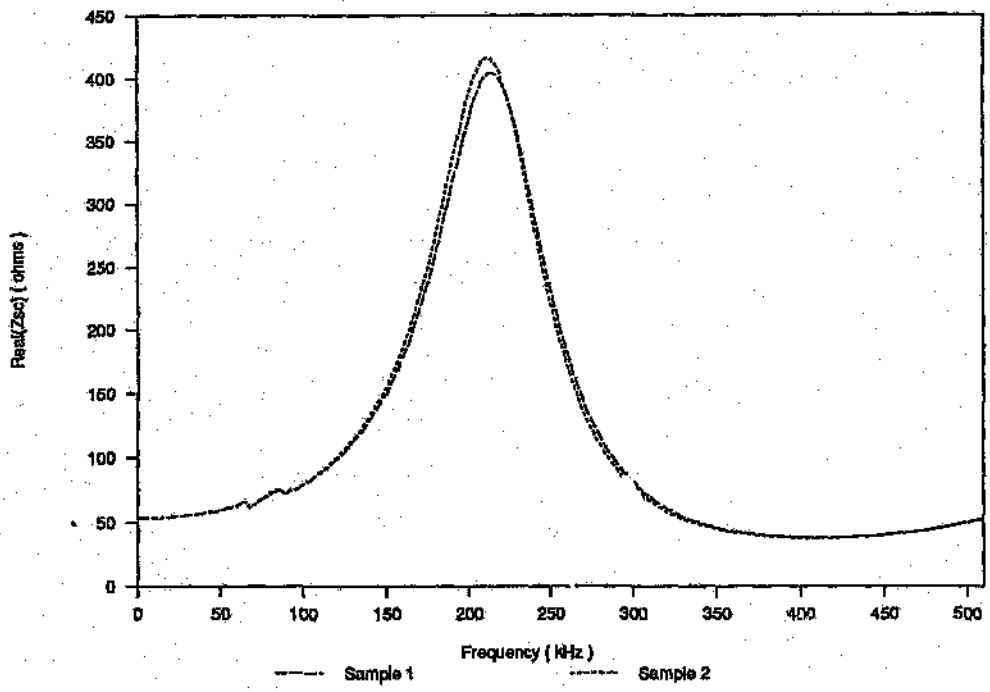

(a)

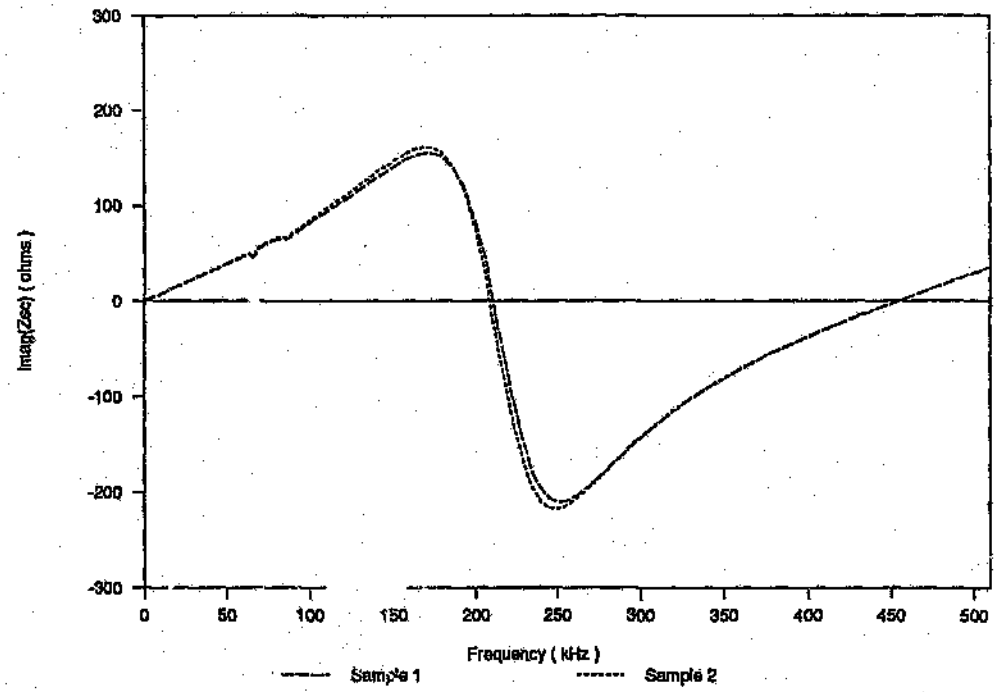

(b)

Figure D.8 Input Impedance, Z_{oc}
Magnitude (a) and phase (b) response of a 200m section of cable gauge type 26 terminated under *open-circuit* conditions.

Appendix E

PRIMARY PARAMETERS

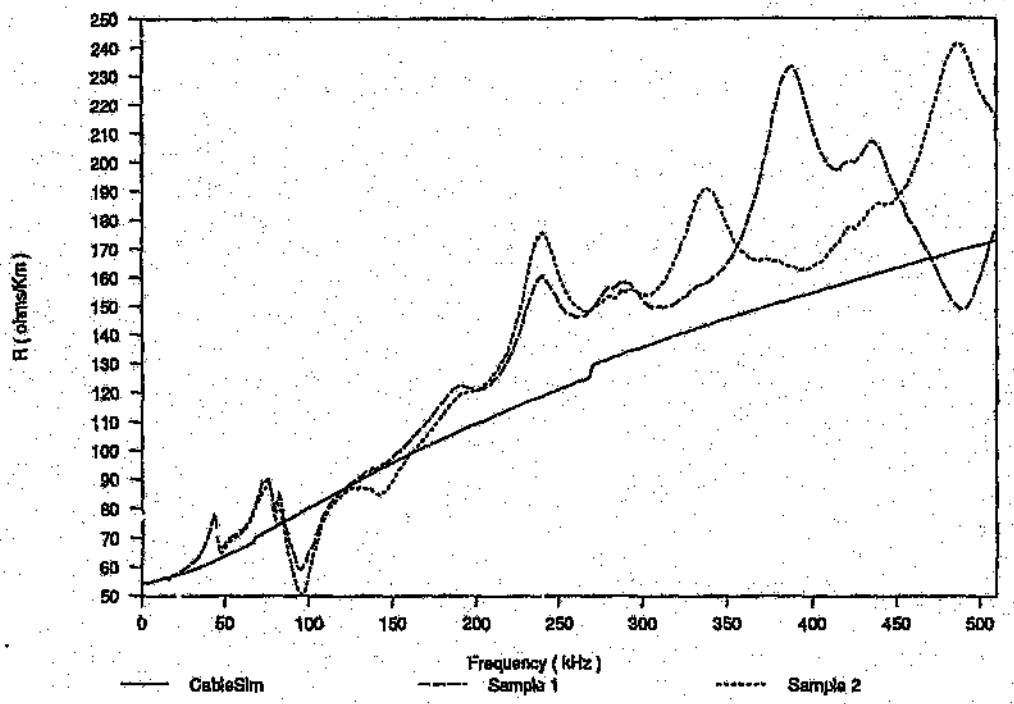

Note : *y-axis zero suppressed*

Figure E.1 Gauge 19 - Resistance

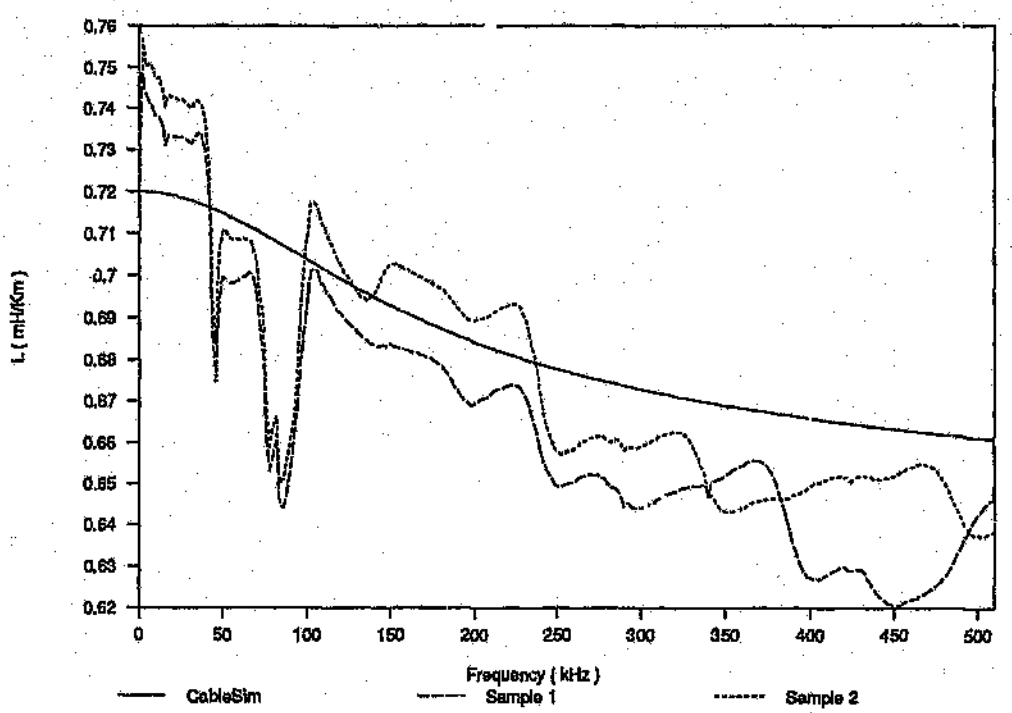

Note : *y-axis zero suppressed*

Figure E.2 Gauge 19 - Inductance

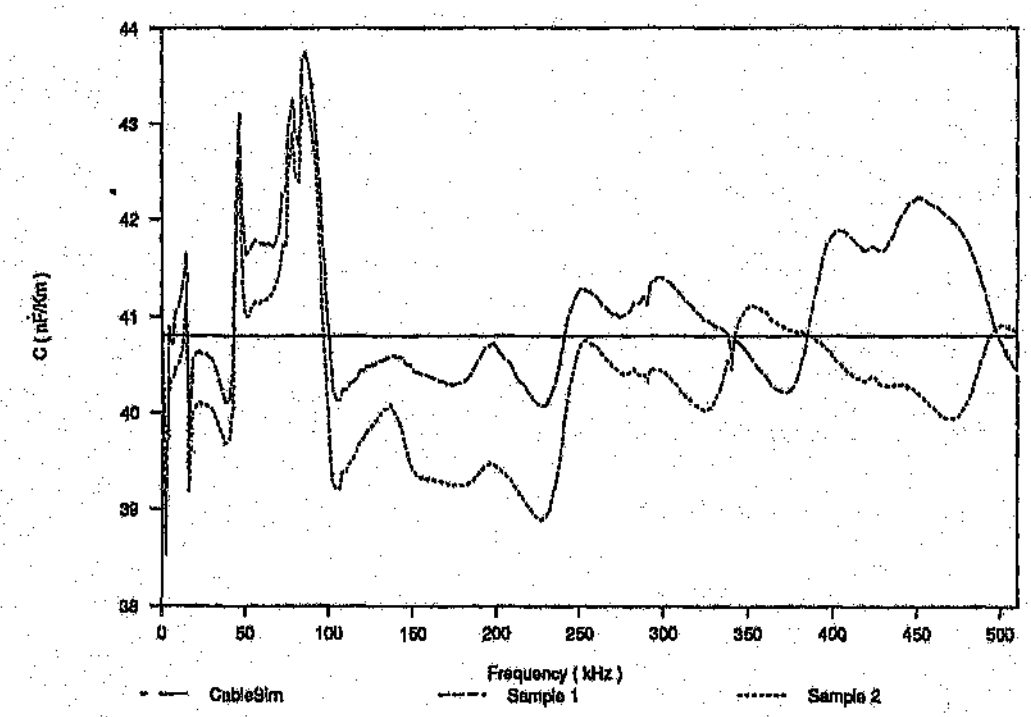

Note : *y-axis zero suppressed*

Figure E.3 Gauge 19 - Capacitance

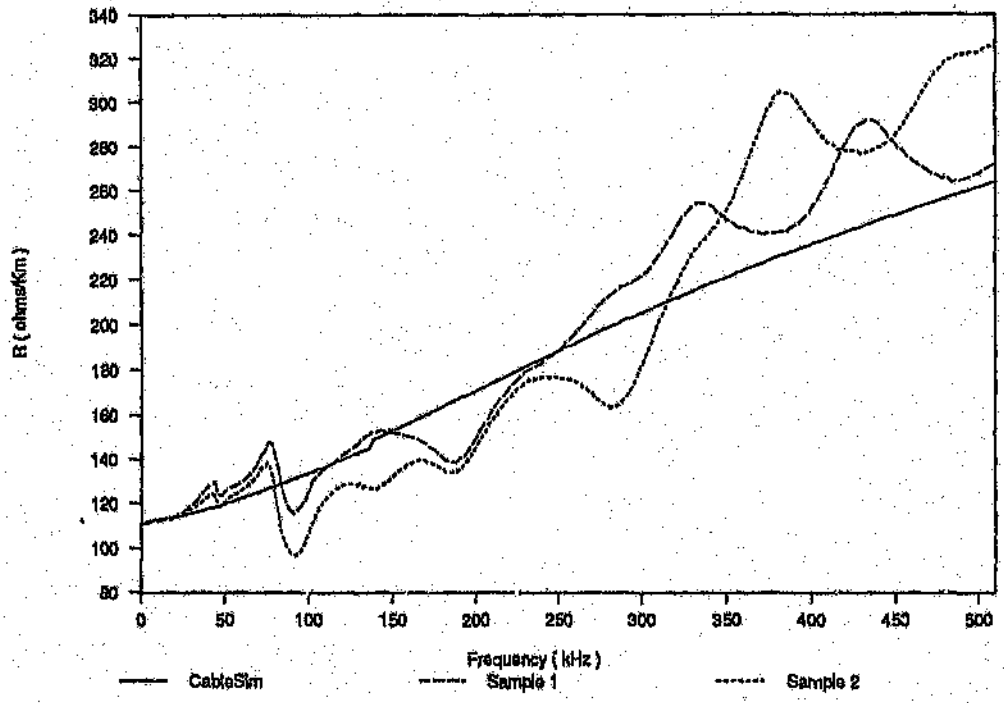

Note : *y-axis zero suppressed*

Figure E.4 Gauge 22 - Resistance

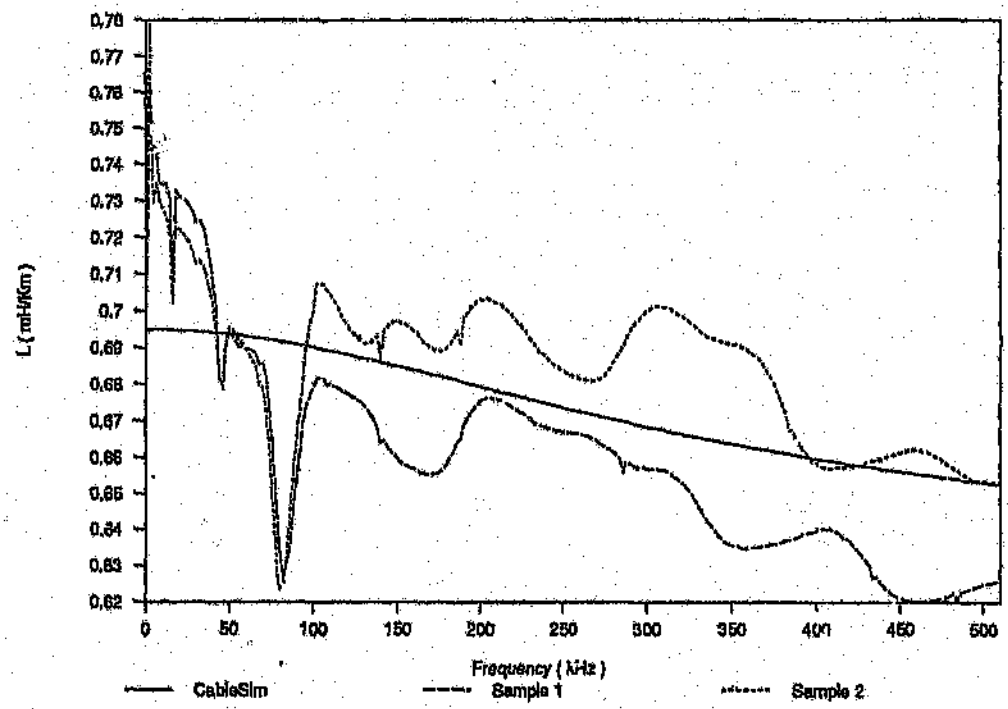

Note : *y-axis zero suppressed*

Figure E.5 Gauge 22 - Inductance

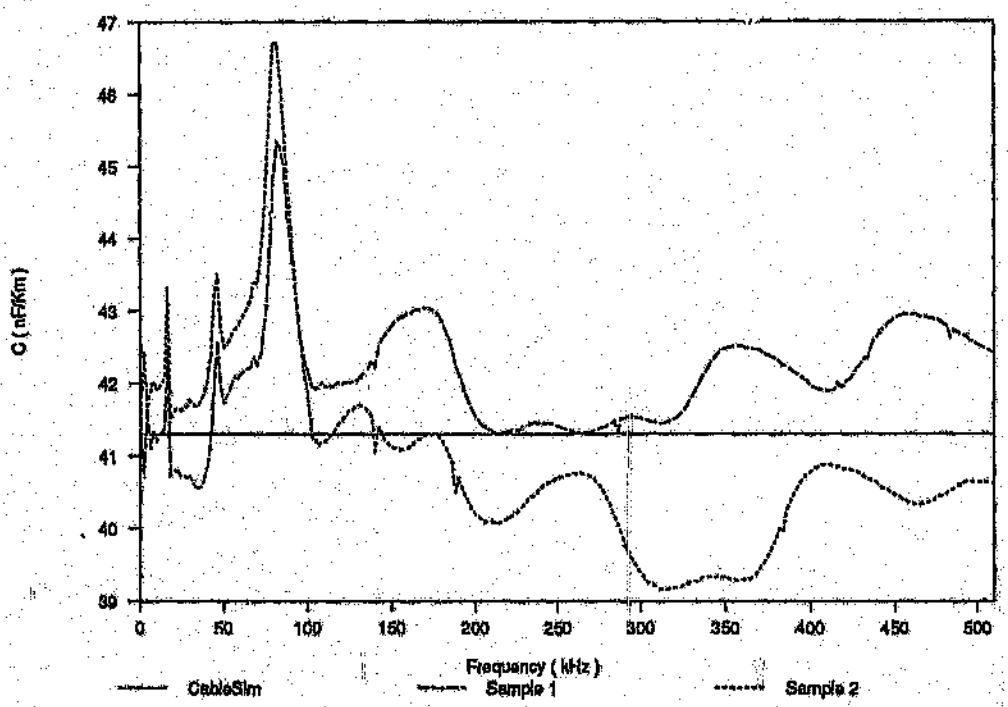

Note : *y-axis zero suppressed*

Figure E.6 Gauge 22 - Capacitance

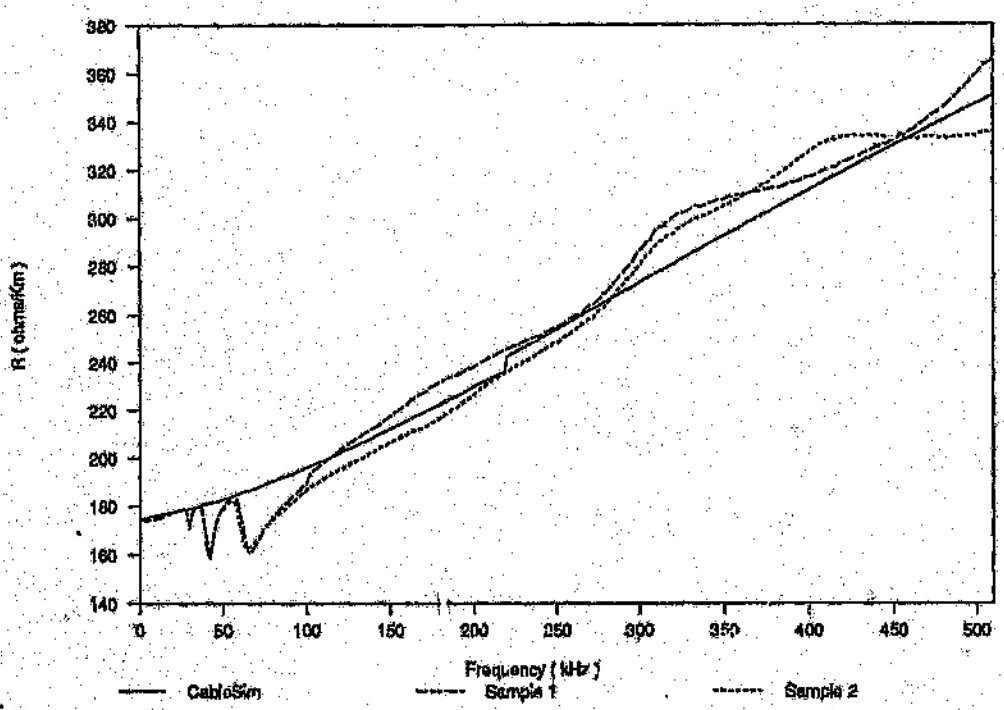

Note : *y-axis zero suppressed*

Figure E.7 Gauge 24 - Resistance

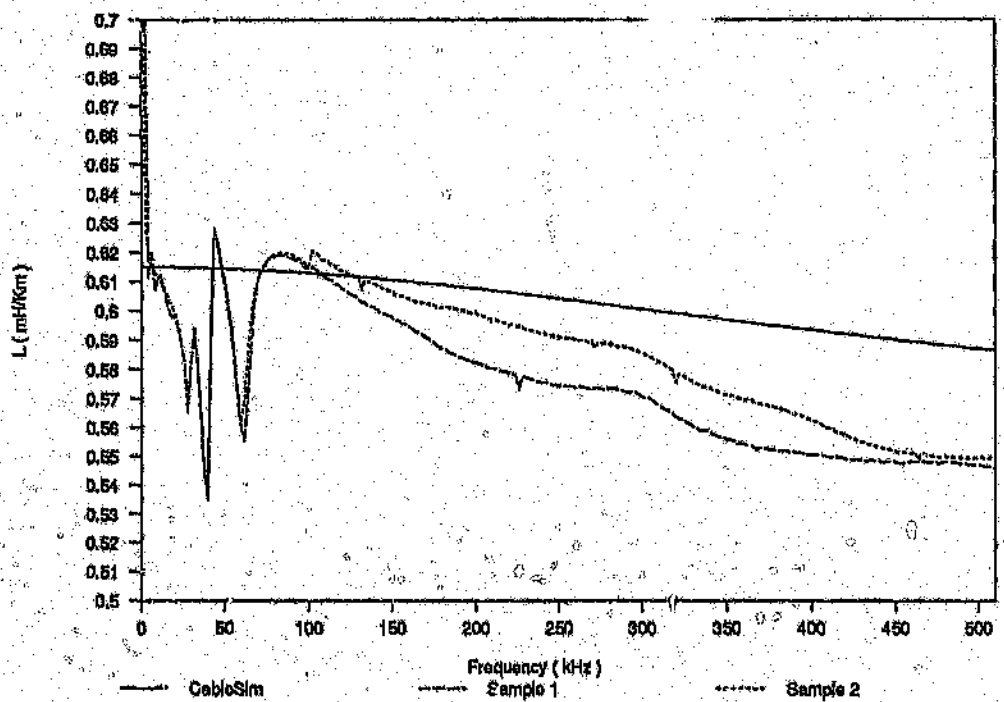

Note : *y-axis zero suppressed*

Figure E.8 Gauge 24 - Inductance

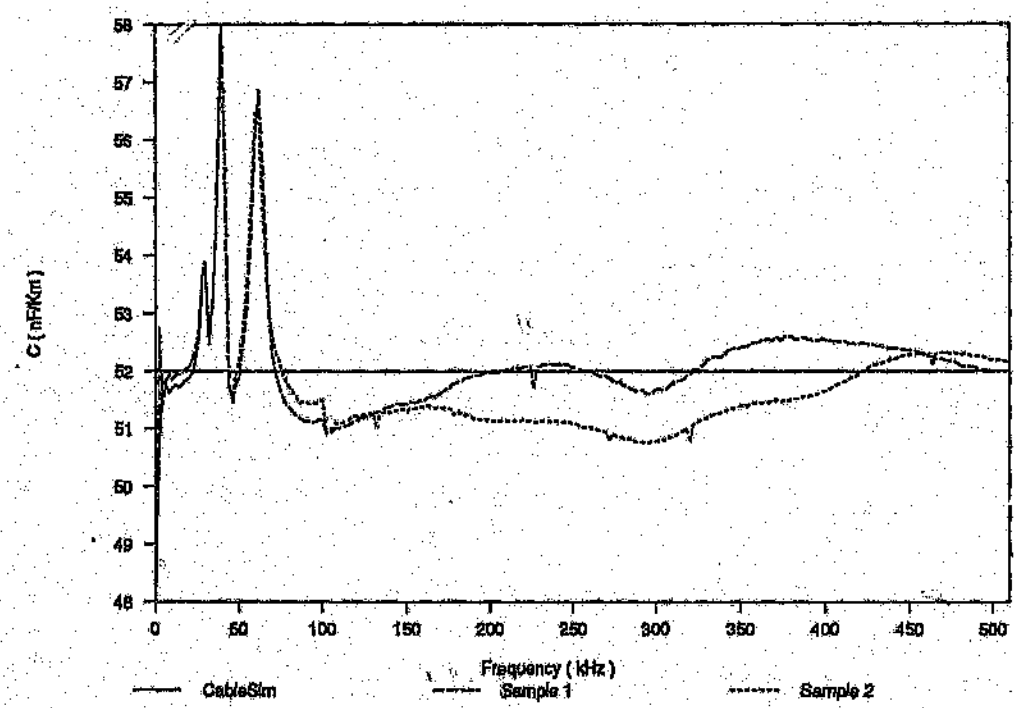

Note : *y-axis zero suppressed*

Figure E.9 Gauge 24 - Capacitance

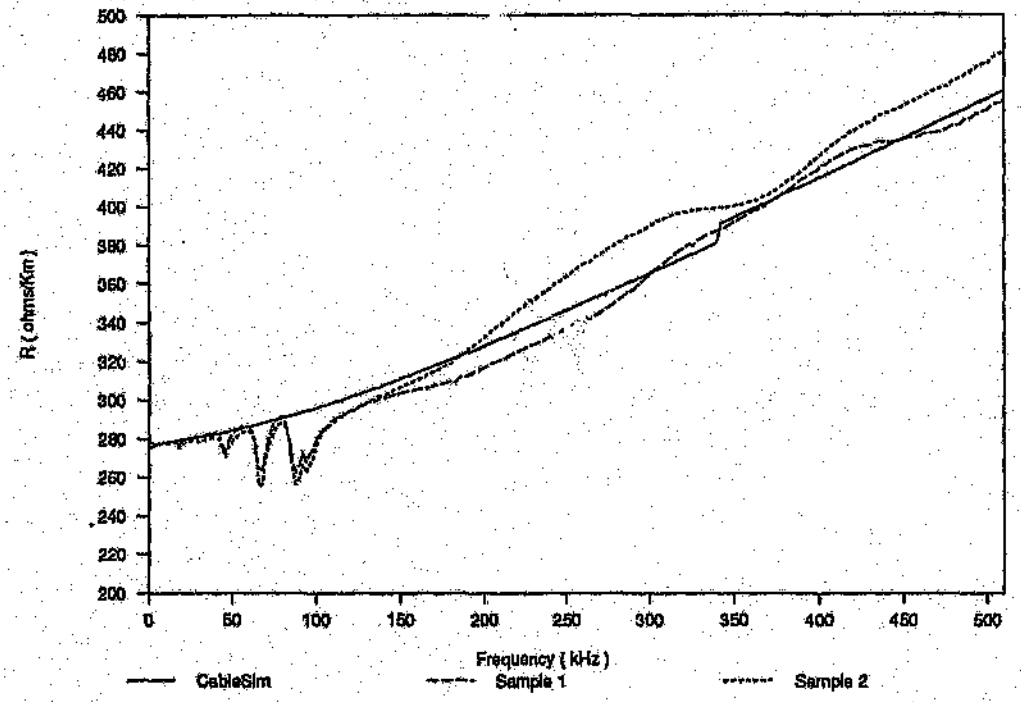

Note : *y-axis zero suppressed*

Figure E.10 Gauge 26 - Resistance

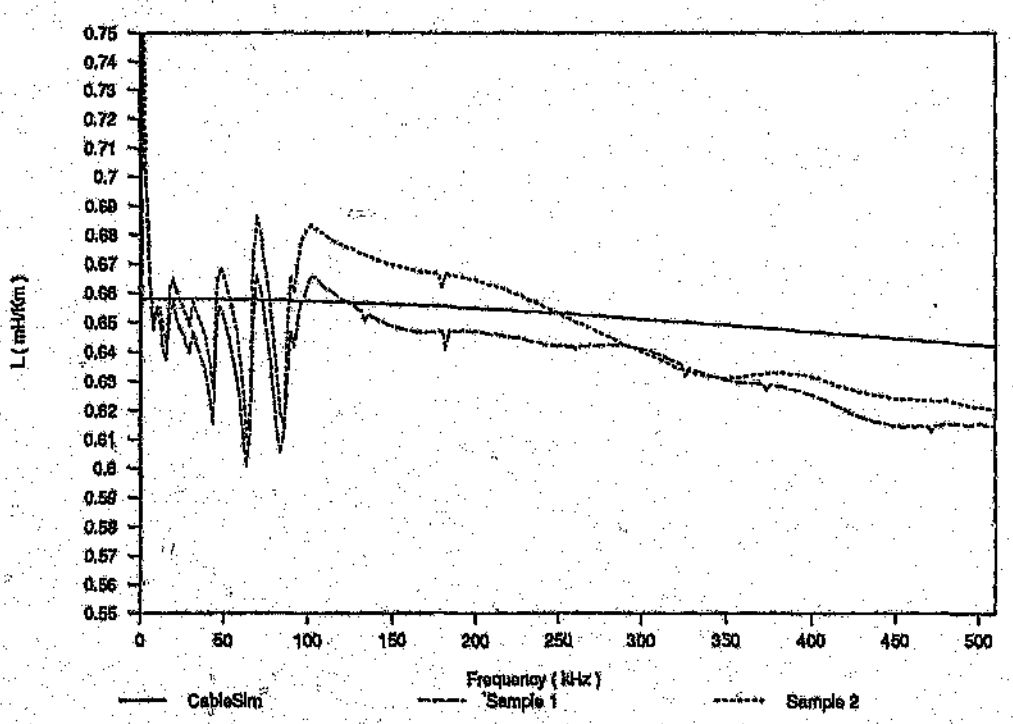

Note : *y-axis zero suppressed*

Figure E.11 Gauge 26 - Inductance

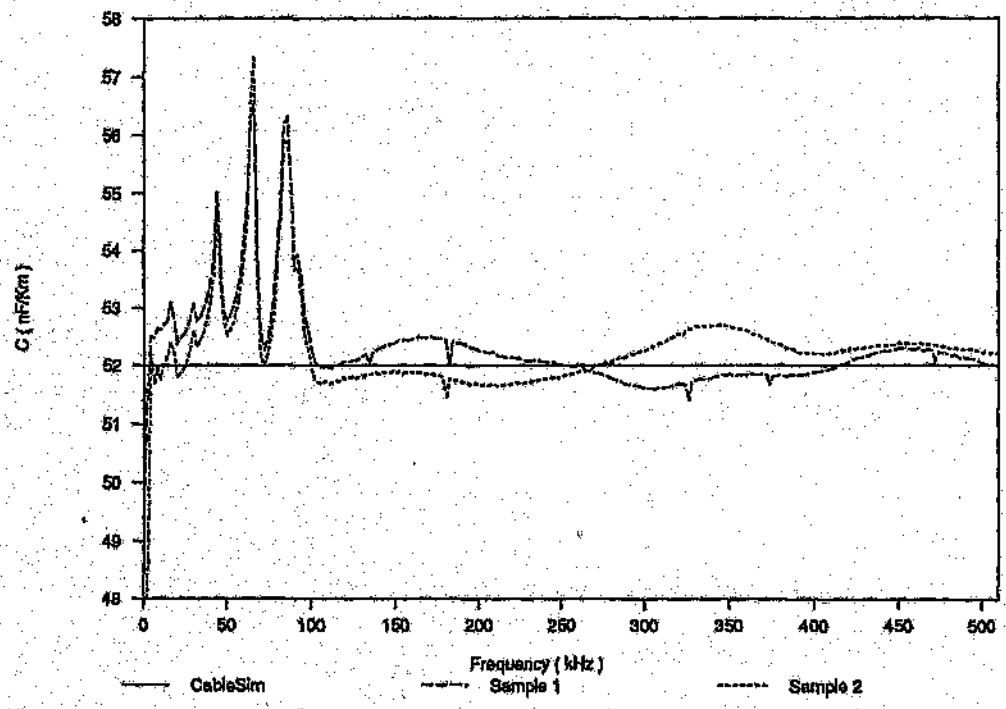

Note : *y-axis zero suppressed*

Figure E.12 Gauge 26 - Capacitance

Appendix F

SECONDARY PARAMETERS

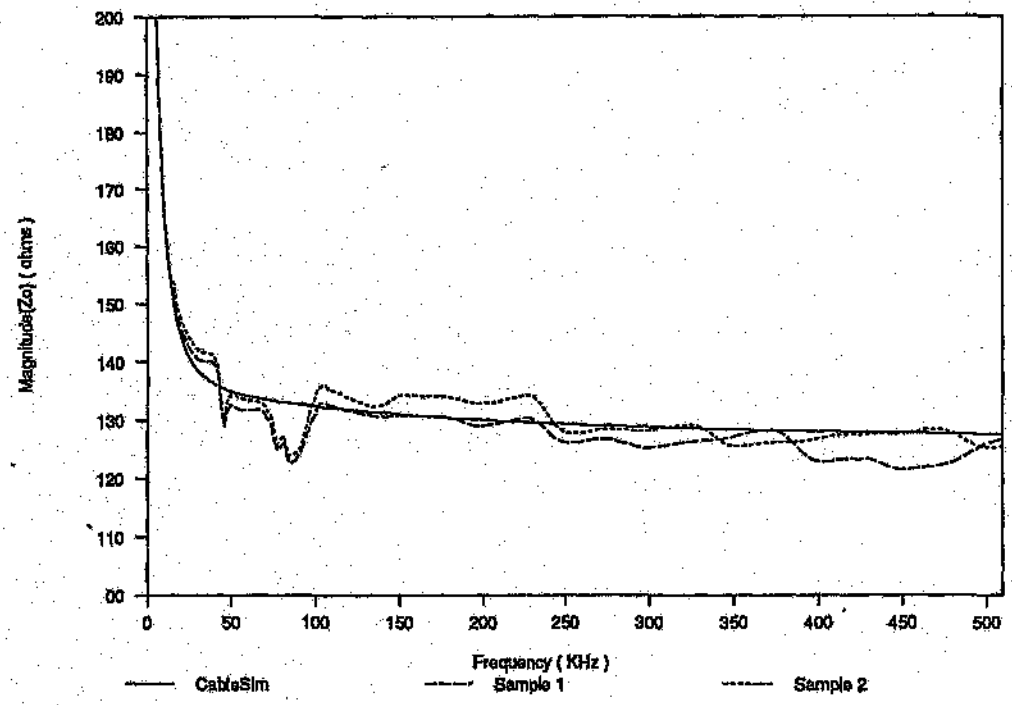

Note : *y-axis zero suppressed*

Figure F.1 Gauge 19 - Magnitude Response(Characteristic Impedance)

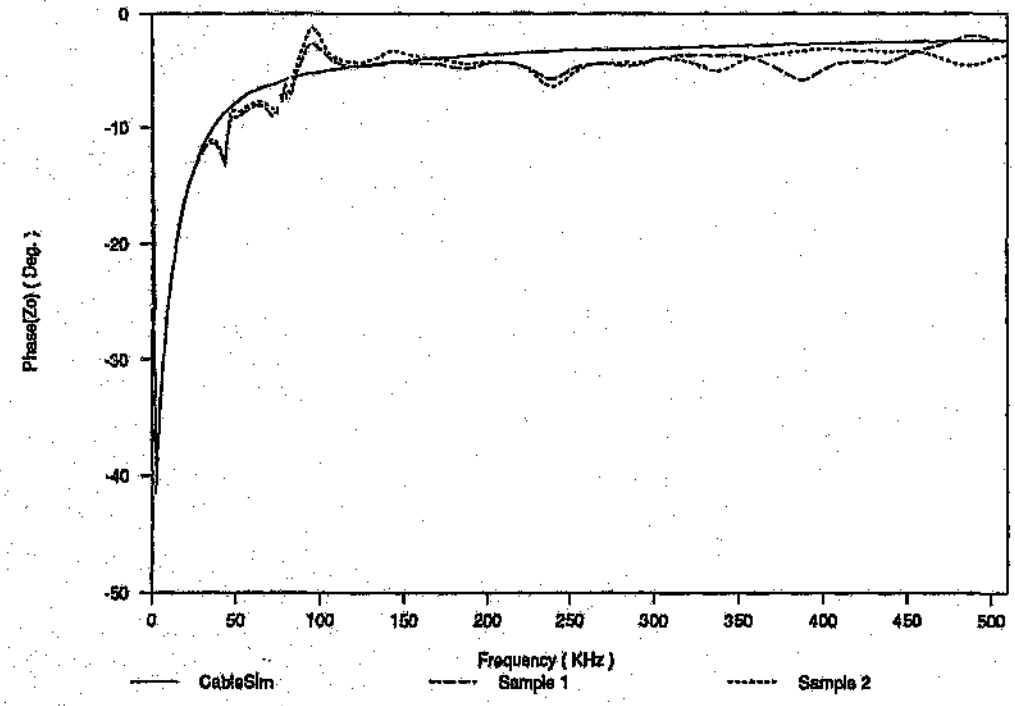

Figure F.2 Gauge 19 - Phase Response(Characteristic Impedance)

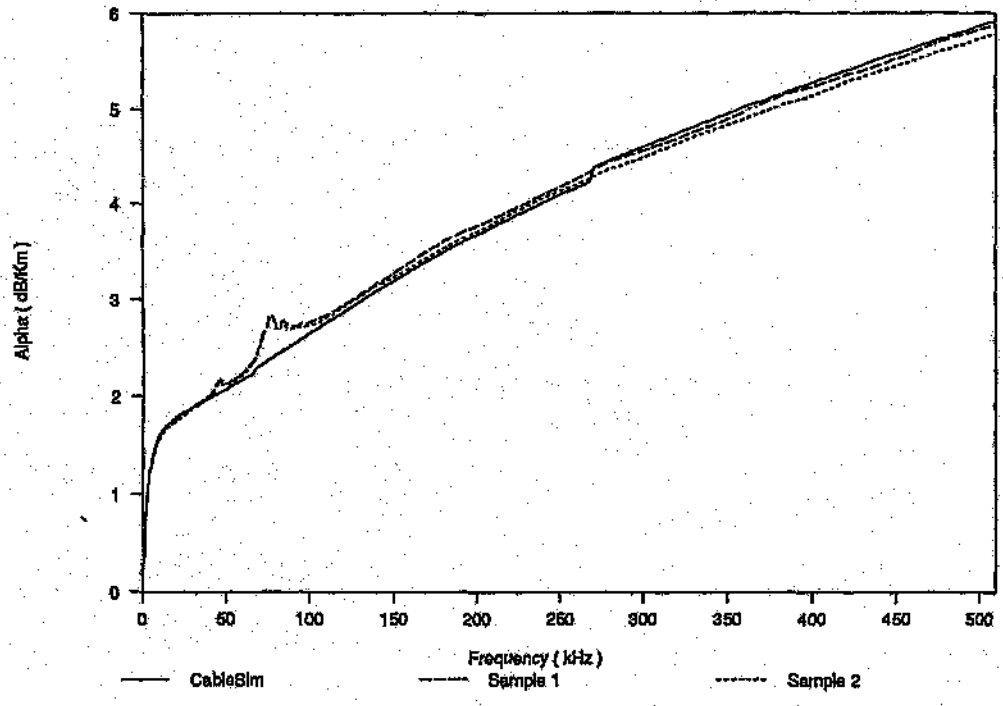

Figure F.3 Gauge 19 - Attenuation Constant

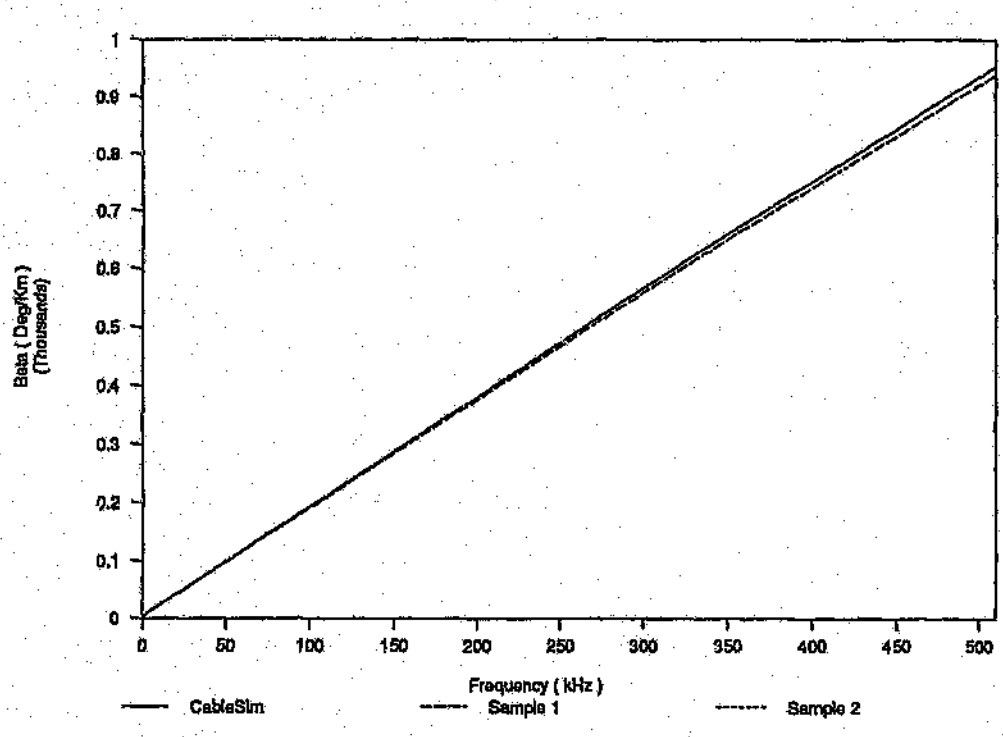

Figure F.4 Gauge 19 - Phase Constant

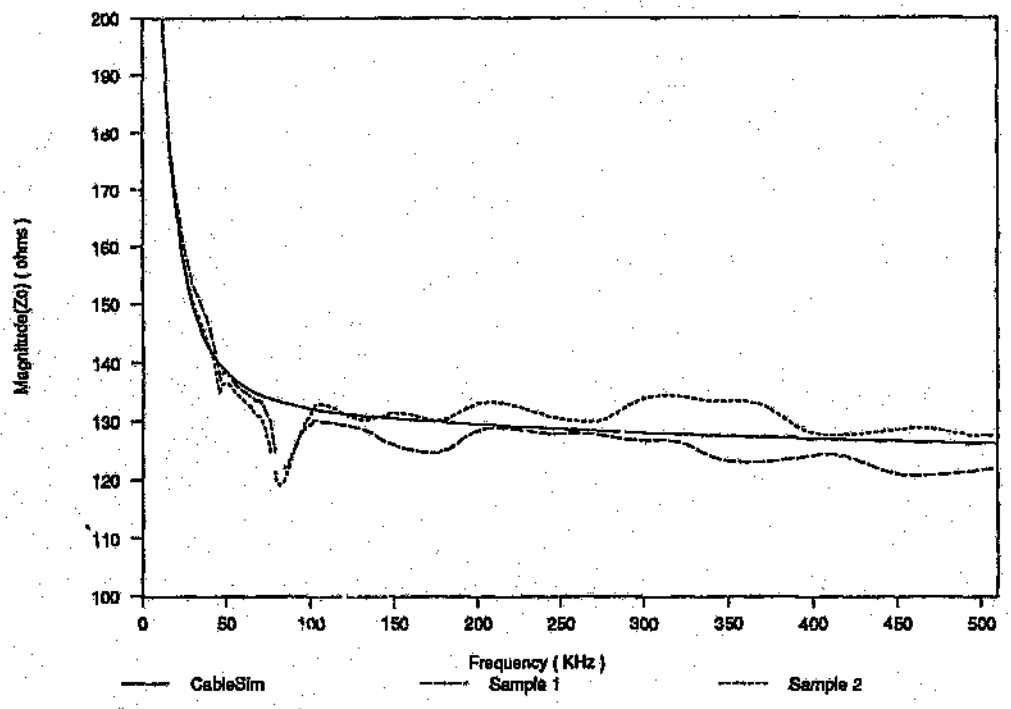

Note : *y-axis zero suppressed*

Figure F.5 Gauge 22 - Magnitude Response(Characteristic Impedance)

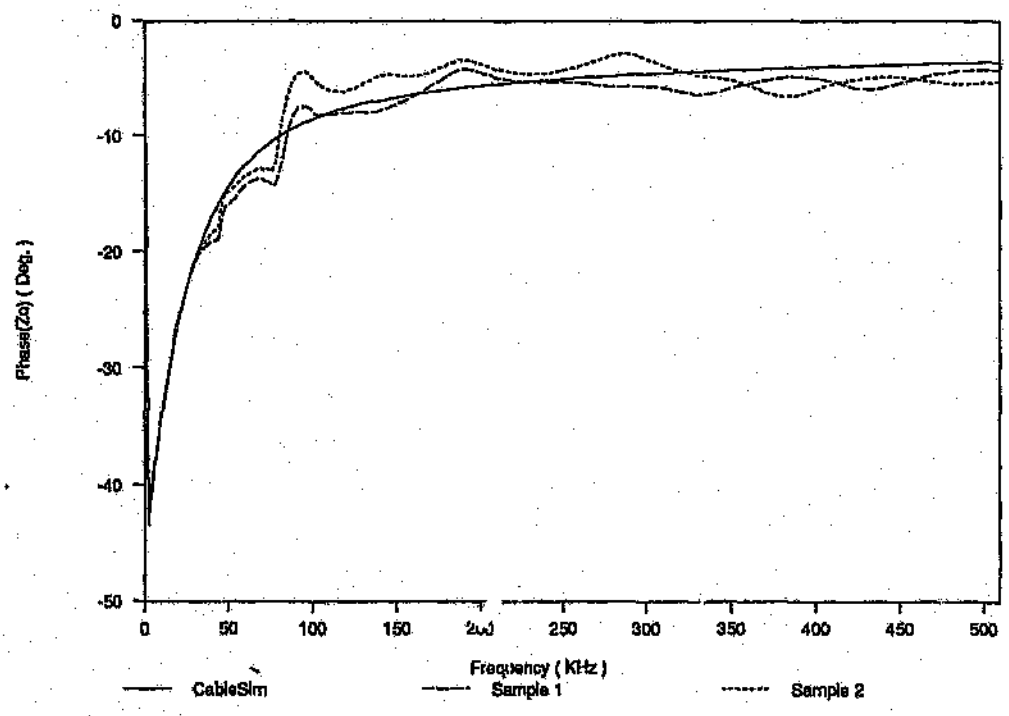

Figure F.6 Gauge 22 - Phase Response(Characteristic Impedance)

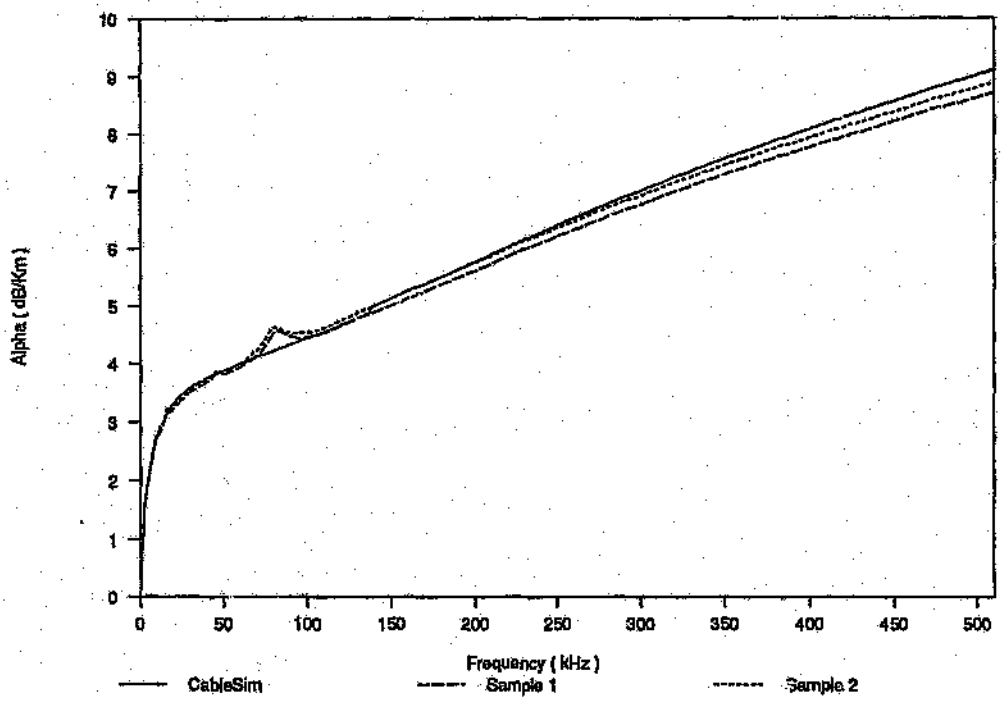

Figure F.7 Gauge 22 - Attenuation Constant

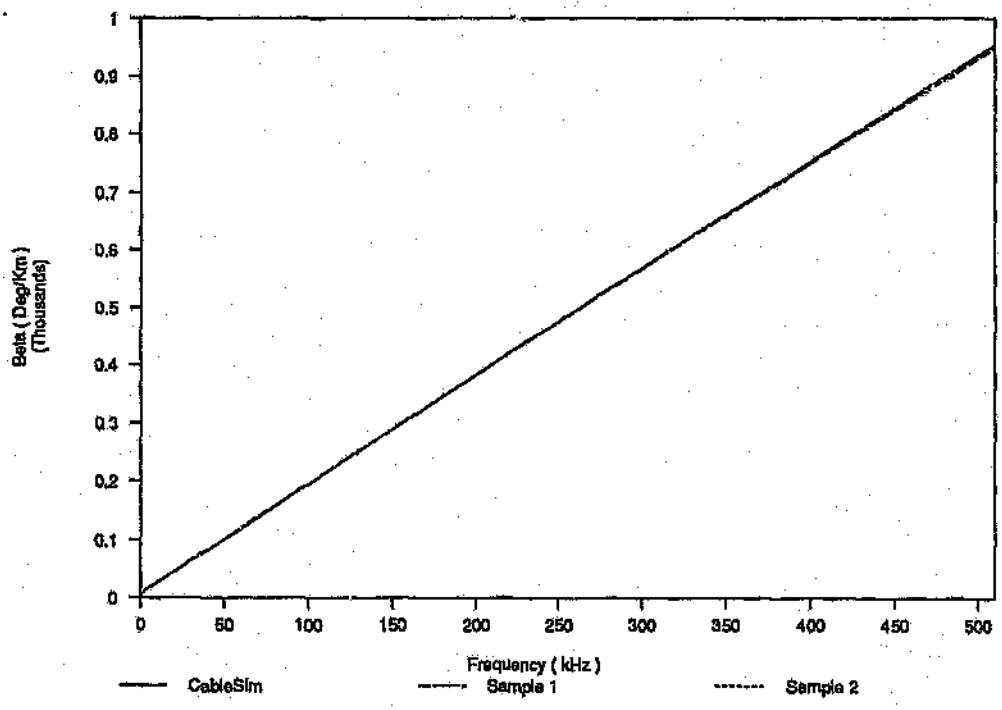

Figure F.8 Gauge 22 - Phase Constant

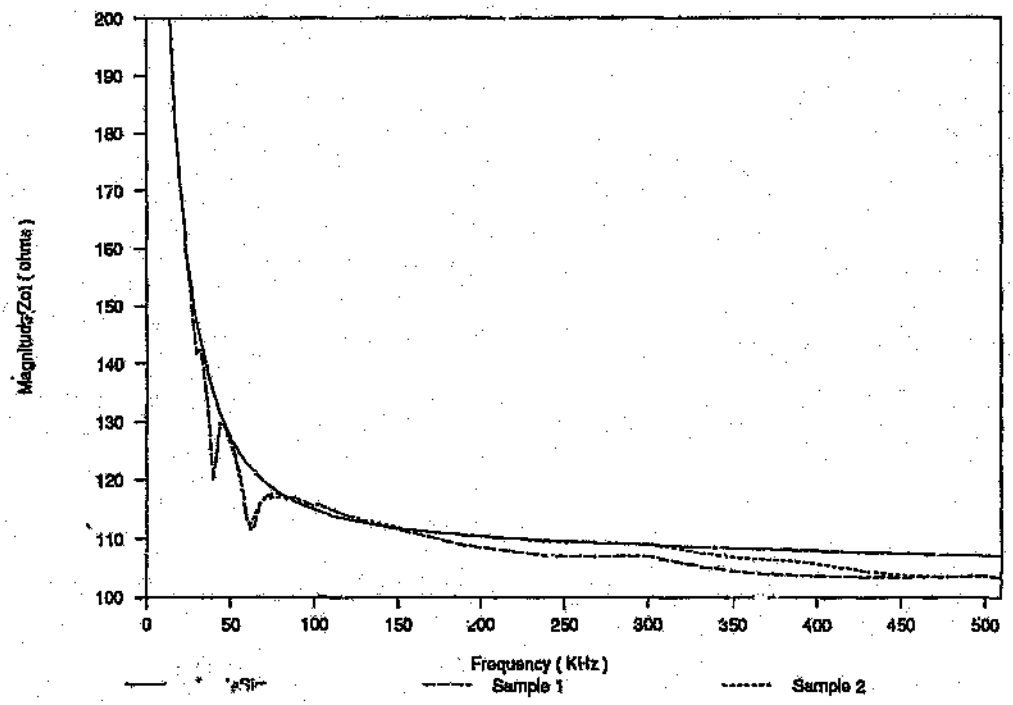

Note : y-axis is zero [illegible]

Figure F.9 [illegible]ude Response(Characteristic Impedance)

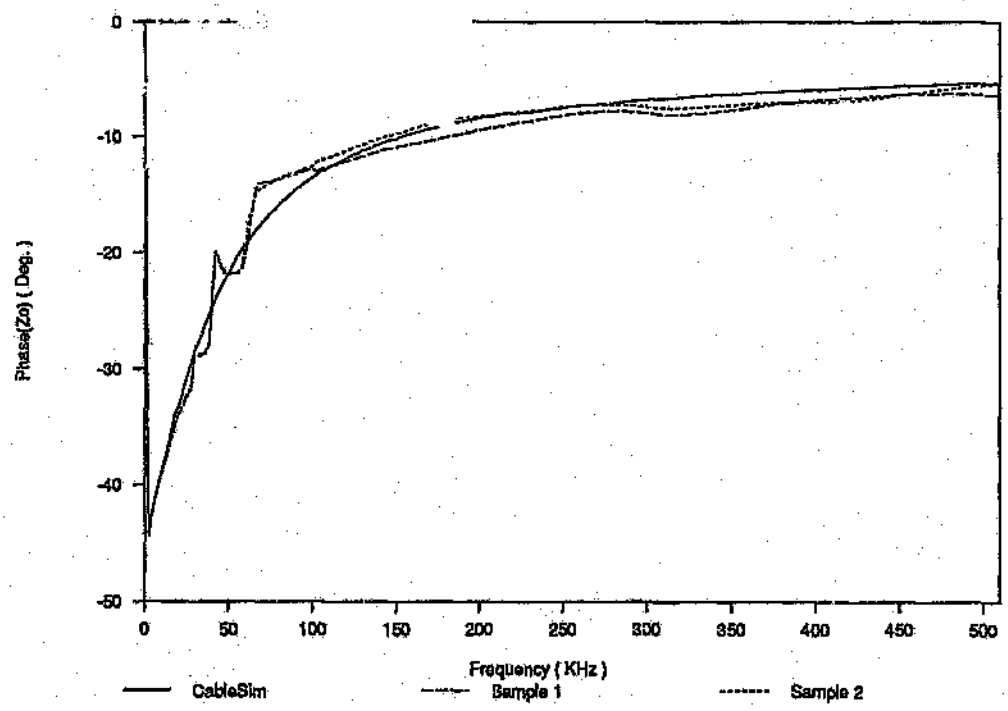

Figure F.10 Gauge 24 - Phase Response(Characteristic Impedance)

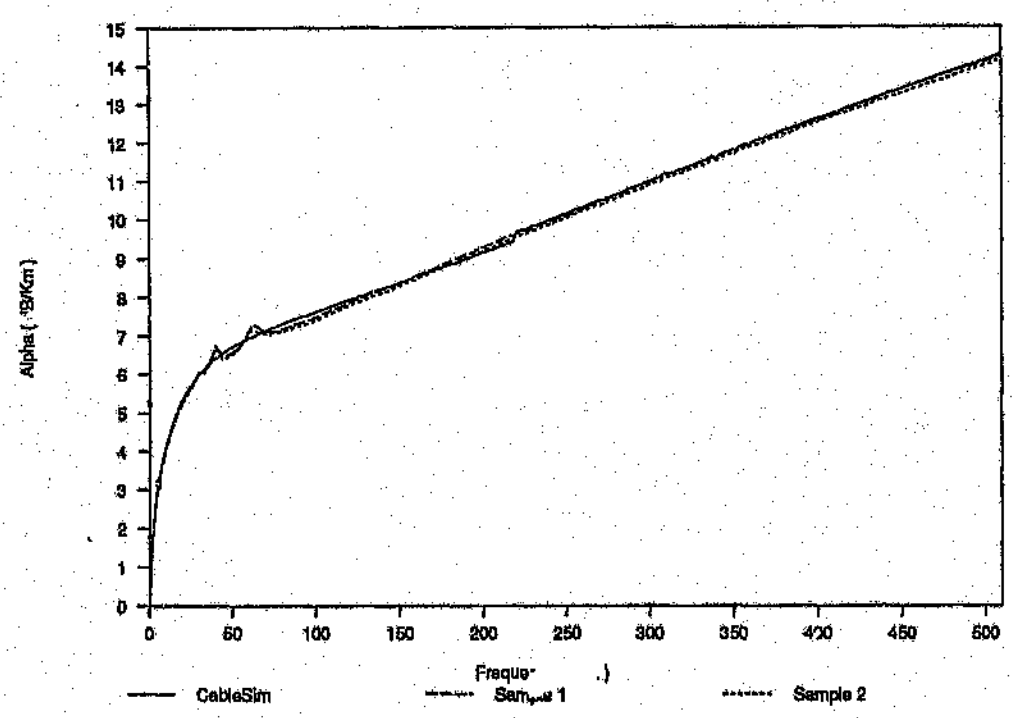

Figure F.11 Gauge 24 - Attenuation Constant

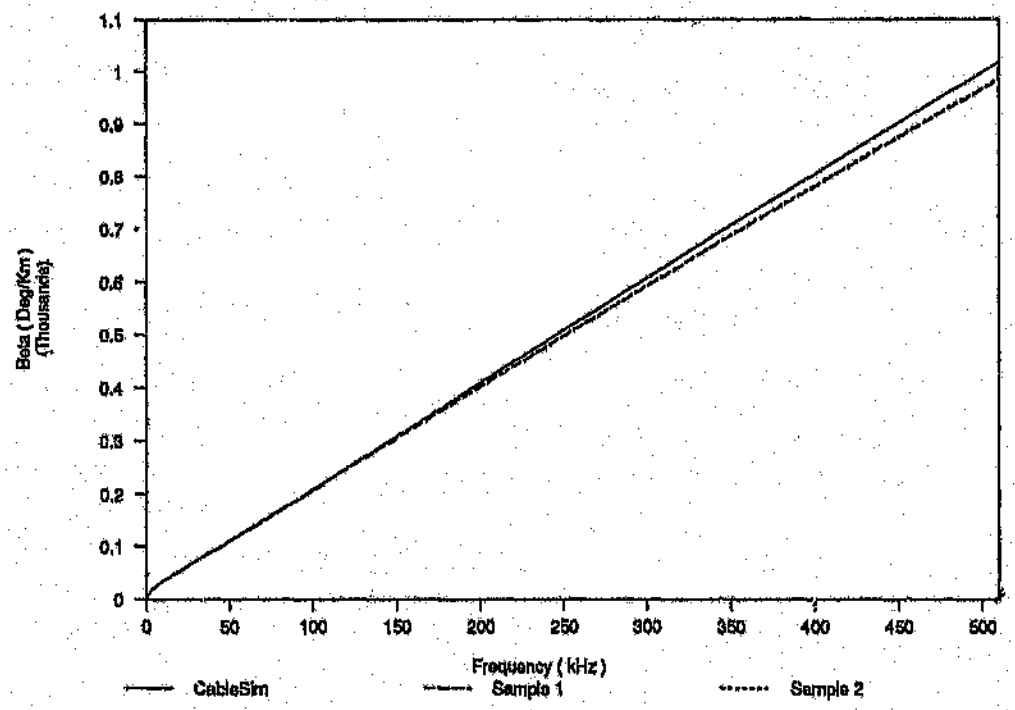

Figure F.12 Gauge 24 - Phase Constant

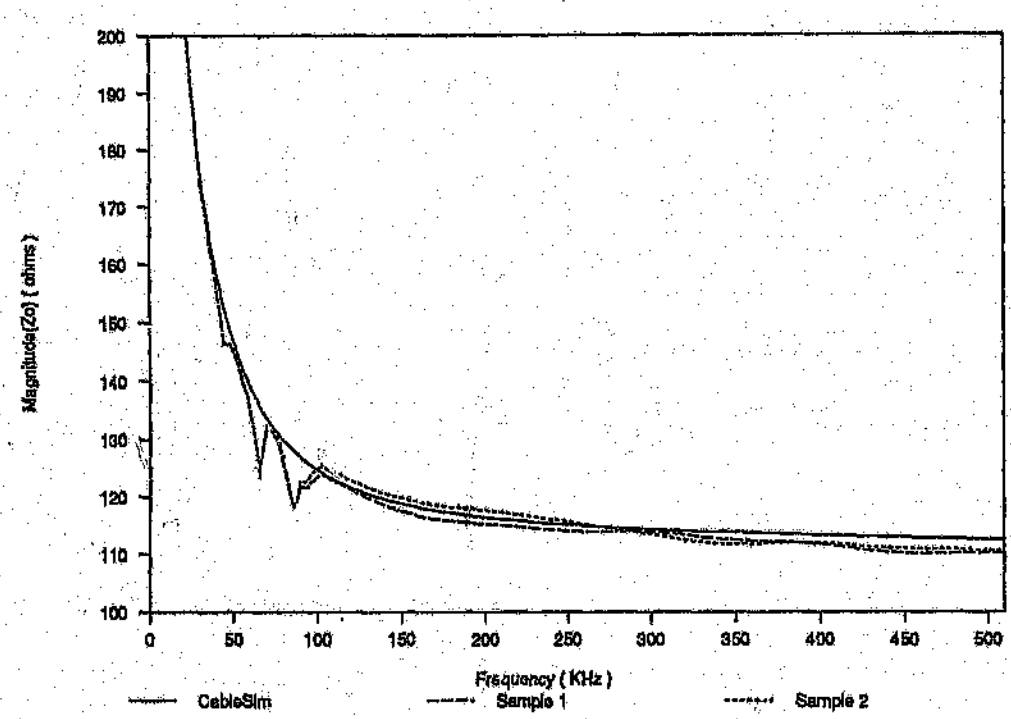

Note : *y-axis zero suppressed*

Figure F.13 Gauge 26 - Magnitude Response(Characteristic Impedance)

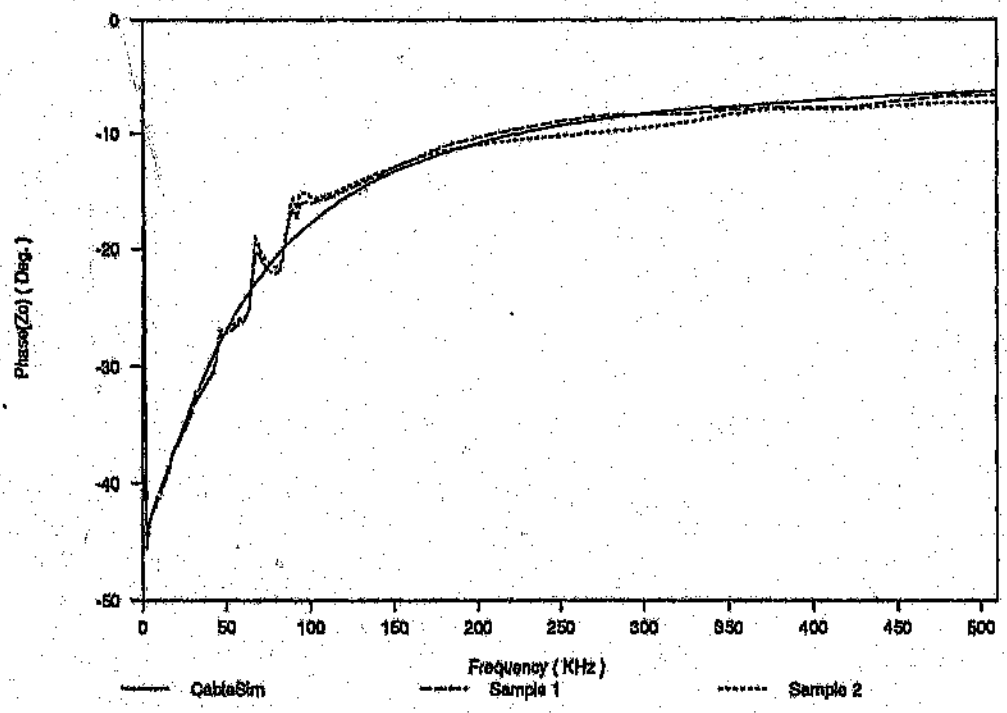

Figure F.14 Gauge 26 - Phase Response(Characteristic Impedance)

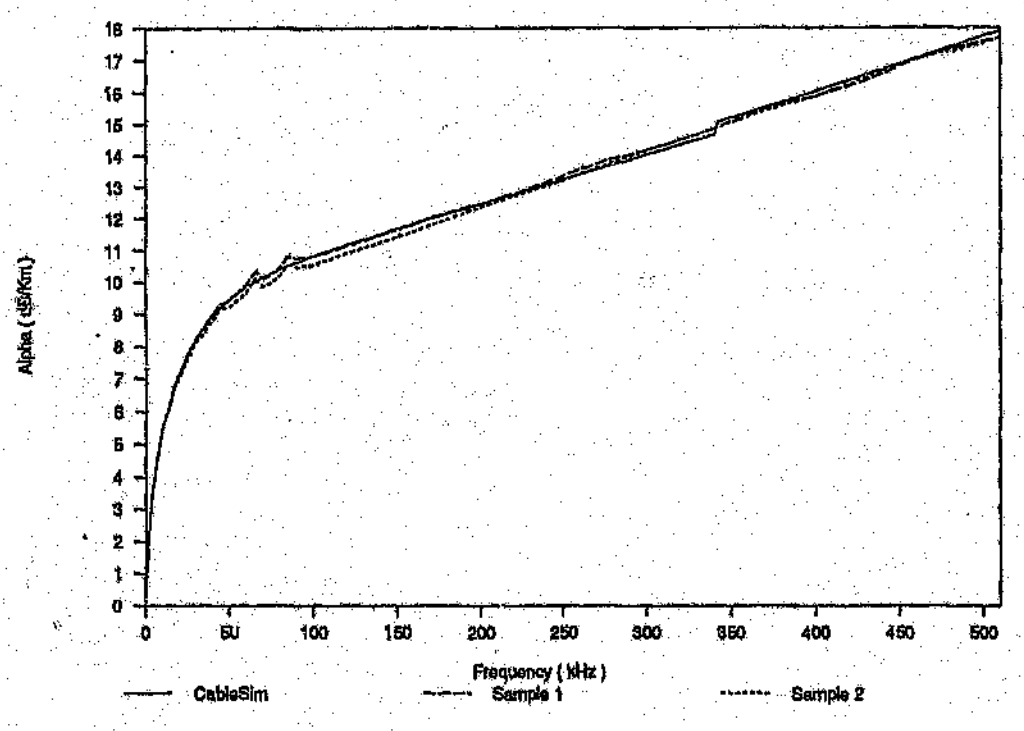

Figure F.15 Gauge 26 - Attenuation Constant

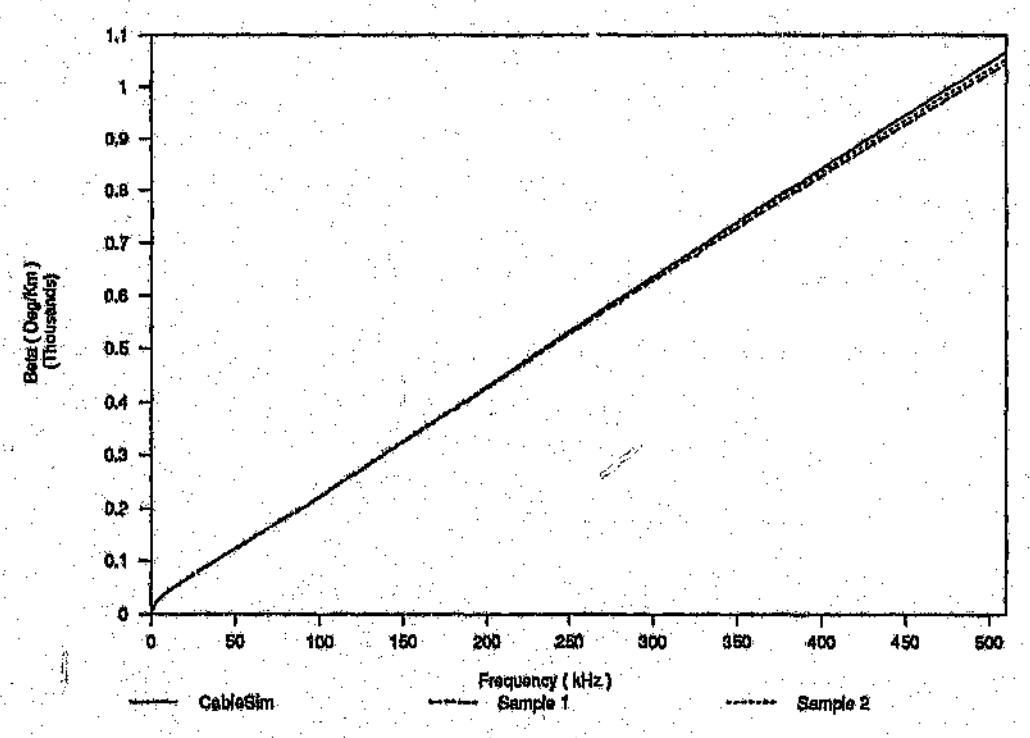

Figure F.16 Gauge 26 - Phase Constant

Appendix G

REFLECTION COEFICIENTS

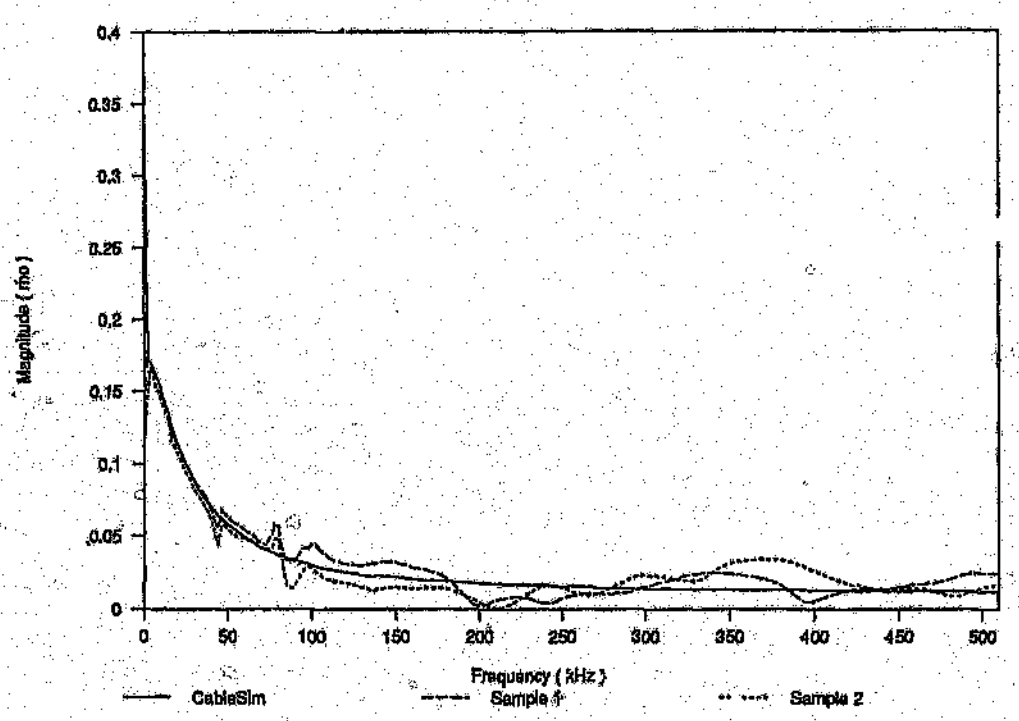

Figure G.1 Gauge 19⇒22 - Reflection Coeficient ($\rho_{19\text{-}22}$)

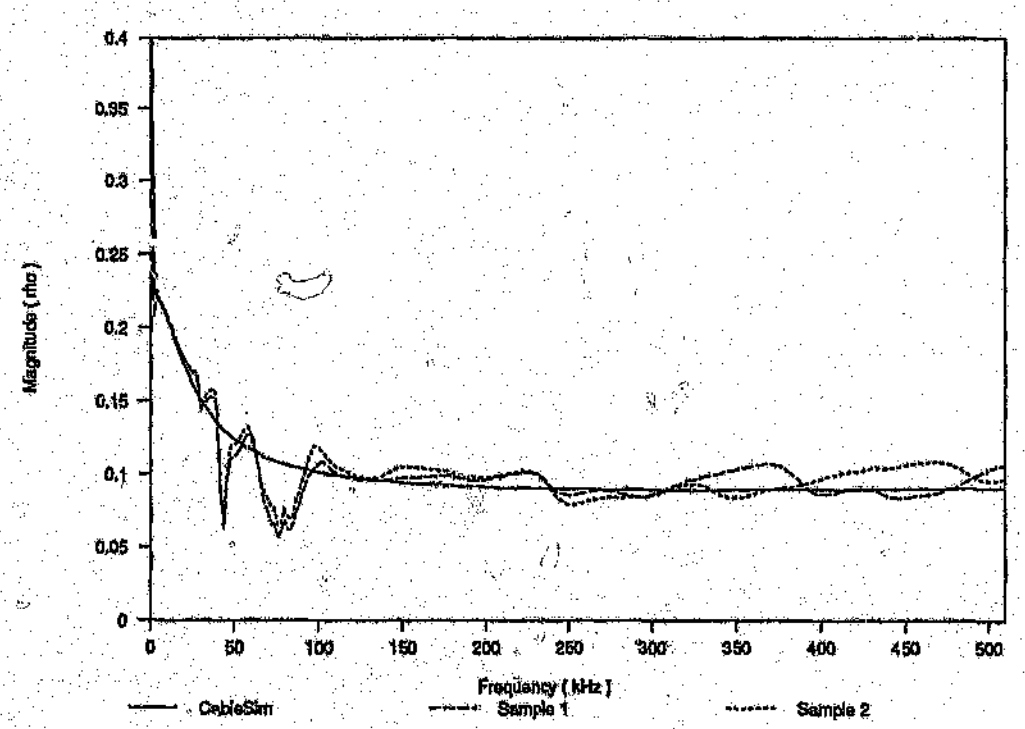

Figure G.2 Gauge 19⇒24 - Reflection Coeficient ($\rho_{19\text{-}24}$)

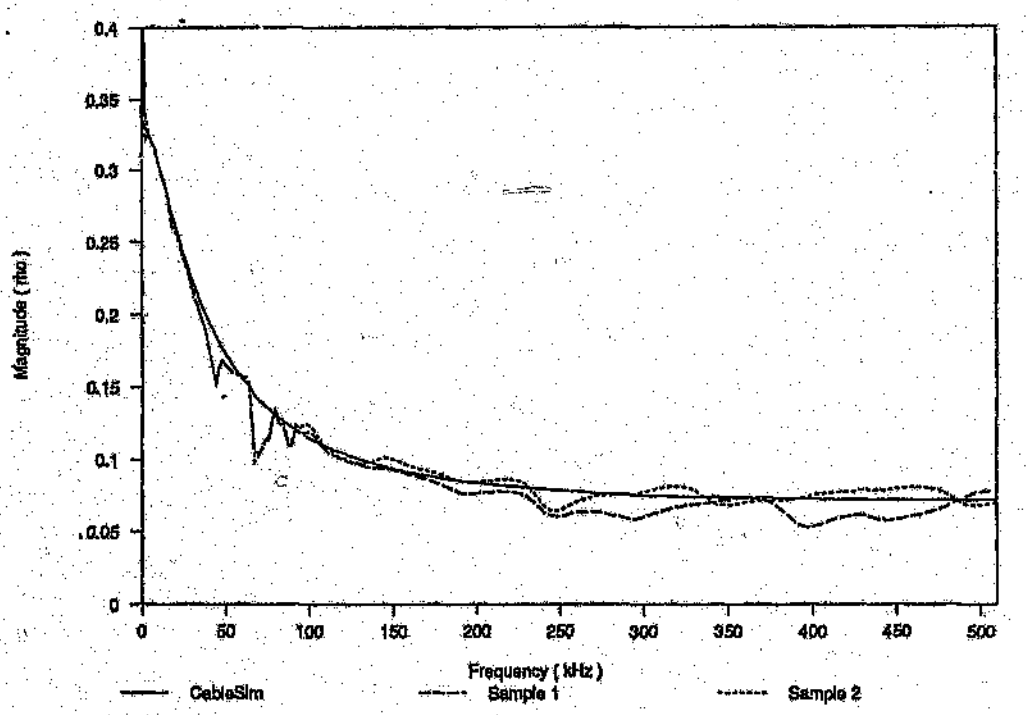

Figure G.3 Gauge 19⇒26 - Reflection Coeficient ($\rho_{19\text{-}26}$)

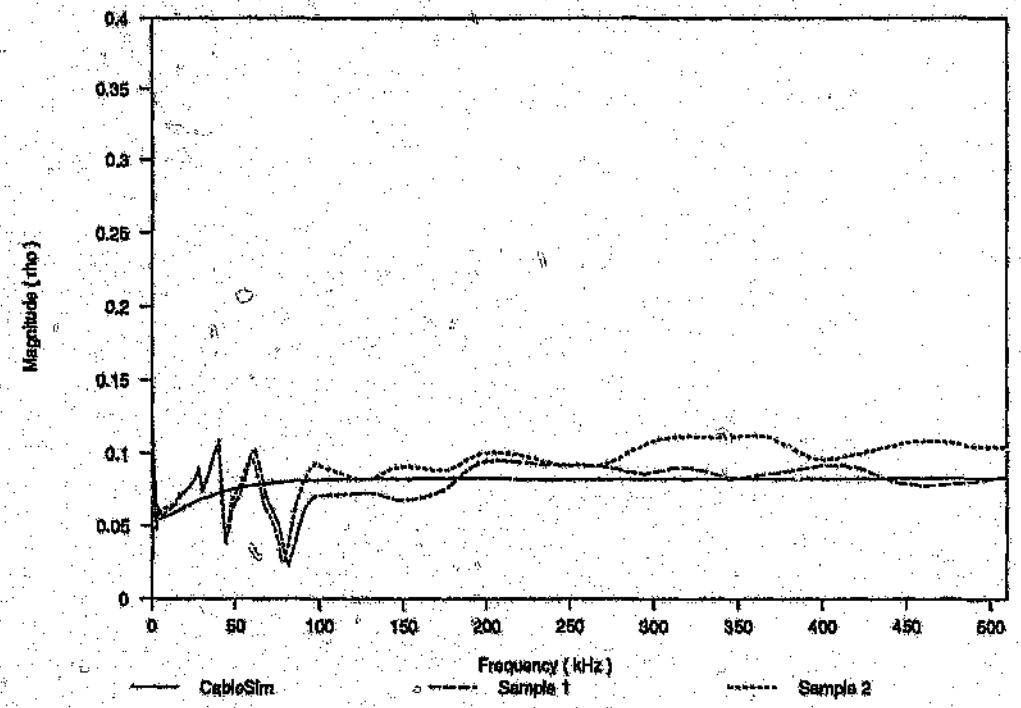

Figure G.4 Gauge 22⇒24 - Reflection Coeficient ($\rho_{22\text{-}24}$)

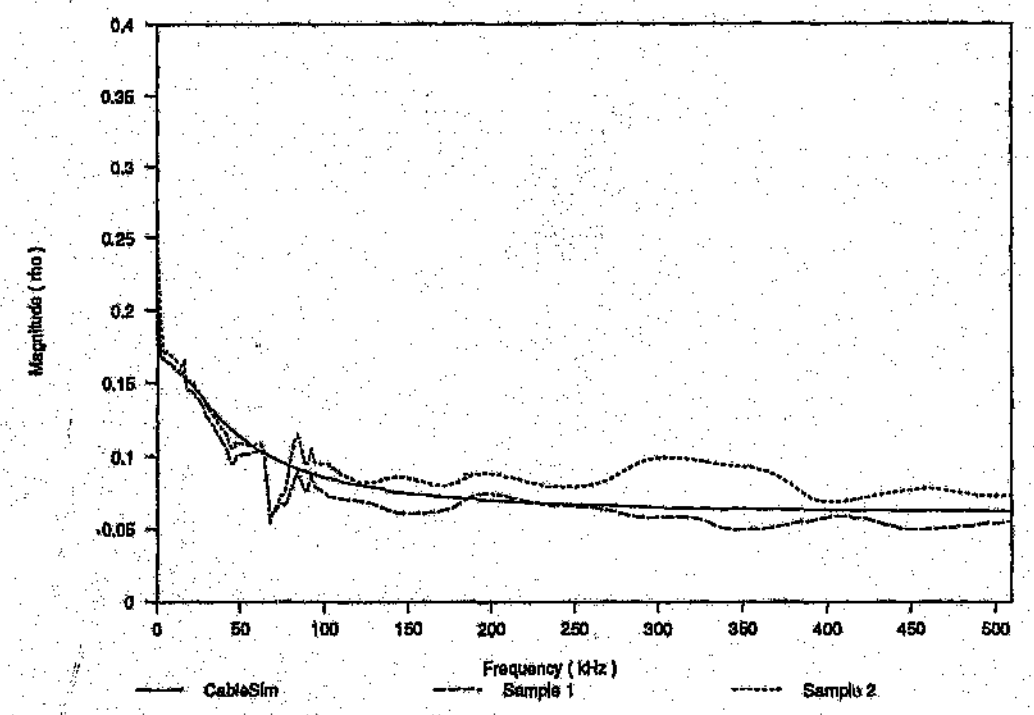

Figure G.5 Gauge 22⇒26 - Reflection Coeficient ($\rho_{22\text{-}26}$)

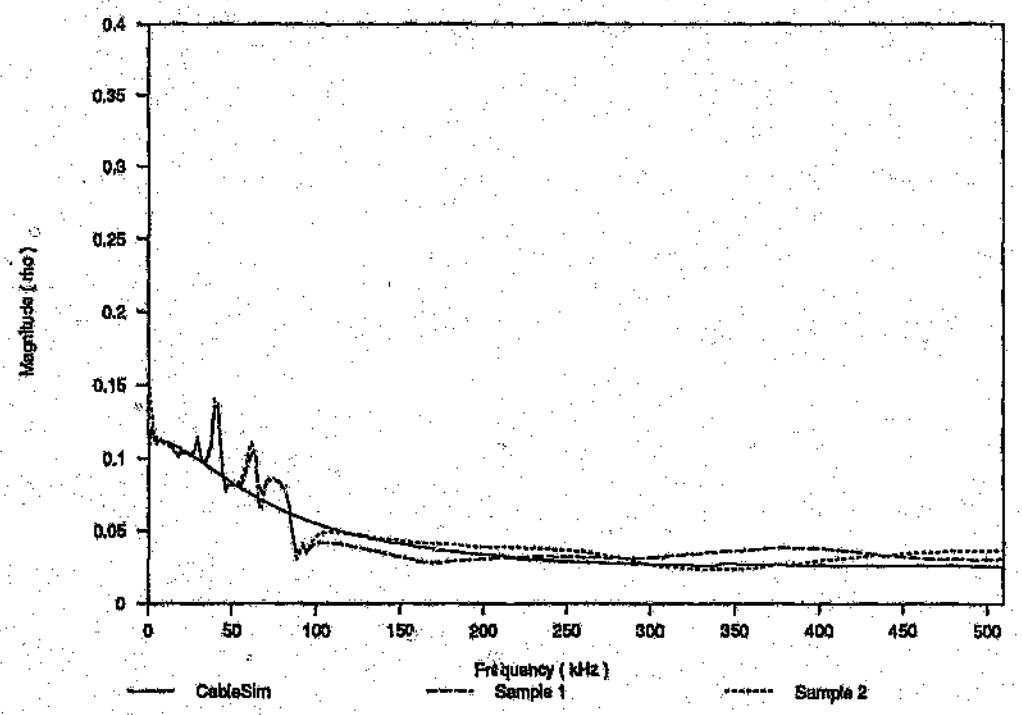

Figure G.6 Gauge 24⇒26 - Reflection Coeficient ($\rho_{24\text{-}26}$)

Appendix H

STEADY STATE TRANSFER FUNCTIONS

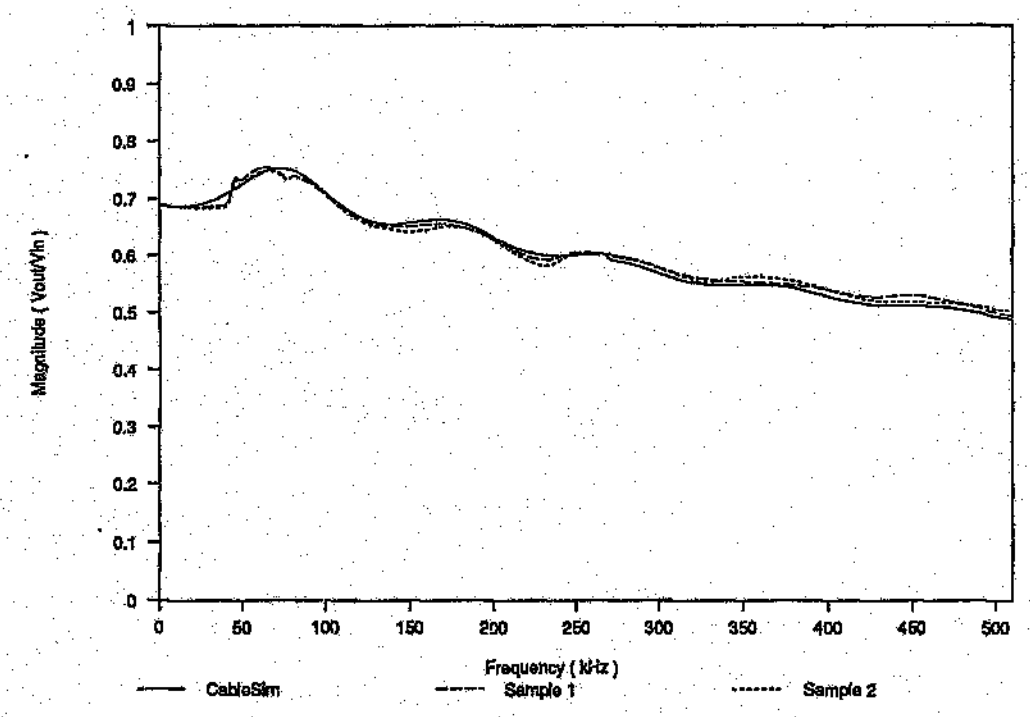

Figure H.1 Gauge 19 - Magnitude Response (Z_{load} = 120+j0 Ω)

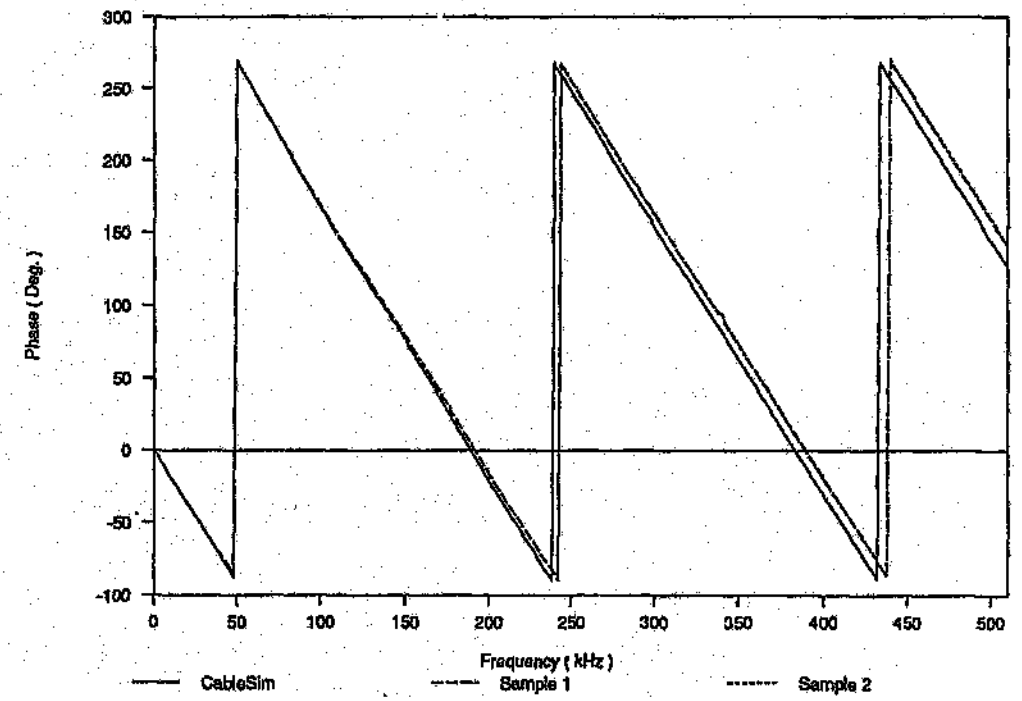

Figure H.2 Gauge 19 - Phase Response (Z_{load} = 120+j0 Ω)

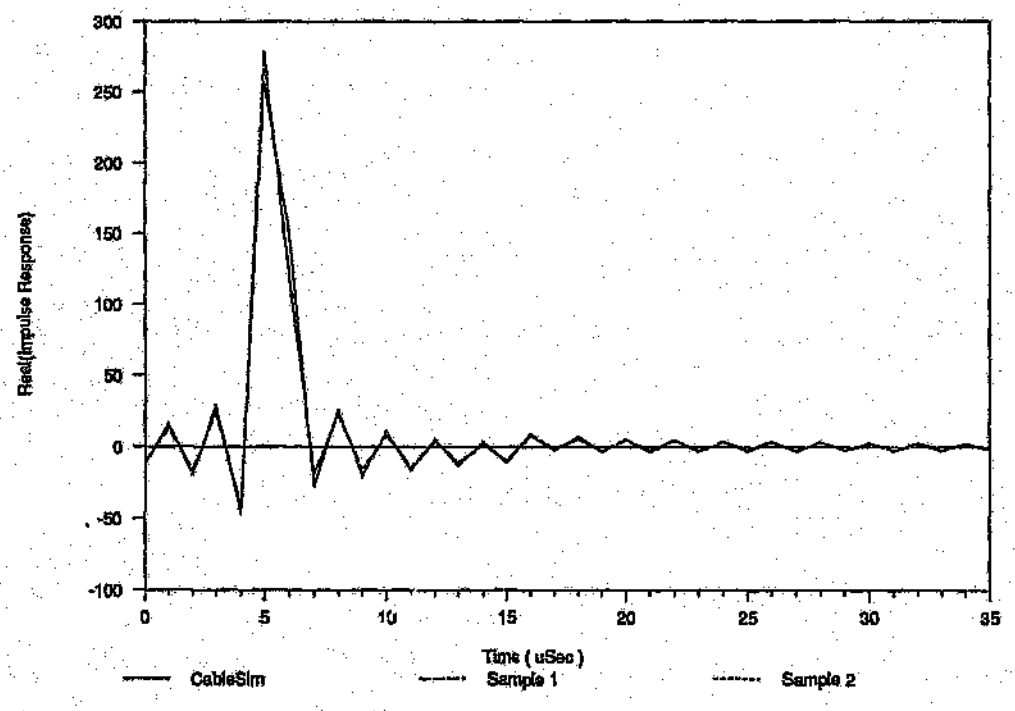

Figure H.3 Gauge 19 - Impulse Response (Z_{load} = 120+j0 Ω)

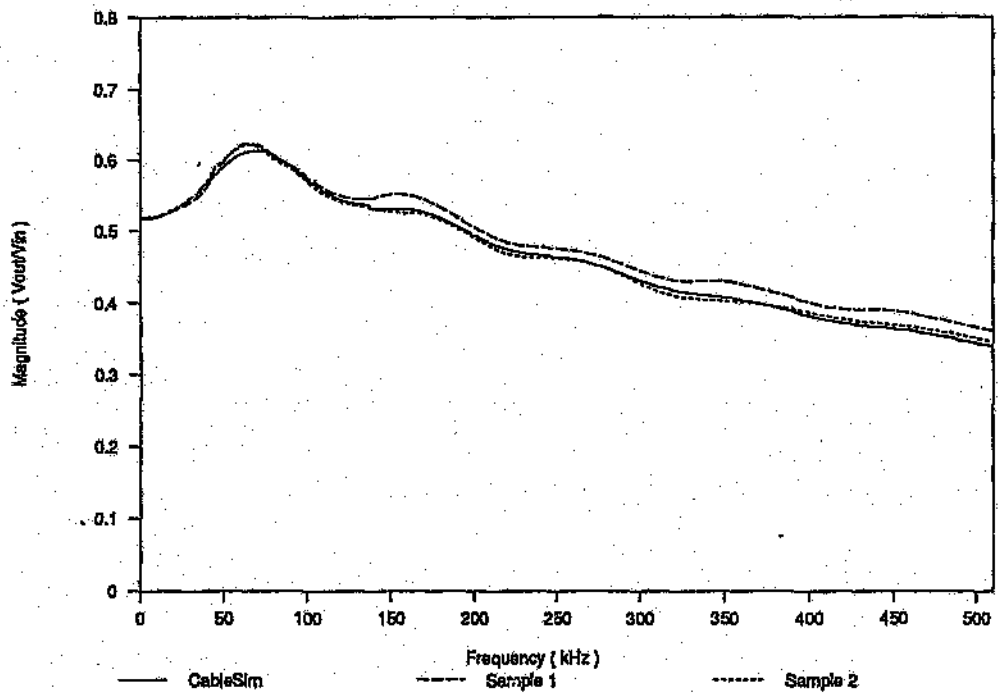

Figure H.4 Gauge 22 - Magnitude Response (Z_{load} = 120+j0 Ω)

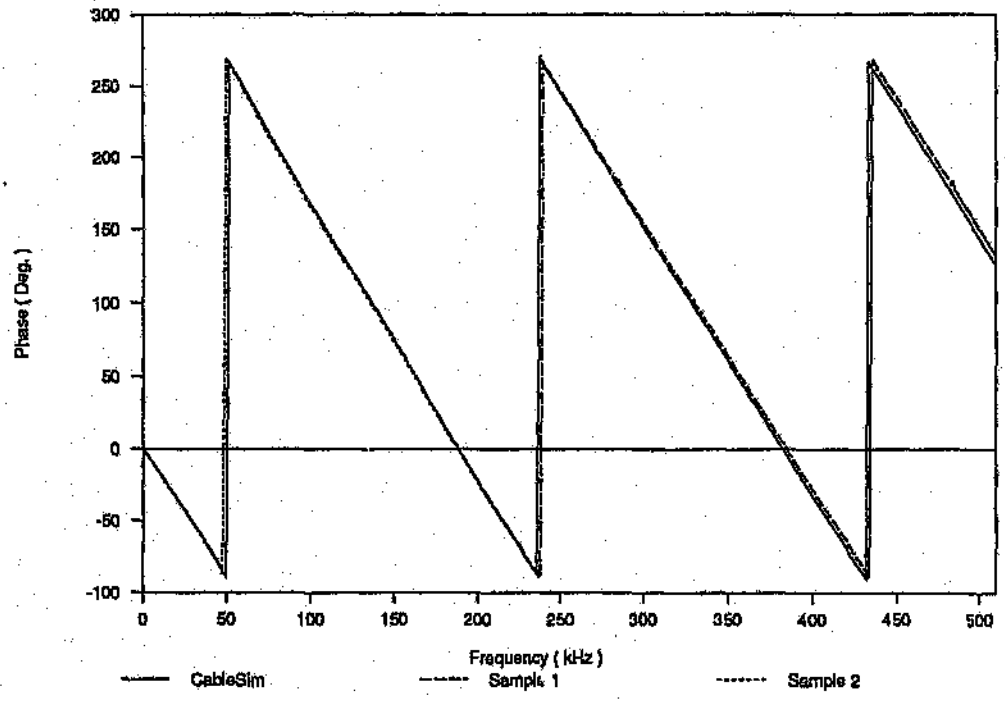

Figure H.5 Gauge 22 - Phase Response (Z_{load} = 120+j0 Ω)

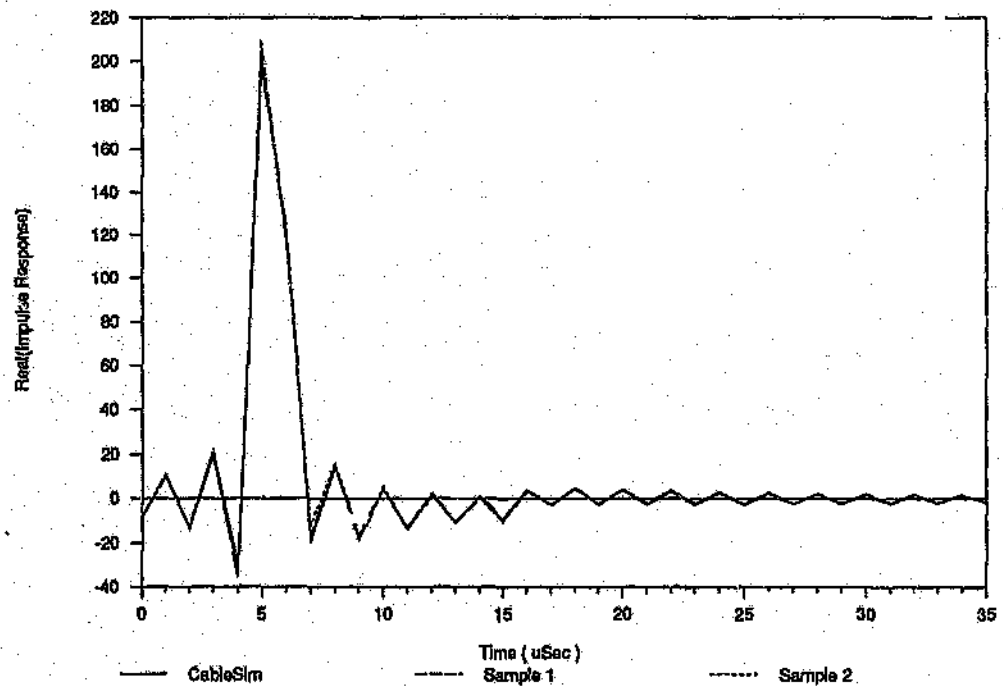

Figure H.6 Gauge 22 - Impulse Response (Z_{load} = 120+j0 Ω)

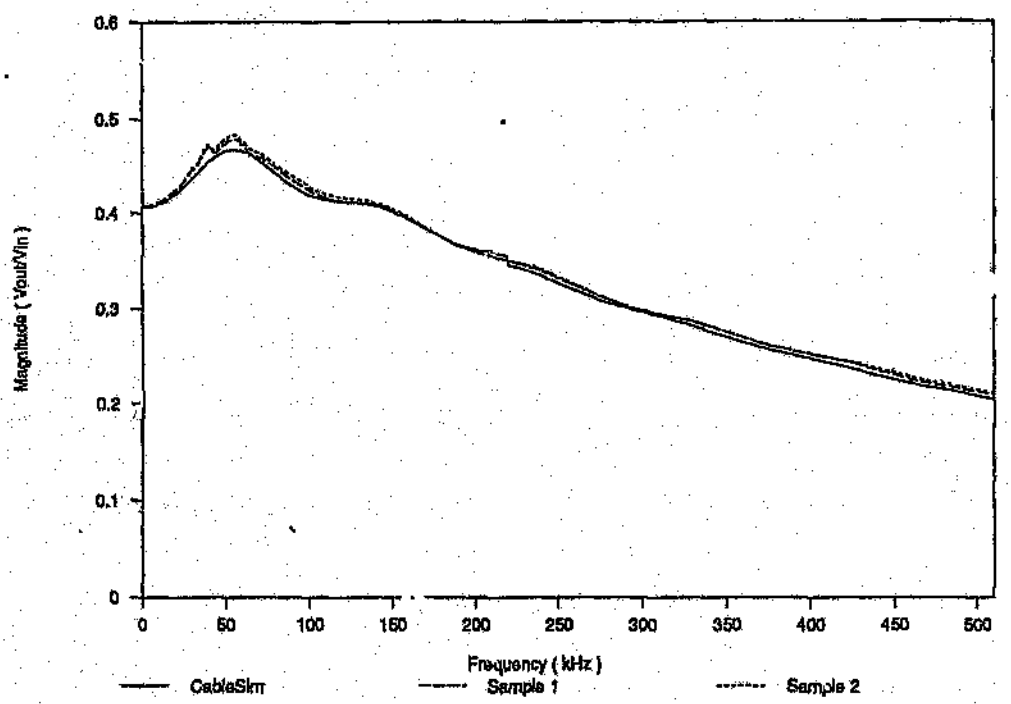

Figure H.7 Gauge 24 - Magnitude Response (Z_{load} = 120+j0 Ω)

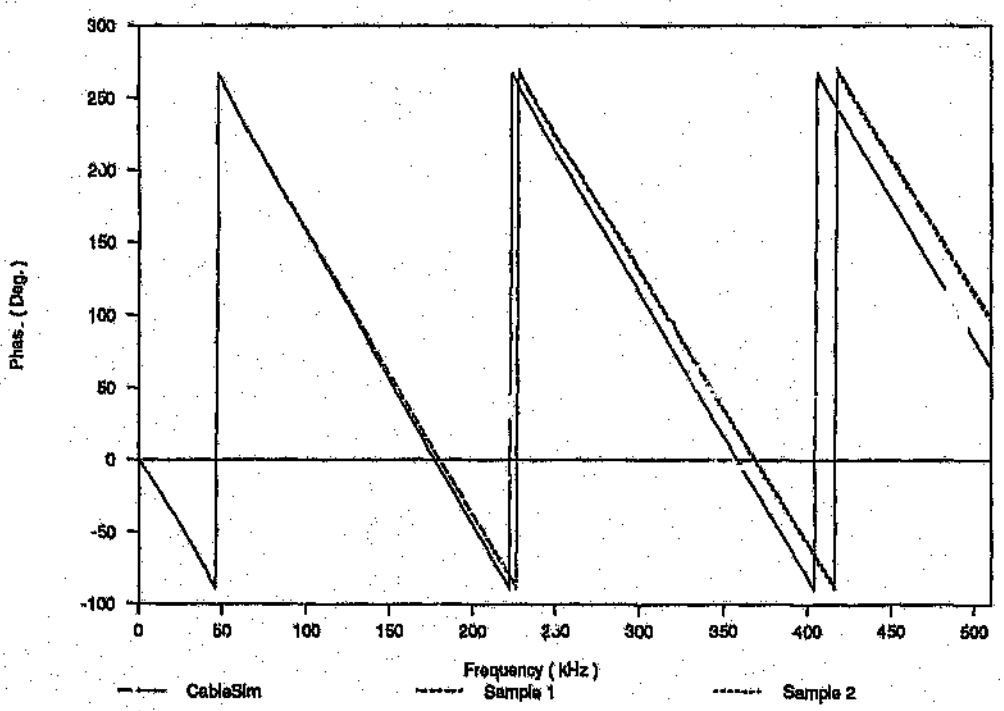

Figure H.8 Gauge 24 - Phase Response (Z_{load} = 120+j0 Ω)

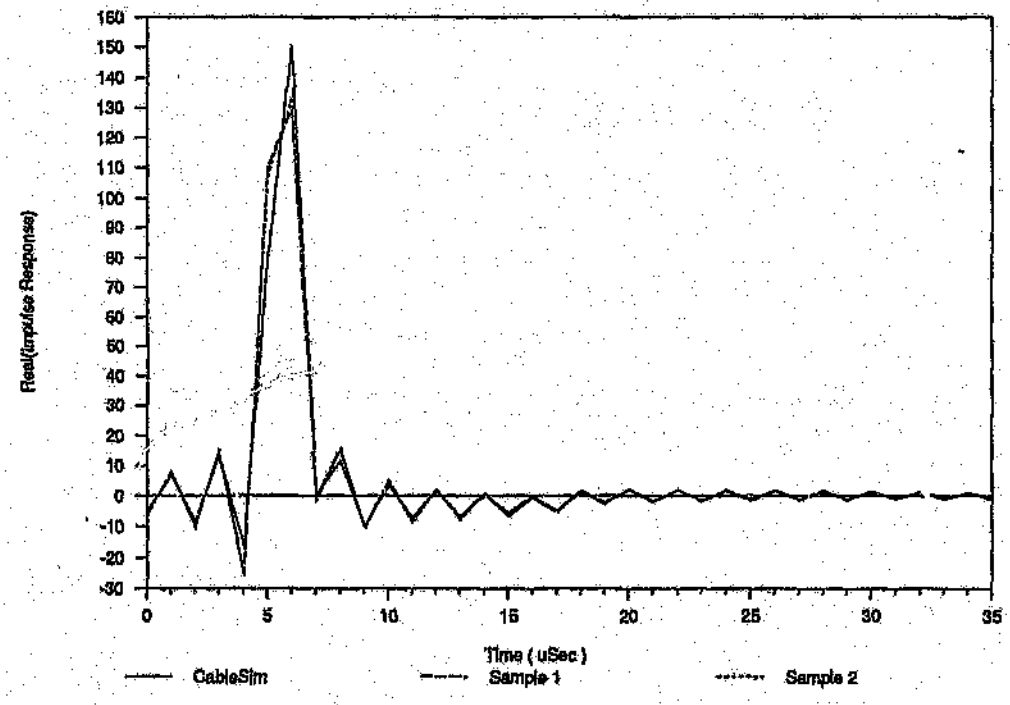

Figure H.9 Gauge 24 - Impulse Response (Z_{load} = 120+j0 Ω)

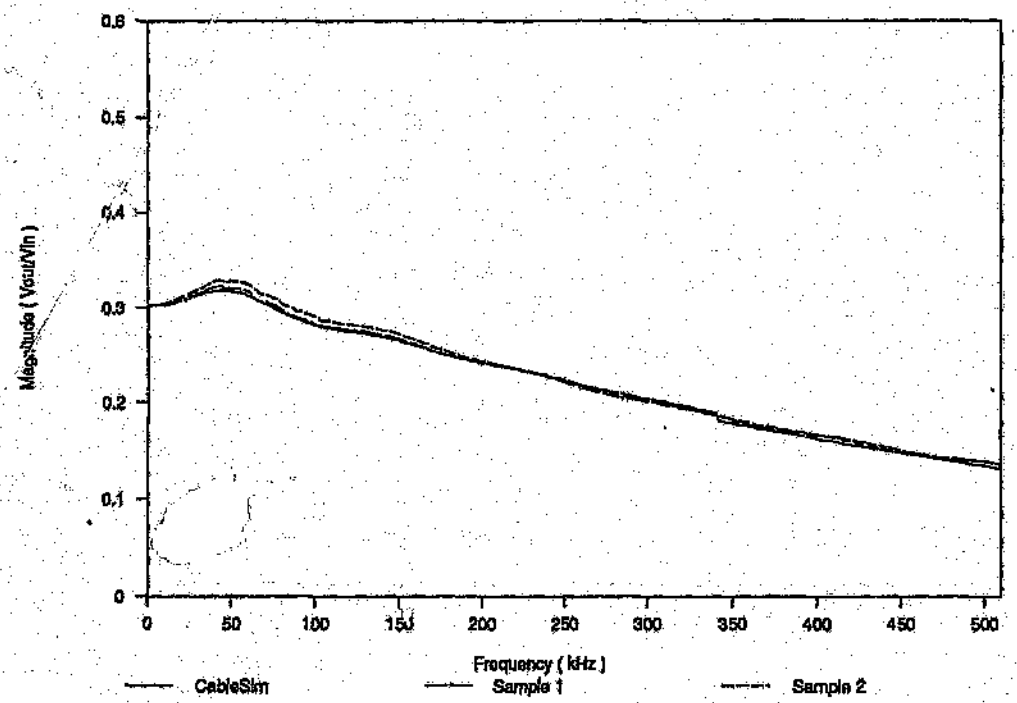

Figure H.10 Gauge 26 - Magnitude Response (Z_{load} = 120+j0 Ω)

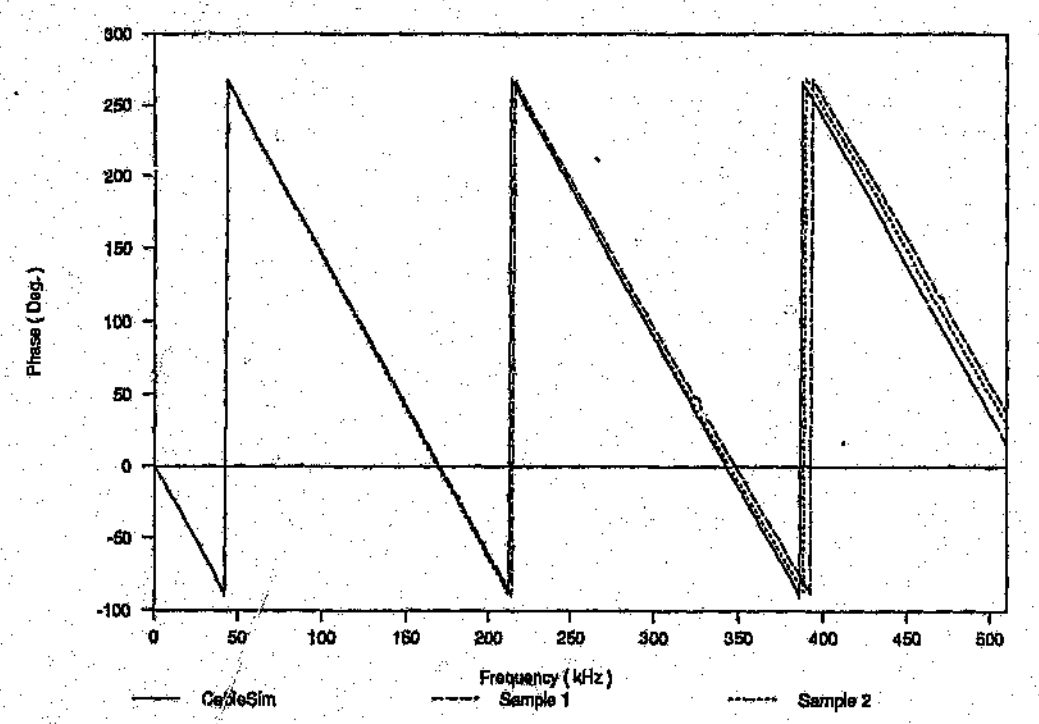

Figure H.11 Gauge 26 - Phase Response (Z_{load} = 120+j0 Ω)

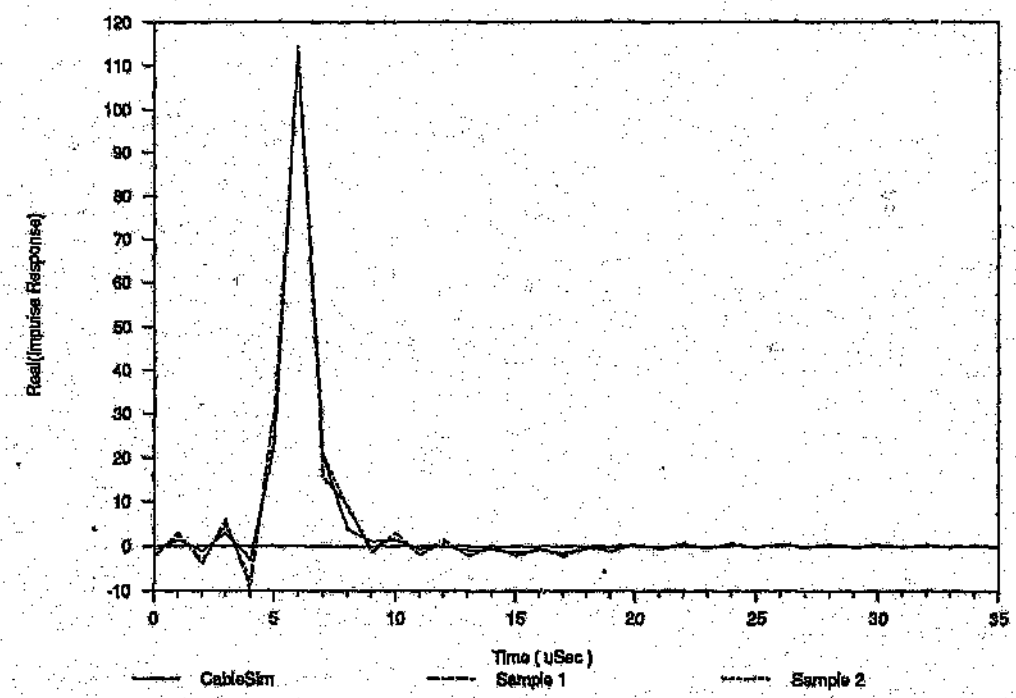

Figure H.12 Gauge 26 - Impulse Response (Z_{load} = 120+j0 Ω)

Appendix I

TRANSIENT STATE TRANSFER FUNCTION

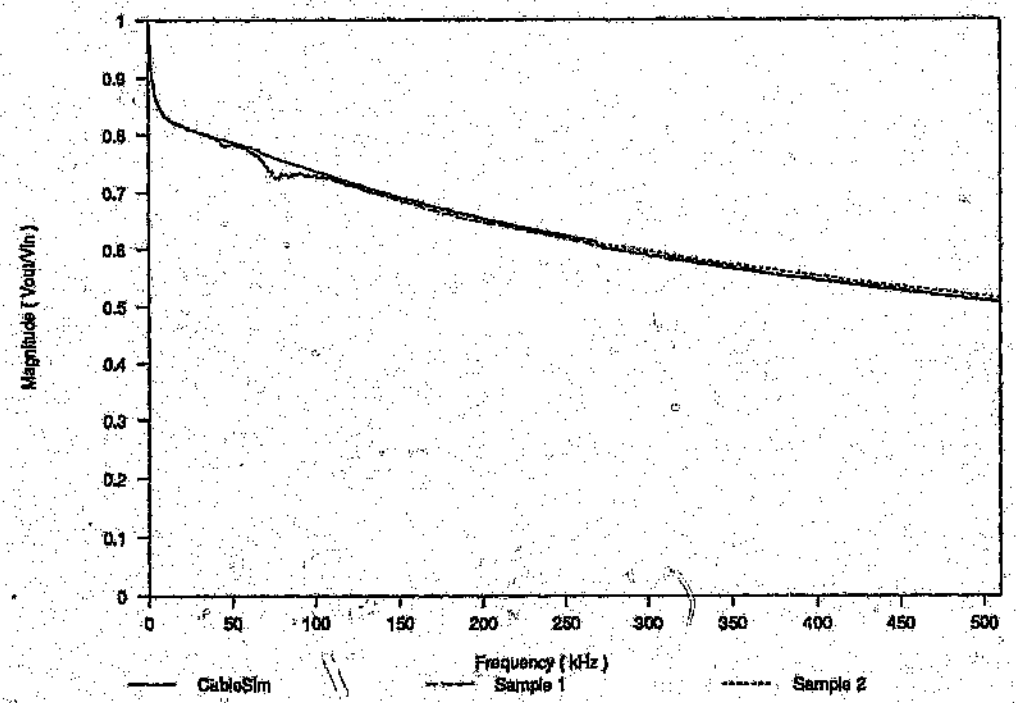

Figure I.1 Gauge 19 - Magnitude Response (Z_{load} = 120+j0 Ω)

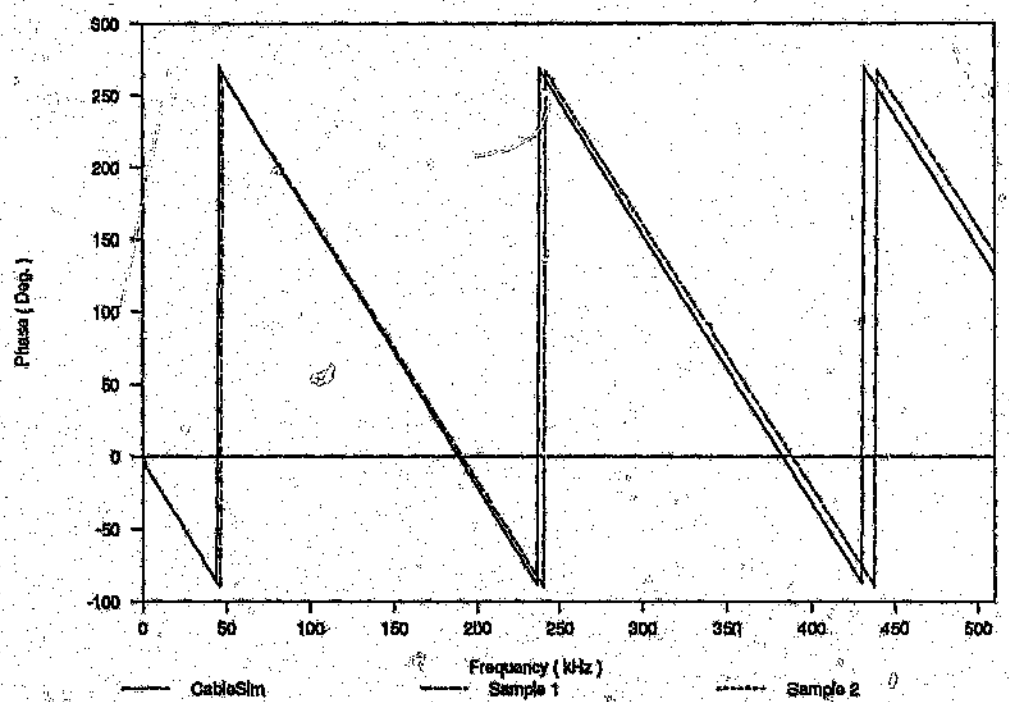

Figure I.2 Gauge 19 - Phase Response (Z_{load} = 120+j0 Ω)

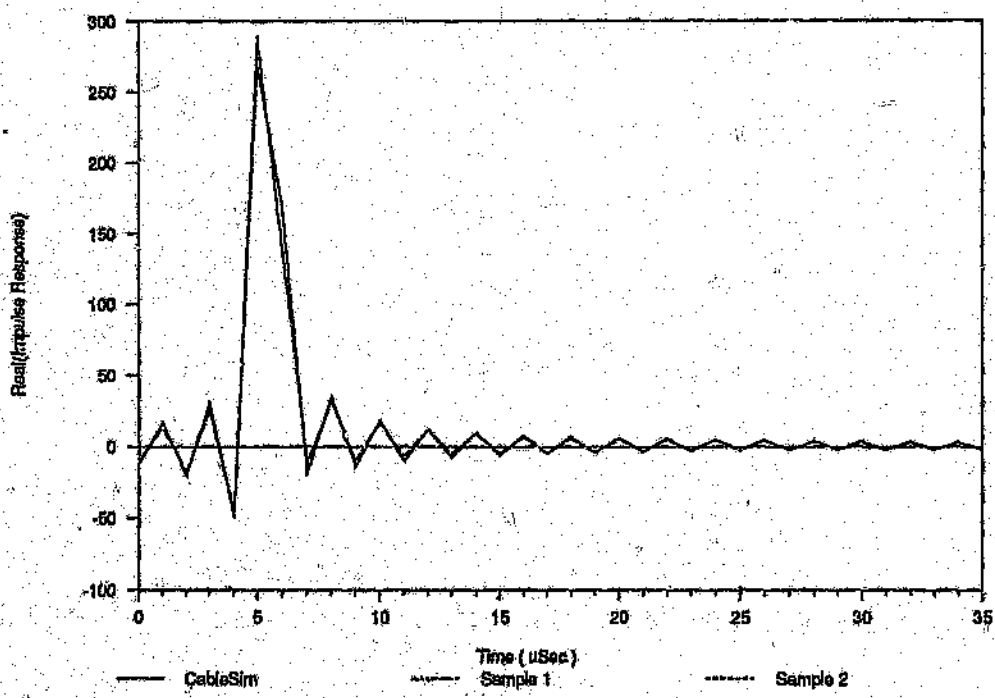

Figure I.3 Gauge 19 - Impulse Response (Z_{load} = 120+j0 Ω)

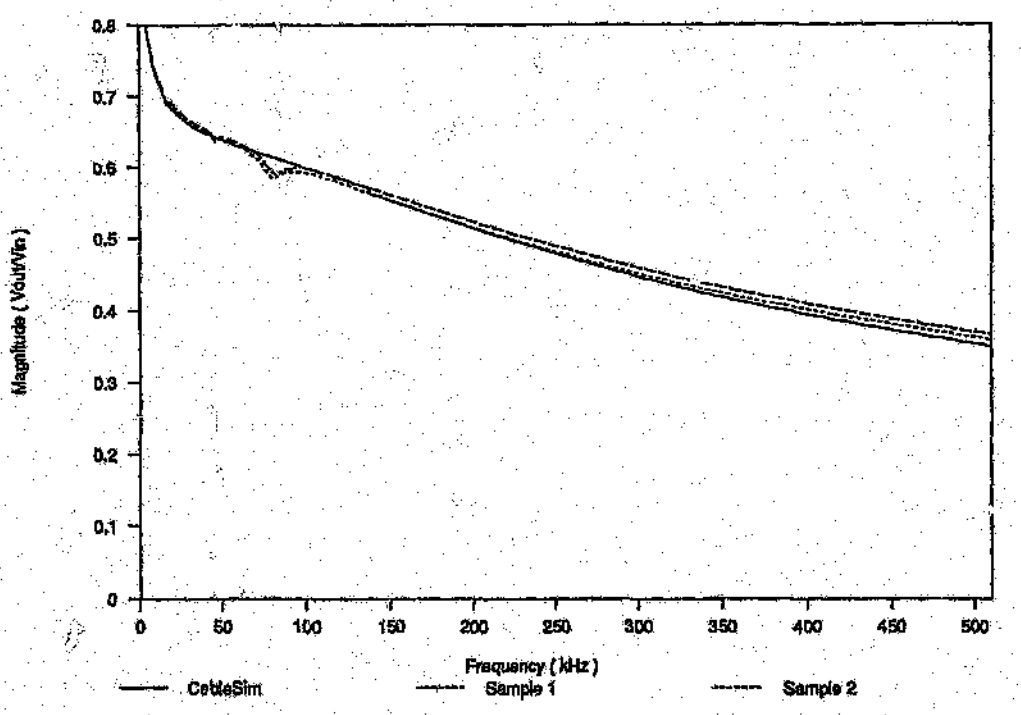

Figure I.4 Gauge 22 - Magnitude Response (Z_{load} = 120+j0 Ω)

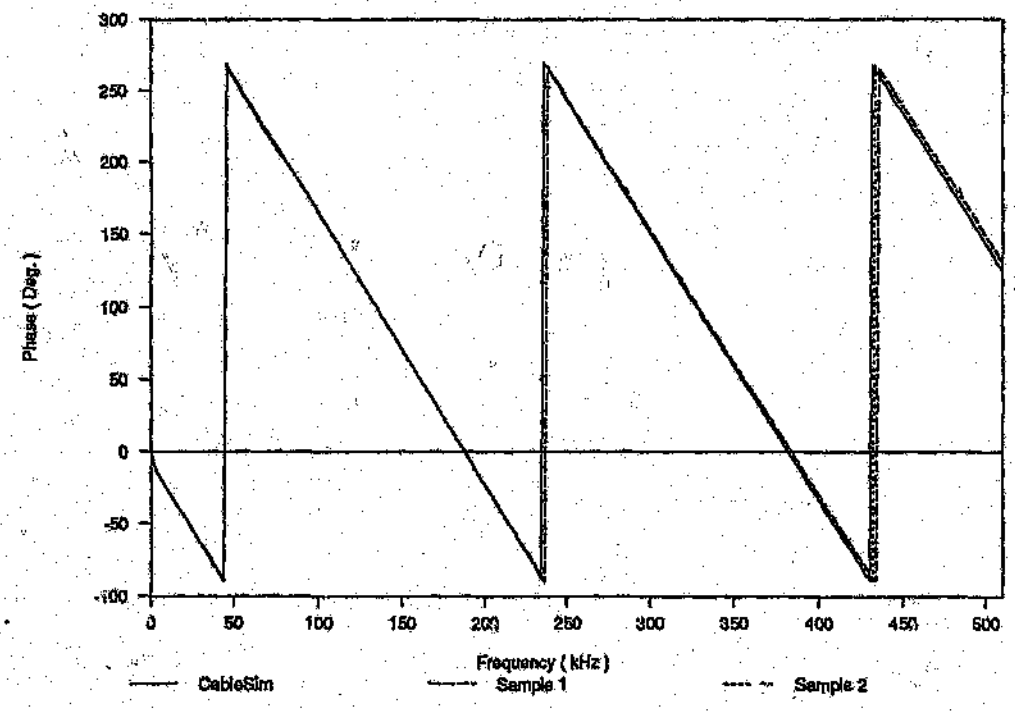

Figure I.5 Gauge 22 - Phase Response (Z_{load} = 120+j0 Ω)

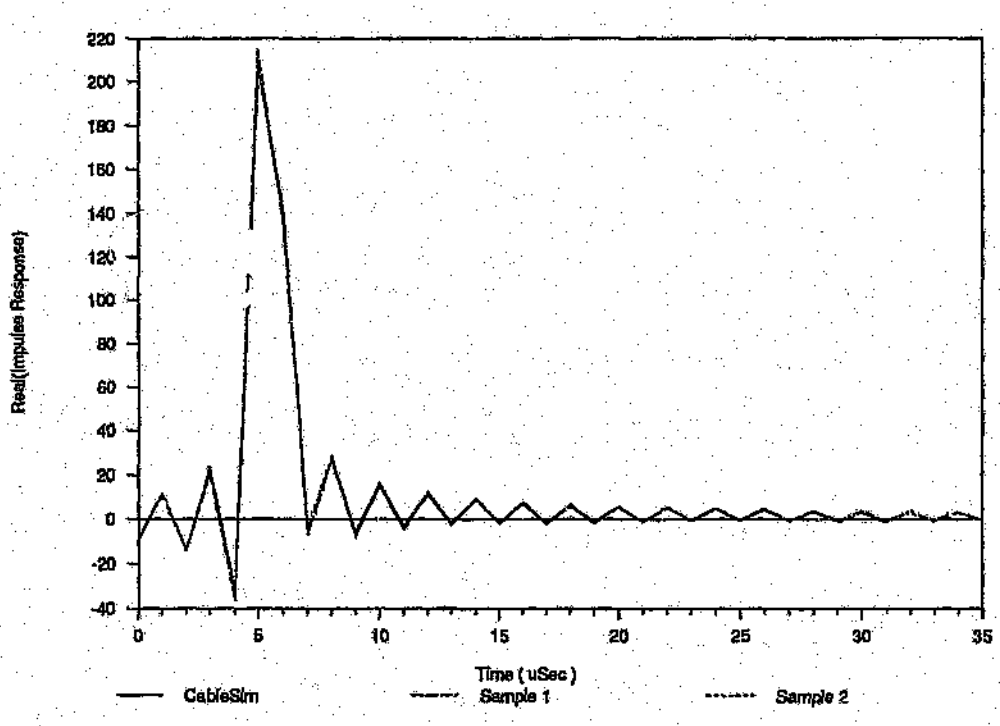

Figure I.6 Gauge 22 - Impulse Response (Z_{load} = 120+j0 Ω)

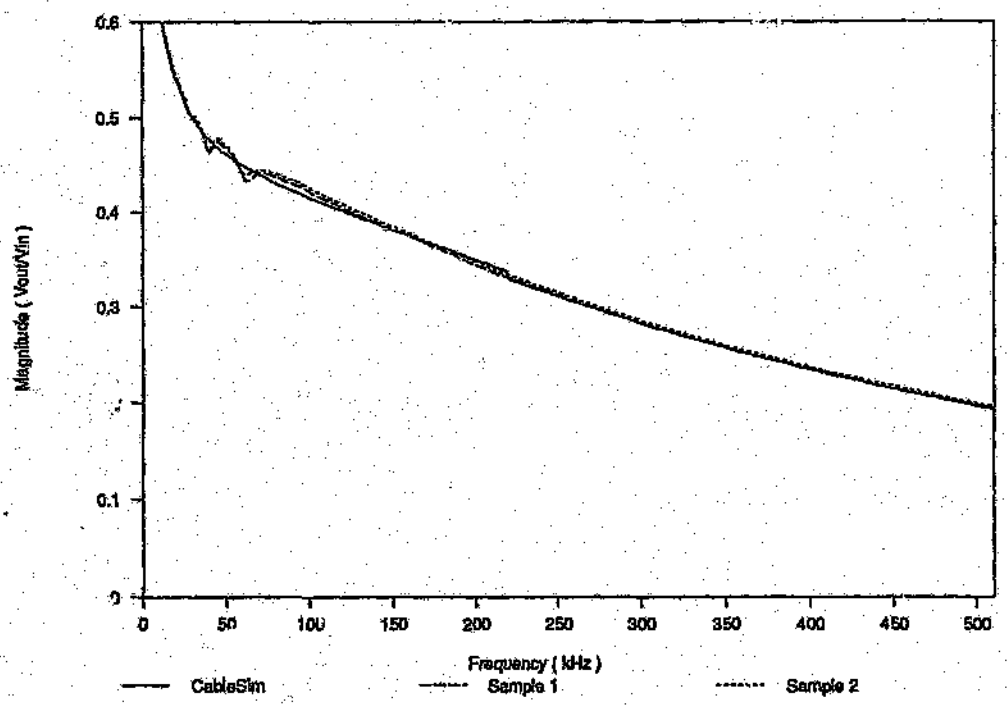

Figure I.7 Gauge 24 - Magnitude Response (Z_{load} = 120+j0 Ω)

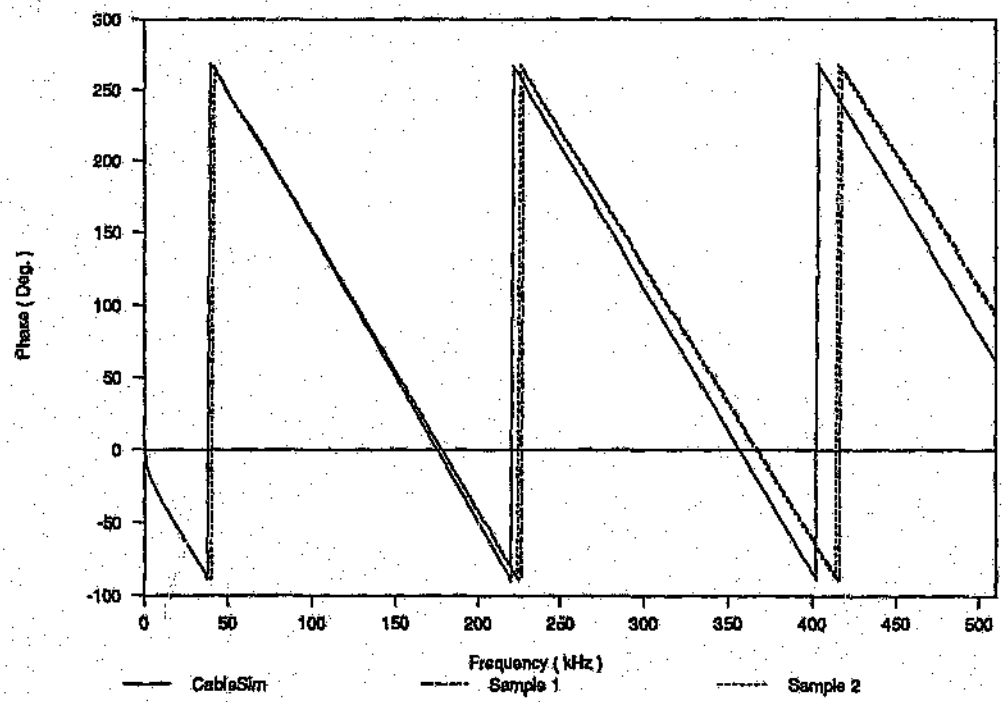

Figure I.8 Gauge 24 - Phase Response (Z_{load} = 120+j0 Ω)

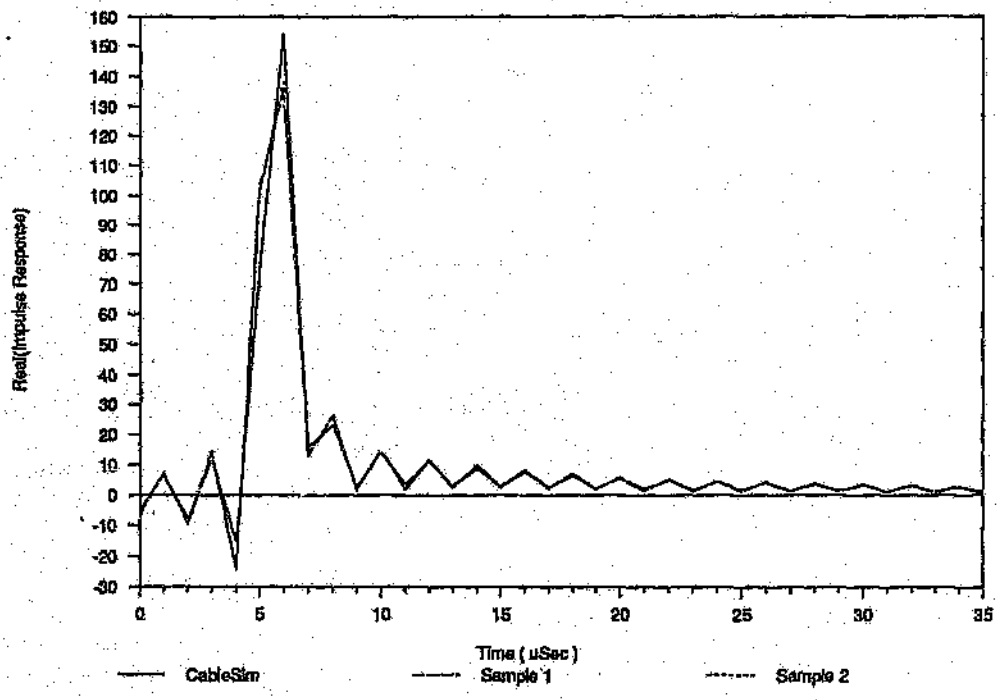

Figure I.9 Gauge 24 - Impulse Response (Z_{load} = 120+j0 Ω)

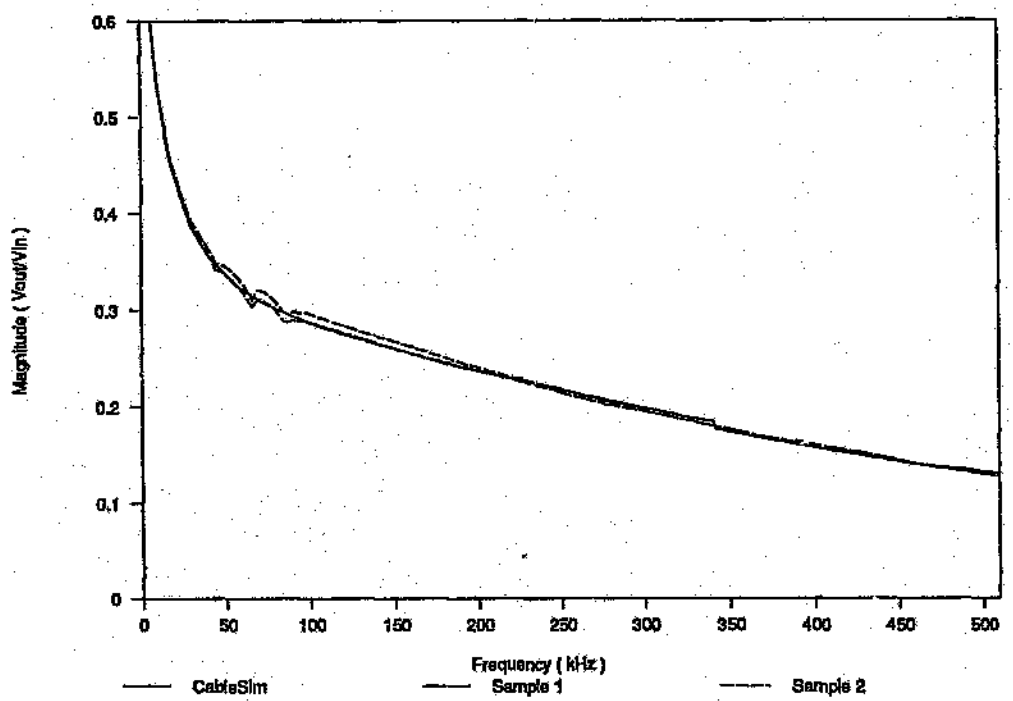

Figure I.10 Gauge 26 - Magnitude Response (Z_{load} = 120+j0 Ω)

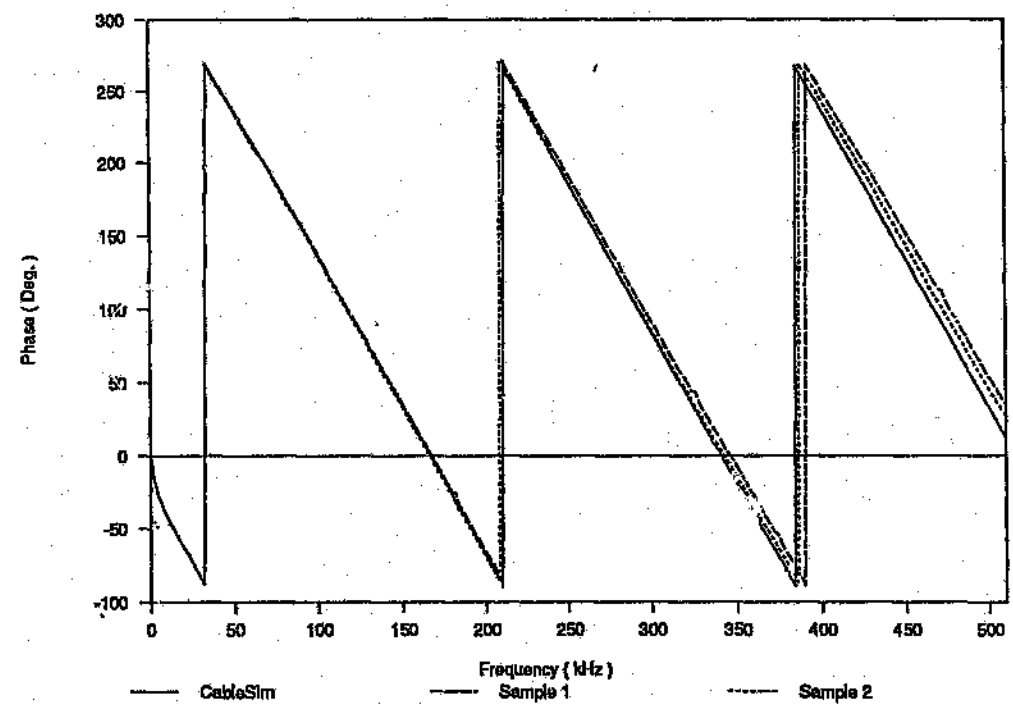

Figure I.11 Gauge 26 - Phase Response (Z_{load} = 120+j0 Ω)

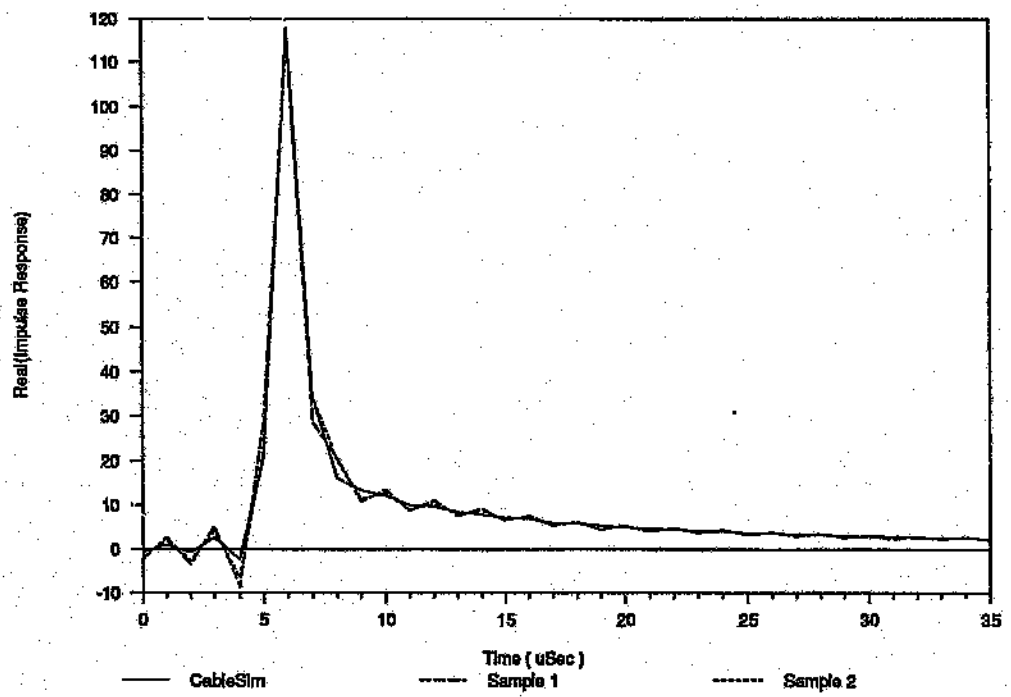

Figure L.12 Gauge 26 - Impulse Response (Z_{load} = 120+j0 Ω)